



UNIVERSIDAD NACIONAL AUTÓNOMA DE MÉXICO

PROGRAMA DE POSGRADO EN CIENCIAS DE LA TIERRA

INSTITUTO DE GEOLOGÍA

ESTACIÓN REGIONAL DEL NOROESTE

“Petrogénesis y metamorfismo del magmatismo Cámbrico de la Formación Cerro Rajón, Sonora, México y su relación con el proceso de rifting en el margen meridional de Laurentia”

T E S I S

QUE PARA OPTAR POR EL GRADO DE:
DOCTOR EN CIENCIAS DE LA TIERRA

PRESENTA:

ARTURO JOAQUÍN BARRÓN DÍAZ

TUTOR:

Dr. Francisco Abraham Paz Moreno
Departamento de Geología, UNISON

COMITÉ TUTOR

Dr. Francisco Abraham Paz Moreno, Departamento de Geología, UNISON.
Dr. Carlos Manuel González León, ERNO, UNAM
Dra. Elena Centeno García, Instituto de Geología, UNAM.

HERMOSILLO, SONORA

ENERO, 2018



Universidad Nacional
Autónoma de México

Dirección General de Bibliotecas de la UNAM

Biblioteca Central



UNAM – Dirección General de Bibliotecas
Tesis Digitales
Restricciones de uso

DERECHOS RESERVADOS ©
PROHIBIDA SU REPRODUCCIÓN TOTAL O PARCIAL

Todo el material contenido en esta tesis esta protegido por la Ley Federal del Derecho de Autor (LFDA) de los Estados Unidos Mexicanos (México).

El uso de imágenes, fragmentos de videos, y demás material que sea objeto de protección de los derechos de autor, será exclusivamente para fines educativos e informativos y deberá citar la fuente donde la obtuvo mencionando el autor o autores. Cualquier uso distinto como el lucro, reproducción, edición o modificación, será perseguido y sancionado por el respectivo titular de los Derechos de Autor.

*Para Graciela y Santiago, los dos faros de mi vida
que me muestran el camino a la verdad...*

...ad maiorem Dei gloriam

AGRADECIMIENTOS

Gracias **Señor** por el don de la ciencia. Que con cada gramo que me regalas de conocimiento, me des también un kilo de humildad para que mi trabajo sea siempre reflejo de tu sencillez y de tu misericordia.

Agradezco profundamente todo el apoyo y la guía que me fue brindada por mi asesor y amigo el **Dr. Francisco Paz** a lo largo de estos años de estudio en el programa de doctorado. Sin su dirección, consejos y revisiones, esta tesis no hubiera podido concluir. Muchas gracias!

Gracias a mi esposa **Graciela Valencia**, por su confianza, cariño y ejemplo que me motivan a diario a ser una mejor persona. También a mi familia política especialmente a **Graciela Murrieta** por su cariño y por todo lo que me ha alimentado.

Le doy las gracias a mi familia, a mi papá **Jesús Barrón** y a mi mamá **Martha Díaz** por todo el apoyo y el cariño de todos estos años y por estar me motivando siempre a mejorar como persona y profesional. También a mis hermanos Anibal y Ana por su apoyo y por su cariño especial de hermanos. Este logro es también de todos ustedes.

A todos los profesores que a lo largo de estos años fueron influyentes en mi trabajo, mi desarrollo profesional y que me apoyaron en varias ocasiones con mi investigación. **Carlos González, Elena Centeno, Saúl Herrera, Ricardo Vega, Jesús Vidal, Martín Valencia, Silvia Martínez, Ricardo Amaya, Diana Meza, Juan Carlos García**. En especial a los colaboradores externos que participaron en las publicaciones y con los que formé un buen equipo de trabajo: **Alex Iriondo, Rufino Lozano, Dan Miggins y James Hagadorn**. Muchas gracias a todos ustedes y a los profesores del departamento de geología y la ERNO que me apoyaron.

Gracias a mis compañeros del programa de posgrado del PCT y PCB que estuvieron ahí para apoyarme y acompañarme a lo largo de estos años. **Alejandra, Iván, Ceci, Rubén, Belem, Alicia, Tomás, Yaz, Ricardo, Adrian, Martha, Yessi, Laura, Karla**, entre otros. Muchas gracias a todos!

Gracias al personal de la ERNO y la UNISON que me apoyó con la fabricación de secciones delgadas y la preparación de muestras para geoquímica. **Sheila, Aimee, Jorge, Elizard y Pablo Peñaflo**.

Un agradecimiento especial a mis amigos y profes locos **Alejandra Gómez** e **Iván Espinoza**. Por todo el apoyo en los momentos buenos y en los momentos difíciles que a lo largo de estos años han ocurrido. Para que siempre sigamos juntos en la amistad y colaborando en lo profesional.

Le agradezco a todo el personal administrativo de la ERNO y el Instituto de Geología por su apoyo en los muchos trámites por los cuales tuvimos que pasar para concluir con este proyecto. **Fátima, Monse, Mónica, María Luisa, Gloria Alba, Erika** y en especial le agradezco a la encargada del posgrado en la ERNO **Uxue Villanueva** por toda su ayuda y atención en mis años de estudio. Muchas gracias!

Mi agradecimiento muy especial para todos los propietarios de las localidades de estudio de la región de Caborca que nos permitieron acceder a los afloramientos de interés. Especialmente al Sr. **Rogelio Lizárraga**. También agradezco a toda la brigada del desierto de Fresnillo por su apoyo y hospedaje en las misiones de campo. Especialmente a mi estimado Omar y a todas las personas que me apoyaron en el campo.

Por último, quiero dar las gracias a mis amigos que aunque no estuvieron directamente involucrados en mi trabajo académico, su apoyo, ejemplo y amistad me ayudaron en esta importante etapa de mi vida. **Roberto, Lizbet, Pepe, Claudia, Esthelita, Rosita, Adolfo, Rosaura...** a todos ustedes que gracias a Dios son muchos. Agradezco también todo el apoyo de mis amistades de la Parroquia Inmaculada Concepción de María y de la Arquidiócesis de Hermosillo por la oportunidad de servirle al Señor al lado de ustedes. Muchas gracias por ser una parte esencial en mi vida.

A todos los que directa o indirectamente me apoyaron y confiaron en mi... muchas gracias!

Petrogénesis y metamorfismo del magmatismo Cámbrico de la Formación Cerro Rajón, Sonora, México y su relación con el proceso de rifting en el margen meridional de Laurentia

En la región de Caborca, al noroeste del estado de Sonora, afloran rocas del Neoproterozoico y Cámbrico que pertenecen a depósitos de plataforma continental. El límite del Neoproterozoico-Cámbrico en esta localidad está marcado por las capas de dolomías de la Fm. La Ciénega (Ediacara) y de la Formación Cerro Rajón (Terrenueviense), esta última previamente identificada como Unidad 1 de la Formación Puerto Blanco. La Formación Cerro Rajón es definida en la presente investigación como una secuencia vulcano-sedimentaria que consiste de interestratificaciones de conglomerados tufáceos, aglomerados, lapillitas, tobas, derrames máficos-ultramáficos, cuarcitas, areniscas, limolitas y conglomerados. Los afloramientos estudiados son escasos y están parcialmente sepultados, sin embargo se pudieron localizar y muestrear ocho localidades donde aflora la Formación Cerro Rajón. Las localidades estudiadas presentan una importante variación en el espesor de las unidades litológicas, especialmente las volcánicas, por lo que se interpreta que la actividad volcánica se llevó a cabo a través de explosiones estrombolianas y la erupción de derrames de pocos metros de espesor. Los estudios petrográficos de los metabasaltos permitieron clasificar las muestras de las lavas como granofels con microfábricas porfidoblásticas. Este metamorfismo de bajo grado fue producido por un importante evento de hidrotermalismo, el cual provocó una alteración propilítica en la mayoría de flujos volcánicos y un carbonatización que se puede observar, principalmente, en los clastos volcánicos de los conglomerados tufáceos. Los metabasaltos presentan una mineralogía secundaria constituida principalmente por clorita, actinolita, epidota, calcita, titanomagnetita, albita y esfena. Sin embargo es posible identificar relictos de la mineralogía primaria como cristales de diopsida e ilmenita. Resultados de geotermometría muestra temperaturas de metamorfismo de 400 a 500 °C para los clastos volcánicos y hasta 548 °C para los derrames. Estos resultados en conjunto con la identificación de la paragénesis metamórfica, permite ubicar a las muestras en las facies superior de esquistos verdes incursionando hacia la facies de epidota-actinolita. La geoquímica obtenida a partir de un total de 36 muestras de clastos volcánicos y derrames, muestra un magmatismo bajo en sílice ($\text{SiO}_2 = 30.50 - 53.11\%$)_N con altas concentraciones de titanio ($\text{TiO}_2 = 2.98 - 7.00\%$)_N. Geoquímicamente se observa un sistema parcialmente abierto afectado por un metasomatismo, que aportó concentraciones de calcio al sistema y empobreció las rocas en sílice y otros elementos mayores. Sin embargo, algunos elementos mayores y principalmente los elementos traza inmóviles se conservaron en la mayoría de las muestras. Los derrames, en general, se clasifican como basaltos alcalinos, aunque muchas de estas rocas provienen de protolitos ultramáficos, de los cuales se identificaron escasas basanitas y picrobasaltos. El magmatismo es del tipo alcalino, anorogénico, con bajas tasas de fusión y se relaciona a un rift del tipo intraplaca continental desarrollado en un margen pasivo. Tiene características de una fuente enriquecida con valores altos en MgV (~70). Los estudios muestran que el último evento de alteración que sufrieron estas rocas fue producido por intrusivos Laramídicos, presentes en la región de estudio. Una granodiorita cercana a las unidades volcánicas fue fechada por U-Pb en zircones en 71.1 ± 0.4 Ma. Estudios de geobarometría en esta granodiorita indican profundidades de emplazamiento de ~8 km. Los resultados de geocronología $^{40}\text{Ar}/^{39}\text{Ar}$ muestran edades de metamorfismo de 55.89 ± 0.6 Ma a 60.26 ± 0.33 Ma para la porción oeste del área de estudio, mientras que la porción este presenta una pérdida de argón que se refleja en edades con alta incertidumbre. La edad de la Formación Cerro Rajón ha sido acotada en un intervalo de entre 530 – 541 Ma. Este rango fue obtenido utilizando la ocurrencia del fósil *Cloudina*, de la fauna Ediacara, observado en la Fm. La Ciénega y en la presencia del icnofósil *Treptichnus pedum* en las capas de areniscas de la Formación Cerro Rajón. Las secuencias estratigráficas han sido correlacionadas con eventos contemporáneos de magmatismo alcalino que se observan en el margen oeste de Laurentia y que están relacionados con un proceso de rifting continental. Se propone que este volcanismo puede haber sido producido por un brazo abortado o bien la parte distal de una rama de ese proceso de rifting continental desarrollado en el margen meridional de Laurentia. Sin embargo, también han sido consideradas otras posibles relaciones del magmatismo de Caborca con eventos de rift contemporáneos.

Petrogenetics and metamorphism from the Cambrian magmatism from the Cerro Rajón Formation, Sonora, Mexico and its relation with the rifting process in the southern margin of Laurentia

Neoproterozoic and Cambrian rocks forming continental platform deposits outcrop in the Caborca region, northwest Sonora. Neoproterozoic and Cambrian boundary locates between the dolostone layers from La Ciénega Fm. (Ediacara) and the volcanism from the Cerro Rajón Formation (Terreneuvian), previously identified as Puerto Blanco Fm. Unit 1. The Cerro Rajón Formation is defined in the present work as a volcano-sedimentary succession consisting of tuffaceous conglomerates, agglomerates, lapillstones, tuffs and mafic-ultramafic flows with minor quartzite, sandstone, mudstones and conglomerates. Studied outcrops are scarce and often observed partially buried or as subcrop. Studied localities show an important variation in the volcanic stratigraphy due to the important volcanic activity which occurred through strombolian eruptions and produced few meters thick volcanic flows. Petrography studies classified the metabasalts as granofels with porphyroblastic microfabrics. The metamorphism was produced with an important hydrothermal event which provoked a propylitic alteration in most of the volcanic flows and a carbonatization more abundant in the tuffaceous conglomerates volcanic clasts. Secondary mineralogy observed in the rocks is formed by chlorite, actinolite, calcite, sphene, epidote, titanomagnetite and albite. Nevertheless, it is possible to observe primary mineralogy as fresh diopside and ilmenite crystals. Geothermometry results show metamorphic temperatures from 400 to 500 °C in the volcanic clasts, and up to 548 °C in the volcanic flows. Metamorphic paragenesis is consistent with upper greenschist facies towards the epidote-actinolite facies. Geochemistry results, obtained from 36 volcanic clasts and volcanic flows samples, show a low silica magmatism ($\text{SiO}_2 = 30.50 - 53.11\%_N$) with high Ti concentrations ($\text{TiO}_2 = 2.98 - 7.00\%_N$). Geochemistry also allowed the recognition of an open system where metasomatism was produced, which add calcium concentrations to the system and depleted the samples in silica and other major oxides. Although, some major oxides and especially immobile trace elements were preserved in most of the samples. Volcanic flows were classified as alkaline basalts, although, many samples came from ultramafic protoliths, from which basanites and picobasalts were identified. Magmatism is alkaline, anorogenic, with low partial melting ratios and related to a continental rift developed in a passive margin. Magmatic source show primary characteristics with high Mg values (~ 70). Study results show that the last metamorphic print was produced by Laramide intrusives observed in the region. A granodiorite near the Cambrian volcanism exposures was dated by U-Pb in zircons in 71.1 ± 0.4 Ma. Geobarometry studies in this granodiorite indicate emplacement depths of ~ 8 km. $^{40}\text{Ar}/^{39}\text{Ar}$ geochronology results in the volcanic flows show a metamorphic age of 55.89 ± 0.6 Ma to 60.26 ± 0.33 Ma for the west portion of the study area, while the east portion show a loss in argon which produced inaccurate metamorphism ages. The deposition age for the Cerro Rajón Formation was constrained from 530 – 541 Ma., obtained through the occurrence of the Ediacaran index fossil *Cloudina*, observed in La Ciénega Fm., and the Cambrian ichnofossil *Treptichnus pedum*, observed in the Cerro Rajón Formation. Stratigraphic successions were correlated to contemporaneous alkaline magmatic events observed in the western margin of Laurentia, which are related to a continental rifting process. We proposed that the Cerro Rajón Formation volcanism may be related to an aborted arm of this system or an aulacogen developed in the southern region of the western Laurentia margin. Although, other possible relations between the Caborca Cambrian volcanism and contemporaneous rift related events in the east Laurentia margin were also considered.

Índice General

Resumen

Abstract

1. Introducción.....	1
1.1 Localización del área de estudio.....	2
1.2 Contexto Geológico.....	3
1.3 Objetivos.....	4
1.4 Metodología.....	5
2. Early Cambrian alkaline volcanism on the southern margin of Laurentia: evidence in the volcanoclastic units from the Puerto Blanco Formation in the Caborca block, NW Mexico.	7
3. The Cerro Rajón Formation—a new lithostratigraphic unit proposed for a Cambrian (Terreneuvian) volcano-sedimentary succession from the Caborca region, northwest Mexico.	27
4. Geochronology and geothermometry of the Laramide metamorphism in the Cambrian metabasalts from the Cerro Rajón Formation, Caborca region, northwest Mexico.	42
5. Características petrogenéticas del magmatismo máfico-ultramáfico de la Fm. Cerro Rajón.....	63
6. Discusión y conclusiones.....	74
7. Referencias.....	81
8. Anexos.....	86

1

INTRODUCCIÓN

INTRODUCCIÓN

Las secuencias del Neoproterozoico y Cámbrico están distribuidas en el estado de Sonora en afloramiento aislados parcialmente cubiertos por vegetación o aluvión y comúnmente presentan metamorfismo (Stewart *et al.*, 2002). Algunas de estas secuencias constituyen depósitos epicontinentales del supercontinente de Rodinia, como el Grupo Las Víboras en la localidad de Cerro de Oro (González-León & Jacques-Ayala, 1988; Stewart *et al.*, 2002). Mientras que las secuencias del Neoproterozoico superior y Cámbrico, entre las cuales se encuentran las localidades de Sahuaripa y Caborca, pertenecen a depósitos de plataforma continental.

La región de Caborca, en el noroeste de Sonora, alberga la sucesión del Neoproterozoico y Cámbrico mejor expuesta en México (Stewart *et al.*, 1984), dicha sucesión está constituida por rocas predominantemente sedimentarias que se atribuyen a la formación de una secuencia de plataforma continental en el margen meridional de Laurentia (Stewart *et al.*, 2002). Las rocas que representan el Cámbrico temprano en la región, están conformadas principalmente por sedimentos relacionados a ambientes marinos someros (Stewart, 1982; Stewart *et al.*, 1984), representados en las capas de la Formación Puerto Blanco. La parte inferior de esta formación (Unidad 1) ha sido redefinida en el presente trabajo y elevada de rango a una nueva unidad litoestratigráfica denominada Formación Cerro Rajón. Esta nueva formación se destaca por presentar la exclusividad de afloramientos de rocas piroclásticas y lávicas relacionadas a un rift continental y su edad ha sido acotada en un rango aproximado entre 530 – 541 Ma, lo cual sitúa a los eventos volcánicos dentro del Fortuniano. El esclarecimiento preciso de la edad de este volcanismo, algo que no se logró en este trabajo, no solo ayudará a precisar el límite del Cámbrico-Precámbrico para la región, sino que permitirá ubicar el evento volcánico dentro de un contexto geodinámico regional que lo relaciona a los eventos ocurridos a inicios del Cámbrico. Este estudio permite establecer una correlación estratigráfica, no solo entre las secuencias de plataforma del Neoproterozoico y Cámbrico de la región, sino también entre eventos volcánicos contemporáneos y petrogenéticamente ligados a los ocurridos a inicios del Cámbrico en Caborca.

A pesar de que el magmatismo Cámbrico aquí reportado de la Formación Cerro Rajón es un evento volcánico importante por su implicación regional, el único trabajo previo donde fue reportado, con un

enfoque petrológico, es el de [Centeno-García et al. \(2002\)](#). Tomando en cuenta estas consideraciones, se estudió este magmatismo desde una visión petrogenética que considerara un estudio detallado de los eventos volcánicos y su distribución espacial, su posición estratigráfica y su génesis. Los resultados de esta investigación están integrados en tres publicaciones científicas en los Capítulos 2, 3 y 4. La primera reporta un estudio geoquímico-petrológico de este magmatismo, enfocado en los clastos volcánicos de los conglomerados tufáceos. Estas unidades son las más representativas de la Formación Cerro Rajón. El estudio permitió reconocer una estrecha relación geoquímica y mineralógica entre los clastos volcánicos y las unidades lávicas de la Formación Cerro Rajón, a la vez que se comprobó que la geoquímica se conserva lo suficiente para permitir la utilización de elementos traza discriminadores de ambientes tectónicos. La segunda publicación es un estudio estratigráfico a detalle de la ocurrencia de las rocas volcánicas y sills relacionados al magmatismo Cámbrico en los alrededores del Rancho Bámori en Caborca. Este estudio era necesario para poder comprender la distribución estratigráfica de los productos volcánicos, sus espesores y el ambiente en el que se depositaron, lo cual permitió explicar la variación litológica y en espesores entre las localidades de estudio. En esta publicación también se define a la Formación Cerro Rajón como una unidad litoestratigráfica formalmente definida con los requisitos de la [Comisión Norteamericana de Nomenclatura Estratigráfica \(2005\)](#). La tercera publicación consiste en un estudio del metamorfismo en las unidades volcánicas y su relación con los intrusivos laramídicos presentes en la región de estudio. El metamorfismo de estas rocas es un elemento clave en la investigación, ya que su estudio permitió identificar los productos volcánicos más viables para análisis geoquímicos y fechamientos radiométricos. En esta publicación se presentan edades de metamorfismo obtenidas por geocronología $^{40}\text{Ar}/^{39}\text{Ar}$, U-Pb en zircones, estudios de geothermobarometría y de química mineral. Por último, debido a la importancia petrogenética de este volcanismo, se agregó un cuarto capítulo con resultados adicionales y una discusión petrogenética más profunda que integra todos los productos magmáticos observados en el área de estudio. Eventualmente este trabajo derivará en una publicación científica y se incluye únicamente como un capítulo adicional de resultados y discusiones que complementa a las tres publicaciones para cumplir con los objetivos del proyecto de doctorado.

1.1. Localización del área de estudio

La presente investigación se llevó a cabo en los alrededores del Rancho Bámori en el municipio de Pitiquito, Sonora, México. Esta zona es internacionalmente conocida como la región de Caborca, debido a la cercanía con dicha ciudad. El área de estudio está ubicada 40 km al sur de la ciudad de Caborca. Desde la capital del estado se puede acceder por la carretera internacional No 15. El área de estudio comprende una superficie aproximada de 800 km², dentro de los cuales se trabajó específicamente en el detalle de

las secuencias cercanas al límite estratigráfico del Cámbrico-Precámbrico. La topografía del área de estudio se puede consultar en las cartas H12-A77 El Prieto, H12-A76 Hilario Gavilondo y H12-A87 La Ciénega, todas con escala 1:50 000.

1.2. Contexto geológico

Las rocas del Neoproterozoico-Cámbrico, en la región de Caborca, afloran como una secuencia homoclinal a lo largo de pequeñas sierras con orientación NW-SE. La secuencia del Neoproterozoico descansa sobre un basamento ígneo-metamórfico de edad Paleoproterozoica conocido como el Complejo Metamórfico Bámori (Longoria *et al.*, 1978). El Neoproterozoico está representado por las formaciones El Arpa, Caborca, Clemente, Pitiquito, Gamuza, Papalote, Tecolote y La Ciénega. Esta última contiene fósiles de la fauna Ediacara (Sour-Tovar *et al.*, 2007) y esta sobreyacida por la secuencia del Cámbrico. La base de la secuencia sedimentaria de edad del Cámbrico está representada por la Formación Cerro Rajón, definida por Barrón-Díaz *et al.* (2019) como una sucesión vulcano-sedimentaria que consiste en conglomerados tufáceos, metabasaltos, tobas máficas, lapillitas máficas, aglomerados máficos y cuarcitas; con limolitas, calizas, dolomías y conglomerados (ver Fig. 4 en Capítulo 3). El magmatismo representado por las rocas volcánicas, presenta características máfico-ultramáficas con firmas primarias relacionadas a un evento de rift del tipo intraplaca continental. La Formación Cerro Rajón aflora en pequeños lomeríos donde los productos volcánicos están parcialmente cubiertos por aluvi3n. La unidad más representativa de esta formaci3n son los conglomerados tufáceos y los aglomerados, ambos son producto de una intensa actividad estromboliana que formó conos cineríticos y pequeños edificios volcánicos. Los derrames de metabasaltos tienen espesores de entre 6 a 25 metros y excepcionalmente aparecen derrames de 60 cm, lo cual es característico de un volcanismo alcalino con bajas tasas de fusi3n. Se interpreta que un magmatismo Laramídico de edad Cretácico tardío - Paleoceno está presente en la zona de estudio. Los afloramientos más cercanos corresponden a granodioritas que afloran en el Cerro El Dátil ubicado aproximadamente a 15 km al suroeste de la localidad del Cerro Calaveras (ver Fig. 1 en el Capítulo 2). Este magmatismo provocó un metamorfismo de bajo grado en facies de esquistos verdes a epidota anfibolita en las secuencias de la Formación Cerro Rajón. El metamorfismo va acompañado de un hidrotermalismo que afecta la mineralogía primaria de las rocas volcánicas y abrió parcialmente el sistema geocronológico (ver Secci3n 4.1.1 en el Capítulo 2).

El límite Cámbrico-Precámbrico para la regi3n de Caborca, se localiza entre la Formaci3n La Ciénega (Ediacara) y la Formaci3n Cerro Raj3n (Fortuniano). La edad de estas formaciones ha sido obtenida mediante la observaci3n de fósiles índice como Cloudina y el icnof3sil Treptichnus pedum (Sour-Tovar *et al.* 2007, ver tambi3n Secci3n 3.3 en el Capítulo 2). La temporalidad del volcanismo en al Formaci3n Cerro

Rajón ha sido recientemente discutida y acotada a través de estudios de bioestratigrafía y chemoestratigrafía, los cuales indican una depositación entre 530 y 541 Ma (ver Sección 3.3 en el Capítulo 2). La datación por métodos radiométricos del volcanismo en la Formación Cerro Rajón no se ha podido obtener con éxito. Esto es debido al metamorfismo que provocó un remplazamiento de la mineralogía primaria, de la cual solo se conservaron algunos clinopiroxenos. Los resultados geoquímicos y petrogenéticos obtenidos de las rocas volcánicas y sills (ver Capítulo 2 y 4), indican que la actividad magmática se produjo en una zona cercana a un rift del tipo intraplaca continental o bien a un rift abortado.

1.3. Objetivos

Objetivo general

Realizar un estudio petrogenético del magmatismo máfico-ultramáfico del Bloque Caborca a través de estudios geocronológicos, trabajos de petrología fina y química mineral, que permitan concluir en una interpretación geodinámica y un contexto tectónico para los eventos ocurridos a inicios del Cámbrico y que contribuyan a calibrar el límite Cámbrico-Precámbrico en la región.

Objetivos específicos

- Realizar un estudio bibliográfico y de investigación detallada sobre los trabajos previos de la región y en específico sobre las formaciones del límite Cámbrico-Precámbrico en Sonora.
- Realizar dos unidades teóricas y de investigación que apoyen el desarrollo de la investigación y permitan una mayor comprensión de los eventos geológicos.
- Realizar misiones de reconocimiento en las localidades de estudio y un mayor detalle en las localidades conocidas, para rastrear afloramientos del volcanismo Cámbrico.
- Medir columnas estratigráficas compuestas y lineales en las principales localidades para comprender la estratigrafía y variaciones litológicas en las localidades.
- Realizar un muestreo sistemático de las unidades volcánicas y sedimentarias cercanas al límite Cámbrico-Precámbrico.
- Realizar secciones delgadas de las muestras volcánicas y sills, para identificar las muestras más adecuadas para los estudios petrográficos, de geoquímica de roca total, química mineral con microsonda electrónica y geocronología.
- Realizar estudios geoquímicos de las muestras más representativas y mejor conservadas.
- Llevar a cabo una separación mineral para estudios de geocronología $^{40}\text{Ar}/^{39}\text{Ar}$ y U-Pb.

- Analizar los resultados obtenidos en conjunto para realizar diagramas geoquímicos, petrogenéticos y de caracterización que apoyen a la comprensión de los eventos geológicos y petrogénesis del magmatismo.
- Redactar tres artículos científicos con las principales temáticas estudiadas, las cuales son la petrogénesis ígnea, estratigrafía y metamorfismo de los eventos ocurridos a inicios del Cámbrico en la región.
- Concluir con la redacción de un documento de tesis que integre las tres publicaciones y los resultados obtenidos del proyecto de doctorado.

1.4. Metodología

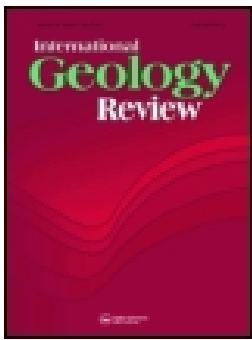
La presente estudio tuvo una importante componente de investigación para rastrear los trabajos previos en la región de estudio, los cuales resultaron ser escasos. Se realizaron al menos 15 misiones de campo para lograr un reconocimiento de las localidades que no se habían podido acceder previamente y para ubicar los afloramientos de rocas volcánicas en la base del Cámbrico para al menos seis localidades de estudio. Las misiones de campo incluyeron un muestreo representativo de las rocas dentro de la Formación Cerro Rajón. Este muestreo se enfocó más en las unidades volcánicas como los aglomerados, conglomerados tufáceos y derrames de metabasaltos. Se obtuvieron muestras para análisis geoquímicos, geocronología y petrografía. El estudio petrográfico se llevó a cabo en los laboratorios de la Universidad de Sonora y la Estación Regional del Noroeste del Instituto de Geología (ERNO-UNAM). Un total de diez muestras de los derrames menos alterados fueron preparadas para estudios de microsonda electrónica, realizando secciones delgadas pulidas con alúmina y posteriormente preparadas con una capa de carbón en el laboratorio Michael J Drake de la Universidad de Arizona. También se realizaron estudios de microsonda electrónica en los derrames con alteración para obtener resultados necesarios para los cálculos de geotermobarometría y caracterización fina de los minerales metamórficos. Los parámetros detallados de este estudio se pueden consultar en la sección de materiales y métodos en el Capítulo 4.

Un total de 40 muestras entre las más representativas y mejor conservadas de los metabasaltos fueron preparadas para estudios geoquímicos. Esta preparación se llevó a cabo en los laboratorios de preparación de muestra de la Estación Regional del Noroeste del Instituto de Geología (ERNO-UNAM) y en el laboratorio de preparación de muestras del Departamento de Geología de la Universidad de Sonora. Las muestras fueron trituradas y posteriormente pulverizadas en un mortero de ágata con canicas de ágata. Se analizaron en los laboratorios de ALS CHEMEX y en el Laboratorio de Fluorescencia de Rayos X del Instituto de Geología de la UNAM. Para los estudios de geocronología $^{40}\text{Ar}/^{39}\text{Ar}$, se tomaron muestras trituradas de los derrames mejor conservados y se separaron según el interés. Las muestras fueron

procesadas en el Oregon State University Argon Geochronology Laboratory en Oregon. El procedimiento de separación consistió en un tamizado de las muestras para obtener una fracción de entre 106 a 355 μm . Posteriormente las muestras tuvieron varios ciclos de baños ultrasónicos, separación por minerales magnéticos con un separador tipo Frantz y tamizado. Cuando se obtuvo una porción considerable de material paramagnético y limpio, éste fue sometido a un lixiviado por ácidos para eliminar los carbonatos y arcillas. Por último las muestras fueron separadas a mano con un microscopio binocular. Se obtuvieron al menos 30 mg de matriz volcánica y 10 mg de flogopita. También se separaron clinopiroxenos pero, debido a su alteración, los resultados obtenidos no fueron concluyentes. Las fracciones separadas se guardaron en contenedores de aluminio y se enviaron a irradiar al reactor nuclear en la misma universidad. Posteriormente los isótopos fueron obtenidos por un espectrómetro de masas ARGUS-VI. Los parámetros detallados de este estudio pueden ser consultados en el apartado de materiales y métodos del Capítulo 4.

2

**EARLY CAMBRIAN ALKALINE VOLCANISM ON THE SOUTHERN MARGIN
OF LAURENTIA: EVIDENCE IN THE VOLCANICLASTIC UNITS FROM THE
PUERTO BLANCO FORMATION IN THE CABORCA BLOCK, NW MEXICO.**





Early Cambrian alkaline volcanism on the southern margin of Laurentia: evidence in the volcanoclastic units from the Puerto Blanco Formation in the Caborca block, NW Mexico

Arturo Joaquín Barrón-Díaz, Francisco Abraham Paz-Moreno, Rufino Lozano-Santa Cruz, Saúl Herrera-Urbina, Elena Centeno-García & Margarita López-Martínez

To cite this article: Arturo Joaquín Barrón-Díaz, Francisco Abraham Paz-Moreno, Rufino Lozano-Santa Cruz, Saúl Herrera-Urbina, Elena Centeno-García & Margarita López-Martínez (2018): Early Cambrian alkaline volcanism on the southern margin of Laurentia: evidence in the volcanoclastic units from the Puerto Blanco Formation in the Caborca block, NW Mexico, International Geology Review, DOI: [10.1080/00206814.2018.1501619](https://doi.org/10.1080/00206814.2018.1501619)

To link to this article: <https://doi.org/10.1080/00206814.2018.1501619>

 View supplementary material 

 Published online: 09 Aug 2018.

 Submit your article to this journal 

 View Crossmark data 

Early Cambrian alkaline volcanism on the southern margin of Laurentia: evidence in the volcanoclastic units from the Puerto Blanco Formation in the Caborca block, NW Mexico

Arturo Joaquín Barrón-Díaz^a, Francisco Abraham Paz-Moreno^b, Rufino Lozano-Santa Cruz^c, Saúl Herrera-Urbina^b, Elena Centeno-García^c and Margarita López-Martínez^d

^aInstituto de Geología, Universidad Nacional Autónoma de México, Hermosillo, México; ^bDepartamento de Geología, Universidad de Sonora, Hermosillo, México; ^cLaboratorio Nacional de Geoquímica y Mineralogía, Instituto de Geología, Universidad Nacional Autónoma de México, Ciudad de México, México; ^dCentro de Investigación Científica y Educación Superior de Ensenada, Ensenada, México

ABSTRACT

Volcanoclastic units are exposed at the base of the Puerto Blanco Formation in the Caborca region, northwestern Mexico. The lower unit reveals the presence of Early Cambrian mafic volcanism in this region. It consists of a volcano-sedimentary sequence represented by tuffaceous conglomerates, agglomerates, lapillistones, tuffs, and altered mafic volcanic flows. Petrographic analysis classified the volcanic clasts as albite-sphene-calcite-actinolite granofels, with a moderate to intense hydrothermal alteration, precisely characterized by EPMA analysis. Albite-actinolite geothermometry indicates temperatures from 400 to 500°C, suggesting metamorphic conditions in the upper temperature greenschist facies. Geochemistry analysis shows a high TiO₂ basic-ultrabasic volcanism that originated the volcanic clasts. Rock protoliths were studied using immobile trace elements, which classified them as OIB-type alkaline basalts with the characteristic spider hump-shaped pattern, situated in an anorogenic intracontinental tectonic setting with enriched mantle signatures. ⁴⁰Ar/³⁹Ar geochronology shows metamorphic ages of 52.58 ± 2.0 and 91.67 ± 0.55 Ma, consistent with the emplacement of Laramidic granitoids identified in the region. Possible correlations of this alkaline volcanism include the Southern Oklahoma Aulacogen and the late stages of the rifting of north western Laurentia represented in western United States.

ARTICLE HISTORY

Received 5 December 2017
Accepted 14 July 2018

KEYWORDS

Lower Cambrian; agglomerates; tuffaceous conglomerates; basic-ultrabasic volcanism; Laramide; granofels; NW Sonora; Mexico; Caborca


1. Introduction

Precambrian and Palaeozoic sequences contained in the Caborca Block, which is located in northwestern Sonora, Mexico, are considered as the most complete in the country (Stewart *et al.* 1984). The Caborca Block was originally conceived as a tectonostratigraphic terrane (Campa and Coney 1983), and it has been treated as an extension of the miogeoclinal prism of North America (Stewart 1982; Stewart *et al.* 1984). One possible explanation for the position of the Caborca Block is a 700–800 km displacement by the hypothetical Mojave–Sonora megashear (Anderson and Silver 1979), which has been used to explain the offset between the miogeoclinal prism sequences in north-west Sonora and southwest United States (Stewart 2005). Figure 1 shows a proposed position for the Mojave–Sonora megashear and its relation with the major North American geologic provinces (see Discussion for details).

In the Caborca region, the Precambrian and Palaeozoic stratigraphic sequences rest over an igneous–metamorphic complex known as the Bámori Metamorphic Complex, established by Longoria *et al.* (1978) as a highly metamorphosed sequence consisting of metaquartzite and slightly carbonaceous pelitic schist of early Precambrian age. Eells (1972) describes the sequence at Sierra La Berruga and divides it into 12 Precambrian units. Unit 12 was defined as a sequence of 90 m of volcanoclastic boulder conglomerate, litharenite, and porphyritic olivine basalt. Currently, Unit 12 is considered the base (Unit 1) of the Puerto Blanco Fm. (Stewart *et al.* 1984), and it is also treated as the base of the Cambrian in the region.

The aim of the present research consists in achieving a petrological characterization of the volcanoclastic sequence of the Puerto Blanco Fm. Unit 1, and their interaction with the sedimentary processes at the beginning of the Cambrian age in the region. The

CONTACT Francisco Abraham Paz-Moreno  francisco.paz@unison.mx  Blvd. Luis Encinas y Rosales S/N, Colonia Centro, CP. 83000, Hermosillo, Sonora, México

 Supplementary data for this article can be accessed [here](#).

© 2018 Informa UK Limited, trading as Taylor & Francis Group

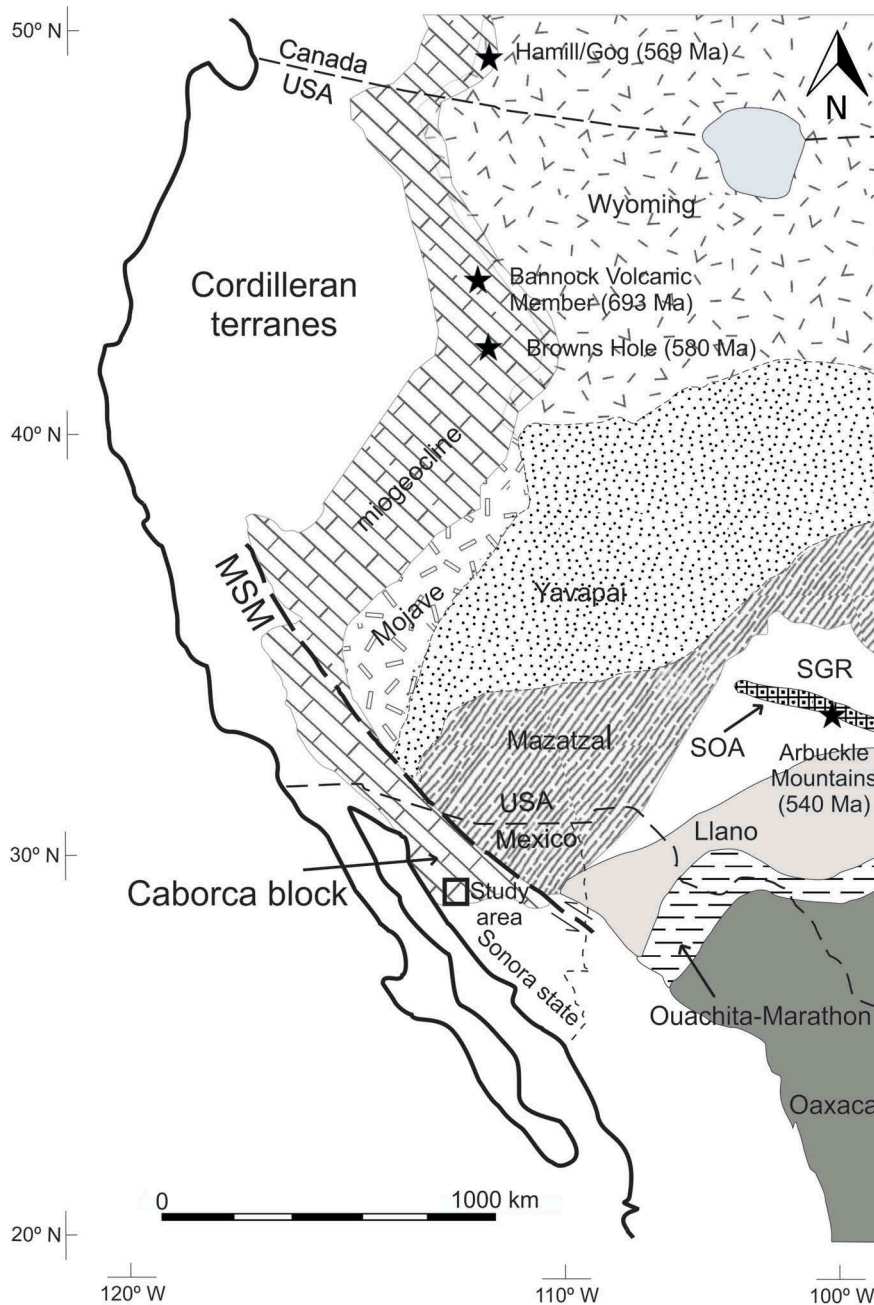


Figure 1. Map of the major North American geologic sequences over the late Neoproterozoic rifting in western Laurentia after Chapman *et al.* (2015). Southern Oklahoma Aulacogen (SOA) and Southern Granite Rhyolite (SGR) after Bickford *et al.* (2015). The hypothetical Mojave–Sonora Megashear (MSM) location, the study area, and the position of rift-related volcanic ages (filled stars); see references in the text.

presence of an alkaline volcanism in the Caborca block has global implications related to the breakup of the Rodinia supercontinent. This rift-related volcanism will allow regional correlations with other contemporaneous rift sequences in northwest United States and Canada, and it opens the possibility of a correlation with the eastern Laurentia margin rifting sequences.

The Puerto Blanco Fm. was originally defined by Cooper and Arellano (1952) 10 km west of the city of Caborca, Sonora. At the type section, only the upper

three units were observed. Nevertheless, Unit 1 outcrops in several localities surrounding the Bámori Ranch, where considerable variations in lithology have been observed (Stewart *et al.* 1984; Barrón-Díaz 2013). In his work on the Sierra La Berruga, Eells (1972) places the Puerto Blanco Fm. at the base of the Cambrian, resting over a volcanoclastic unit that defines as Unit 12, at the top of the Precambrian sequence. Later, Longoria (1981) included basalt flows, volcanic agglomerate, and volcanic breccia in the Puerto Blanco Fm.

These units are in fact similar to Unit 12 from Eells (1972), and for this reason, Stewart *et al.* (1984) added Unit 12 in the base of the Puerto Blanco Fm. as Unit 1. Stewart *et al.* (1984) described the Puerto Blanco Fm., exposed in the Cerro Rajón, as a 717 m thick sequence divided in the following units: Unit 1 is 285.5 m thick and is characterized by volcanoclastic rocks and greenstones. Unit 2 is 173 m thick and contains mainly siltstone and quartzite. Unit 3 is 117 m thick and includes archaeocyath-bearing limestones, siltstones, and quartzites. Unit 4 is 141 m thick and includes limestones, siltstones, quartzites, and dolostones. The Puerto Blanco Fm. is overlain by the Provedora Quartzite and underlain by dolostone packages of the La Ciénega Fm. This last formation also contains a few greenstones exposed as sills. In other studies of the Puerto Blanco Fm., the conglomeratic units are not mentioned (Maytorena-Silva and Durazo-Tapia 1982; Sour-Tovar, 2006).

Petrology studies of these rocks are scarce. Centeno-García *et al.* (2002) made geochemical and isotopic analyses on the volcanic rocks from La Ciénega Fm. in Cerro Calaveras. The results show basaltic rocks with low silica (29–44%) and high K related to an intracontinental rift. The work of Barrón-Díaz (2013) showed an extensive study in the southern part of the Caborca region, concluding that the volcanism at the base of the Puerto Blanco Fm. is characterized by alkaline magmas, which were emplaced as sills in the La Ciénega Fm. and as flows in the Puerto Blanco Fm. Unit 1. They were described as anorogenic picrobasalts, metabasalts, and metabasalts, related to an intracontinental rift.

This study was made 40 km south of the city of Caborca, in a region that is accessible by highway 15. Several reconnaissance field missions were made to systematically sample the volcanic and sedimentary units in the localities surrounding the Bámori Ranch (Figure 2).

2. Geological setting

2.1. The Puerto Blanco Formation Unit 1 and its occurrence in the Caborca region

The Puerto Blanco Fm. outcrops in several localities of Sonora (Stewart *et al.* 2002); nevertheless, the most complete sequences are restricted to the Caborca region, where it was possible to find the formation's four units. The three upper units are represented by sedimentary and meta-sedimentary rocks, including large sequences of siltstones, limestones, and quartzites. Some of them contain lower Cambrian fossils (Eells 1972; Stewart *et al.* 1984). These top three units

can be observed with a similar stratigraphy in the localities surrounding the Bámori Ranch (Stewart *et al.* 1984).

The Puerto Blanco Formation Unit 1 varies considerably in thickness and lithology from one locality to another (Eells 1972; Stewart *et al.* 1984; Barrón-Díaz 2013). For this research, we sampled four localities (Figure 2), where the lithology is represented mainly by tuffaceous conglomerates, quartzites, sandstones, mafic-ultramafic flows, tuffs, lapillistones, and mafic agglomerates. Siltstones, limestones, and mudstones were also found in minor proportions (Figure 3). Cerro Rajón locality, in the northeast side of the study area, is recognized as the most complete and representative sequence of the Puerto Blanco Fm. Unit 1. In this locality, the tuffaceous conglomerates are 20 m thick and are located at the base of the sequence; the agglomerates are 80 m thick and are located at the base and the top of the sequence. Cerro San Agustín, in the east of the study area, is the smallest sequence, where only 10 m of partially buried tuffaceous conglomerates can be found. In Cerro Calaveras, located in the west of the study area, the tuffaceous conglomerates are approximately 80 m thick and are located at the top of the sequence. Finally, in Cerros de la Ciénega located in the south of the study area, the sequence is mainly pyroclastic and it varies from a tuffaceous conglomerate in the east of this locality, to an agglomerate in the west.

The tuffaceous conglomerates in the Puerto Blanco Fm. Unit 1 are the most characteristic volcanoclastic lithology of this unit (Figure 4a). They consist of rounded, mafic, volcanoclastic conglomerates cemented by a mixture of sedimentary material, carbonates, and mafic lapilli and ashes. In the Cerro Rajón locality, they can be 20 m thick, and their lower boundary contains a dolostone breccia with clasts up to 1.5 m in size. In the Cerros de la Ciénega locality, its distribution changes from a tuffaceous conglomerate in the east to an agglomerate to the west. The tuffaceous conglomerates in this locality are more than 50 m thick. In the Cerro San Agustín locality, tuffaceous conglomerates were only observed in a small layer a couple of metres thick. Finally, in Cerro Calaveras, the volcanic clast showed deformation probably due to burial pressures. The tuffaceous conglomerates in this locality are 60 m thick.

The agglomerates are a key unit to understand the pyroclastic-volcanic events during the Cambrian for this region. These agglomerate sequences can be up to 50 m thick in Cerro Rajón and Cerros de la Ciénega and are represented mainly by decimetric cracked volcanic bombs up to half a metre in diameter, which are cemented by mafic pyroclastic material (Figure 4b). Occasionally, it is possible to observe interbedded

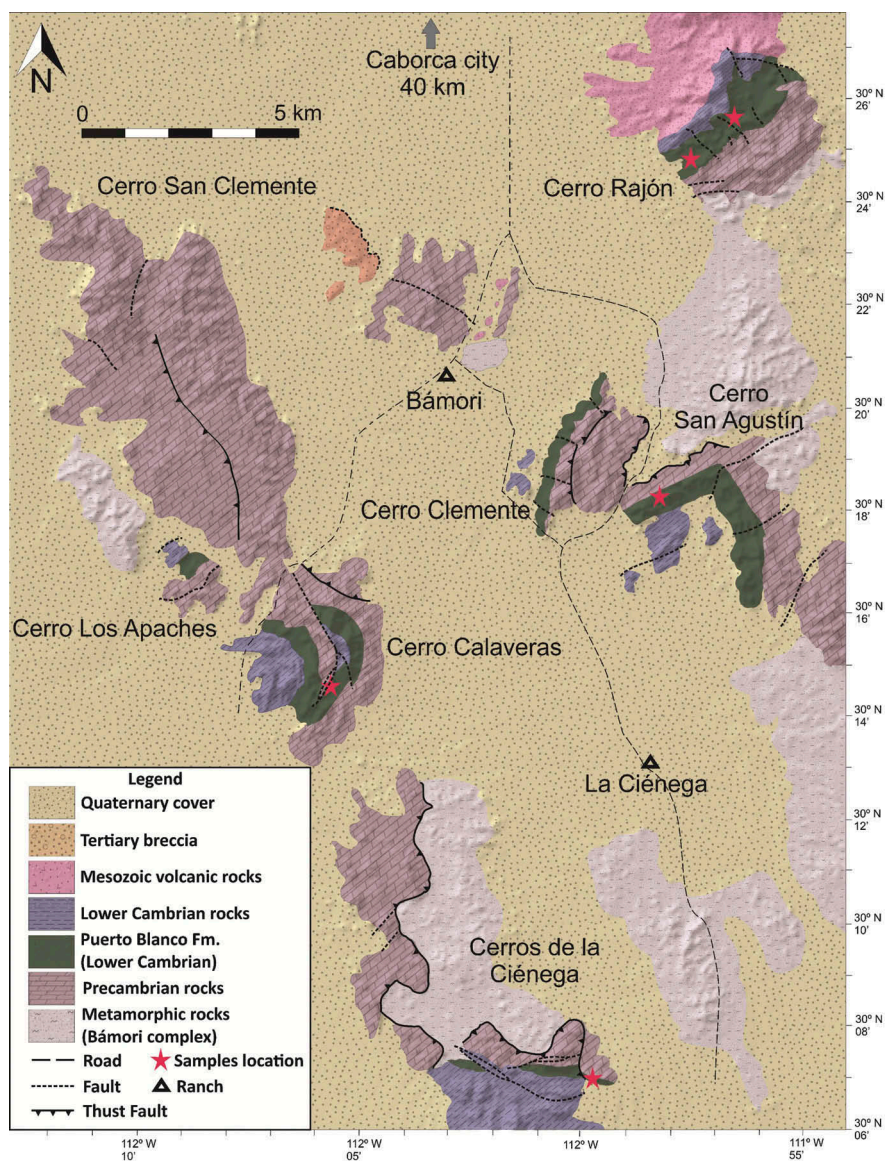


Figure 2. Simplified geologic map of the Caborca Region and localities surrounding the Bámori Ranch. The red stars indicate the localities where the samples were taken. Redrawn and modified from Stewart *et al.* (1984), Maytorena-Silva and Durazo-Tapia (1982), Eells (1972), and Anderson and Silver (1981).

lapillistones in levels of 30–60 cm thick within the agglomerate sequences. The agglomerates represent an important pyroclastic activity that can be observed towards the top of Unit 1 in Cerro Rajón and generally among the whole Unit 1 sequence in Cerros de la Ciénega. The occurrence of these agglomerates can be explained as having been formed by destruction of small strombolian cinder cones; therefore, it can only be observed in a few localities.

In this study, we also present the petrographic and geochemical analysis from a picrobasalt from the Cerro San Agustín locality (sample AB10–06A). This sample represents the volcanic flows mostly found at the top of the Puerto Blanco Fm. Unit 1. It is 6 m in thickness and its volcanic features are clearly represented in the

upper part of the flow with columnar prisms, and its scoriaceous base rich in calcite amygdaloids and vesicles. The picrobasalt flow is located 100 m from the volcanic clast samples AB14–05A and AB14–05B.

2.2. Nomenclature

An effort was made to properly name these so-called volcanoclastic rocks. By using petrologic criteria, the samples were classified as pyroclastic rocks. The nomenclature of tuffaceous conglomerates was obtained by applying the recommendations of the International Union of Geological Sciences Subcommittee on the Systematics of Igneous Rocks (Le Maitre *et al.* 2002), which states that for a mixture of pyroclastic and epiclastic rocks, the

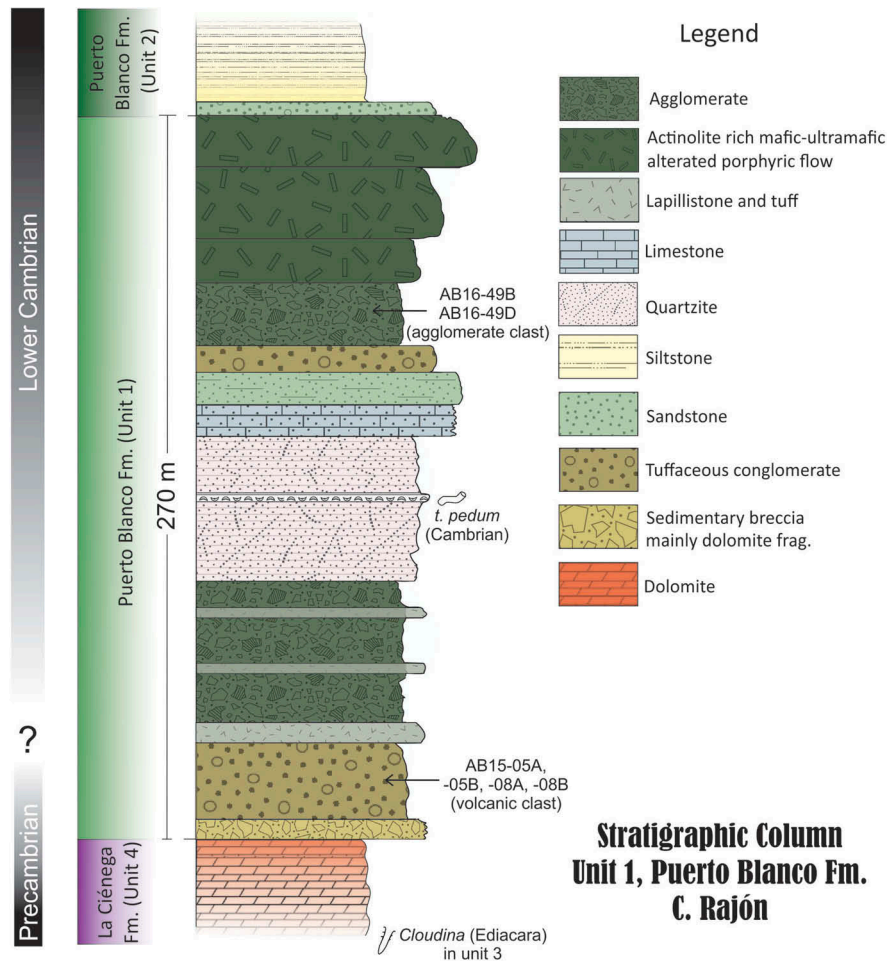


Figure 3. Stratigraphic column from the Cerro Rajón locality showing the position where the samples were taken. This sequence is considered as the most representative from the Puerto Blanco Fm. Unit 1. Stratigraphic position of *Cloudina* and *T. pedum* were taken from sour-tovar *et al.* (2006) and Loyd *et al.* (2012), respectively.

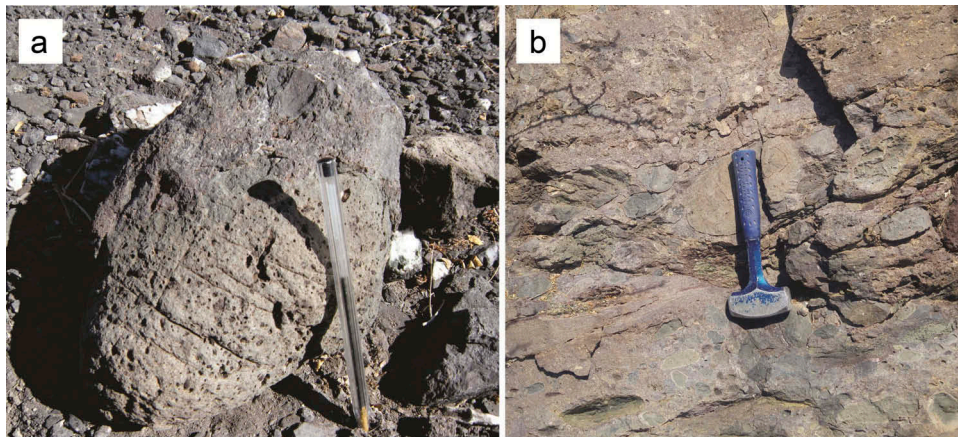


Figure 4. (a) Photograph of a slightly deformed volcanic clast from the tuffaceous conglomerate unit. The groundmass is mainly carbonates and epiclastic material. (b) Agglomerate from mainly mafic volcanic bombs cemented by volcanic ashes. The picture was taken at the upper sequence of the Cerro Rajón.

classification of Schmid (1981) should be used. Regarding these rocks, most of the conglomerates are close to 50% volcanic material; therefore, they were classified as

tuffaceous conglomerates. The units that have more than 90% of pyroclastic material were classified as agglomerates, as these rocks consist primarily of tephra

(cracked bombs > lapilli and ash fragments). Finally, it was possible to observe thin layers of conglomerate (<20% of pyroclastic material) that were not directly related to pyroclastic activity.

3. Materials and methods

A difficulty experienced during this research was the work invested in locating and sampling the volcanoclastic units. Puerto Blanco Fm. Unit 1 is generally associated with low terrain or heavily eroded and buried areas. These conditions made it especially difficult to locate the thin volcanic units and the less obvious volcanoclastic rocks.

Taking this into consideration, six field missions were made to systematically sample the rock units, including the less altered or metamorphosed rocks in the volcanoclastic units. Thirty samples were collected, varying from 15 to 30 cm in diameter. The thin sections, for petrographic studies, were made at the Geology Department of Universidad de Sonora and the Estación Regional del Noroeste of Universidad Nacional Autónoma de México (ERNO-UNAM). Results of the 19 samples chosen for geochemical analysis are hereby presented; only the most representative and least altered samples were analysed. Preparations for the geochemical analysis were made at the ERNO-UNAM laboratory using a Braun Chipmunk crusher with steel plates and a Rescht S100 mill with an agate container and 12 agate balls. Major elements analysis was done at the XRF Laboratory of the UNAM Institute of Geology in Mexico City, following the methodology described by Lozano-Santa Cruz and Bernal (2005). Standard and detection limits for XRF analysis are presented in Supplementary file 3 and 5. Trace elements analysis was performed at ALS labs in Vancouver, CA, using the ICP-MS method. For mineral chemistry, an electron microprobe (CAMECA SX100 and SX50) was used at the Michael J. Drake Microprobe Laboratory of the University of Arizona. $^{40}\text{Ar}/^{39}\text{Ar}$ geochronology studies were made at the Geochronology Laboratory at the CICESE, B.C., Mexico, using a VG5400 spectrometer. Sample measurements were made on volcanic groundmass and were irradiated by the research reactor at McMaster University in Canada.

4. Results

4.1. Petrography

Petrography studies made on the volcanic clasts from the tuffaceous conglomerates and agglomerates of the

Puerto Blanco Fm. Unit 1 show important alteration observed in all the samples and can replace almost the entire rock mineralogy, excluding the Fe-Ti oxides phenocrysts, which are only partially affected. Using petrographic criteria, the volcanic clasts can be classified as granofels. The descriptions are presented in Supplementary File 1.

The picrobasalt flow preserves most of its primary mineralogy and texture. It shows a porphyritic texture formed by fresh diopside crystals up to 7 mm long (Figure 5k). The groundmass consists of a second generation of diopside microcrystals, sphene, and titanomagnetite oxides (Figure 5l). Plagioclase is also present in the groundmass in a late stage of crystallization and in less than 5% in abundance. Sphene presents a cloudy habit, probably due to a slight hydrothermal alteration that relocated the Ti from the larger titanomagnetite phenocryst (previously ilmenite?). These petrographic characteristics evidence an ultramafic flow which is further supported by the geochemical analysis.

The tuffaceous conglomerates clasts textures are porphyritic to micro-porphyritic, with some of them showing abundant calcite amygdalae. Actinolite and chlorite completely replace the primary clinopyroxene phenocrysts. The original olivine crystals are always replaced by carbonates and Fe-Ti oxides, forming the borders and filling the fractures of the crystal. Fe-Ti oxides are abundant in the samples as partially altered phenocrysts or as microcrystals. In most of these rocks, hydrothermal albite is abundant in the groundmass. The presence of carbonate and feldspar veins is one example of evidence of this hydrothermal alteration. Sphene, present in a cloudy or earthy habit, is another characteristic, and it is an abundant mineral in the groundmass, probably produced by the Ti mobilization during hydrothermal alteration. Actinolite, in a decussate texture, is also abundant in the groundmass, and it is produced by the alteration of clinopyroxene microcrystals. Figure 5 shows several microphotographs of thin sections, where different alteration grades can be observed.

The volcanic clasts can mainly be classified as fine-grained albite-sphene-calcite-actinolite granofels. Sample AB11-20D shows an aphanitic texture, but a mafic volcanic protolith can be described, based on its melanocratic features and geochemical characteristics. Sample AB11-39 was taken from a block within the tuffaceous conglomerate. Apparently, this rock is a mixture of volcanic flow and unconsolidated sedimentary material. Sample AB1-06B can be classified as an ankaramite flow by its petrographic characteristics such as diopside as the main constituent of the rock and a virtual absence of plagioclase.

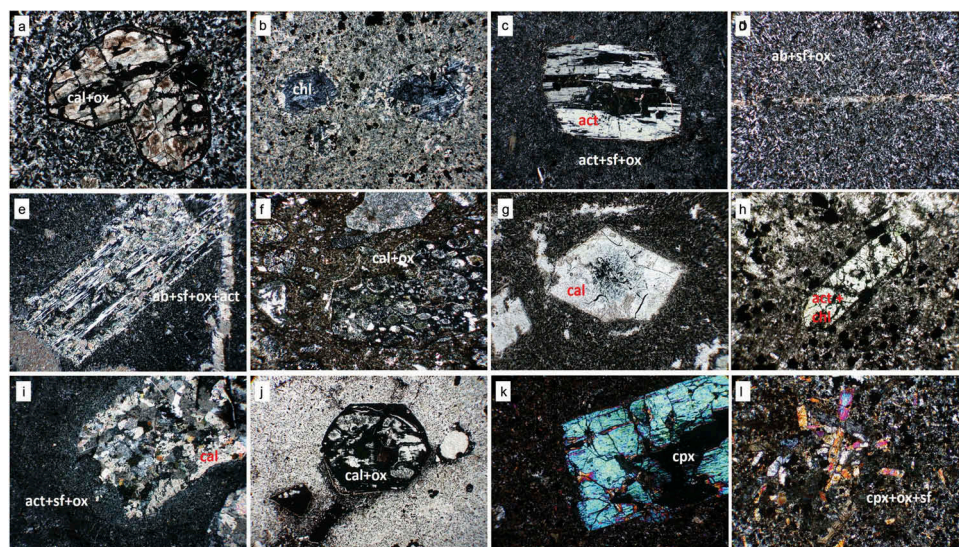


Figure 5. Microphotographs of the volcanic clasts from the tuffaceous conglomerate and picrobasalt flow. The porphyroclasts are mainly formed of carbonates and actinolite and it can be appreciated on most of the images shown. Microphotographs correspond to the following samples: (a) AB11–20C, (b) AB14–05A, (c) AB15–08B, (d) AB11–20L, (e) AB16–02C, (f) AB11–39, (g) AB16–02A, (h) AB15–05A, (i) AB15–05B, (j) AB11–40C, (k) AB10–06B, and (l) AB10–06B. Microphotograph F corresponds to a mixture of volcanic flow and sedimentary material. Small rounded quartz grains are also observed. All images are taken with the 4× objective and NX, the wide of each image represents 1.5 mm, except for the letter L. This last image corresponds to the groundmass of the previous sample and is taken with a 10× objective.

ab = albite, chl = chlorite, cpx = clinopyroxene (diopside), cal = calcite, act = actinolite, sf = sphene, ox = Fe-Ti oxides (mainly titanomagnetite).

Considering the groundmass of the samples, two groups can be observed: the granofels coming from a mafic volcanic protolith, showing albite replacing other plagioclase crystals present only in the groundmass; and the granofels coming from an ultramafic volcanic protolith, showing none to scarce interstitial albite grains and more abundant actinolite microcrystals, which probably reveal an original clinopyroxene-rich groundmass. This division is supported by the geochemical results. The volcanic flows interbedded in the Puerto Blanco Fm. Unit 1 can also be divided into two groups of mafic and ultramafic rocks (Barrón-Díaz 2013).

4.1.1. Hydrothermal alteration

The identification of hydrothermal alteration mineralogy and metamorphic facies in the studied samples provide important information about the source of primary volcanic clasts. The mineral aggregates present in most samples show clinopyroxene pseudomorphs and relatively less abundant olivine pseudomorphs, although this proportion between them may be reversed in some samples. The primary olivine phenocrysts are principally replaced by carbonates and Fe-Ti oxides, while the mineral composition of clinopyroxene pseudomorphs strongly varies in direct relation to the alteration grade. The alteration of primary clinopyroxene phenocrysts begins with a gradual transformation

to an actinolite aggregate but preserves most of the optical characteristics of a pyroxene, with the exception of an almost parallel extinction and a weak pleochroism. Additionally, it is possible to observe aggregates of chlorite replacing the clinopyroxene phenocrysts. In some cases, the alteration allows the development of subhedral to euhedral epidote crystals in the same pseudomorph phenocryst. Finally, under stronger hydrothermal alteration, the clinopyroxene pseudomorphs are generally composed of carbonates or titanomagnetite, which is possibly due to the mobilization of Fe in the rock. In these cases, the alteration may complicate the reconnaissance of primary crystals.

The hydrothermal alteration mineralogy in the studied samples is composed of albite, sphene, calcite, actinolite, chlorite, and epidote, in order of relative abundance. This mineral paragenesis is indicative of a typical propylitic alteration. With the purpose of confirming this metamorphic facies hypothesis, an amphibole-plagioclase geothermometer (Blundy and Holland 1990) was utilized on samples AB15–05A (Cerro Rajón locality) and AB16–02C (Cerro Calaveras locality). In these samples, using 10 analysed amphibole-plagioclase pairs in each one, the corresponding temperatures were calculated. In the first sample, temperatures varied from 429 to 487°C, with an average temperature of 455°C, and a standard deviation of 21. In the second sample, temperatures varied from 451 to

518°C, with an average temperature of 493°C and a standard deviation of 20. These two calculated average temperatures indicate that the metamorphism event in the studied region is a low-grade metamorphism developed in the upper-temperature albite-epidote hornfels facies or upper-temperature greenschist facies. Geothermometry results are provided in Supplementary File 2.

4.2. Geochemistry

A total of 19 rock samples, systematically selected as more representative and less altered, were used for geochemical analysis. Sixteen samples correspond to volcanic clasts from the tuffaceous conglomerates, two are rounded blocks from the agglomerates picked towards the top of the Puerto Blanco Fm. Unit 1 in the Cerro Rajón and one sample corresponds to the picrobasalt flow. The two agglomerate clasts samples were re-collected to compare these volcanic elements with the tuffaceous conglomerate clasts. The picrobasalt flow is presented as a comparison with the volcanic clasts to analyse a possible relationship. All major-oxide mayor oxide values were normalized to 100% on an anhydrous basis (subscript $_N$) and the results can be found in Supplementary File 3.

Geochemical results show that the volcanic clasts came from low-silica volcanism with values of $SiO_{2N} = 34.32\text{--}48.21\%$. The MgO_N values vary from one locality to another. In the Cerros de la Ciénega, the MgO was lixiviated and replaced by calcite carbonates, while in the rest of the localities, the concentration of MgO_N remains above 5.10%. The high TiO_{2N} concentrations of 3.63–7.52% are another characteristic

signature of this magmatism. The concentrations of $Fe_2O_{3N} = 9.58\text{--}21.06\%$ and the high Fe_2O_{3N}/FeO_N ratio show an important oxidation stage, probably due to hydrothermal alteration. The $Mg\#$ [$100 * Mg / (Mg + Fe^{2+})$] is from very low values (<10) to 67.58 for sample AB14–05B in Cerro San Agustín. Due to metamorphism, $Mg\#$ does not reflect real rock characteristics in the volcanic clasts. It is presented to support a relation with sample AB10–06B ($Mg\# = 67.58$).

All the samples are mildly alkaline (Figure 6a) in the TAS diagram from Le Bas *et al.* (1989). The objective of using this diagram was to compare the volcanic clasts with the volcanic flows (Barrón-Díaz 2013) within the Puerto Blanco Fm. Unit 1, and it is not for classification purposes. The results show a close relation, with a slight increase in alkalis from the volcanic clasts. For proper classification purposes, the Nb/Y–Zr/Ti diagram from Pearce (1996) and the software MagClAMSys (Verma *et al.* 2017) were used. Pearce (1996) diagram uses immobile trace elements that may remain unaffected by the alteration. The results show that most samples plot in the alkali basalt field towards the foidite field. All samples plot within the mafic volcanic flows field (Figure 6b). Verma *et al.* (2017) classification software utilizes a multidimensional scheme applied to altered igneous rocks. Using mayor element analysis can determine the ultramafic, mafic, intermediate, and felsic characteristics of the rocks. The results indicate five samples correspond to basic rocks and 14 to ultrabasic rocks. It is important to mention that none of these rocks present strong ultramafic characteristics due to being close to the mafic boundary. The ultrabasic evidence of this volcanism is supported in sample AB10–06B by the SiO_2 concentration and the absence of

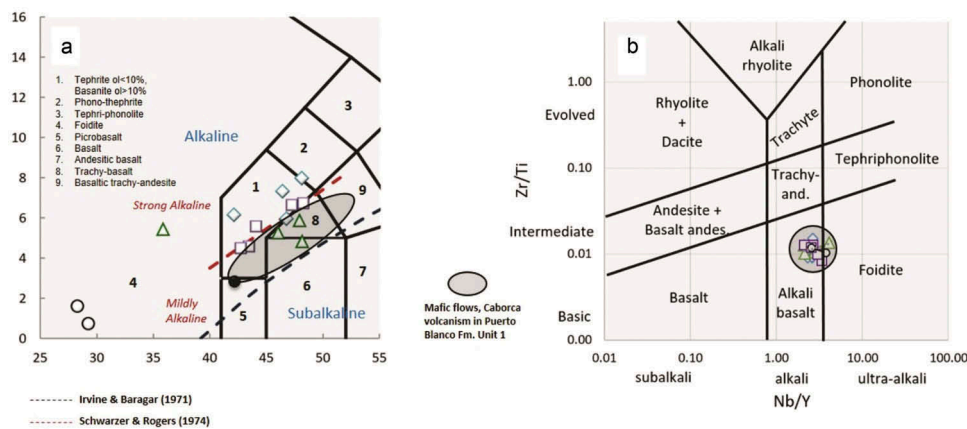


Figure 6. (a) Total alkalis vs. silica diagram from Le Bas *et al.* (1986), including the alkaline-subalkaline and strong-middle alkaline discrimination lines. The TAS diagram is shown as a comparison between the volcanic clast and the volcanic flows analysis, and is not meant for classification purposes due to the alteration of the rocks. (b) Diagram Zr/Ti vs. Nb/Y from Pearce (1982); this diagram is used to give a classification of the volcanic clast as well as a comparison with the volcanic flows. The diagram uses immobile elements that are less susceptible to alteration and metamorphism.

plagioclase (<5%). All results can be found in Supplementary File 4.

Trace element analysis was done on the 17 samples, and 11 of the most representative samples were further analysed by ICP-MS. Primary magma characteristics were preserved for several samples. High Cr and Ni values for samples AB14-05B (Cr = 660 ppm) and AB15-08A (Cr = 549 ppm) are consistently the highest in $Mg\# = 67.58$, and remain as a primary magma signature. Nevertheless, these are not the most common characteristics for the volcanic clasts due to the mobilization of trace elements probably by the hydrothermal alteration. Some samples also preserve high values in Cr, but a significant absence in Ni is always observed, along with low values in $Mg\#$. This absence is due to the complete alteration of olivine crystals and possibly its fractionation.

Although, the volcanic clasts present significant alteration and metasomatism, the affinity between these clasts and the sample AB10-06B (picrobasalt) is evident. The volcanic flow shows low LOI values (2.38%), high $TiO_{2N} = 6.7\%$, Cr = 400 ppm, and Ni = 236. This sample is low silica-undersaturated with normative Ne = 2.44%, implying that, while some trace elements may have suffered a loss or enrichment due to the metasomatism, most of the values remain similar to the results from the volcanic flow.

Spider diagrams show a typical hump-shaped spectrum related to OIB type magmas and marked by a Nb-Ta positive anomaly (Figure 7). LILE shows a greater dispersion, especially the strongly negative K and Sr anomalies. The LILE dispersion can be explained by the hydrothermal alteration, as mentioned by Rollinson (1993) and therefore, this is not a primary characteristic of the magmas. The strong Pb positive anomaly can be explained as sediment contamination

and is more punctuated in sample AB11-39, a mixture of volcanic flows and sediments. In contrast, the HFSE, controlled by the chemistry of the magma source, shows a more uniform spectrum. Sample AB10-06B shows the same pattern that of the volcanoclastic units. This indicates that immobile trace elements did not suffer an important mobilization and may be used for discrimination diagrams.

The REE diagram normalized with chondritic values from Sun and McDonough (1989) shows a strong light-REE enrichment and low concentrations in heavy-REE (Figure 8). The complete REE slope yields $(La/Lu)_N$ ratios from 17.3 to 31.1, except sample AB11-39, which yields a ratio of 37.3. The LREE slopes have more constrained $(La/Sm)_N$ ratios between 2.7 and 3.6, whereas the HREE slopes are more scattered $(Gd/Lu)_N = 3.5-5.8$. There is no Eu anomaly for any of the samples ($Eu/Eu^* = 0.91-1.05$). This is evidence that no plagioclase was fractionated. All samples, excluding AB11-39, conserve a parallel spectrum, indicating genetic filiation. Trace element results can be found in the Supplementary File 5.

4.2.1. Mineral chemistry

The main objective of the electron microprobe analysis for the volcanoclastic units was to determine if any primary crystals from the protolith volcanic rock were conserved. Therefore, samples AB15-05A and AB16-02C were selected from Cerro Rajón and Cerro Calaveras, respectively. Both samples show phenocrysts with optical characteristics similar to clinopyroxene. The phenocrysts and microcrystals of what were formerly clinopyroxene are being replaced by amphiboles, classified as actinolite in the Leake *et al.* (1997) diagram (Figure 9a). Albite crystals were also identified, mostly in interstitial spaces (Figure 9c). These minerals were used for

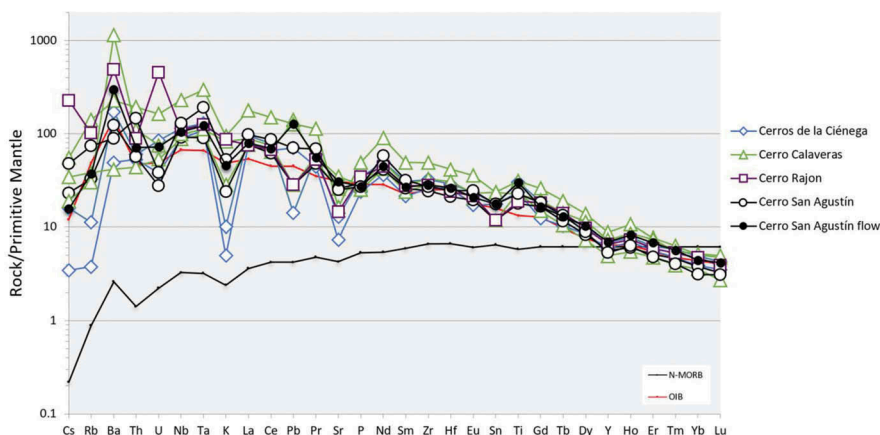


Figure 7. Spider diagram spectrum normalized with primitive mantle for the volcanic clasts from the tuffaceous conglomerates and agglomerates in the Puerto Blanco Fm. Unit 1 and the picrobasalt flow. Normalization values, OIB and N-MORB values are from Sun and McDonough (1989).

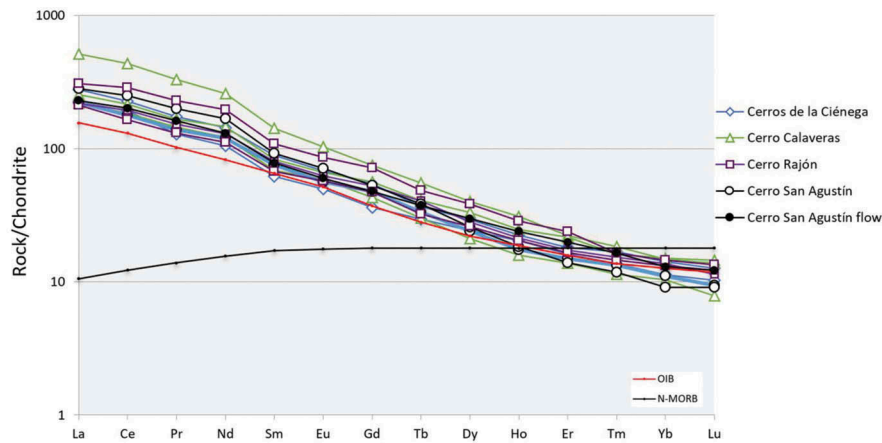


Figure 8. Diagram showing the REE spectrum normalized with chondrite for the volcanic clasts from the tuffaceous conglomerates and agglomerates in the Puerto Blanco Fm. Unit 1 and the microbasalt flow. The upper triangle sample from Cerro Calaveras is the clast with the mixture of sedimentary and volcanic material. OIB and N-MORB values are from Sun and McDonough (1989).

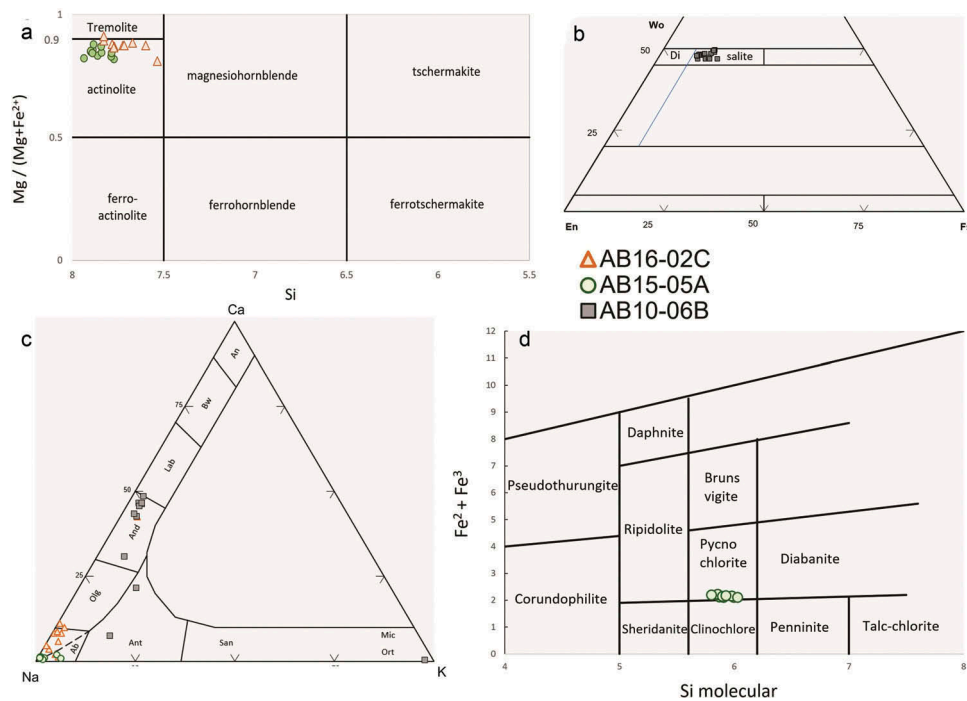


Figure 9. Mineral characterization diagrams. (a) Amphibole characterization after Leake *et al.* (1997). (b) Diagram for pyroxene characterization after Morimoto *et al.* (1988). (c) Feldspar nomenclature in An-Ab-Or diagram. (d) Chlorite characterization after Baley (1980).

geothermometric calculations. Chlorite crystals were classified as pycnochlorite using the Baley (1980) diagram (Figure 9d). Additionally, sphene, titanomagnetite, epidote, orthoclase, and quartz crystals were identified.

Sample AB10-06B presents fresh diopside phenocrysts that were classified in the Morimoto *et al.* (1988) diagram. A second generation of diopside microcrystals is present as a main mineral in the groundmass. Diopside crystals contain unusually high TiO_2 concentrations, which suggest a relationship with ultramafic magmas (Gerke *et al.*

2005). Groundmass also contains titanomagnetite and sphene in a cloudy habit and late stage crystallization andesine (Figure 9c). The presence of andesine in the groundmass indicates that the volcanic flow did not suffer a complete albitization, due to hydrothermal metamorphism, as occurred in the volcanic clasts.

The electron microprobe analysis confirms that metamorphism affected the volcanic clasts and almost entirely replaced the original mineralogy. Due to the poor preservation of the minerals, radiometric analysis

cannot achieve a crystallization age by analysing the groundmass. However, sample AB10–06B and other volcanic flows within the Puerto Blanco Fm. Unit 1 preserve unaltered clinopyroxene crystals (Barrón-Díaz 2013). Microprobe analysis results are provided in Supplementary File 6.

4.3. Biostratigraphy and metamorphic age

Through biostratigraphy studies, Sour-Tovar *et al.* (2007) constrained the location of the Cambrian–Eldiacaran boundary. The study was made in the Cerros de la Ciénega locality. Sour-Tovar *et al.* (2007) observed that the packstones and wackestones from Unit 3 of the La Ciénega Fm. have the last occurrences of *cloudiniids*, an Eldiacaran index fossil. They also reported the Cambrian index fossil *Treptichnus pedum* within the Puerto Blanco Fm. Unit 1. Taking this into consideration, the volcanic event must be located near the Cambrian–Precambrian boundary. While Sour-Tovar *et al.* (2007) mentioned that the *T. pedum* was found on a dolomitic sandstone towards the top of the Puerto Blanco Fm. Unit 1, it must be considered that the sequence at the Cerros de la Ciénega locality is not the most representative of this unit. This locality lacks the volcanic flows that were recognized in the other studied localities.

Loyd *et al.* (2012) recognized the *T. pedum*, at the sequence from the Cerro Rajón, within the base of the Puerto Blanco Fm. Unit 1. They mentioned that the fossils occur below an extensive boulder

conglomerate. We consider these rocks as agglomerates that underlie and overlie the fossil-bearing sandstones (Figure 3). This implies that the appearance of the *T. pedum* fossil is contemporaneous with the volcanic events.

Acquiring a radiometric age for this volcanic event has been difficult. On a first attempt to date these rocks, two volcanic flows from the studied localities were analysed by $^{40}\text{Ar}/^{39}\text{Ar}$ geochronology. The sample AB10–06B from Cerro San Agustín was classified as a porphyritic clinopyroxene picrobasalt flow. Sample AB 11 46 from Cerro Calaveras is slightly more differentiated and was thus classified as a metabasalt flow (Barrón-Díaz 2013). Through groundmass analysis, two ages were obtained at 52.58 ± 2 Ma and 91.67 ± 0.55 Ma (Figure 10). These results were interpreted as metamorphism ages considering that the hydrothermal processes made a partial or complete reset on the radiogenic argon contained in the crystals.

Geochronology results may be best explained as a metamorphic print of Laramidic intrusives, which were dated at 90.1 ± 1.1 and 69.4 ± 1.2 Ma near the study region (Ramos-Velázquez *et al.* 2008). These intrusive bodies were also reported in the study region by Radelli *et al.* (2008). More recently, Leyva-Ruiz (2017) reported Laramidic intrusives outcropping in the Cerro El Dátil, 15 km west of the Cerros de la Ciénega. The Laramidic batholith was produced by the magmatism derived from the subduction of the Farallon Plate during the Cretaceous to the Eocene. Its age is temporally constrained from 90 to 40 Ma (Damon *et al.* 1983).

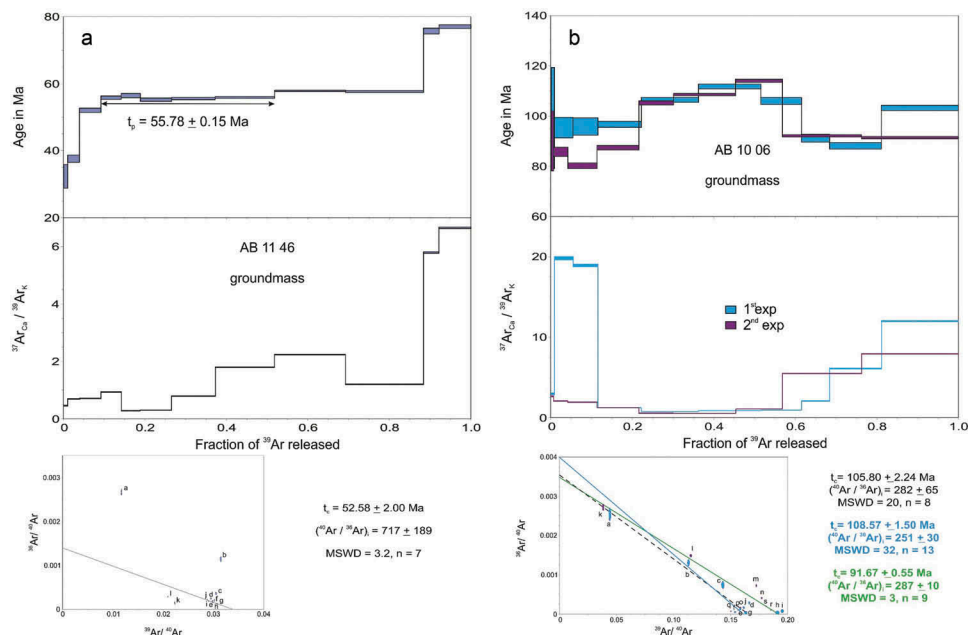


Figure 10. $^{40}\text{Ar}/^{39}\text{Ar}$ geochronology graphics made for two volcanic flow samples from the Puerto Blanco Fm. Unit 1. Samples AB 11 46 and AB 10 06 were identified as a metabasalt and a picrobasalt, respectively.

5. Discussion and conclusions

The volcanic activity recorded in the study area mostly corresponds to a pyroclastic activity, where the volcanic vents were mostly destroyed to form agglomerates to tuffaceous conglomerates. The tuffaceous conglomerates represent the erosion and destruction of the cinder cones that were produced by a strombolian activity or could have been formed in areas distant from the main source of the pyroclastic activity. In any scenario, most of these volcanic clasts correspond to slightly rework volcanic bombs. In contrast, the agglomerates represent the closest locations to the volcanic structures, where the cinder cones collapsed. Some of the agglomerates were probably preserved due to further effusive events that sealed the sequence and prevented further degradation, as can be observed at the top of the Cerro Rajón sequence (Figure 3).

One particular consideration that must be taken while interpreting the geochemical analysis is that the volcanic units were exposed to metamorphism and metasomatism. In order to address this issue, we needed to be sure that at least the immobile trace elements represent the original concentration of the volcanic flows. A key element to resolve this was found in sample AB10–06B, a picrobasalt flow with fresh primary mineralogy. The low silica and very low concentrations of plagioclase in the picrobasalt reveal the presence of ultramafic rocks temporally close to the Cambrian–Precambrian boundary for the Caborca region. Using this picrobasalt flow sample and other mafic-ultramafic flows (Barrón-Díaz 2013) from the Caborca region, we were able to justify that even though hydrothermal alteration affected the volcanoclastic rocks, the original protolith signatures are preserved in at least half of the analysed samples.

We assume that the volcanic clasts were produced by the same volcanic events that produced the volcanic flows within the Puerto Blanco Fm. Unit 1. The petrography and geochemical data show that the volcanism has ultrabasic to slightly basic characteristics. The volcanic bombs, sampled from the agglomerate units in the Cerro Rajón locality, preserve the same geochemical characteristics of the volcanic clasts of the tuffaceous conglomerates. The volcanic clasts should be treated as metamorphic rocks due to their degree of alteration and described as granofels by their petrographic characteristics. Nevertheless, the combined results of this work allowed the identification of an igneous protolith. Therefore, the volcanic clasts can be classified as alkaline metabasalts and metabasalts.

One particular characteristic of this volcanism is the relatively high TiO_2 concentrations ($\text{TiO}_{2\text{N}} = 3.63\text{--}7.52\%$)

also observed in another mafic alkaline flows (Keeley 2011; Zhang *et al.* 2012). This characteristic is a primary signature which is also revealed by the unusually high TiO_2 values obtained from the diopside microprobe analysis. $\text{TiO}_2/\text{Mg}\#$ ratios can be used to obtain the estimated crystallization pressures for the clinopyroxene crystals, where $\text{TiO}_2 > 3\%$ indicates low crystallization pressures for the clinopyroxene (Wass 1979). By doing this, we found that the diopside crystals were formed at low pressures. This is further supported by the Alvi and Aliv values in the diopside crystals (Alvi/Aliv < 0.03), inside the field of igneous rocks (< 0.25), which indicate non-metamorphic characteristics for these pyroxenes (Aoki and Kushiro 1968).

The alteration of the rocks is controlled by the geological history of each particular locality. Samples from the eastern part of the study area, including Cerro San Agustín and Cerro Rajón, are generally less altered and the agglomerate units were better preserved. Samples from Cerro Calaveras and Cerros de la Ciénega, in the western part of the study area, suffered a more intense alteration and are mostly represented by tuffaceous conglomerates. This might be explained by the proximity of the intrusive bodies located west to the study area (Leyva-Ruiz, 2017). The metamorphism facies identified in the volcanoclastic units and the geothermometry results suggest that this metamorphic event was strong enough to transform the original mineralogy, which is especially noted in the altered clinopyroxene crystals, commonly a resilient mineral in a low-grade metamorphism. On the other side, the picrobasalt flow was preserved in its middle unit, where diopside phenocrysts and microcrystals remain fresh. Moreover, metamorphism also affected the late stage plagioclase in the groundmass and partially removed the Ti in the large Fe-Ti oxide phenocrysts, causing the presence of secondary sphene in a cloudy habit and the relicts of ilmenite phenocrysts now transformed to skeletal titanomagnetite. Laramidic intrusives may explain the hydrothermal alteration and the younger metamorphism suggested by the $^{40}\text{Ar}/^{39}\text{Ar}$ ages.

5.1. Tectonic setting

The preservation of immobile trace elements, such as Hf, Nb, Ta, Th, and Zr, was used to plot the samples in the discrimination diagrams of Wood (1980). These diagrams allowed location of the protolith of the samples within a tectonic setting. Volcanic clast samples plot in the alkaline within-plate basalts field (Figure 11b). The other two diagrams show consistent results, which support the alkaline and intracontinental characteristic of the volcanism. This is also sustained by the results of

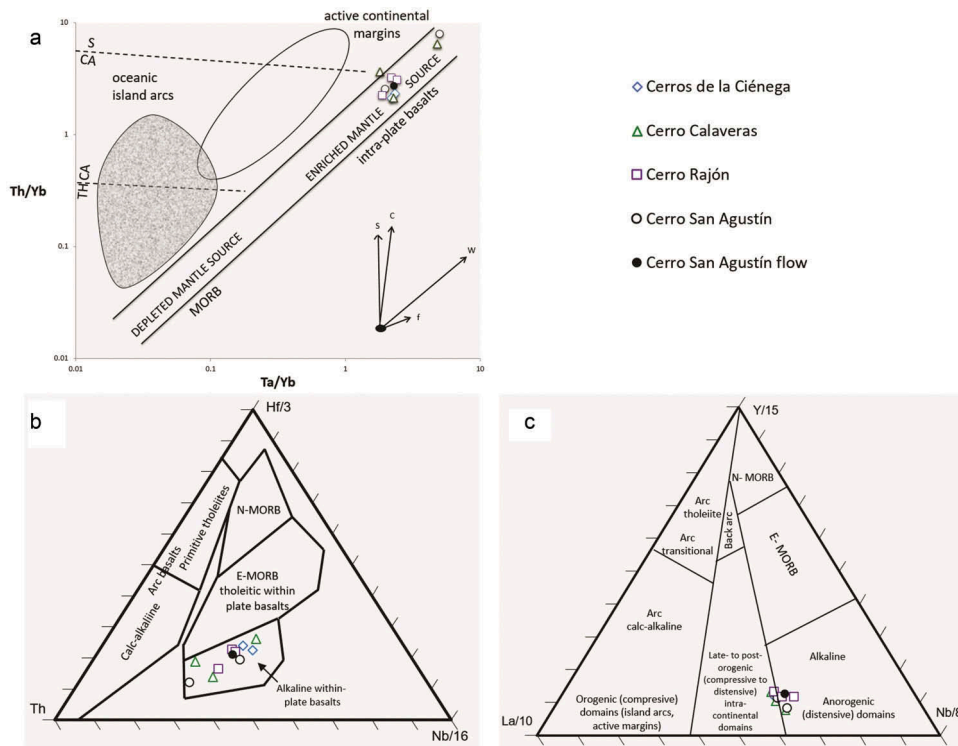


Figure 11. (a) Pearce (1983) diagram used to show the difference between depleted and enriched magma sources. Vectors shown indicate the influence of subduction components (S), within-plate enrichment (W), crustal contamination (C), and fractional crystallization (F). Dashed lines separate the boundaries of the tholeiitic (TH), calc-alkaline (CA), and shoshonitic (S) fields. (b) Tectonic setting discrimination diagram Th-Hf/3-Nb/16 from Wood (1980), used for the volcanic units in the Puerto Blanco fm. Unit 1. (c) Tectonic setting diagram from Cabanis and Lecolle (1989).

the Cabanis and Lecolle (1989) diagram, where samples plot in the anorogenic distensive domains towards the intra-continental domain (Figure 11c). A Pearce (1983) diagram is used to show the difference between depleted and enriched mantle sources. Once again, the trace elements remain consistent for all the samples, locating the original volcanism within an enriched mantle source (Figure 11a), related to OIB-type volcanism. All diagrams present a close relation between the volcanoclastic units and the picrobasalt flow. These results are in concordance with the classification diagrams for tectonomagmatic discrimination from Verma and Rivera-Gómez (2013), where the Puerto Blanco Fm. Unit 1 samples plot within the OIB field (Figure 12). These diagrams were specifically made to be used in basic and ultrabasic rocks and were applied in ancient rocks.

The tectonic setting results suggest a volcanic event related to an intracontinental rift, although the small volume of volcanic products is consistent with low melting ratios (Figure 13). To explain this, we suggest the original volcanism that formed these rocks is not related to an axial zone rift but to a distant branch or an aulacogen, where the volcanic activity could occur in small volumes and over a small span of time. Further

petrology studies on the volcanic flows are needed to properly understand this volcanic event. Figure 14 summarizes the main results while comparing the differences between the east and west part of the study area.

The Puerto Blanco Fm. has been correlated with the miogeoclinal prism sequences in southwestern of the United States (Stewart *et al.* 1984). The Cambrian sequences are correlated through stratigraphy and palaeontology, although no volcanic events had been reported for the Cambrian in southwestern United States. In Idaho and Utah, Harper and Link (1986) reported alkaline basalts of Neoproterozoic age related to an intra-continental rift with high TiO_2 values. This volcanic event is known as the Bannock Volcanic Member (Keeley 2011), associated with the rifting process on the western part of the Laurentia margin, which was active 780–570 Ma ago (Lund *et al.* 2003). Another possible correlation to the volcanism in the Puerto Blanco Fm. Unit 1 is the Hamill/Gog Group in the southeastern Canadian Cordillera, identified as the latest Neoproterozoic rifting along western Laurentia (Colpron *et al.* 2002). The volcanic group was dated by U-Pb zircon geochronology at 569.6 ± 5.3 Ma. In their work, Colpron *et al.* (2002) suggest that the age difference between the Hamill/Gog Group and other rift-related events in the NW margin of North America may be

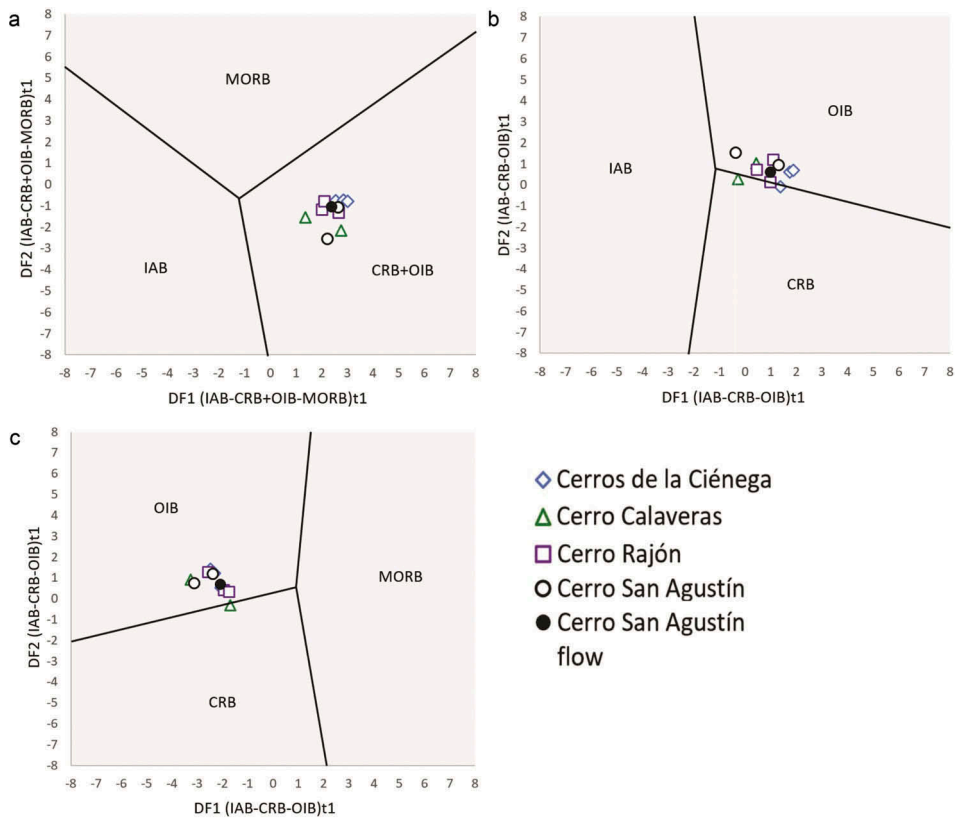


Figure 12. Diagrams for tectonomagmatic discrimination from Verma and Rivera-Gómez (2013) for the volcanoclastic units and picobasalt flow from the Puerto Blanco Fm. Unit 1.

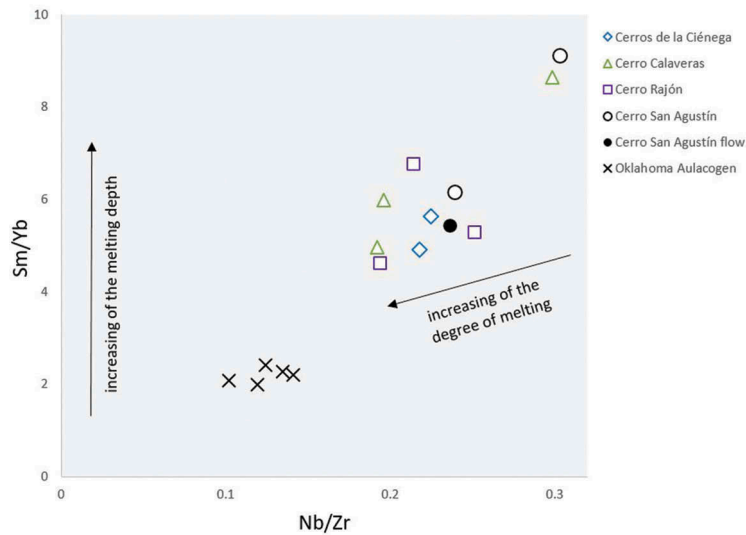


Figure 13. Plot Sm/Yb vs. Nb/Zr and Dy/Yb vs. La/Sm for the tuffaceous conglomerates, agglomerate, and picobasalt flow from the Puerto Blanco Fm. Unit 1. Samples were compared with the Oklahoma Aulacogen basaltic flows (Brueseke *et al.* 2016). Plots from the Caborca region are related to a lower degree of melting. Sample AB11–39, a mixture of volcanic and sedimentary material, plots outside the main cluster of samples, along with sample AB14–05A, a very altered and lixiviated sample from Cerro San Agustín. Vectors after He *et al.* (2010).

explained by considering the following: first, a continental separation and passive margin development along the margin of northern Laurentia during the Neoproterozoic; and second, the breakup of a second crustal block from

western Laurentia. This scenario also explains the simultaneous occurrence of volcanism and passive margin deposition during the Cambrian–Precambrian boundary, the same scenario that develops during the lower

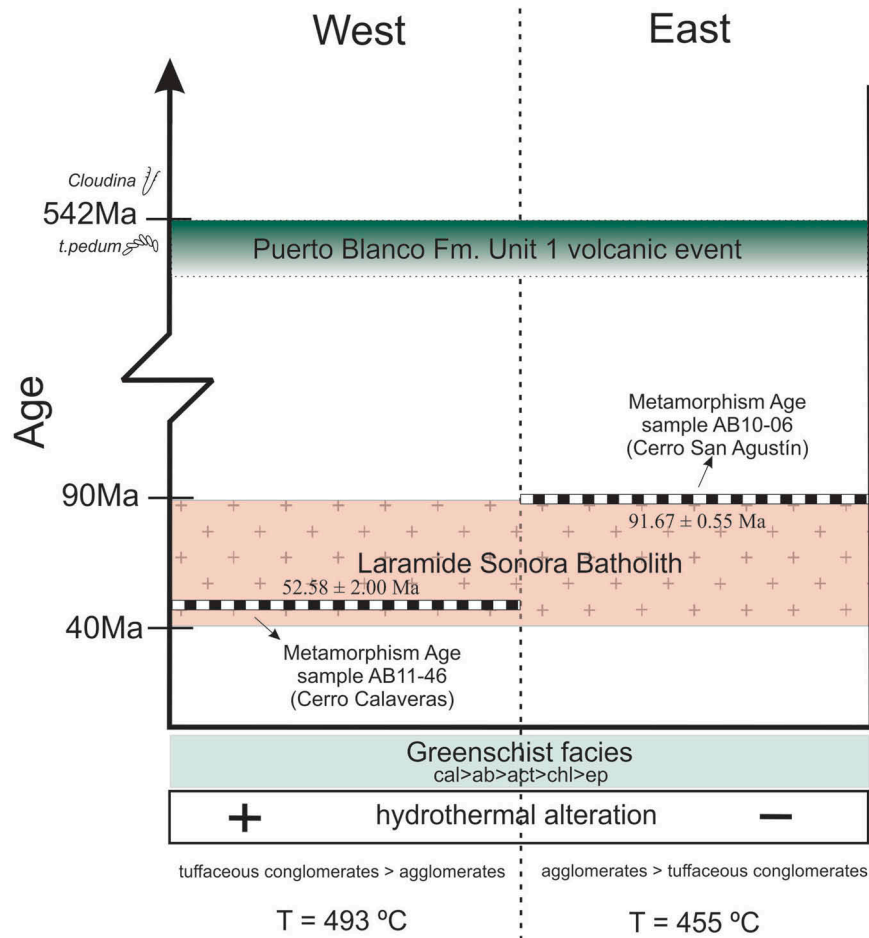


Figure 14. Age vs. study area indicating the temporal and spatial position of the two radiometric ages obtained. Both samples can be included within the Sonora Laramide batholith timespan (Damon *et al.* 1983; Ramos-Velázquez *et al.* 2008). Other important differences between the east and west part of the study area are presented.

Cambrian in the Caborca region sequence. Hamill/Gog Group greenstones present up to 4.58% of TiO_2 , a particular similitude with the Caborca region volcanic units.

Other possible correlations with this magmatism include Skinner Cove Fm. in Newfoundland and the early Cambrian volcanism in the Southern Oklahoma Aulacogen (SOA; Figure 1). The volcanic event that formed the Skinner Cove Fm. was dated in an ankaramite flow at 550.5 ± 3 Ma, an event that provides evidence of a rift–drift transition ca. 540–535 Ma (Cawood *et al.* 2001). The minimum age for the SOA volcanic event was dated on the Arbuckle Mountains in 540 Ma (Thomas *et al.* 2012). Mafic volcanism in the SOA is represented by subalkaline, tholeiitic basalts, and andesites (Brueseke *et al.* 2016). The SOA volcanic events show notable differences with the magmatism in the Caborca region, such as low Ti concentrations, a higher degree of melting (Figure 13), and more differentiated products. Nevertheless, estimated primary magmas by Brueseke *et al.* (2016) are similar in composition and mineralogy with the volcanism in Caborca.

Acknowledgements

We thank the support of James Hagadorn in the field work and location of some Cerros de la Ciénega and Cerro Rajón localities. We thank Aimé Orcí from ERNO-UNAM and Sheila Corral from UNISON for their valuable work in the preparation of thin sections. Our thanks to Pablo Peñaflor from ERNO-UNAM for the assistance in the use of the sample preparation laboratory and to Ken Domanik for his assistance in the electron microprobe analysis.

Disclosure statement

No potential conflict of interest was reported by the authors.

Funding

This work was supported by Universidad de Sonora (PIFI 2015–2016 grant) and the Institute of Geology–UNAM (special grant 2016).

References

- Anderson, T.H., and Silver, L.T., 1979, The role of the Mojave-Sonora megashear in the tectonic evolution of northern Sonora, in Anderson, T.H., and Roldán-Quintana, J., eds., *Geology of northern Sonora*, Geological Society of America Annual Meeting, guidebook trip 27, Pittsburgh, Pa., University of Pittsburgh and Hermosillo, Sonora, Instituto de Geología, U.N.A.M., p. 59–68
- Anderson, T.H., and Silver, L.T., 1981, An overview of Precambrian rocks in Sonora, Univ. Nal. Autón. México, *Instituto Geología, Revista*, v. 5, no. 2, p. 131–139
- Aoki, K.I., and Kushiro, I., 1968, Some clinopyroxenes from ultramafic inclusions in Dreiser weeber, Eifel, *Contributions to Mineralogy and Petrology*, v. 18, p. 326–337.
- Bailey, S.W., 1980, Summary of recommendations of AIPEA nomenclature committee on clay minerals, *American Mineral*, v. 65, p. 1–7.
- Barrón-Díaz, A.J., 2013, Caracterización petrogenética de las metabasitas anorogénicas del límite cámbrico-precámbrico, Municipio de Pitiquito, Sonora, México [M.S. thesis], Universidad de Sonora, 95 p.
- Bickford, M.E., Van Schmus, W.R., Karlstrom, K.E., Mueller, P.A., and Kamenov, G.D., 2015, Mesoproterozoic-trans-laurentian magmatism: A synthesis of continent-wide age distributions, new SIMS U–Pb ages, zircon saturation temperatures, and Hf and Nd isotopic compositions, *Precambrian Research*, v. 265, p. 286–312. doi: [10.1016/j.precamres.2014.11.024](https://doi.org/10.1016/j.precamres.2014.11.024)
- Blundy, J.D., and Holland, T.J.B., 1990, Calcic amphibole equilibria and a new amphibole-plagioclase geothermometer, *Contributions to Mineralogy and Petrology*, v. 104, p. 208–224. doi: [10.1007/BF00306444](https://doi.org/10.1007/BF00306444)
- Brueseke, M.E., Hobbs, J.M., Bulen, C.L., Mertzman, S.A., Puckett, R.E., Walker, J.D., and Feldman, J., 2016, Cambrian intermediate-mafic magmatism along the Laurentian margin: Evidence for flood basalt volcanism from well cuttings in the Southern Oklahoma Aulacogen (U.S.A.), *Lithos*, v. 260, p. 164–177. doi: [10.1016/j.lithos.2016.05.016](https://doi.org/10.1016/j.lithos.2016.05.016)
- Cabanis, B., and Lecolle, M., 1989, Le diagramme La/10–Y/15–Nb/8; un outil pour la discrimination des series volcaniques et la mise en evidence de processus de melange et/ou de contamination crustale, *C R Academic Sciences Series II*, v. 309, p. 2023–2090.
- Campa, U.M.F., and Coney, P.J., 1983, Tectono-stratigraphic terranes and mineral resource distributions in Mexico, *Canadian Journal of Earth Sciences*, v. 20, p. 1040–1051. doi: [10.1139/e83-094](https://doi.org/10.1139/e83-094)
- Cawood, P.A., McCausland, P.J.A., and Dunning, G.R., 2001, Opening Iapetus: Constraints from the Laurentian margin in Newfoundland, *GSA Bulletin*, v. 113, no. 4, 443–453. doi: [10.1130/0016-7606\(2001\)113<0443:OICFTL>2.0.CO;2](https://doi.org/10.1130/0016-7606(2001)113<0443:OICFTL>2.0.CO;2)
- Centeno-García, E., Maytorena, F., Calmus, T., Solis-Pichardo, G., and Lozano-Santa Cruz, R., 2002, Proterozoic OIB magmatism in the Caborca terrane, northwestern Mexico, *in* Denver Annual Meeting, Colorado Convention Center: C205, Session No. 245. doi: [10.1044/1059-0889\(2002\)er01](https://doi.org/10.1044/1059-0889(2002)er01)
- Chapman, A.D., Ernst, W.G., Gottlieb, E., Powerman, V., and Metzger, E., 2015, Detrital zircon geochronology of neoproterozoic-lower Cambrian passive margin strata of the white-ino range, east-central California: implications for the Mojave-snow lake fault hypothesis, *GSA Bulletin*, v. 127, p. 926–944.
- Colpron, M., Logan, J.M., and Mortensen, J.K., 2002, U–Pb zircon age constraint for late neoproterozoic rifting and initiation of the lower paleozoic passive margin of western Laurentia, Canada *Journal Earth Science*, v. 39, p. 133–143. doi: [10.1139/e01-069](https://doi.org/10.1139/e01-069)
- Cooper, G.A., and Arellano, A.R.V., 1952, Introduction and stratigraphy, Cooper, G.A., Arellano, A.R.V., Johnson, J.H., Okulitch, V.J., Stoyanow, A., and Lochman, C., eds., *Cambrian stratigraphy and paleontology near Caborca, northwestern Sonora, Mexico: Smithsonian Miscellaneous Collections*, v. 119, no. 1, p. 1–23
- Damon, P.E., Shafiqullah, M., Roldán-Quintana, J., and Cochemé, J.J., 1983, El Batolito Laramide (90–40 Ma) de Sonora, *Asociación de Ingenieros de Minas, Metalurgistas y Geólogos de México (AIMMGM), Convención Nacional XV, Guadalajara, Jal.*, p. 63–95.
- Eells, J.L., 1972, *Geology of the sierra de la berruga, northwestern Sonora, Mexico* [M.S. thesis], San Diego, California State University, 77 p.
- Gerke, T.L., Kilinc, A.I., and Sack, R.O., 2005, Ti-content of high-Ca pyroxenes as a petrogenetic indicator: An experimental study of mafic alkaline rocks from the Mt. Erebus volcanic region, Antarctica, *Contributions to Mineralogy and Petrology*, v. 148, p. 735. doi: [10.1007/s00410-004-0636-5](https://doi.org/10.1007/s00410-004-0636-5)
- Harper, G.D., and Link, P.K., 1986, Geochemistry of upper proterozoic rift-related volcanics, northern Utah and southeastern Idaho, *Geology*, v. 14, p. 864–867. doi: [10.1130/0091-7613\(1986\)14<864:GOUPRV>2.0.CO;2](https://doi.org/10.1130/0091-7613(1986)14<864:GOUPRV>2.0.CO;2)
- He, Q., Xiao, L., Balta, B., Gao, R., and Chen, J., 2010, Variety and complexity of the Late-Permian Emeishan basalts: Reappraisal of plume–Lithosphere interaction processes, *Lithos*, v. 119, p. 91–107. doi: [10.1016/j.lithos.2010.07.020](https://doi.org/10.1016/j.lithos.2010.07.020)
- Irvine, T.N., and Baragar, W.R.A., 1971, A guide to the chemical classification of the common volcanic rocks, *Canadian Journal of Earth Science*, v. 8, p. 523–548. doi: [10.1139/e71-055](https://doi.org/10.1139/e71-055)
- Keeley, J.A., 2011, *Stratigraphy, geochemistry and geochronology of the Bannock volcanic and Scout mountain members, Pocatello Fm, and structure of Oxford Ridge, SE Idaho* [M.S. thesis], Pocatello, Idaho State University.
- Le Bas, M.J., Le Maitre, R.W., Streckeisen, A., and Zanettin, B., 1986, A chemical classification of volcanic rocks based on the total alkali–silica diagram, *Journal of Petrology, Oxford*, v. 27, p. 745–750. doi: [10.1093/petrology/27.3.745](https://doi.org/10.1093/petrology/27.3.745)
- Le Maitre, R.W., (editor), Streckeisen, A., Zanettin, B., Le Bas, M. J., Bonin, B., Bateman, P., Bellieni, G., Dudek, A., Efremova, S., Keller, J., Lameyre, J., Sabine, P.A., Schmid, R., Sørensen, H., and Woolley, A.R., 2002, *Igneous rocks: A classification and glossary of terms: Recommendations of the international union of geological sciences, subcommission on the systematics of igneous rocks: Cambridge, U.K., Cambridge University Press*, 236 p.
- Leake, B.E., Woolley, A.R., Arps, C.E.S., Birch, W.D., Gilbert, M. C., Grice, J.D., Hawthorne, F.C., Kato, A., Kisch, H.J., Krivovichev, V.G., Linthout, K., Laird, J., Mandarino, J.A., Maresch, W.V., Nickel, E.H., Rock, N.M.S., Schumacher, J.C., Smith, D.C., Stephenson, N.C.N., Ungaretti, L., Whittaker, E. J.W., and Guo, Y., 1997, *Nomenclature of amphiboles: Report of the subcommittee on amphiboles of the international mineralogical association, commission on new minerals and mineral names, Canadian Mineralogist*, v. 35, p. 219–246.

- Leyva-Ruiz, N., Barrón-Díaz, A.J., Lozano-Santa Cruz, R., and Paz-Moreno, F.A., 2017, Petrografía y geoquímica de los intrusivos granitoides en el cerro El Dátil, municipio de Pitiquito, Sonora, México, XXVII Congreso Nacional de Geoquímica, Actas INAGEQ, v. 23, p. 104.
- Longoria, J.F., 1981, Geologic features of northwest Sonora, *in* Longoria, J., ed., Regional geology of northwest Sonora: Geological Society of America, Cordilleran Section Annual Meeting, Hermosillo, Sonora, Mexico, Proceedings, p. 1–48.
- Longoria, J.F., and González, M.A., 1981, Descripción de las localidades a ser visitadas durante la excursión de campo de la GSA no. 4, *in* Longoria, J., Regional geology of northwest Sonora, Geological Society of America, Cordilleran Section, Annual Meeting, Hermosillo, Sonora, Mexico, p. 49–64.
- Longoria, J.F., González, M.A., Mendoza, J.J., and Pérez, V.A., 1978, Consideraciones estructurales en el cuadrángulo Pitiquito-La Primavera, NW de Sonora, Boletín Del Departamento De Geología UNISON, v. 1, no. 1, p. 61–67.
- Loyd, S.J., Marengo, P.J., Hagadorn, J.W., Lyons, T.W., Kaufman, A.J., Sour-Tovar, F., and Corsetti, F.A., 2012, Sustained low marine sulfate concentrations from the Neoproterozoic to the Cambrian: Insights from carbonates of northwestern Mexico and eastern California, Earth and Planetary Science Letters, v. 339–340, p. 79–94. doi: [10.1016/j.epsl.2012.05.032](https://doi.org/10.1016/j.epsl.2012.05.032)
- Lozano-Santa Cruz, R., and Bernal, J.P., 2005, Characterization of a new set of eight geochemical reference materials for XRF major and trace element analysis, Revista Mexicana De Ciencias Geológicas, v. 22, no. 3, p. 329–344.
- Lund, K., Aleinikoff, J., Evans, K., and Fanning, C., 2003, SHRIMP U-Pb geochronology of Neoproterozoic windermere supergroup, central Idaho, implications for rifting of western Laurentia and synchronicity of Sturtian glacial deposits, GSA Bulletin, v. 115, no. 3, 349–372. doi: [10.1130/0016-7606\(2003\)115<0349:SUPGON>2.0.CO;2](https://doi.org/10.1130/0016-7606(2003)115<0349:SUPGON>2.0.CO;2)
- Maytorena-Silva, J.F., and Durazo-Tapia, G.E., 1982, Bosquejo geológico y estructural de los cerros Clemente y San Agustín, cuadrángulo pitiquito-la primavera, noroeste del estado de Sonora [Bachelor thesis], Universidad de Sonora, 45 p.
- Morimoto, N., Fabries, J., Ferguson, A., Ginzburg, I., Roos, M., Seifert, F., and Zussman, J., 1988, Nomenclature of pyroxenes, American Mineralogist, v. 73, p. 1123–1133.
- Pearce, J.A., 1982, Trace elements characteristics of lavas from destructive plate boundaries, *in* Thorpe, R. S., Andesites: Wiley & Sons, p.525–548.
- Pearce, J.A., 1983, Role of the subcontinental lithosphere in magma genesis at continental margins, *in* Hawkesworth, C. J., and Norry, M.J., Eds., Continental Basalts and Mantle Xenoliths, Cheshire: Shiva Publishing, p. 230–249.
- Pearce, J.A., 1996, A user's guide to basalt discrimination diagrams, *in* Wyman, D.A., ed., Trace Element Geochemistry of Volcanic Rocks: Applications for Massive Sulphide Exploration: Geological Association of Canada, Short Course Notes, v. 12, p. 79–113.
- Radelli, L., Solis-Weiss, V., Dórame-Navarro, M., De La Cruz-Ortega, L.C., and Urrutia, J., 2008, Fossil content and structural relationships of the San Luis zone and Caborca zone of NW Sonora, Mexico. Suppression of the precambrian Z. of Caborca, Boletín De Geología Universidad Industrial De Santander, Colombia, v. 30, no. 2, p. 1–34.
- Ramos-Velázquez, E., Calmus, T., Valencia, V., Iriondo, A., Valencia-Moreno, M., and Bellon, H., 2008, U-Pb and 40Ar/39Ar geochronology of the coastal Sonora batholith: New insights on Laramide continental arc magmatism, Revista Mexicana De Ciencias Geológicas, v. 25, no. 2, p. 314–333.
- Rollinson, H.R., 1993, Using geochemical data: Evaluation, presentation and interpretation, Longman, Harlow, 352 p.
- Schmid, R., 1981, Descriptive nomenclature and classification of pyroclastic deposits and fragments: Recommendations of the IUGS subcommission on the systematics of igneous rocks, Geology, v. 9, p. 41–43. doi: [10.1130/0091-7613\(1981\)9<41:DNACOP>2.0.CO;2](https://doi.org/10.1130/0091-7613(1981)9<41:DNACOP>2.0.CO;2)
- Schwarzer, R.R., and Rogers, J.J.W., 1974, A worldwide comparison of alkali olivine basalts and their differentiation trends, Earth Planet Science Letters, v. 23, p. 286–296. doi: [10.1016/0012-821X\(74\)90117-4](https://doi.org/10.1016/0012-821X(74)90117-4)
- Sour-Tovar, F., Hagadorn, J.W., and Huitrón-Rubio, T., 2007, Ediacaran and Cambrian index fossils from Sonora, Mexico, Paleontology, v. 50, no. Part 1, 169–175. doi: [10.1111/j.1475-4983.2006.00619.x](https://doi.org/10.1111/j.1475-4983.2006.00619.x)
- Stewart, J.H., 1982, Regional relations of proterozoic Z and lower Cambrian rocks in the western United States and northern Mexico, *in* Cooper, J.D., Troxel, B.W., and Wright, L.A., eds., Geology of selected areas in the San Bernardino Mountains, western Mojave Desert, and southern Great Basin, California, Geological Society of America, Cordilleran Section Annual Meeting, Anaheim, California, Guidebook and Volume, p. 171–186.
- Stewart, J.H., 2005, Evidence for Mojave-Sonora megashear; systematic left lateral offset of neoproterozoic to lower Jurassic strata and facies, western United States and northwestern Mexico, *in* Anderson, T.H., ed., The Mojave-Sonora megashear hypothesis: Development, assessment, and alternatives: Geological Society of America Special Paper, v. 393, p. 209–231.
- Stewart, J.H., Amaya-Martinez, R., and Palmer, A.R., 2002, Neoproterozoic and Cambrian strata of Sonora, Mexico: Rodinian supercontinent to Laurentian cordilleran margin, Geológicas Society of América, Special Paper, v. 365, p. 5–48.
- Stewart, J.H., McMenamin, A.S., and Morales-Ramirez, J.M., 1984, Upper proterozoic and Cambrian rocks in the Caborca region, Sonora, Mexico. Physical stratigraphy, biostratigraphy, paleocurrents studies and regional relations., U. S. Geological Survey Professional Paper 1390.
- Sun, S.S., and McDonough, W.F., 1989, Chemical and isotopic systematics of oceanic basalts: Implications for mantle composition and processes, *in* Saunders, A.D., and Norry, M.J., Eds., Magmatism in the ocean basins, Vol. 42: Geological Society, Special Publications, London, p. 313–345.
- Thomas, W.A., Tucker, R.D., Astini, R.A., and Denison, R.E., 2012, Ages of pre-rift basement and synrift rocks along the conjugate rift and transform margins of the Argentine Precordillera and Laurentia, Geosphere, v. 8, p. 1–18. doi: [10.1130/GES00800.1](https://doi.org/10.1130/GES00800.1)
- Verma, S.P., and Rivera-Gómez, M.A., 2013, New computer program TecD for tectonomagmatic discrimination from discriminant function diagrams for basic and ultrabasic magmas and its

- application to ancient rocks, *Journal of Iberian Geology*, v. 39, p. 167–179. doi: [10.5209/rev_JIGE.2013.v39.n1.41757](https://doi.org/10.5209/rev_JIGE.2013.v39.n1.41757)
- Verma, S.P., Rivera-Gómez, M.A., Díaz-González, Pandarinath, K., Amezcua-Valdez, A., Rosales-Rivera, M., Verma, S.K., Quiroz-Ruiz, A., Armstrong-Altrin, J.S., and Díaz-González, L., 2017, Multidimensional classification of magma types for altered igneous rocks and application to their tectonomagmatic discrimination and igneous provenance of siliciclastic sediments, *Lithos*, v. 278–281, no. p, 321–330. doi: [10.1016/j.lithos.2017.02.005](https://doi.org/10.1016/j.lithos.2017.02.005)
- Wass, S.Y., 1979, Multiple origins of clinopyroxenes in alkali basaltic rocks, *Lithos*, v. 12, p. 115–132. doi: [10.1016/0024-4937\(79\)90043-4](https://doi.org/10.1016/0024-4937(79)90043-4)
- Wood, D.A., 1980, The application of a Th-Hf-Ta diagram to problems of tectonomagmatic classification and to establishing the nature of crustal contamination of basaltic lavas of the British tertiary volcanic province, *Earth and Planetary Science Letters*, v. 50, p. 11–30. doi: [10.1016/0012-821X\(80\)90116-8](https://doi.org/10.1016/0012-821X(80)90116-8)
- Zhang, Z., Kang, J., Kusky, T., Santosh, M., Huang, H., Zhang, D., and Zhu, J., 2012, Geochronology, geochemistry and petrogenesis of neoproterozoic basalts from Sugetbrak, northwest Tarim block, China: Implications for the onset of Rodinia supercontinent breakup, *Precambrian Research*, v. 220–221, p. 158–176. doi: [10.1016/j.precamres.2012.08.002](https://doi.org/10.1016/j.precamres.2012.08.002)

3

**THE CERRO RAJÓN FORMATION—A NEW LITHOSTRATIGRAPHIC UNIT
PROPOSED FOR A CAMBRIAN (TERRENEUVIAN) VOLCANO-
SEDIMENTARY SUCCESSION FROM THE CABORCA REGION,
NORTHWEST MEXICO.**



The Cerro Rajón Formation—a new lithostratigraphic unit proposed for a Cambrian (Terreneuvian) volcano-sedimentary succession from the Caborca region, northwest Mexico

Arturo J. Barrón-Díaz^{a,b,*}, Francisco A. Paz-Moreno^b, James W. Hagadorn^c

^a Posgrado en Ciencias de la Tierra, Instituto de Geología (ERNO-UNAM), Hermosillo, Mexico

^b Departamento de Geología, Universidad de Sonora (UNISON), Hermosillo, Mexico

^c Department of Earth Sciences, Denver Museum of Nature & Science, Denver, CO, USA

ABSTRACT

A new mappable rock unit, the Cerro Rajón Formation, is proposed for the Cambrian succession of the Caborca region, Sonora, México. Formerly Unit 1 of the Puerto Blanco Formation, the Cerro Rajón Formation is interpreted as a volcano-sedimentary succession deposited along the coast of a passive margin that was impacted by rift-related volcanism. At its proposed type locality, in Cerro Rajón, the Cerro Rajón Formation consists of 270–285 m of tuffaceous conglomerate, metabasalt, mafic tuff, mafic lapillistone, mafic agglomerate, and quartzite with minor siltstone, limestone, and dolostone- and quartzite-dominated conglomerate. The unit contains a major disconformity near its base, where m-to-dm-thick conglomerate locally replaces the fine-grained clastics that make up the base of the Cerro Rajón Formation. $\delta^{13}\text{C}$ chemostratigraphy and biostratigraphy of the Rajón and its bounding strata limits Rajón deposition to the Fortunian Stage of the Terreneuvian Series. Volcanic rocks in the Cerro Rajón Formation are represented by mafic to ultramafic flows, including picobasalts and metabasalts with hydrothermal alteration characteristics, evidenced by replacement of clinopyroxenes by chlorite, actinolite, and epidote. The mineral paragenesis of these volcanic rocks suggests the succession experienced greenschist grade metamorphism. Basalt geochemistry is consistent with low silica (34.32–48.21%) magmatism with high TiO_2 concentrations (3.63–7.52%), related to continental rift volcanism with OIB characteristics. This volcanism could represent the last southern evidence of the rifting process that occurred along the western margin of Laurentia or could be related to volcanic rift deposits further afield.

1. Introduction

The Caborca region contains the most extensive succession of Neoproterozoic and Cambrian rocks in Mexico (Fig. 1; Cooper and Arellano, 1946, 1952; Eells, 1972; Stewart et al., 1984). This succession overlies a crystalline basement first described by Damon et al. (1962), and later defined as the Bámori Metamorphic Complex (Longoria et al., 1978), a highly metamorphosed sequence consisting of metaquartzite and slightly carbonaceous pelitic schist of early Precambrian age. The Aibo Granite, a granite of 1.1 Ga produced from anatexis of the local Precambrian basement (Farmer et al., 2005) is overlain by the Neoproterozoic strata, which are thought to represent an extension of the North American miogeoclinal prism (Stewart, 1982).

The Puerto Blanco Formation is the lowest Cambrian unit within this succession. It was first defined by Cooper and Arellano (1952) based on exposures on the west side of Cerro de la Proveedora, located just west of the town of Caborca where it consists of 293 m of green shale, sandstone and limestone that contain diagnostic Cambrian fossils such as archaeocyathids and olenelloid trilobites. No igneous rocks were reported from the type section. The Puerto Blanco Formation was

later described by Eells (1972) based on exposures in Cerro Aquituni, Cerro Calaveras, Cerro Clemente, and Cerro de la Ciénega. Westerfield (1988) also studied the unit in Cerro Clemente and Cerro Llano Verde. Eells (1972) described the unit as being over 250 m thick and dominated by siltstone, quartzarenite, subarkose and archaeocyathid-bearing limestone. These strata conformably overlie his unit 12, a succession composed of 90 m of volcanoclastic boulder conglomerate litharenite, and trachyoidal porphyritic olivine basalt with olivine, clinopyroxene, plagioclase, chloritized olivine and opaques (Eells, 1972). The Proterozoic succession, including these units, was further delineated by Longoria et al. (1978) and Longoria and Gonzalez (1981), with Longoria (1981) noting the presence of volcanic agglomerates and volcanic breccia in Unit 12. Stewart et al. (1984) integrated these contributions in his analysis of the exposures at Cerro Rajón, formally incorporating this volcanic unit into the Puerto Blanco Formation as its basal member. Thus Eells' (1972) Unit 12 became Stewart et al.'s (1984) Unit 1 of the Puerto Blanco Formation. The main reason for integrating this succession into the Puerto Blanco Formation was the interstratification of the volcanic and volcanoclastic rocks with siltstones and quartzite that are more typical of the lithologies seen at the type section

* Corresponding author. Posgrado en Ciencias de la Tierra, Instituto de Geología (ERNO-UNAM), Hermosillo, Mexico.

E-mail address: arturo.barron@unison.mx (A.J. Barrón-Díaz).

<https://doi.org/10.1016/j.jsames.2018.11.003>

Received 8 October 2018; Received in revised form 1 November 2018; Accepted 2 November 2018

Available online 10 November 2018

0895-9811/ © 2018 Elsevier Ltd. All rights reserved.

at Cerro de la Proveedora. Stewart et al. (1984) indicated that the facies of Puerto Blanco Formation Unit 1 were distinct from the rest of the Neoproterozoic-Cambrian succession in the Caborca region, and that more work was needed to delineate and characterize them.

Sour-Tovar et al. (2007) and Loyd et al. (2012, 2013) built on this earlier work by refining the biostratigraphic framework for the succession and augmenting it with a $\delta^{13}\text{C}$ and $\delta^{34}\text{S}$ chemostratigraphic framework. This work identified the isotopic nadirs associated with the Wonoka-Shuram event and the Precambrian-Cambrian boundary, fostering correlation between the strata of Sonora and comparable strata in Death Valley, California and elsewhere. It also helped refine the position of the Ediacaran-Cambrian boundary, suggesting it occurs above the $\delta^{13}\text{C}$ isotopic nadir in Unit 4 of the La Ciénega Formation, but below the occurrence of *Treptichnus pedum* in the basal portion of Unit 1 in the Puerto Blanco Formation. The volcanic and volcanoclastic portion of Unit 1 thus reflects events that transpired shortly after the Ediacaran-Cambrian transition.

This volcano-sedimentary succession is dominated by mafic pyroclastic rocks and mafic volcanic flows that have basic to ultrabasic geochemical characteristics consistent with formation in an intracontinental rift zone (Hagadorn, 2009; Barrón-Díaz, 2013; Hagadorn and Holm-Denoma, 2016; Barrón-Díaz et al., 2018). The metabasalts and metabasalts of Puerto Blanco Formation Unit 1 are hydrothermally altered. These rocks and the other Proterozoic-Paleozoic strata of the region have also been intruded by the Sonora Laramide Batholith (Ramos-Velázquez et al., 2008; Radelli et al., 2008; Leyva-Ruiz et al., 2017). Contact metamorphism from this magmatic event inhibits dating of volcanic sequences of the Puerto Blanco Formation Unit 1 using conventional approaches like $^{40}\text{Ar}/^{39}\text{Ar}$ (Barrón-Díaz, 2013; Barrón-Díaz et al., 2018). Nevertheless, picobasalt flows are still preserved in the unit, and they have primary diopside crystals that suggest alkaline magmatism with low fusion rates. Although volcanic rocks occur elsewhere in Sonora's Neoproterozoic succession (Stewart et al., 1984; Centeno-García et al., 2002; Barrón-Díaz, 2013), these mafic flows likely represent sills intercalated between underlying sedimentary rocks and are not treated here.

Given its timing, the rift-related nature of its volcanism, and our refined understanding of its depositional-setting, Unit 1 of the Puerto Blanco Formation merits elevation from member status to a formal formation designation. Below we describe this unit based on analyses of seven measured sections in the vicinity of Rancho Bámori, we interpret its depositional and petrogenic history, and we propose naming it the Cerro Rajón Formation, after the localities in which it is best exposed.

2. Geological setting

This volcano-sedimentary succession is best exposed in the southern portion of Cerro Rajón (Figs. 1 and 3), where it is sandwiched in an ~2 km thick Neoproterozoic-Cambrian package of sedimentary rocks that nonconformably overlie metamorphic basement to the southeast. Elsewhere in the region, the easily-weathered volcanic flows and pyroclastic rocks of the proposed new formation are often completely covered by alluvium, or are identifiable by subcrop or volcanic residuum. Exceptions include Cerro San Agustín, Cerro los Apaches, Cerro Calaveras, and Cerro de la Ciénega, where much of the succession is visible.

3. Results

3.1. The Cerro Rajón Formation

Owing to the volcanic nature of its constituent lithologies, Stewart et al. (1984) indicated that Puerto Blanco Formation Unit 1 differed substantially from the rest of the formation, and intimated that it merited different consideration from the rest of the succession. Our proposal to elevate Puerto Blanco Formation Unit 1 to have its own new formation name follows Stewart's (1984) work and is grounded in four observations:

i) the unit sharply differs from lithologies of the underlying La Ciénega Formation and the overlying Unit 2 of the Puerto Blanco Formation; ii) the unit's contacts can locally be walked out for 100s of meters laterally (Fig. 2); iii) the unit is thick enough (90–270 m) and lithologically different enough from adjacent rocks such that its subcrop and residuum is still mappable and topographically distinctive from adjacent rocks; and iv) the unit can be readily mapped across many kilometers of exposure in the Caborca region (*sensu* Eells, 1972; Longoria, 1981).

The description of the Cerro Rajón Formation type section follows, and adheres to requirements of the North American Commission on Stratigraphic Nomenclature (2005; see summary in Table 1).

The Cerro Rajón Formation (previously Unit 1 of the Puerto Blanco Formation) is defined as a volcano-sedimentary succession of tuffaceous conglomerate, metabasalt, mafic tuff, mafic lapillistone, mafic agglomerate and quartzite with minor siltstone, limestone, dolostone and sedimentary conglomerate (Fig. 3). The relative abundance of each of the Cerro Rajón Formation lithologies varies considerably from one locality to another within the Caborca region, but at all studied localities the primary and reworked volcanic rock types predominate. At or just above its base the Cerro Rajón often has a massive quartzite- and dolostone-dominated conglomerate that locally grades into breccia; its clasts are remarkably similar to lithologies known from underlying clastic and carbonate units. Locally this conglomerate incises thinly bedded siltstone and quartzite but elsewhere these are absent and the conglomerate lies directly atop dolostone of the underlying Unit 4 of the La Ciénega Formation. The top of the Cerro Rajón Formation is typically characterized by up to 55 m of basalt that is locally incised by the basalmost conglomerate or very coarse-grained quartzite of Unit 2 of the Puerto Blanco Formation.

In many localities, the Cerro Rajón Formation is heavily eroded or buried. However, even when less resistant beds within the unit are only visible as subcrop or residuum, many of the thicker volcanic flows are visible as outcrop because they are capped by more erosion-resistant quartzites.

3.1.1. Cerro Rajón (type section)

Cerro Rajón exhibits the most complete and representative succession of the proposed Cerro Rajón Formation and is proposed as the type section for the unit. The base of the measured section and graphic log of the type Cerro Rajón Formation is at 30°25'10.99"N, 111°56'50.54"W and its top is at 30°25'21.47"N, 111°56'58.97"W (Fig. 3).

In the type section, the Cerro Rajón Formation is 270 m thick (Fig. 4). Its base consists of up to 21.5 m of medium grained trough cross-bedded to planar-bedded orthoquartzite with minor intercalated purple mudstone that bears a suite of characteristically Phanerozoic trace fossils including *Aulichmites*, *Diplichnites*, *Gordia*, *Planolites*, *Skolithos*, and *Treptichnus*. Along strike this clastic sequence is truncated from above by massive (up to 10 m thick) cliff-forming conglomerate (Fig. 5A). The conglomerate is locally a breccia and is dominated by clast-supported pebble-to ≤ 1.5 m-diameter boulder-sized subrounded to tabular clasts of quartzite, sandy dolostone, and dolostone with minor limestone, basalt, and mudstone clasts. Inclined internal stratification, normally-graded bedding and imbricated clasts occur, and the conglomerate has a well-rounded very coarse to granular quartz groundmass (Fig. 5B). This conglomerate is overlain by tuffaceous pebble to boulder conglomerate (Fig. 6A) which progressively has more volcanic material, until it becomes a mafic agglomerate over 50 m thick (Fig. 6B). It is intercalated with mafic tuff and lapillistone. This portion of the unit is overlain by up to 45 m of laminated very fine-grained quartzite and shale that locally exhibits burrowing (including *Planolites*, *Skolithos*, *Treptichnus*), ripple cross-lamination, and flute and groove casts. It is overlain by up to 12 m of intraformational limestone-dolostone conglomerate that bears tabular dolostone clasts and by sandy cf. *Arenicolites* burrow-mottled limestone and medium grained quartzite. Above this portion of the succession is up to 30 m of intercalated lapillistone, tuff, tuffaceous conglomerate, sandy limestone, and very fine quartzite and mudstone. The upper part of the

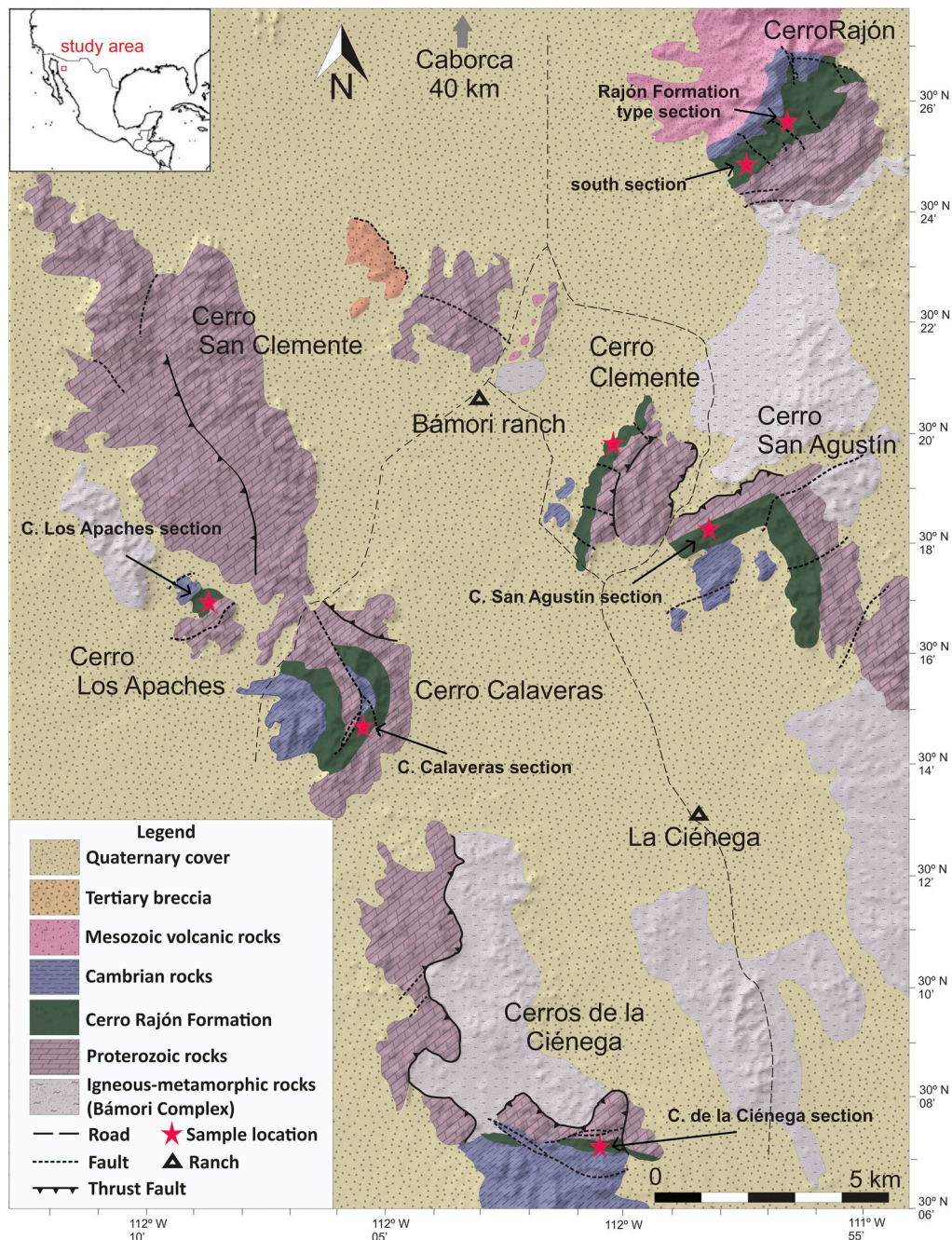


Fig. 1. Simplified geologic map of the study area, south of the city of Caborca, Sonora, México. Sample locations and measured section locations are included. Modified from Barrón-Díaz et al. (2018).

Cerro Rajón Formation is characterized by up to 35 m of tuffaceous conglomerate and minor fine grained quartzite that grades upward into agglomerate rich in volcanic bombs up to 1 m in diameter (Fig. 6B), overlain by up to 55 m of metabasalt. The latter contains three flows which are, from bottom to top, ~14, ~17, and ~24 m thick. The uppermost metabasalt has abundant actinolite crystals derived from the alteration of the clinopyroxene and the lowermost metabasalt has abundant actinolite and calcite veining. Olivine pseudomorphs and large Fe–Ti oxides also occur as phenocrysts (Barrón-Díaz et al., 2018).

The thick metabasalt that defines the top of the Cerro Rajón Formation is overlain by a 10–50 cm thick conglomerate that grades upward into an up to 3 m thick trough cross-bedded coarse quartzite (Fig. 7A) that was originally included in Unit 1 of the Puerto Blanco Formation (Stewart et al., 1984). The basal conglomerate of Unit 2 of the Puerto Blanco Formation is dominated by quartz and basalt pebbles

and cobbles (Fig. 7B). Because this contact is sharp and readily identified in the field, we remove this conglomerate-quartzite from Unit 1 of the Puerto Blanco (the Cerro Rajón Formation proposed herein) and refer to it as the base of Unit 2 of the Puerto Blanco Formation (Fig. 3). The upper portions of this quartzite and the overlying 11 m of very fine to very coarse quartzite are intercalated with thin ribbon limestone and intraformational limestone- and dolostone-conglomerate. 28 m above the top of the Cerro Rajón Formation, *Obolella*-like brachiopod pavements occur on bed tops of thin limestones.

3.1.2. Cerro Rajón South

In the southern portion of Cerro Rajón, the Cerro Rajón Formation is ~250 m thick (Fig. 8). The base consists of a highly tectonized 7 m thick quartzite that directly overlies the upper dolostone of Unit 4 of the La Ciénega Formation. The quartzite is overlain by ~100 m of partially

	Cooper and Arellano (1952)	Eells (1972)	Longoria and González (1981)	Stewart et al. (1984)	Sour-Tovar et al. (2007)	Barrón-Díaz et al. (2018)	This study	
Cambrian	Provedora Quartzite		Provedora Quartzite		Provedora Quartzite		Provedora Quartzite	
	Puerto Blanco Fm.	Upper	Puerto Blanco Fm.	Upper	Puerto Blanco Fm.	Unit 4	Puerto Blanco Fm.	Unit 4
		Middle		Middle		Unit 3		Unit 3
		Lower		Lower		Unit 2		Unit 2
Not Exposed		Unit 12	Gachupín Group	Unit 1	Unit 1	Unit 1	Cerro Rajón Fm.	
		Unit 11		La Ciénega Fm.	La Ciénega Fm.	La Ciénega Fm.	La Ciénega Fm.	
				Tecolote Quartzite	Tecolote Quartzite	Tecolote Quartzite	Tecolote Quartzite	

Fig. 2. Evolution of stratigraphic lexicon for the Puerto Blanco Formation (in gray), including the proposed Cerro Rajón Formation, and the relative position of the Ediacaran-Cambrian boundary (dark line).

buried tuffaceous conglomerate, which weathers to volcanoclastic subcrop and residuum. This conglomerate has up to 30 cm wide volcanic clasts of metabasalt with propylitic alteration and near its base has 10 cm diameter quartzite clasts. The top 10 m of the tuffaceous conglomerate is intercalated with a laminated sandstone with thin quartzite beds. The quartzite is overlain by a 6 m thick metabasalt whose base has a tempered and scoriaceous surface. Silica veins occur in the

lower and top members of the metabasalt, whereas the middle member contains epidote veins and fresh diopside phenocrysts. The upper part of the Cerro Rajón Formation consists of ~100 m of *Skolithos*-bearing quartzite, siltstone and tuffaceous conglomerate. Dolostones up to 30 cm thick occur in the middle and upper portions of the quartzite. Overlying a suite of pyroclastic rocks, an up to 6 m thick volcanic metabasalt occurs at the top of the Cerro Rajón Formation. It contains

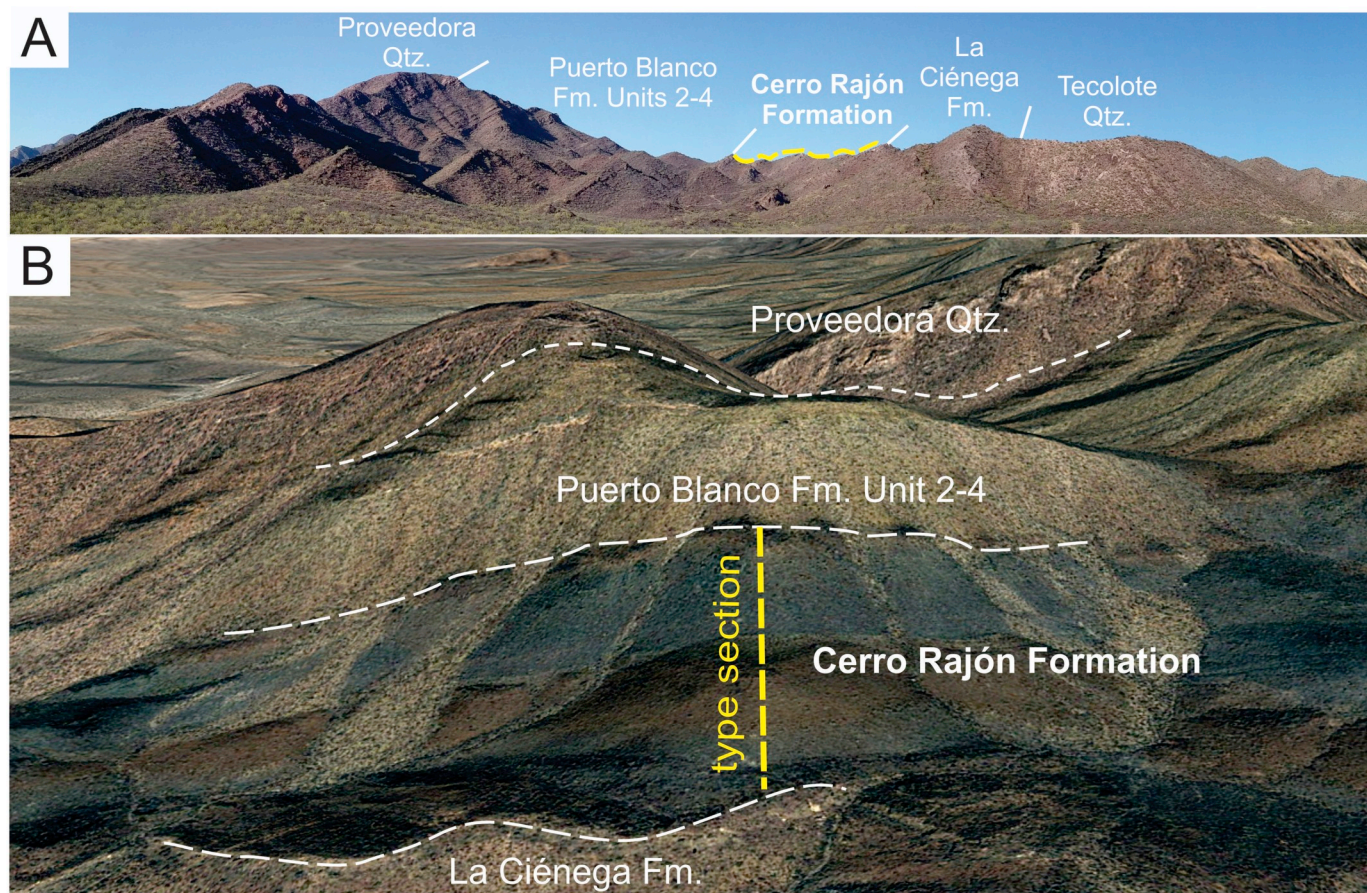


Fig. 3. A. Panoramic image of the western flank of Cerro Rajón, illustrating the proposed type section for the Cerro Rajón Formation (yellow dashed line) and some of the major ridge-forming units in the succession. B. Northwest oblique satellite image of the area surrounding the proposed type section (yellow dashed line), and approximate unit contacts (white dashed lines). Field of view in A is ~6.5 km wide; B is ~1.3 km wide; B is from Google Earth. (For interpretation of the references to color in this figure legend, the reader is referred to the Web version of this article.)

Table 1

Summary of how the proposed Cerro Rajón Formation meets the requirements for formally naming geologic units according to the [North American Commission on Stratigraphic Nomenclature \(2005\)](#).

The Cerro Rajón Formation		
Requirements for naming a new stratigraphic unit		
Article	Article name	Description
5	Intent and utility	See description in section 4.1
6	Category and rank	Lithostratigraphic
7	Name	Cerro Rajón Formation
8	Stratotype	Cerro Rajón type section Fig. 3
8a	Type locality	Cerro Rajón
9	Unit description	See description in section 3.1
10	Boundaries	Upper contact at base of basal quartzite/ conglomerate of Puerto Blanco Fm. Unit 2. Lower contact with top of uppermost dolostone of La Ciénega Fm. Unit 4
11	Historical background	See description in section 1
12	Dimensions and regional relations	See discussions in section 4.1
13	Age	Terreneuvian (Cambrian)
14	Correlation	See discussion in section 4.2
15	Genesis	Alkaline rift-related volcanism, coastal continental and marine sedimentation. See details in section 4

abundant amygdules and vesicles at the bottom of the unit that are sometimes filled with detrital material. A mixture of fine-grained detrital material within the basalt is observed towards the top of this unit. As in the Cerro Rajón type section, this basalt is capped by a conglomeratic-to coarse-quartzite, which defines the base of Unit 2 of the Puerto Blanco Formation.

3.1.3. Cerro San Agustín

At Cerro San Agustín, the Cerro Rajón Formation is estimated to be ~100 m thick based on the projected thickness of volcano-sedimentary outcrop and residuum that lies between the dolostone of the La Ciénega Unit 4, and the basal quartzite-conglomerate of Puerto Blanco Unit 2 ([Fig. 8](#)).

Here the basalmost portion of the Cerro Rajón Formation is covered, and the first identifiable outcrop is a tuffaceous conglomerate ~40 m above the uppermost exposed dolostone of the La Ciénega Formation. Higher in the section there are mafic tuffs, trough cross-bedded quartzites and a distinctive 6 m thick picobasalt. The latter appears to be the least altered example of a volcanic flow in the region. The picobasalt is characterized by a scoriaceous base with abundant quartz- and carbonate-amygdules and olivine pseudomorphs, a well preserved middle member with porphyritic texture and clinopyroxene phenocrysts, and columnar jointing ([Fig. 9](#)). This particular picobasalt is described in greater detail in [Barrón-Díaz \(2013\)](#) and [Barrón-Díaz et al. \(2018\)](#). 5 m above the quartzite of Unit 2 of the Puerto Blanco Formation is 30 m of intercalated limestone and mudstone that bears rynchonelliform brachiopods, similar to those observed in comparable strata in the Cerro Rajón type section.

3.1.4. Cerros Los Apaches

At Cerro Los Apaches, the Cerro Rajón Formation is ~270 m thick and dominated by quartzite, metabasalt and polymict conglomerate ([Fig. 8](#)). Mafic agglomerate, tuffaceous conglomerate and mafic tuff also occur in the lower portion of this section. The succession is vertical and at its base the section can be repeated by faults, leading to over-estimation of its true thickness. Thus the lower limit of the Cerro Rajón Formation is hard to determine in this locality. Although obscured, this boundary could be in two locations. The first possible basal contact could be between the basalmost tuffaceous conglomerate and a nearby outcrop of dolostone, a relationship also observed in the type section

and in the Cerro Rajón South section. A second possible lower limit is at the base of a *Skolithos*-bearing quartzite that contains two greenstones up to 60 cm thick and is overlain by a polymict conglomerate that bears abundant quartzite clasts. We tentatively favor the first interpretation.

As interpreted, the base of the Cerro Rajón Formation in Cerros Los Apaches consists of ~30 m of tuffaceous conglomerate, mafic agglomerate, mafic tuff and a 3 m thick quartzite overlain by 21 m of sandstone intercalated with thin mudstone. A 1 m thick greenstone rests atop the sandstone unit. It is overlain by 15 m of pink quartzite, followed by another 60 cm thick bed of greenstone. This greenstone has a 15 cm thick black base (hypothesized to be dominated by Mn-oxides) overlain by a porphyritic center and a tempered top. These strata are overlain by up to 40 m of *Skolithos*-bearing quartzite which is then overlain by conglomerate with fragments of the underlying quartzite. Higher in the section the uppermost part of the unit has at least two metabasalts with abundant large titanomagnetite phenocrysts. These metabasalts are intercalated with quartzite and their thickness varies laterally. The upper contact of the metabasalt is covered but approximately 2 m above the uppermost metabasalt is a 1.5 m thick limestone overlain by a quartzite and a 12 m thick Fe-rich sandstone. The limestone-sandstone-quartzite relationship continues for at least 100 m.

3.1.5. Cerro Calaveras

In Cerro Calaveras, the Cerro Rajón Formation is at least 200 m thick but this is an incomplete thickness because the section is overturned and its base is faulted. We measured a partial section through the unit where it is relatively thick yet reasonably well exposed ([Figs. 1 and 8](#)).

Here the lower half of the Cerro Rajón Formation consists of ~100 m of intercalated metabasalt, tuffaceous conglomerate and mafic tuff, resting over a ~20 m thick sandstone. Four metabasalts, each ~20 m thick, occur above this sandstone. The lower two exhibit ultramafic characteristics, porphyritic texture and large clinopyroxene and titanomagnetite oxides ([Fig. 9](#); [Barrón-Díaz et al., 2018](#)). The upper flow is slightly more differentiated with a porphyritic lower member and an aphanitic top. This last volcanic flow rests atop a tuffaceous conglomerate ~55 m thick with abundant metabasalt clasts up to 30 cm in diameter. The clasts are strongly deformed and crushed, and some clasts have merged with others. A 20 m thick cliff-forming suite of intercalated sandy limestones and Fe-rich sandstone caps the succession here. They weather blue to yellow and bear distinctive 1 cm diameter purple oxidized pyrite crystals.

The lower contact of the Cerro Rajón Formation is a structural contact that brings the basal sandstone close to the dolostone of Unit 4 of the La Ciénega Formation. Similarly, the upper contact of the Cerro Rajón Formation is truncated by a fault and is not exposed.

3.1.6. Cerros de la Ciénega

At Cerros de la Ciénega, the lithology of the Cerro Rajón Formation varies considerably—from a tuffaceous conglomerate-dominated succession to the east, to a pyroclastic- and agglomerate-dominated succession to the west. At our measured section, the top of the unit is not exposed but the unit is at least 100 m thick ([Fig. 8](#)). The base of the formation consist of ~30 m of mafic tuff and lapillistones. The basal part of the succession directly overlies intercalated dolostone and sandstone, and is mainly subcrop and residuum. It contains a ~10 m thick interval dominated by tuffaceous conglomerate that appears to grade laterally into agglomerate. This succession is overlain by a distinctive ~20 m thick mafic tuff with agglomerate ([Fig. 10A](#)). The mafic tuff has notable *Gordia*-, *Planolites*-, and *Teichichnus*-like burrows and *Harlaniella*-like fossils ([Fig. 10B](#)). A metabasalt 4.5 m thick occurs in the middle of the section. It has a porphyritic texture with clinopyroxene phenocrysts and calcite veins. The uppermost portion of the Cerro Rajón Formation consists of ~40 m of tuffaceous conglomerate with metabasalt clasts, which gradually becomes a mafic agglomerate up section. It is overlain by a prominent cliff-forming mafic tuff. The upper

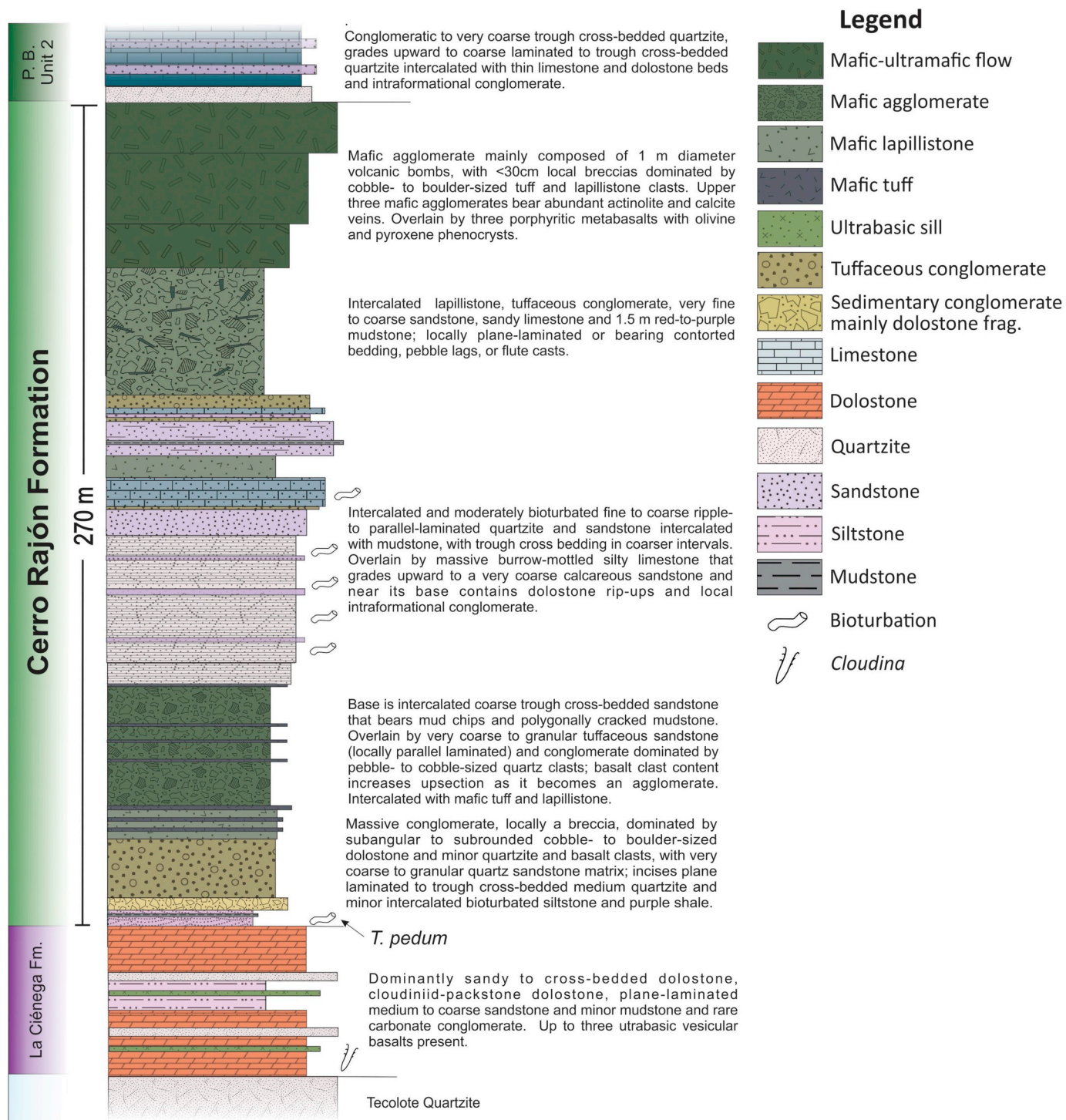


Fig. 4. Condensed graphic log of the type section of the Cerro Rajón Formation, illustrating predominant lithologies, bedforms and key fossil occurrences.

contact of the Cerro Rajón Formation is obscured by alluvium, but stratigraphically above this interval lie carbonates like those of Unit 2 of the Puerto Blanco Formation. It is unclear how much section is covered or missing near this contact.

3.1.7. Cerro Clemente and Cerro Llano Verde

The Cerro Rajón Formation also occurs along the northwest flank of Cerro Clemente (Fig. 1). Here the thickness of the unit is uncertain because its upper portions are obscured by alluvium. Westerfield (1988) logged at least 61 m of basalt, volcanoclastic sandstone, and volcanoclastic conglomerate and sandstone in this region. In the western portions of

Cerro Clemente, the Cerro Rajón Formation exposures consists of a Fe-rich sandstone overlain by a 5 m thick metapicrobasalt with a porphyritic texture, diopside and phlogopite phenocrysts and an absence of plagioclase (Barrón-Díaz, 2013). This volcanic rock varies considerably in texture along strike. For example, ~200 m south along strike, the unit's phenocrysts are bigger and it has a scoriaceous, vesicular base. The metapicrobasalt contains phlogopite crystals and weathers yellow.

3.1.8. Cerro Pozo Serna

Farmer et al. (2001) identified Unit 1 of the Puerto Blanco Formation in a locality 11 km southwest from Cerro Calaveras known as Cerro

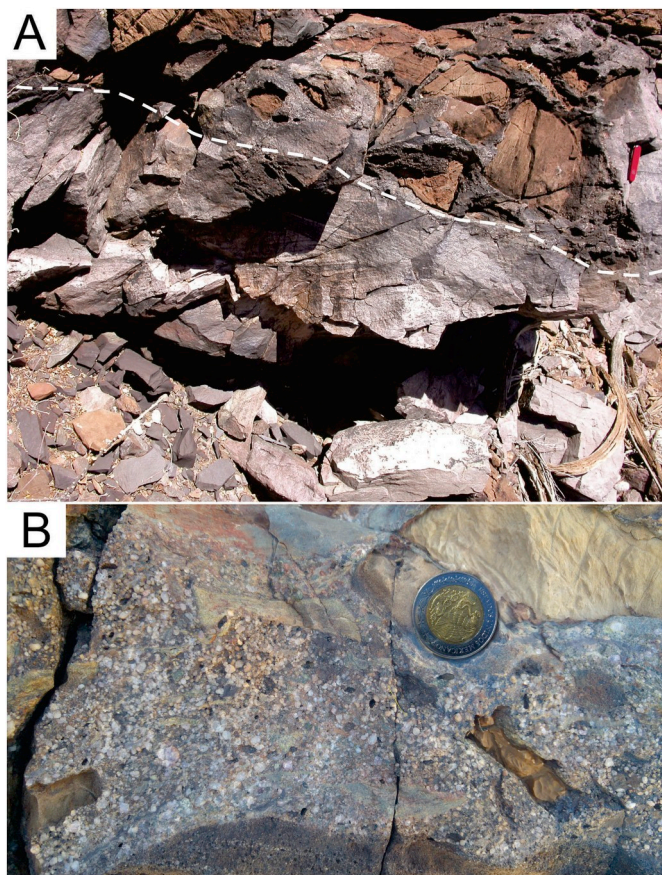


Fig. 5. A. Brecciated portion of the massive dolostone conglomerate that incises (dashed line) the basal quartzites of the Cerro Rajón Formation; Cerro Rajón. B. Typical granular to very coarse quartz-dominated groundmass of the conglomerate; Cerro Rajón. Knife in A is 8.5 cm long and coin in B is 2.5 cm wide.

Pozo Serna. No volcanic rocks were reported from this locality and we were unable to confirm the presence of the Cerro Rajón Formation here.

3.2. Petrography

The volcanic flows and volcanic clasts from the tuffaceous conglomerates and agglomerates can be divided into two groups. The ultramafic group is characterized by abundant clinopyroxene crystals, mostly altered to actinolite, and an absence of plagioclase. The mafic group contains slightly more differentiated rocks, where albitized plagioclase is common in the groundmass.

Volcanic rocks exhibit considerable variation in hydrothermal alteration – both within the succession and between localities (Barrón-Díaz et al., 2018). For example, the tuffaceous conglomerate clasts show total replacement of their primary mineralogy. Calcite, chlorite, actinolite, sphene and epidote are the dominant metamorphic minerals. Calcite veins and carbonatization occurs in some clasts (Fig. 9). Large titanomagnetite phenocrysts also occur, and exhibit a skeletal habit. Such crystals could have formed from ilmenite, which due to the alteration, were transformed to titanomagnetite.

Yet some volcanic flows preserve primary mineralogy such as diopside crystals. Fresh clinopyroxene cores also occur, and confirm the alkaline and anorogenic signature of this volcanism (Barrón-Díaz, 2013).

3.3. Biostratigraphy & chemostratigraphy

The Cerro Rajón Formation is biostratigraphically underlain by latest Ediacaran cloudinids, which in the type section occur between

49 and 88 m below the contact with the Cerro Rajón Formation in Unit 1 of the La Ciénega Formation and whose uppermost occurrence in the type section coincides with the end-Ediacaran $\delta^{13}\text{C}$ isotopic nadir (Lloyd et al., 2013). The Cerro Rajón Formation contains a diverse suite of bed-penetrating and bed-parallel trace fossils (Figs. 10 and 11). Body fossils were not observed in its carbonate nor its clastic facies. The first macroscopic Cambrian body fossils occur 28 m above the top of the Cerro Rajón Formation in the type section, and include Cambrian Stage 2 (Terreneuvian) rhynchonelliform brachiopods similar to *Obolella* (Fig. 11; also see Stewart et al., 1984). Elsewhere, for example in Cerro San Agustín, these brachiopods occur 60 m above the inferred top of the Cerro Rajón Formation. In Cerro Rajón, *Fritzaspis* Assemblage Zone trilobites appear 16 m above these brachiopods, signaling the arrival of the first trilobites and onset of Series 2 Cambrian time. Systematic variations in the $\delta^{13}\text{C}$ and $\delta^{34}\text{S}_{\text{CAS}}$ chemostratigraphy of Unit 2 of the Puerto Blanco Formation are similar to those exhibited by Stage 2 successions in Death Valley and elsewhere in the world (Lloyd et al., 2012, 2015). Collectively these fossils and isotopic signatures restrict deposition of the Cerro Rajón Formation to Fortunian time. If chemostratigraphic correlations are correct and if bounding fossils represent last and first fossil occurrences, correlation of these events to geochronologically better constrained successions (e.g., Maloof et al., 2005; Fike et al., 2006; McFadden et al., 2008; Schmitz, 2012) constrains deposition of the Cerro Rajón Formation to an interval between ~530 and 541 Ma.

3.4. Geochemistry

The volcanic flows and the volcanic clasts from tuffaceous conglomerates and agglomerates are derived from low-silica volcanism ($\text{SiO}_{2\text{N}} = 34.32\text{--}48.21\%$) with high TiO_2 concentrations (3.63–7.52%).

Geochemical analyses support the presence of a mafic and ultramafic group of volcanic rocks. This interpretation is reinforced by the primary mineralogy preserved in the picrobasalts and metabasalts, as well as in the tuffaceous conglomerate's volcanic clasts (Barrón-Díaz et al., 2018). Hypabyssal sills from the La Ciénega Formation also have ultrabasic characteristics (Centeno-García et al., 2002).

Metamorphic events considerably impacted the SiO_2 , Na_2O and K_2O concentrations of the Cerro Rajón Formation magmatism. Hydrothermal alteration caused propylitic alteration and carbonatization in most of the magmatic products in this formation.

Given these constraints, the Cerro Rajón Formation volcanic flows and volcanic clasts protoliths can all be classified, in a board spectrum, as alkaline basalts, and their geochemistry implies emplacement via intraplate volcanism and OIB-type magmatism. Detailed geochemical descriptions are in Barrón-Díaz et al. (2018).

4. Discussion and implications

The Cerro Rajón Formation is a distinctive volcanic and volcanoclastic unit, containing metabasalts, picrobasalts, tuffaceous conglomerates, mafic tuffs, mafic lapillistones and mafic agglomerates. These rock types and their associated structures and spatial relationships are interpreted to represent volcanic flows, pyroclastic falls and collapse of volcanic structures. Rocks representing these phenomena are present at every known major exposure of the unit, albeit the distribution of such features varies from section to section. Such variation probably represents different volcanic centers, which mainly started with Strombolian-type eruptions, producing volcanic structures such as cinder cones, where all the volcanic activity occurred over a geologically short period of time. Pyroclastic events are intercalated with low volume effusive events. These volcanic flows probably were only a few meters thick and their preservation was controlled by the paleotopography. Outcrops with thicker volcanic packages may correspond to inverted topography, whereby several volcanic flows were deposited in a paleochannel or paleolow. This interpretation helps explain the

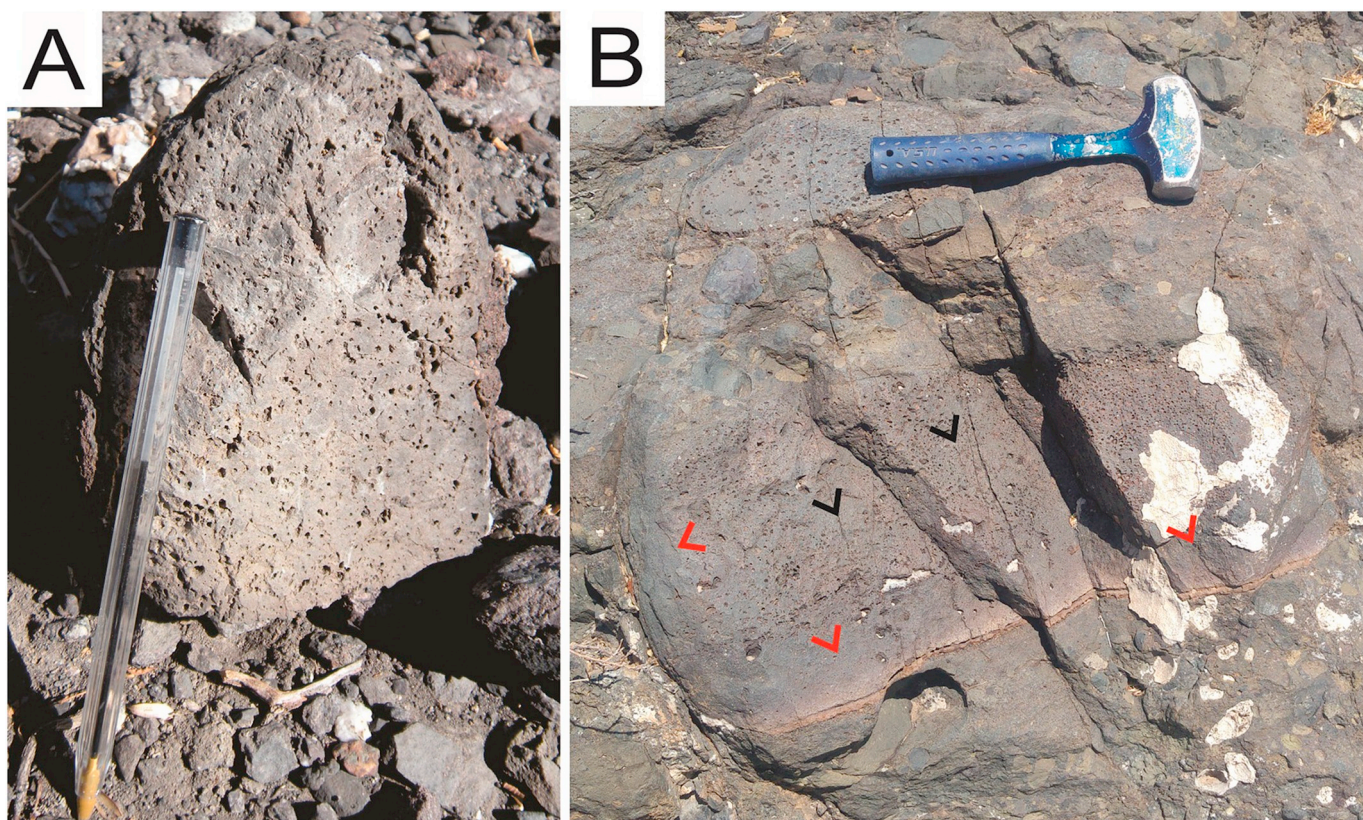


Fig. 6. A. Metabasaltic volcanic clast from the tuffaceous conglomerate facies that dominates the lower half of Cerro Rajón Formation; Cerro Calaveras. B. Mafic agglomerate that overlies the tuffaceous conglomerate in the lower half of the Cerro Rajón Formation; Cerro Rajón. A large volcanic bomb lies below the rock hammer. Red arrowheads indicate the tempered base where the bomb hit the ground and the sides where the bomb is inferred to have hit previously unconsolidated material or been cooled by the atmospheric contrast of temperatures, causing the center of the bomb to cool more slowly and develop a porphyritic texture (black arrowheads). White crust at right is caliche. Pen in A is 15 cm long; hammer in B is 30 cm long. (For interpretation of the references to color in this figure legend, the reader is referred to the Web version of this article.)

uneven lateral distribution of Cerro Rajón Formation volcanism, whereby the detailed characteristics and distribution of preserved volcanic rocks in each studied locality is controlled by the particular volcanic history in that region, and the subsequent effects of erosion. For example, the measured section in Cerros de la Ciénega records the most intense pyroclastic activity in the region, as represented by ~100 m of mafic tuff, mafic lapillistone and mafic agglomerate—indicating proximity to a volcanic vent.

Although we do not have sufficient geochronologic control to constrain the nuances of differential erosion between our studied sections, the major erosional unconformities are similar between our seven studied sections, such as the conglomerate-filled paleo-incision near the base of the Cerro Rajón Formation, and the conglomeratic-to very coarse quartzite that represents reworking of the uppermost Cerro Rajón Formation metabasalts.

The Cerro Rajón Formation is not the first succession whose volcanic event stratigraphy rapidly changes laterally from one locality to another. Rather, this phenomenon typifies certain types of low-volume volcanic fields whose overall preservational potential is low. Where their remnants are preserved, their most resistant elements, such as volcanic flows, predominate. For example, the Quaternary Pinacate Volcanic Field in northwest Mexico is also dominated by alkaline basalt representing emplacement in a setting dominated by several maars, hundreds of cinder cones and associated lava flows (Lynch, 1981; Lynch et al., 1993). Such features were emplaced, like the Cerro Rajón Formation's volcanics, close to a plate margin in an extensional tectonic setting.

The Cerro Rajón Formation volcanic rocks have alkaline within-plate basalt signatures (Barrón-Díaz, 2013; Barrón-Díaz et al., 2018) that demonstrate they were emplaced as volcanic flows in a continental

intraplate setting. The succession is affected by a greenschist grade metamorphism observed in the metamorphic mineralogy (actinolite, albite, chlorite, calcite and epidote) of the volcanic flows and tuffaceous conglomerates volcanic clasts. Barrón-Díaz et al. (2018) described this alteration in the tuffaceous conglomerates and approximate metamorphism temperatures from 400 to 500 °C. The volcanic flows often show evidence of interaction with shallow water environments. This relationship is observed in the quench surfaces, columnar jointing and scoriaceous bases observed in some volcanic lavas. For example, the thinnest (~60 cm) volcanic flows in the region are from Cerro Los Apaches (Fig. 8), where their tops are fine grained and greenish in color - features often related to water interaction. The base of these flows also contain thin carbonate layers, indicating that carbonate rich sediments were present during emplacement of the flow. Similarly, the thick volcanic flow at the top of the Cerro Rajón Formation in the Cerro Rajón South section (Fig. 8) bears evidence for interaction of a lava flow with unconsolidated muds, which produced a peperite (Fig. 7C and D). Although such characteristics illustrate interaction of volcanism with water and with hydrated sediment, no pillow structures were found, despite the presence of abundant spheroidal weathering. We interpret the absence of such pillow structures to indicate that the depocenter lacked significant water depth at the time when flows impacted the water, either because of local buoying of the landscape associated with maar development, or because of eustatic or within-basin sea level lowstand.

The Cerro Rajón Formation igneous and volcanoclastic strata are bounded by and contain clastic and carbonate strata that bear fossils, structures, fabrics, and bedforms consistent with deposition in subtidal to peritidal coastal marine to continental settings (see syntheses in Stewart et al., 1984, Sour-Tovar et al., 2007; Pope et al., 2012). Even in

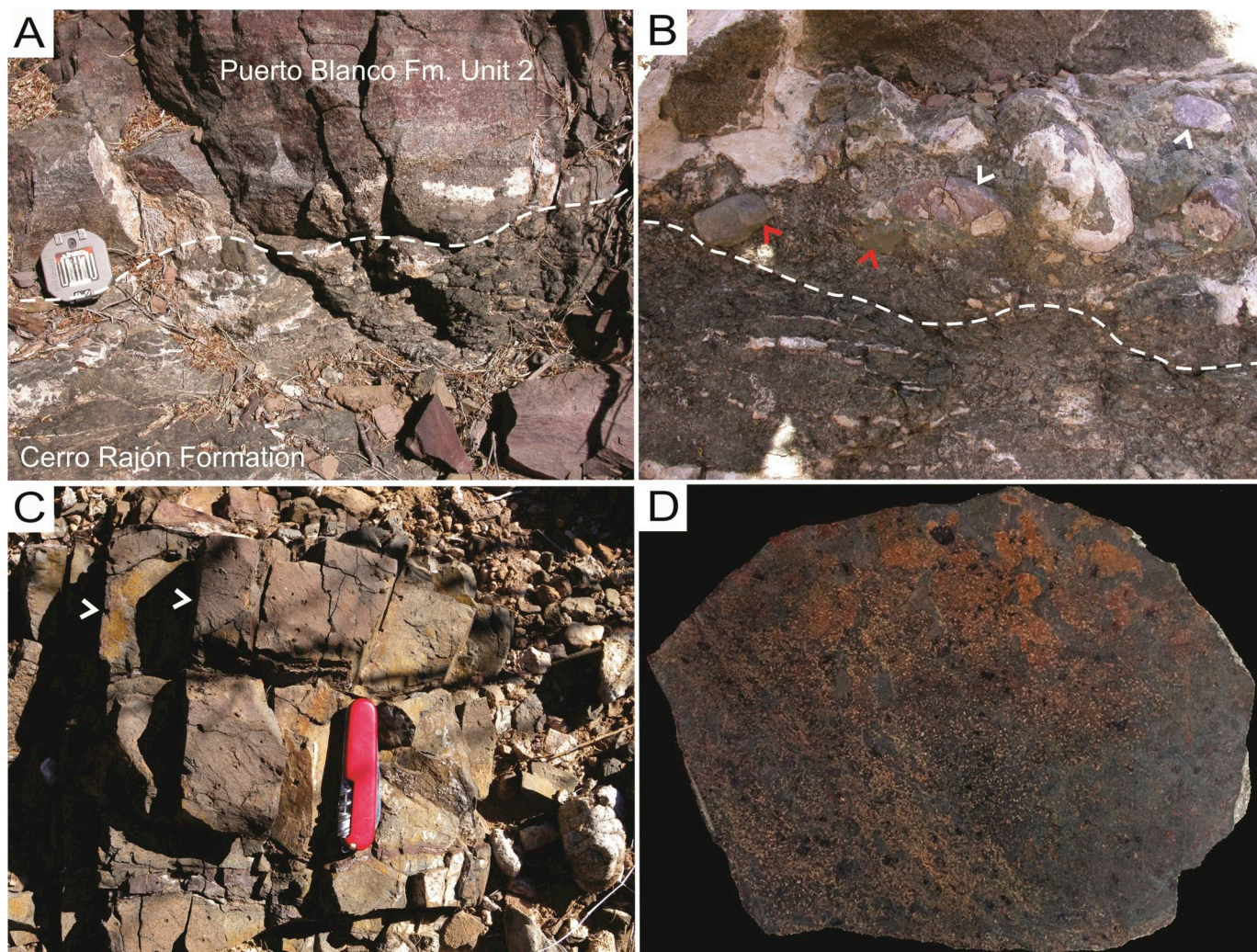


Fig. 7. A. Erosive contact at the top of the Cerro Rajón Formation (dashed line); here the basal portion of Unit 2 of the Puerto Blanco Formation is characterized by a granular to pebbly lag; Cerro Rajón. B. Close-up of the basal conglomeratic quartzite of Unit 2 of the Puerto Blanco Formation (contact is dashed), illustrating reworked rounded metabasalt (red arrowheads) and quartz cobbles (white arrowheads); Cerro Rajón. C. Cross-sectional view of picrobasalt, illustrating incipient columnar jointing (white arrowheads) developed at the top of the flow; Cerro San Agustín. D. Polished slab of the peperite that caps the Rajón South section. Orange to yellow grains are sedimentary material, whereas gray and darker areas represent the volcanic flow. Brunton compass in A is 7.5 cm wide. Field of view in B is 50 cm wide. Knife in C is 7.6 cm long. Field of view in D is 25 cm wide. (For interpretation of the references to color in this figure legend, the reader is referred to the Web version of this article.)

the face of intense pyroclastic activity, possibly including deposition of airborne tephra and or lahars, marine organisms thrived. In this vein, the bioturbated tuff and agglomerates in the Cerros de la Ciénega succession illustrate not only to the ability of marine animals to colonize volcanic deposits, but reinforces evidence from peperites in the succession that volcanic activity occurred in and adjacent to very shallow marine and intermittently emergent environments.

These observations are internally consistent with the broader paleoenvironmental and paleogeographic context hypothesized for Sonora's Cambrian successions (Lochman-Balk, 1956; Stewart et al., 2001, 2002; Hagadorn, 2011), indicating that the volcanic loci were within and along the coastline of a shallow continental platform.

4.1. Local correlations

The Cerro Rajón Formation only occurs in the Caborca region of Sonora, despite the presence of abundant Cambrian (including possibly Terreneuvian) successions in other localities in Sonora (Stewart et al., 2002). These other successions are sedimentary in origin and lack pre-Jurassic volcanic rocks. Geochemical characteristics of the Cerro Rajón

Formation volcanism indicate low melting rates (Barrón-Díaz, 2013) and a lack of extensive magma differentiation. These features imply that only low volumes of volcanic products were produced. These characteristics are also consistent with the volcanic material being produced at the end of a non-developed rift arm or aulacogen, where the volcanism began as fissure volcanism and then later aborted. In either scenario, the Cerro Rajón Formation volcanics indicate a low volume of produced material, and help explain the restriction of the Cerro Rajón Formation volcanic activity to the Caborca Region. The Moctezuma volcanic field provides some contextual framework for the spatial scale of the Rajón volcanics. In this intraplate volcanic event, $\sim 2 \text{ km}^3$ of volcanic deposits were produced across $\sim 400 \text{ km}^2$, in a setting dominated by fissure volcanism rather than by pyroclastic vents (Paz-Moreno et al., 2003).

Whereas it is possible that there are Cambrian volcanic or volcanoclastic deposits outside of the Caborca region in Sonora, such successions are may be buried or temporally unconstrained enough to correlate. For example, intercalated in strata exposed near Banjamín Hill in central Sonora, there are undated volcanoclastic rocks similar to the Cerro Rajón Formation's tuffaceous conglomerates, that lie close to Proterozoic basement.

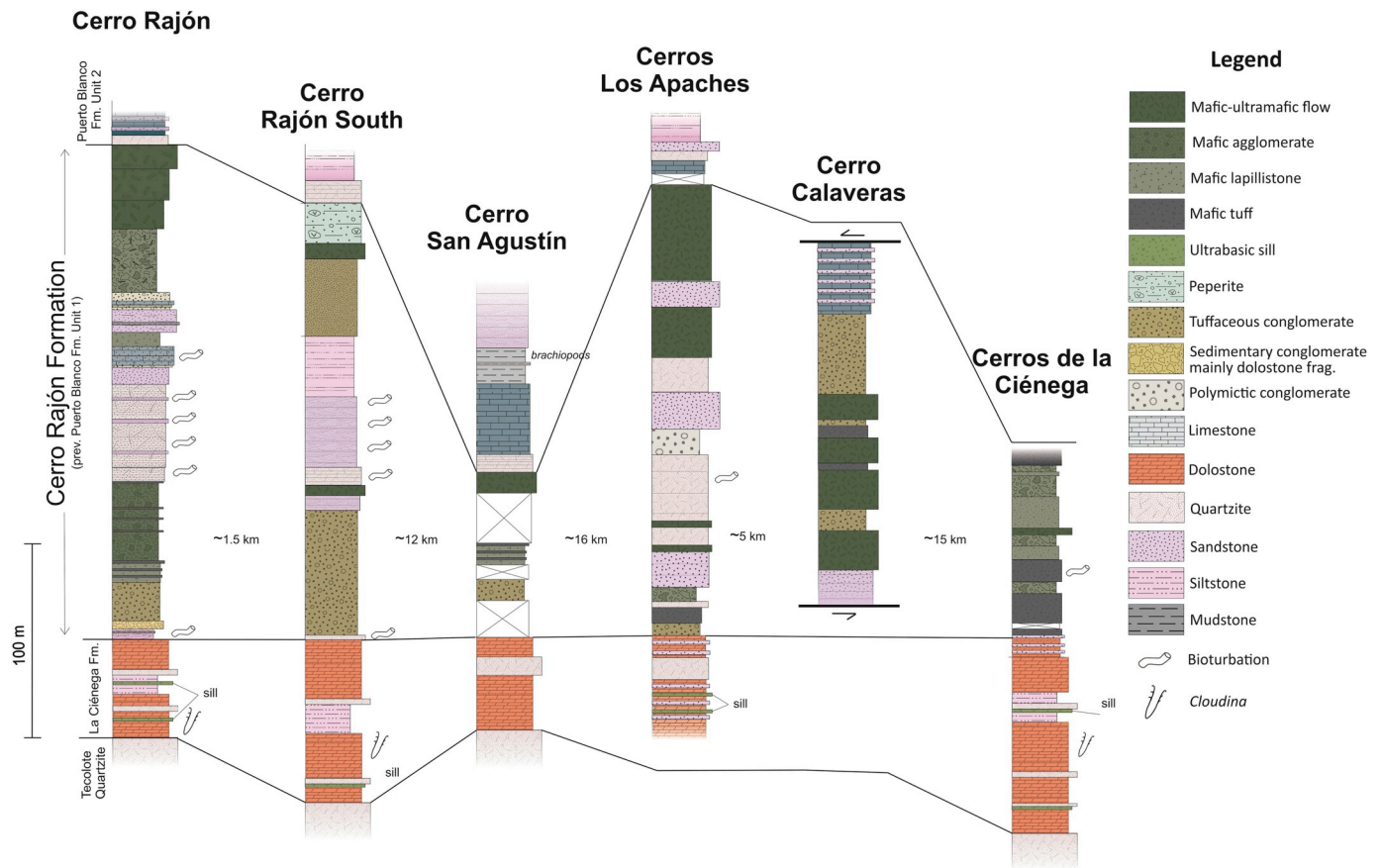


Fig. 8. North-to-south panel diagram of graphic logs of measured sections of the Cerro Rajón Formation (see Fig. 1). White X-bearing boxes indicate where section is covered, and arrows at Cerro Calaveras indicate where section is truncated by faulting. Approximate distance between the studied localities is indicated near bottom.

Within the Caborca region, the Cerro Rajón Formation can readily be correlated across studied localities. The outcrops vary considerably in the details of their lithologies from one locality to another, probably due to the local paleogeographic conditions during volcanic emplacement and due to different erosion rates each locality may have experienced. The proximity of the localities to the different sources of volcanic activity may have also mitigated preservation of these rocks.

Tuffaceous conglomerate is present in five of the six studied localities. These volcanic products may have been formed by destruction of cinder cones or in areas distant from the main source of the pyroclastic activity, where volcanic detrital material was more abundant (Barrón-Díaz et al., 2018). For example, in the Cerros de la Ciénega locality, the tuffaceous conglomerate outcrops in the east section, but is absent in the west section (measured section in Fig. 8) where the volcanic activity is represented by agglomerates instead. If these strata are coveval, these relationships suggest that the west section could be closer to the source of the pyroclastic activity.

Similarly, mafic agglomerates occur in Cerro Rajón, Cerros de la Ciénega and Cerro Los Apaches. These agglomerates are defined by having more than 90% volcanic products, which sometimes include large blocks of lapillistones and tuffs. This concentration indicates that these rocks were probably produced by the collapse of the volcanic structures. As a result, their presence at only three localities may mean that these sites were the closer to the emission vents of the volcanism.

Different volcanic flows occur in all the studied localities. Their individual thickness and chemistry varies from the 6 m thick picobasalt in Cerro San Agustín, to the ~20 m metabasalt visible at the tops of the Cerro Rajón, Cerro Calaveras and Cerros Los Apaches sections. This thickness variation may be due to a slight increase in the melting rate of the magmatism, produced towards the end of the volcanic activity, considered in light of the local paleotopographic conditions. Barrón-Díaz

(2013) used the cores of the diopside crystals to compare the melting rate of the picobasalts and metabasalts from Cerro San Agustín and Cerro Calaveras respectively, observing that the picobasalts had a lower melting rate than metabasalts. The thicker volcanic flows are also more differentiated, which indicates discrete evolution of the magmatism. Because the picobasalt flows are relatively thin, they are not as well preserved and are more easily eroded. Quartzites located at the top of some volcanic flows may have aided in preserving some of the units, a relationship observed in three of the studied localities (Figs. 7A and 8).

Regional variations in the nature of the disconformable upper contact of the Cerro Rajón Formation with the overlying quartzite of Unit 2 of the Puerto Blanco Formation may reflect differential reworking of the metabasalt at the top of the unit. Yet everywhere it is exposed, a chert-pebble lag sits atop the uppermost metabasalt in the Cerro Rajón Formation - signaling at the very least, a regional flooding event and sequence boundary.

Everywhere it is exposed, near the base of the Cerro Rajón Formation lies another disconformity, where incision locally removes the basal bioturbated clastics of the unit. Together with the character of the cobble-to-boulder conglomerates that cap and fill depressions in this surface, this event represents another sequence boundary. It may stem from erosion due to a regional sea level drawdown, or potentially erosion triggered by uplift associated with regional volcanism.

Ironically this volcanic-volcaniclastic succession is not exposed at the type section for the Puerto Blanco Formation at Cerro de la Proveedora because the basal portion of the succession is covered by alluvium (Cooper and Arellano, 1952; Stewart et al., 1984). Its absence reinforces the rationale for removing Unit 1 from the Puerto Blanco Formation and elevating it to its own formation. Renaming the remaining units (Units 2–4) of the Puerto Blanco Formation is beyond the scope of this contribution, but is a logical next step in the evolution of

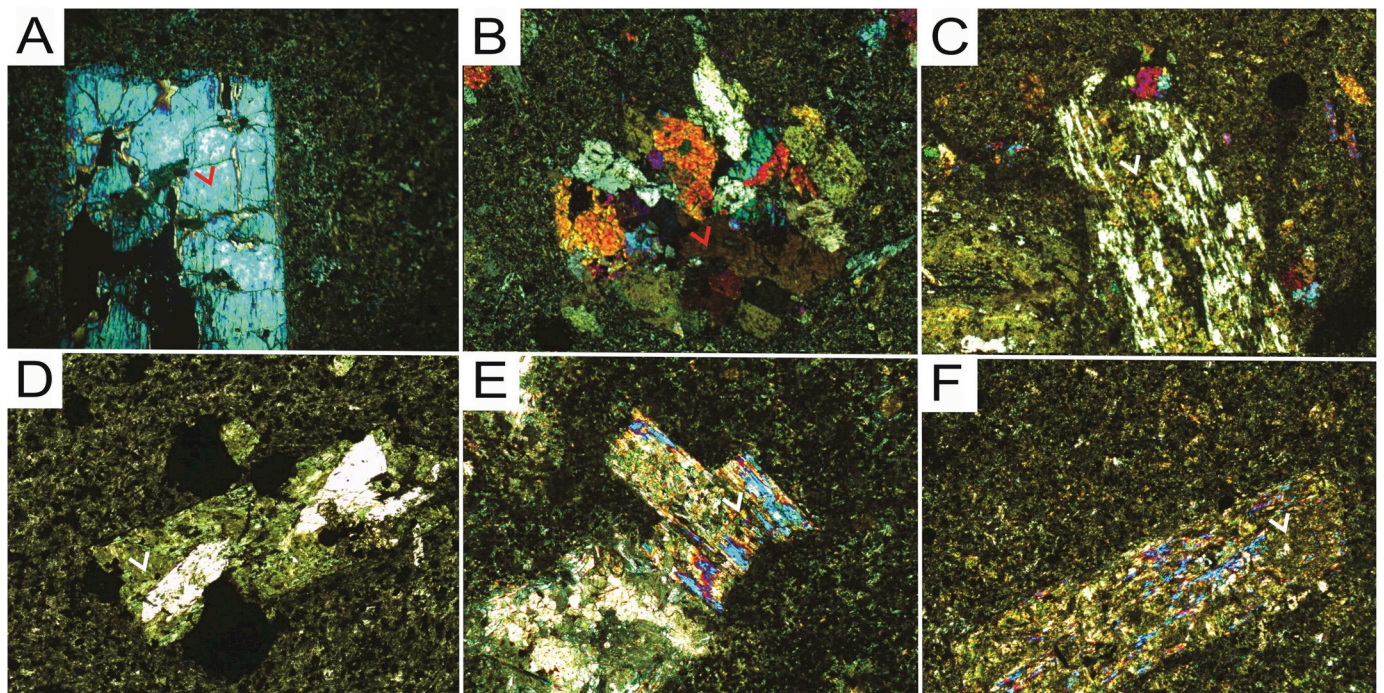


Fig. 9. Photomicrographs of volcanic flows in the Cerro Rajón Formation. A. Microbasalt exhibiting fresh diopside phenocrysts (red arrowhead) in a diopside-sphenetitanomagnetite-albite groundmass; uppermost Cerro Rajón Formation, Cerro San Agustín. B. Epidote crystals, including an epidote accumulate (red arrowhead) in a metabasalt; lower Cerro Rajón Formation, Cerro Calaveras. C. Actinolite-chlorite porphyroblast formed from a clinopyroxene, with chlorite aggregates (white arrowhead); lower Cerro Rajón Formation, Cerro Calaveras. D. Actinolite-chlorite porphyroblast with large titanomagnetite crystals and chlorite aggregates (white arrowhead); lower Cerro Rajón Formation, Cerro Calaveras. E. Actinolite-chlorite porphyroblast with calcite. The actinolite is being altered to chlorite (white arrowhead); middle Cerro Rajón Formation, Cerro Calaveras. F. Actinolite-chlorite porphyroblast in an actinolite-sphene-chlorite-titanomagnetite groundmass. Green colors in B-F represent the greenschist facies related mineralogy, which affects the volcanic signatures in the Cerro Rajón Formation. Field of view is 1.5 mm wide for each photomicrograph. (For interpretation of the references to color in this figure legend, the reader is referred to the Web version of this article.)

the region's stratigraphy, especially given emerging detrital zircon, strontium isotope, and trilobite data for the younger Cambrian portions of the succession (e.g., Cuen-Romero et al., 2016; Hagadorn and Holm-Denoma, 2016).

4.2. Regional correlations

The Cerro Rajón Formation and its bounding units exhibit broad similarities to Ediacaran-Cambrian successions exposed along the North

American Cordillera—from Sonora to British Columbia (see summaries in Lochman-Balk, 1956; Stewart et al., 1990; Stewart et al., 2002; Corsetti et al., 2007; Hagadorn, 2009). We support this correlation and suggest that the mafic volcanism in Caborca is related to rifting processes active in the western margin of Laurentia (Fig. 12; see also Stewart et al., 1990; Centeno-García et al., 2002; Hagadorn, 2009; Barrón-Díaz et al., 2018).

For example, in the Canadian Cordillera, the Neoproterozoic-Cambrian sedimentary strata of the Hamill Group contain 569.6 ± 5.3 Ma mafic volcanics and volcanoclastics (Colpron et al.,

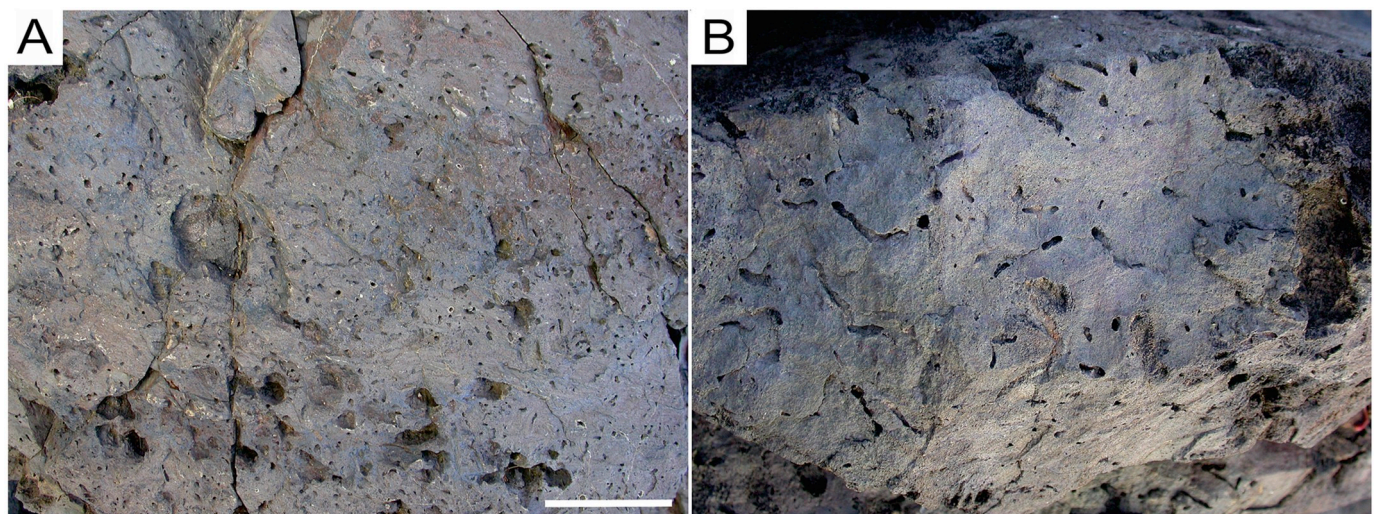


Fig. 10. A. Bioturbated intraclastic mafic tuff and B. bioturbated fine grained mafic tuff. Middle Cerro Rajón Formation, Cerros de la Ciénega. Scale bar in A is 8 cm and for B is 4 cm.

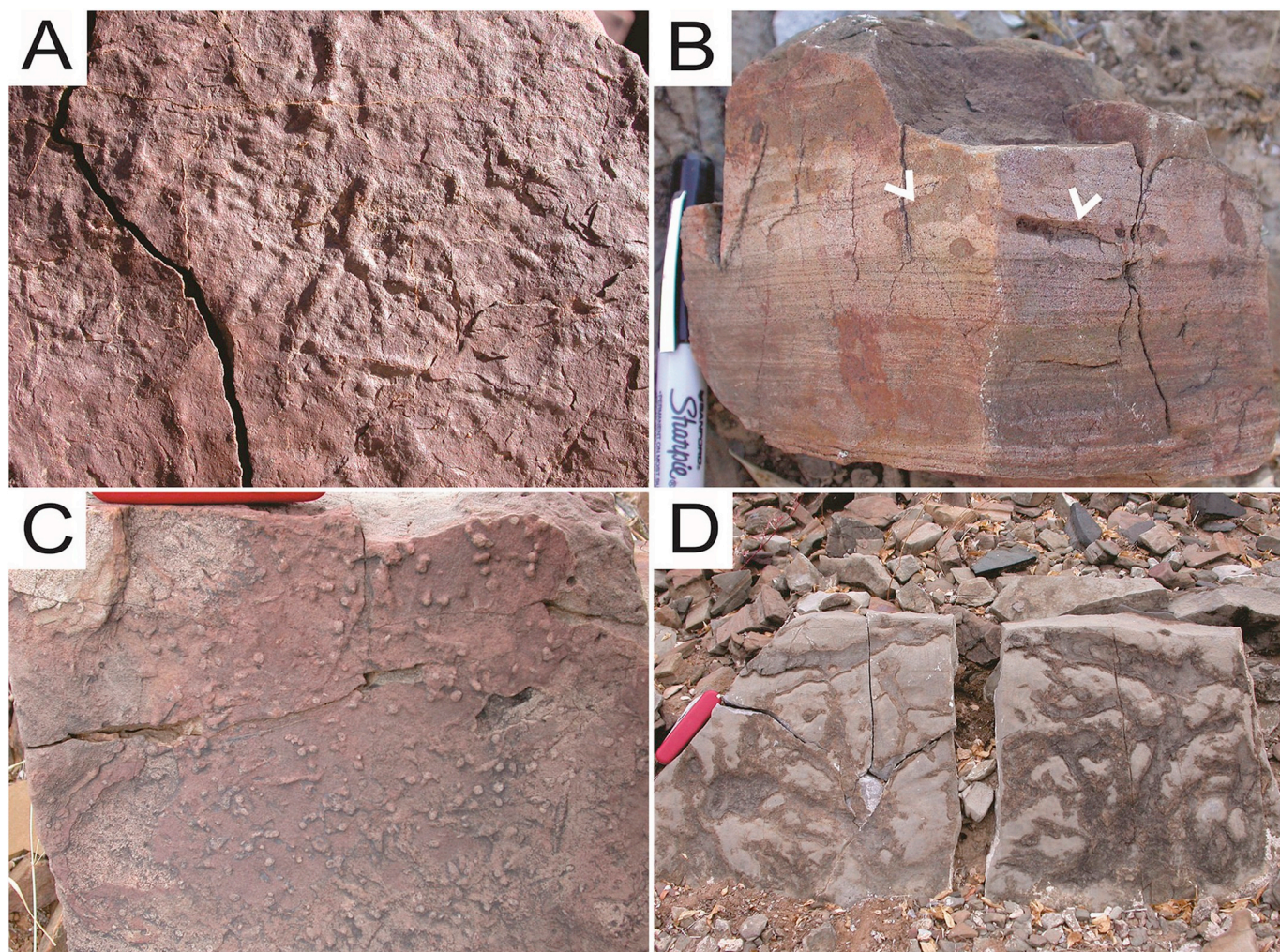


Fig. 11. Typical Cerro Rajón Formation trace fossils from the type section in Cerro Rajón. A. Bed sole view of *Planolites* and *Trepichnus* from the basal quartzites. B. Cross-sectional view of bed penetrative bioturbation (white arrowheads) typical of the laminated quartzites of the middle Cerro Rajón Formation. C. Bed sole view of *Planolites* and *Skolithos* from sandstone-mudstone interbeds in the middle Cerro Rajón Formation. D. Bed top view of cruzianiform- and *Teichichnus*-dominated silty limestones of the middle-upper Cerro Rajón Formation. Field of view in A is 6 cm, pen cap in B is 4.5 cm tall and knife in C, D is 8.5 cm long.

2002). Both the Hamill and the Rajón volcanic rocks have high TiO_2 concentrations, a geochemical characteristic not common in rift-related volcanic deposits. In Idaho and Utah, Harper and Link (1986) report alkaline basalts of Neoproterozoic age that also exhibit high TiO_2 concentrations. In northern Utah, the Ediacaran-Cambrian succession also contains volcanic rocks that are intercalated in sedimentary strata, including mafic agglomerates and 580 ± 7 Ma trachybasalt flows (Crittenden and Wallace, 1973). Other Early Cambrian rift-related volcanic rocks occur in central-southern Utah, intercalated in the Ediacaran-Cambrian Tintic Formation and Prospect Mountain Quartzite (see summary in Yonkee et al., 2014). Further south, in the Egan Range of Nevada, mafic volcanic flows are intercalated in the Ediacaran-Cambrian Stirling Quartzite and Wood Canyon Formation (Kellogg, 1963; Stewart, 1972).

Well cuttings from the Southern Oklahoma Aulacogen (SOA) cut through 577–528 Ma basaltic and intermediate subalkaline to tholeiitic rocks of the Carlton Rhyolite Group (Hames et al., 1998; Lambert et al., 1988; Bowring and Hoppe, 1982; Hogan and Amato, 2015; Brueseke et al., 2016), associated with intrusive and subvolcanic exposures of the Wichita Granite Group in the Wichita Mountains. Some samples show relatively high TiO_2 concentrations, similar to the Cerro Rajón Formation volcanism—but with much higher melting rates. The SOA rifting process is hypothesized to be related to the breakup of Pannotia and the formation of a failed arm of a three armed radial system (Brueseke

et al., 2016). Although this volcanism is related to an axial zone of a rift, where higher volcanic volumes were produced (vs. the Cerro Rajón Formation volcanism), it is important to explore the possibility that the Cerro Rajón Formation volcanic rocks were produced at the end of one of these failed arms, where the volcanism wasn't able to evolve.

All these previous volcanic events may be related to rifting processes in the western margin of Laurentia, a tectonic setting which was active from 780 to 570 Ma (Lund et al., 2003) and in some cases well into the Cambrian (Karlstrom et al., 2018). The Cerro Rajón Formation volcanic rocks may represent the southern arm of this rifting activity, where the axial zone of the rift was not fully developed, explaining the lack of evolution in the volcanism and the low melting rates. The absence of proven early Cambrian rift related volcanism observed between Utah and Idaho, and the Caborca Block (Fig. 1 in Barrón-Díaz et al., 2018), may be because its products have mostly been eroded or buried (Stewart et al., 1990). This situation leaves geologists the challenge to sift through the remnants of these events that are scattered through the Cordillera, and the opportunity to try to correlate and better understand their genesis, by linking their occurrence in stratigraphic successions which are challenging to geochronologically constrain and correlate.

The eastern Laurentian margin also has similar age volcanics that are worth comparing to Cerro Rajón Formation volcanism. For example, the Skinner Cove Formation in Newfoundland contains a

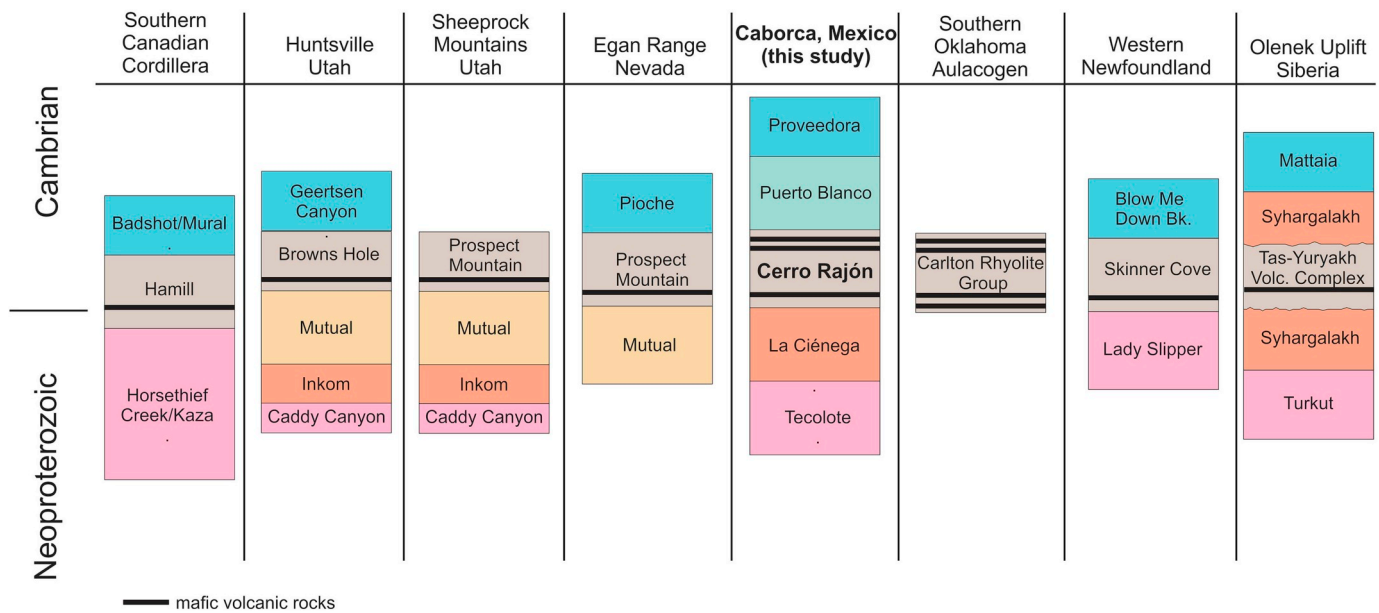


Fig. 12. Comparison of the Caborca region's stratigraphy, including the Cerro Rajón Formation, with other Ediacaran-Cambrian rift-related volcanics from the western and eastern margins of Laurentia and Siberia. Unit thicknesses and ages are depicted stylistically, and are intended to illustrate candidates for possible correlation.

550.5 ± 3 Ma ankaramite flow that also provides evidence of a rift-drift transition (Cawood et al., 2001).

Further afield, in the Olenek Uplift of Siberia, the Tas-Yuryakh Volcanic Complex forms a diatreme where a 543.9 ± 0.24 Ma tuff breccia (Bowring et al., 1993) occurs in *T. pedum*-bearing sedimentary rocks of the Syhargalakh Formation (Rogov et al., 2015). Like the Cerro Rajón Formation rift-related volcanism, the Tas-Yuryakh volcanism presents a paradox in its timing because it significantly post-dates the Laurentian margin: Evidence for flood basalt volcanism from well cuttings in the Southern Oklahoma Aulacogen (U.S.A.). *Lithos* 260, 164–177.

Further work to constrain the radiometric age of the volcanism in the Cerro Rajón Formation, as well as its petrogenetic and facies relationships with potential adjacent and conjugate successions are thus ripe targets for further inquiry.

Acknowledgements

We are grateful to the many colleagues who have helped us in the field and shepherded our understanding of these rocks, including R. Amaya-Martinez, J. Collette, F. Corsetti, C. Gonzalez-Leon, S. Hollingsworth, C. Holm-Denoma, S. Loyd, J. MacDonald, K. Marengo, P. Marengo, A. Morales, E. Smith, F. Sour-Tovar, J. Stewart, and C. Wyshnytsky. We are also thankful to the many local landowners who gave us permission to view outcrops on their property, especially R. Lizarraga and to the Fresnillo mining company for assistance in Caborca. Financial support for this project was generously provided by the University of Sonora PIFI (2015–2017) and patrons of the Denver Museum of Nature & Science. We thank Aimeé Orcí from ERNO-UNAM and Sheila Corral from UNISON for their work fabricating thin sections and R. Lozano for his help with XRF analyses. We thank three anonymous reviewers and editor F. Vega for their comments and suggestions about the manuscript.

References

Barrón-Díaz, A.J., 2013. Caracterización petrogenética de las metabasitas anorogénicas del límite Cámbrico-Precámbrico, Municipio de Pitiquito, Sonora, México. M.S. thesis. Universidad de Sonora, pp. 95.

Barrón-Díaz, A.J., Paz-Moreno, F.A., Lozano-Santa Cruz, R., Herrera-Urbina, S., Centeno-García, E., López-Martínez, M., 2018. Early Cambrian alkaline volcanism on the southern margin of Laurentia: evidence in the volcanoclastic units from the Puerto

Blanco Formation in the Caborca block, NW Mexico. *Int. Geol. Rev.* <https://doi.org/10.1080/00206814.2018.1501619>.

Bowring, S.A., Grotzinger, J.P., Isachsen, C.E., Knoll, A.H., Pelechaty, S.M., Kolosov, P., 1993. Calibrating rates of early Cambrian evolution. *Science* 261, 1293–1298.

Bowring, S.A., Hoppe, W.J., 1982. U–Pb zircon ages from mount Sheridan Gabbro, Wichita Mountains. In: Gilbert, M.C., Donovan, R.N. (Eds.), *Geology of the Eastern Wichita Mountains, Southwestern Oklahoma*, vol. 21. Oklahoma Geological Survey Guidebook, pp. 54–59.

Brueseke, M.E., Hobbs, J.M., Bulen, C.L., Mertzman, S.A., Puckett, R.E., Walker, J.D., Feldman, J., 2016. Cambrian intermediate-mafic magmatism along the Laurentian margin: Evidence for flood basalt volcanism from well cuttings in the Southern Oklahoma Aulacogen (U.S.A.). *Lithos* 260, 164–177.

Cawood, P.A., McCausland, P.J.A., Dunning, G.R., 2001. Opening Iapetus: Constraints from the Laurentian margin in Newfoundland. *GSA Bull.* 113 (4), 443–453.

Centeno-García, E., Maytorena, F., Calmus, T., Solís-Pichardo, G., Lozano-Santa Cruz, R., 2002. Proterozoic OIB magmatism in the Caborca terrane, northwestern Mexico. In: Denver Annual Meeting. Colorado Convention Center: C205 Session No. 245.

Colpron, M., Logan, J.M., Mortensen, J.K., 2002. U–Pb zircon age constraint for late Neoproterozoic rifting and initiation of the lower Paleozoic passive margin of western Laurentia. *Can. J. Earth Sci.* 39, 133–143.

Cooper, G.A., Arellano, A.R.V., 1946. Stratigraphy near Caborca, northwest Sonora, Mexico. *Bull. Am. Assoc. Pet. Geol.* 30, 606–611.

Cooper, G.A., Arellano, A.R.V., 1952. Introduction and stratigraphy. In: Cooper, G.A., Arellano, A.R.V., Johnson, J.H., Okulitch, V.J., Stoyanow, Alexander, Lochman, Christina (Eds.), *Cambrian Stratigraphy and Paleontology Near Caborca, Northwestern Sonora*, vol. 119. Smithsonian Miscellaneous Collections, Mexico, pp. 1–23 no. 1.

Corsetti, F.A., Stewart, J.H., Hagadorn, J.W., 2007. Neoproterozoic diamicite-cap carbonate succession and $\delta^{13}\text{C}$ chemostratigraphy from eastern Sonora, Mexico. *Chem. Geol.* 237, 129–142.

Crittenden Jr., M.D., Wallace, C.A., 1973. In: Possible Equivalents of the Belt Supergroup in Utah, Belt Symposium, vol. 1. Idaho Bureau of Mines and Geology, Moscow, Idaho, pp. 116–138.

Cuen-Romero, Francisco Javier, Valdez Holguín, José Eduardo, Buitrón, Blanca Estela, Monreal, Rogelio, Sundberg, Frederick, Montijo González, Alejandra, Minjarez Sosa, Ismael, 2016. Cambrian Stratigraphy of San José de Gracia, Sonora, Mexico: El Gavilán Formation, a new lithostratigraphic unit of middle Cambrian open shelf environment. *Bol. Soc. Geol. Mex.* 68 (3), 429–441.

Damon, P.E., Livingston, D.E., Mauger, R.L., Gilletti, B.J., y Pantoja-Alor, Jerjes, 1962. Edad del Precámbrico anterior y de otras rocas del zócalo de la región de Caborca-Altar, en la parte noroccidental del Estado de Sonora, vols. 64–2. Universidad Nacional Autónoma de México, Instituto de Geología Boletín, pp. 11–44.

Eells, J.L., 1972. Geology of the Sierra de La Berruga, north-western Sonora, Mexico. M.S. thesis. California State University, San Diego, pp. 77.

Ernst, R.E., Hamilton, M.A., Soderlund, U., Hanes, J.A., Gladkochub, D.P., Okrugin, A.V., Kolotilina, T., Mekhonoshin, A.S., Bleeker, W., LeCheminant, A.N., Buchan, K.L., Chamberlain, K.R., Didenko, A.N., 2016. Long-lived connection between southern Siberia and northern Laurentia in the Proterozoic. *Nat. Geosci.* 9, 464–469.

Farmer, G.L., Espinoza, G., Morales, M., Martin, M.W., Bowring, S.A., 2001. Nd isotope constraints on sources of Neoproterozoic to Early Cambrian siliciclastic sedimentary rocks in northern Sonora. *J. S. Am. Earth Sci.* 14 (5), 437–446.

- Farmer, G.L., Bowring, S.A., Matzel, J., Espinosa-Maldonado, G., Fedo, C., Wooden, J., 2005. Paleoproterozoic Mojave province in northwestern Mexico? Isotopic and U-Pb zircon geochronologic studies of Precambrian and Cambrian crystalline and sedimentary rocks, Caborca, Sonora, The Mojave-Sonora Megashear Hypothesis. *Dev. Assess. Altern.* 393, 183–198.
- Fike, D.A., Grotzinger, J.P., Pratt, L.M., Summons, R.E., 2006. Oxidation of the Ediacaran ocean. *Nature* 444, 744–747.
- Hagadorn, J.W., Holm-Denoma, C.S., 2016. Linking Neoproterozoic to Cambrian strata from Sonora to Utah. *Geol. Soc. Am. Abstr. Programs* 48 (7).
- Hagadorn, J.W., 2011. The Sonoran succession: Life and death in the shadow of glaciers, tropical beaches, and volcanoes: XII Congreso Nacional de Paleontología. *Libro de Resúmenes*, pp. 22–23.
- Hagadorn, J.W., 2009. Ediacaran-Early Cambrian Cordilleran volcanism and incision: Evidence for rifting and eustatic lowstand? *Geol. Soc. Am. Abstr. Programs* 41, 181.
- Hames, W.E., Hogan, J.P., Gilbert, M.C., 1998. Revised granite-gabbro age relationships, Southern Oklahoma Aulacogen, U.S.A. In: Hogan, J.P., Gilbert, M.C. (Eds.), *Basement Tectonics Proceedings of the Twelfth International Conference on Basement Tectonics* 12. Kluwer, Dordrecht, The Netherlands, pp. 247–249.
- Harper, G.D., Link, P.K., 1986. Geochemistry of Upper Proterozoic rift-related volcanics, northern Utah and southeastern Idaho. *Geology* 14, 864–867.
- Hogan, J.P., Amato, J.M., 2015. Confirmation of temporally distinct magmatic events in the Wichita Mountains. In: *Oklahoma Presented at the Geological Society of America South Central Section Meeting*, pp. 13 no. 47.
- Karlstrom, K., Hagadorn, J., Gehrels, G., Matthews, W., Schmitz, M., Madronich, L., Mulder, J., Pecha, M., Giesler, D., Crossey, L., 2018. Cambrian Sauk transgression in the Grand Canyon region redefined by detrital zircons. *Nat. Geosci.* 11, 438–443.
- Kellogg, H.E., 1963. Paleozoic Stratigraphy of the Southern Egan Range, Nevada. *GSA Bull.* 74, 685–708.
- Leyva-Ruiz, N., Barrón-Díaz, A.J., Lozano-Santa Cruz, R., Paz-Moreno, F.A., 2017. Petrografía y geoquímica de los intrusivos granitoides en el cerro El Dátil, municipio de Pitiquito, Sonora, México, XXVII Congreso Nacional de Geoquímica. *Actas INAGEQ* 23, 104.
- Lambert, D.D., Unruh, D.M., Gilbert, M.C., 1988. Rb-Sr and Sm-Nd isotopic study of the Glen Mountains Layered Complex: initiation of rifting within the Southern Oklahoma aulacogen. *Geology* 16, 13–17.
- Lochman-Balk, C., 1956. The Cambrian of the Rocky Mountains and southwest deserts of the United States and adjoining Sonora province, Mexico. v. 2, pt. 2. In: Rogers, J. (Ed.), *El Sistema Cámbrico, su paleogeografía y el problema de su base*, vol. 20. Congreso Geológico Internacional, Australia, América, pp. 529–560 México.
- Longoria, J.F., Gonzalez, M.A., Mendoza, J.J., Perez, V.A., 1978. Consideraciones estructurales en el Cuadrángulo Pitiquito-La Primavera, NW de Sonora [Structural considerations in the Pitiquito-La Primavera quadrangle, northwestern Sonora, Mexico], vol. 1. Universidad de Sonora, Departamento de Geología Boletín, pp. 61–67.
- Longoria, J.F., 1981. Geologic features of northwest Sonora. In: Longoria, Jose (Ed.), *Regional Geology of Northwest Sonora: Geological Society of America, Cordilleran Section Annual Meeting*, Hermosillo, Sonora, Mexico, Proceedings, pp. 1–48.
- Longoria, J.F., Gonzalez, M.A., 1981. Description of the localities to be visited during the Geological Society of America Field excursion n. 4. In: Longoria, J.F. (Ed.), *Regional Geology of Northwest Sonora, Geological Society of America, Cordilleran Section, Annual Meeting*, Hermosillo, Sonora, Proceedings, pp. 49–64.
- Loyd, S.J., Marengo, P.J., Hagadorn, J.W., Lyons, T.W., Kaufman, A.J., Sour-Tovar, F., Corsetti, F.A., 2012. Sustained low marine sulfate concentrations from the Neoproterozoic to the Cambrian: Insights from carbonates of northwestern Mexico and eastern California. *Earth Planet Sci. Lett.* 339–340, 79–94.
- Loyd, S.J., Marengo, P.M., Hagadorn, J.W., Lyons, T.W., Kaufman, A.J., Sour-Tovar, F., Corsetti, F.A., 2013. Local $\delta^{34}\text{S}$ variability in ~580 Ma carbonates of northwestern Mexico and the Neoproterozoic marine sulfate reservoir. *Precambrian Res.* 224, 551–569.
- Loyd, S.J., Corsetti, F.A., Shen, Y., Eagle, R., Hagadorn, J.W., Shen, Y., Zhang, X., Bonifaci, M., Tripathi, A.K., 2015. Evolution of Neoproterozoic Wonoka-Shuram Anomaly-aged carbonates: Evidence from clumped isotope paleothermometry. *Precambrian Res.* 264, 179–191.
- Lund, K., Aleinikoff, J., Evans, K., Fanning, C., 2003. SHRIMP U-Pb geochronology of Neoproterozoic Windermere Supergroup, central Idaho: Implications for rifting of western Laurentia and synchronicity of Sturtian glacial deposits. *Bull. Geol. Soc. Am.* 115 (3), 349–372.
- Lynch, D.J., 1981. Genesis and Geochronology of Alkaline Volcanism in the Pinacate Volcanic Field of Northwestern Sonora, Mexico. Ph.D. thesis. University of Arizona, Tucson, pp. 215.
- Lynch, D.J., Musselman, T.E., Gutmann, J.T., Patchett, P.J., 1993. Isotopic Evidence for the origin of Cenozoic volcanic rocks in the Pinacate volcanic field, northwestern Mexico. *Lithos* 29, 295–302.
- Maloof, A.C., Schrag, D.P., Crowley, J.L., Bowring, S.A., 2005. An expanded record of Early Cambrian carbon cycling from the Anti-Atlas Margin, Morocco. *Can. J. Earth Sci.* 42, 2195–2216.
- McFadden, K.A., Huang, J., Chu, X., Jiang, G., Kaufman, A.J., Zhou, C., Yua, X., Xiao, S., 2008. Pulsed oxidation and biological evolution in the Ediacaran Doushantuo Formation. *Proc. Natl. Acad. Sci. Unit. States Am.* 105, 3197–3202.
- North American Commission on Stratigraphic Nomenclature, 2005. *North American Stratigraphic Code*. AAPG (Am. Assoc. Pet. Geol.) Bull. 89 (11), 1547–1591.
- Paz-Moreno, F.A., Demant, A., Cochemé, J.-J., Dostal, J., Montigny, R., 2003. The Quaternary Moctezuma volcanic field: A tholeiitic to alkali basaltic episode in the central Sonoran Basin and Range Province, México. In: Johnson, S.E., Paterson, S.R., Fletcher, J.M., Girty, G.H., Kimbrough, D.L., Martín-Barajas, A. (Eds.), *Tectonic Evolution of Northwestern México and the Southwestern USA*. Geological Society of America Special Paper 374, Boulder, Colorado, pp. 439–455.
- Pope, M.C., Hollingsworth, J.S., Dilliard, K., 2012. Overview of Lower Cambrian mixed carbonate-siliciclastic deposition along the western Laurentian passive margin. In: Derby, J.R., Fritz, R.D., Longacre, S.A., Morgan, W.A., Stembach, C.A. (Eds.), *The Great American Carbonate Bank: the Geology and Economic Resources of the Cambrian-Ordovician Sauk Megasequence of Laurentia*. AAPG Memoir 98, pp. 735–750.
- Ramos-Velázquez, E., Calmus, T., Valencia, V., Iriondo, A., Valencia-Moreno, M., Bellon, H., 2008. U-Pb and $^{40}\text{Ar}/^{39}\text{Ar}$ geochronology of the coastal Sonora batholith: New insights on Laramide continental arc magmatism. *Rev. Mex. Ciencias Geol.* 25 (2), 314–333.
- Radelli, L., Solis-Weiss, V., Dórame-Navarro, M., De la Cruz-Ortega, L.C., Urrutia, J., 2008. Fossil content and Structural relationships of the San Luis zone and Caborca zone of NW Sonora, Mexico. *Suppression of the precambrian Z. of Caborca*. *Bol. Geol. Univ. Ind. Santander, Colombia* 30 (2), 1–34.
- Rogov, V., Karlova, G.A., Marusin, V., Kochnev, B., Nagovitsin, K., Grazhdankin, D., 2015. Duration of the first biozone in the Siberian hypostratotype of the Vendian. *Russ. Geol. Geophys.* 56, 573–583.
- Schmitz, M.D., 2012. Appendix 2 – Radiometric ages used in GTS2012. In: Gradstein, F.M., Ogg, J.G., Schmitz, M.D., Ogg, G.M. (Eds.), *The Geologic Time Scale 2012*. Elsevier, Boston, pp. 1045–1082.
- Sour-Tovar, F., Hagadorn, J.W., Huitrón-Rubio, T., 2007. Ediacaran and Cambrian index fossils from Sonora, Mexico. *Paleontology* 50 (1), 169–175.
- Stewart, J.H., 1972. Initial deposits of the Cordilleran geosyncline: evidence of a late Precambrian (850 m.y.) continental separation. *Geol. Soc. Am. Bull.* 83, 1345–1360.
- Stewart, J.H., 1982. Regional relations of Proterozoic Z and Lower Cambrian rocks in the western United States and northern Mexico. In: Cooper, J.D., Troxel, B.W., Wright, L.A. (Eds.), *Geology of Selected Areas in the San Bernardino Mountains, Western Mojave Desert, and Southern Great Basin, California: Geological Society of America, Cordilleran Section Annual Meeting*, Anaheim, California, pp. 171–186 1982, Guidebook and Volume.
- Stewart, J.H., McMenamin, A.S., Morales-Ramirez, J.M., 1984. Upper Proterozoic and Cambrian Rocks in the Caborca Region, Sonora, Mexico. *Physical Stratigraphy, Biostratigraphy, Paleocurrents Studies and Regional Relations*. U. S. Geological Survey Professional Paper 1390.
- Stewart, J.H., Gehrels, G.E., Barth, A.P., Link, P.K., Christie-Blick, N., Wrucke, C.T., 2001. Detrital zircon provenance of Mesoproterozoic to Cambrian arenites in the western United States and northwestern Mexico. *Geol. Soc. Am. Bull.* 113 (10), 1343–1356.
- Stewart, J.H., Amaya-Martinez, R., Palmer, A.R., 2002. Neoproterozoic and Cambrian Strata of Sonora, Mexico: Rodinian Supercontinent to Laurentian Cordilleran Margin. *Geológicas Society of América*, pp. 5–48 Special Paper 365.
- Stewart, J.H., Poole, F.G., Ketner, K.B., Madrid, R.J., Roldán-Quintana, Jaime, Amaya-Martínez, Ricardo, 1990. Tectonics and stratigraphy of the Paleozoic and Triassic southern margin of North America, Sonora, Mexico. In: Gehrels, G.E., Spencer, J.E. (Eds.), *Geologic Excursions through the Sonoran Desert Region, Arizona and Sonora*. Arizona Geological Survey Special Paper 7, pp. 183–202.
- Westerfield, M.J., 1988. *Geology and Magnetism of the Cerros Clemente-Llano Verde, Northwestern Sonora, Mexico* (M.S. thesis). University of Cincinnati, Cincinnati, Ohio, pp. 124.
- Yonkee, W.A., Dehler, C., Link, P.K., Balgord, E.A., Keeley, J.A., Hayes, D.S., Wells, M.L., Fanning, C.M., Johnston, S.M., 2014. Tectono-stratigraphic framework of Neoproterozoic to Cambrian strata, west-central U.S.: Protracted rifting, glaciation, and evolution of the North American Cordilleran margin. *Earth Sci. Rev.* 136, 59–95.

4

**GEOCHRONOLOGY AND GEOTHERMOMETRY OF THE LARAMIDE
METAMORPHISM IN THE CAMBRIAN METABASALTS FROM THE CERRO
RAJÓN FORMATION, CABORCA REGION, NORTHWEST MEXICO.**

Geochronology and geothermometry of the Laramide metamorphism in the Cambrian metabasalts from the Cerro Rajón Formation, Caborca region, northwest Mexico.

Barrón-Díaz Arturo J.^{a,b,*}, Paz-Moreno Francisco A.^b, Miggins Daniel P.^c Iriondo Alexander^d

^aEstación Regional del Noroeste - ERNO (Universidad Nacional Autónoma de México), Hermosillo, Mexico.

^bDepartamento de Geología, Universidad de Sonora (UNISON), Hermosillo, Mexico

^cCollege of Earth, Ocean, and Atmospheric Sciences, Oregon State University, Corvallis, Oregon, USA

^dCentro de Geociencias, Universidad Nacional Autónoma de México, Querétaro, Mexico

ABSTRACT

Early Cambrian volcanic rocks characterized by pyroclastic and lava flows of basaltic composition from the Cerro Rajón Formation are exposed in the Caborca region, northwest Sonora, Mexico. These rocks underwent greenschist facies metamorphism characterized by a metamorphic paragenesis of actinolite, sphene, chlorite, epidote and calcite with minor interstitial albite. This mineralogical association was characterized by electron microprobe analysis. Metamorphic temperatures were calculated by amphibole-plagioclase geothermometry, which indicates temperatures as high as 548 ± 40 °C. U-Pb geochronology of the pluton that may cause the metamorphism yielded an age of 71.1 ± 0.4 Ma, and an average estimated temperature of 664 ± 40 °C. Preliminary pressures in this intrusive show an average of 3.08 ± 1.5 kbar. Two metamorphic events were identified by $^{40}\text{Ar}/^{39}\text{Ar}$ geochronology. Metabasalt samples from the western part of the study area yielded ages from 55.89 ± 0.6 Ma to 60.26 ± 0.33 Ma, while an age of 81.37 ± 0.81 Ma was obtained from a sample collected in the eastern part. Combined results suggest that Laramide intrusives metamorphosed the Neoproterozoic and Cambrian rocks in the Caborca region.

1. Introduction

Neoproterozoic and Paleozoic sedimentary rocks crop out in the northwest part of Mexico, in the Caborca Block (Eells, 1972; Longoria, 1981; Stewart *et al.*, 1984; Stewart *et al.*, 2002). This succession is regionally affected by an extensive magmatic event occurred during the late Cretaceous and early Tertiary, which is contemporaneous with the Laramide Orogeny (Coney and Reynolds, 1977). Evidence of this magmatism are widespread along western Mexico (Valencia-Moreno *et al.*, 2001; Iriondo *et al.*, 2004; Valencia-Moreno *et al.*, 2006; Ramos-Velázquez *et al.*, 2008). In northwestern Sonora, this magmatism probably started since late Permian (Arvizu *et al.*, 2009). Late Cretaceous to middle Eocene magmatism are related to the Laramide plutonic belt, dated by K-Ar (Damon *et al.*, 1983a) and by $^{40}\text{Ar}/^{39}\text{Ar}$ and U-Pb from 90 to 40 Ma (Valencia-Moreno *et al.*, 2006, Ramos-Velázquez *et al.*, 2008).

The present study is focused on the volcanic rocks of the Cerro Rajón Fm., previously named as the unit 1 of the Puerto Blanco Fm. (Cooper and Arellano, 1952; Barrón-Díaz *et al.*, 2019). The succession is characterized by rift-related alkaline pyroclastic deposits and volcanic basaltic flows produced at the beginning of the Cambrian (Barrón-Díaz *et al.*, 2018; Barrón-Díaz *et al.*, 2019). Previous attempts to date this volcanism were unsuccessful (Barrón-Díaz, 2013). The difficulty lies on the alteration and metamorphism affecting the volcanic rocks. The best approximation to define the Cambrian-Precambrian transition in northwestern Mexico has been done by means of fossils found at the top of the Neoproterozoic succession and the base of the early Cambrian Cerro Rajón Fm. (Sour-Tovar *et al.*, 2007; Loyd *et al.*, 2013). Cloudina family fossils, representing the Ediacaran fauna, and the ichnofossil *Treptichnus pedum* (Cambrian) had also been reported from the La Ciénega Fm. and Cerro Rajón Fm., respectively (Sour-Tovar *et al.*, 2007; Barrón-Díaz *et al.*

al. 2019). The occurrence of cloudiniids in the Cerro Rajón locality coincides with the end-Ediacaran $\delta^{13}\text{C}$ isotopic nadir (Loyd *et al.*, 2013).

The main goal of this research is to describe the metamorphic characteristics from the Cerro Rajón Fm. volcanic rocks and their metamorphic age produced by Laramide intrusions, mapped near the study area (Radelli *et al.*, 2008; Leyva-Ruiz *et al.*, 2017). While describing the metamorphism in the volcanic clasts in the Cerro Rajón Fm., Barrón-Díaz *et al.* (2018) suggested that Laramide intrusives were the source of the metamorphism for these rocks. This time, we want to provide harder evidence of this metamorphism using detailed $^{40}\text{Ar}/^{39}\text{Ar}$ geochronology and geothermobarometry. As well as dating a Laramide intrusive within the study area and discuss its interaction with the Neoproterozoic and Cambrian succession.

2. Geologic setting

Caborca region successions are observed in a basin and range taphrogen (Dickinson, 2002), developed after extensional efforts in the region. This geologic setting formed buried ranges (Raisz, 1964) where the Cerro Rajón Fm. volcanic rocks can be observed as subcrop or discrete outcrops. The study area is located in the surrounding of the Bámori Ranch. Studied localities include the Cerro Rajón, Cerro Calaveras, Cerros de la Ciénega, Cerro los Apaches and Cerro San Agustín (Fig. 1). These localities show sedimentary successions from platform deposits that developed during the late Neoproterozoic and early Cambrian (Stewart *et al.*, 1984). Exposures of this succession show semi vertical layers resting over an igneous-metamorphic basement identified as the Bámori Metamorphic Complex (Longoria *et al.*, 1978).

The Cambrian-Precambrian boundary is represented by the Ediacaran La Ciénega Fm. and the Cambrian Cerro Rajón Fm., defined by Barrón-Díaz *et al.* (2019) as a volcano-sedimentary succession consisting of tuffaceous conglomerate, metabasalt, mafic tuff, mafic lapillistone, mafic agglomerate, and quartzite with minor siltstone, limestone, dolostone, and sedimentary conglomerate (Fig. 2). Volcanism during this period is related to an alkaline continental rift with OIB type characteristics (Barrón-Díaz *et al.*, 2018). Metabasalt outcrops are scarce, often partially buried and show porphyritic textures with large clinopyroxene crystals (Fig. 3A, 3C). Metabasalt layers are commonly a few meters thick, and often exhibit a scoriaceous base and columnar jointing (Fig. 3B).

Barrón-Díaz *et al.* (2018) classified the volcanic clasts from the Cerro Rajón Fm. as metapicrobasalts, metabasalts and metabasalts that show basic and ultrabasic characteristics. The study was made in the volcanic clasts from the tuffaceous conglomerate units, a distinctive unit of this formation. Barrón-Díaz *et al.* (2018) propose that hydrothermal fluids caused the metamorphism of the volcanic rocks.

Laramide intrusives had been reported for northwestern Sonora (Valencia-Moreno *et al.*, 2001). The closest Laramide intrusive bodies to the study area include the granitic bodies 40 km north, dated by K-Ar from 66 – 74 Ma (Valencia-Moreno *et al.*, 2006). The late Cretaceous monzonitic porphyry from Cerro Gasolinera, 10 km north of Caborca Sonora, showed a $^{40}\text{Ar}-^{39}\text{Ar}$ age of 75.9 ± 0.4 Ma in amphibole and a U-Pb age of 76.3 ± 0.4 in zircons (Paz-Moreno *et al.*, 2018). A similar age of ~ 72 Ma was calculated 25 km west from the Cerro Calaveras locality (Roldán-Quintana, oral commun., 2018). A granodiorite from Cerro El Dátil, located 20 km west from Cerros de la Ciénega, is described in this work and is considered the closest reported Laramide intrusive to the Cerro Rajón Fm. rocks.

3. Materials and methods

Samples from each lava flow were characterized through a petrographic analysis in the department of geology of the University of Sonora. Electron Microprobe analyses (EMPA) were performed using the CAMECA SX100 microprobe at the Lunar and Planetary Laboratory of the University of Arizona. Analyses for silicates and oxides were performed at 15kV, 20na, using a focused beam and counting 20 seconds on peak and 20 seconds on background for all elements. Plagioclase and mica analyses were performed using a 2 μm defocussed beam at 15 Kv, 10na, 10 second peak, and 10 second background time for Na and K, and a 2 μm beam at 15kv, 20na, and 20 second peak and 20 second background

times for all other elements. Well characterised, natural and synthetic materials were used as standards for all elements. Geothermometry calculations were made in a MS Excel spreadsheet prepared by Lawford Anderson from the University of Southern California (see Supplementary File 4 and 5 for calculations and Supplementary File 2 for results).

The metamorphic minerals in the groundmass of the metabasalts were used to obtain a minimum age for the metamorphism through $^{40}\text{Ar}/^{39}\text{Ar}$ geochronology. The process for obtaining a clean groundmass started with the crushing and the sieving of the sample until a fraction between 106 and 355 μm was obtained. Fractions were cleaned with ultrasonic baths, and magnetic materials were separated with a Frantz magnetic separator. These last three steps were repeated several times to obtain a clean material. Groundmass fractions were leached with acids to remove carbonate alterations from the rock. Finally, the remaining fractions were separated by handpicking using a binocular microscope and stored in aluminium containers for irradiation.

Groundmass fractions of the metabasalts were separated in the OSU Argon Geochronology Laboratory in Oregon State University. $^{40}\text{Ar}/^{39}\text{Ar}$ ages were obtained by incremental heating methods using an ARGUS-VI mass spectrometer. Groundmass samples were irradiated for 6 hours (Irradiation 15-OSU-07) in the TRIGA CLICIT nuclear reactor at Oregon State University, along with the FCT sanidine (28.201 ± 0.023 Ma, 1σ) flux monitor (Kuiper *et al.*, 2008). Individual J-values for each sample were calculated by parabolic extrapolation of the measured flux gradient against irradiation height and typically gave 0.2-0.3% uncertainties (1σ). The ARGUS-VI mass spectrometer at Oregon State University has 5 Faraday collectors (all fitted with 10^{12} Ohm resistors) and 1 ion-counting CuBe electron multiplier (located in a position next to the lowest mass Faraday collector). This allowed us to measure simultaneously all argon isotopes, with mass 36 on the multiplier and masses 37 through 40 on the four adjacent Faradays. This configuration provides the advantages of running in a full multi-collector mode while measuring the lowest peak (on mass 36) on the highly sensitive electron multiplier (which has an extremely low dark-noise and a very high peak/noise ratio). Irradiated samples were loaded into Cu-planchettes in an ultra-high vacuum sample chamber and incrementally heated by scanning a defocused 25 W CO_2 laser beam in pre-set patterns across the sample, in order to release the argon evenly. After heating, reactive gases were cleaned up using an SAES Zr-Al ST101 getter operated at 400°C for ~ 10 minutes and two SAES Fe-V-Zr ST172 getters operated at 200°C and room temperature, respectively. All ages were calculated using the corrected Steiger and Jäger (1977) decay constant of $5.530 \pm 0.097 \times 10^{-10}$ 1/yr (2σ) as reported by Min *et al.* (2000). For all the other constants used in the age calculations we refer to Table 2 in Koppers *et al.* (2003). Incremental heating plateau ages and isochron ages were calculated as weighted means with $1/\sigma^2$ as weighting factor (Taylor, 1997) and as YORK2 least-square fits with correlated errors (York, 1969) using the ArArCALC v2.6.2 software from Koppers (2002) available from the <http://earthref.org/ArArCALC/> website.

Zircon mineral separation for granodiorite sample NL16-04 ($\sim 1\text{kg}$) was produced in the Laboratorio de Caracterización Mineral (CarMINLab) at Centro de Geociencias, Universidad Nacional Autónoma de México, using conventional methods (crushing, sieving, magnetic separation, and heavy liquids). Zircons for U-Pb geochronology were mounted in epoxy resin and grounded to nearly half their thickness using abrasives. Transmitted and reflected-light photos (not shown) were taken of all mounted zircon grains to aid in the spot selection to perform the laser ablation ICP-MS studies. In addition, scanning electron microscope-cathodoluminescence images (SEM-CL) of all zircons were obtained at the CarMINLab and used to reveal internal zoning related to chemical composition variations in order to avoid possible problematic areas within grains (Fig. 7C).

U-Th-Pb zircon geochronology of the granodiorite sample was conducted in the Laboratorio de Estudios Isotópicos (LEI) at Centro de Geociencias, Universidad Nacional Autónoma de México, using a Resonetics Workstation model M050 equipped with a LPX220 excimer laser coupled with a Thermo ICap Qc quadrupole ICP-MS (inductively coupled plasma-mass spectrometer), following analytical techniques similar to those reported in previous publications by Solari *et al.* (2010) and González-León *et al.* (2016).

Sample spot beam locations are $\sim 23\mu\text{m}$ in diameter. To account for down-hole fractionation observed in the primary standard zircon, the data reduction was performed using the commercial software "Iolite 2.5" by Paton *et al.* (2010, 2011), employing the VisualAge data reduction scheme presented in Petrus and Kamber (2012). The primary zircon-bracketing standard used was 91500 (Wiedenbeck *et al.*, 1995; TIMS age of $1065.4 \pm 0.6\text{Ma}$) whereas PLE standard (Plešovice; Sláma *et al.*, 2008; TIMS age of $337.13 \pm 0.37\text{Ma}$) was used as secondary standard control. All uncertainties were propagated using Iolite protocols and are reported at 2-sigma level of precision (Supplementary File 6). The data were exported from Iolite and plotted with computational software "Isoplot 3.0" (Ludwig, 2003) and shown in a concordia diagram and a weighted mean age plot (Fig. 7A & B). No common Pb correction was applied to the geochronology data because the ^{204}Pb signal is insignificant in comparison to the overwhelming ^{204}Hg signal present in the system.

4. Mineral chemistry and geothermometry

The thermal metamorphism of the volcanic rocks is characterized by the presence of actinolite, chlorite and calcite pseudomorphs, which are mainly produced from the alteration of clinopyroxene and olivine phenocrysts (Fig. 4A-4C). Titanomagnetite phenocrysts were partially leached forming skeletal crystals. Diopside crystals were preserved in sample AB10-06B from Cerro San Agustín (Fig. 4D, see also Supplementary File 1). The groundmass consists of titanomagnetite, sphene, actinolite, chlorite, and late crystallized albite microcrystals (Fig. 4E,4F). Actinolite in the groundmass shows an acicular habit and is often found as micro pseudomorph crystals derived from primary clinopyroxene. These particular replacements are better understood when observing the picobasalt flow groundmass which is formed by diopside microcrystals. Quartz, feldspar and calcite veins are observed in veins and amygdaloid textures.

EMPA analyses were performed on four lava flow samples from the Cerro Rajón Fm. Actinolite was identified and characterized in all the samples (Fig. 5A). Late stage interstitial crystallization of albite was also observed in all the samples (Fig. 5B). Titanomagnetite phenocrysts from up to 5mm thick are common in the volcanic flows. Only one ilmenite crystal was properly measured from a volcanic flow in the Cerros de la Ciénega locality. This crystal shows high TiO_2 and MnO values ($\text{TiO}_2 \leq 48.79\%$ and $\text{MnO} \leq 10.23\%$). Mineral chemistry can be found in the Supplementary File 1.

Actinolite and albite compositions results were used to calculate metamorphic temperatures in the volcanic flows using the calculations of Holland & Blundy (1994). These calculations were calibrated for amphiboles and plagioclase thermometry reaction to edenite + 4 quartz = tremolite + albite. While the actinolite lacks sufficient aluminum for the geobarometry calculations, a geothermometer can be utilized. Results from the Cerro Rajón metabasalt (AB16-53A) show an average metamorphism temperature of $481 \pm 40^\circ\text{C}$ with a standard deviation of 30°C . Cerro Calaveras flow (AB11-46) shows an average metamorphism temperature of $548 \pm 40^\circ\text{C}$ with a standard deviation of 40°C . Cerro Los Apaches flow (AB15-20) shows an average metamorphism temperature of $482 \pm 40^\circ\text{C}$ with a standard deviation of 29°C . Cerros de la Ciénega flow (AB15-24) shows an average metamorphism temperature of $529 \pm 40^\circ\text{C}$ with a standard deviation of 39°C .

Being recognized as the closest granitic intrusive to the Cambrian volcanism, the granodiorite from Cerro El Dátil was collected and analyzed for mineral chemistry and geochronology. EMPA results from the granodiorite sample (NL16-04) contain oligoclase (Fig. 5B) and magnesiohornblende (Fig. 5A). Amphiboles in this sample show a slight alteration to actinolite in the borders. Geothermometry calculations for the granodiorite were made using a calibration reaction edenite + albite = richterite + anorthite from Holland & Blundy (1994). The calculations of this sample show an average crystallization temperature of 664°C with a standard deviation of 26°C . While Holland & Blundy (1994) calculations for estimated temperatures were adequate, the geobarometer proved to be unsuccessful, probably due to the actinolite alteration of the hornblende. Therefore, Molina *et al.* (2015) calibrations for amphibole-plagioclase Al-Si partitioning were used. This calculation proved to be more adequate due to the regression methods based on the MM-

estimator utilized. The average pressure for the granodiorite samples is 3.08 kbar with a standard deviation of 0.75. Molina *et al.* (2015) geobarometry calculations report an error of ± 1.5 kbar. These calculations were not fitted for the volcanic flows due to the greenschist facies metamorphism observed.

5. $^{40}\text{Ar}/^{39}\text{Ar}$ and U-Pb geochronology

Groundmass separates were obtained from volcanic lava flows in three localities in the east and west portions of the study area (Cerro Calaveras, Cerro Los Apaches, and Cerro San Agustín; Fig. 1). Two samples from the first mentioned localities were characterized as metabasalts. These samples show a metamorphic groundmass formed by actinolite, chlorite, titanomagnetite and late stage albitized plagioclase. Two groundmass separates from sample AB15-20 (Cerro Los Apaches) were prepared for $^{40}\text{Ar}/^{39}\text{Ar}$ age determinations. Both analyses yielded plateau ages of 56.86 ± 0.57 Ma and 55.89 ± 0.6 Ma (Fig. 6A, 6B). Two analyses from sample AB11-46 (Cerro Calaveras) yielded complex age spectra and suggested ages of 57.31 ± 0.57 Ma and 60.26 ± 0.33 Ma (Fig. 6C, 6D).

While samples from the western part of the study area indicate Paleocene age for the metamorphosed lava flows, sample AB10-06B, from Cerro San Agustín, yields a weighted mean age of 81.37 ± 0.81 Ma, which places it in the late Cretaceous. This sample was characterized as a picobasalt with fresh diopside phenocrysts and microcrystals (Fig. 4D). It also exhibits alkaline feldspar in an interstitial position. $^{40}\text{Ar}/^{39}\text{Ar}$ groundmass ages from Cerro San Agustín are consistent with preliminary results from Barrón-Díaz *et al.* (2018). In samples AB15-20 and AB11-46, the groundmass is formed by metamorphic reactions of actinolite, titanomagnetite and late stage crystallization albite. Sphene is also abundant in a cloudy habit. Sample AB10-06B indicated a similar metamorphic paragenesis, with the exception of diopside microcrystals in the groundmass that have not been transformed into actinolite.

Approximately 150 zircons, mostly euhedral crystals of ~ 50 – 200 μm in size, were mounted and characterized using transmitted and reflected-light microscopy images, in addition to scanning electron microscope-cathodoluminescence images (SEM-CL; e.i., Fig. 7C). Based on these zircon images we selected the best 30 grains for perform the U-Pb zircon geochronology using the laser ablation ICP-MS technique (see Supplementary File 6). The collected U-Th-Pb zircon data were plotted in a Terra-Wasserburg concordia diagram (Fig. 7A), and a group of the most concordant zircon analyses were selected to calculate a $^{206}\text{Pb}/^{238}\text{U}$ weighted mean age of 71.1 ± 0.4 Ma (Fig. 7B; Mean Squares of Weighted Deviates = MSWD = 1.06, $n = 19$) that we interpret as the age of crystallization of the Cerro El Dátil granodiorite sample NL16-04.

6. Discussions and conclusions

Metamorphic minerals in the Cambrian lava flows appear to be controlled by the hydrothermal alteration affecting the succession (Fig. 4A-4C). Minerals vary based in the degree of alteration received by each locality. Ilmenite and diopside phenocrysts were the only primary minerals preserved from the rock protolith (see Supplementary File 1). Hydrothermal processes lixiviated Ti from the ilmenite phenocrysts, probably producing the sphene in a cloudy habit observed as a secondary mineral in the groundmass (Fig. 4E, 4F). Diopside and olivine crystals were also affected by the hydrothermal alteration, producing actinolite-chlorite pseudomorphs and calcite pseudomorphs when reaching higher alteration temperatures. Diopside phenocrysts and microcrystals in the picobasalt lava flows from Cerro San Agustín allow to suggest that the actinolite microcrystals in the volcanic lava flows were produced from these primary clinopyroxenes. Furthermore, the picobasalt sample lacks of plagioclase, consistent of ultramafic rocks. Ultramafic characteristics of the protoliths of this volcanism were suggested using geochemical criteria in the volcanic clasts (Barrón-Díaz *et al.*, 2018).

Metamorphic mineral paragenesis of albite, actinolite, calcite, chlorite and epidote are typical of greenschist facies metamorphism (Fettes *et al.*, 2007). Although, the abundance of epidote, the presence of magnesiohornblende, and a metamorphic temperature of 548 $^{\circ}\text{C}$ in sample AB11-46 may indicate that this sample is close to the boundary of the epidote-amphibolite facies, which is defined by Eskola (1920, 1939) and recommended by Fettes *et al.* (2007). Epidote-amphibolite facies require slightly higher metamorphic pressure conditions than the ones reported herein. Although,

other studies in central Sonora report Laramide intrusives with the required pressures (Barra *et al.*, 2005). Geothermometry results from the lava flows are consistent with metamorphism temperatures obtained from the tuffaceous conglomerate volcanic clasts of the Cerro Rajón Fm. (Barrón-Díaz *et al.*, 2018).

Geothermometry results in the metamorphic minerals are consistent with high temperature greenschist facies rocks. This metamorphic overprint may be due to the granitic intrusions observed close to the study area (Radelli *et al.*, 2008; Leyva-Ruíz *et al.*, 2017). Although no plutonic bodies were observed in direct contact with the Neoproterozoic-Cambrian succession, petrographic and geothermometric results indicate that Laramide age batholithic bodies affected the sequence and probably uplifted the volcanic succession (Fig. 8). This geologic setting where a Laramide intrusive uplifts a Proterozoic succession is also observed in the Sierrita Prieta locality approximately 40 km southeast from Bámori area. In this locality, the San Hipólito batholith, is associated with other Laramide batholiths from the Central Sonora region, due to its geochemical and mineralogical characteristics (Urrutia-Bañuelos *et al.*, 2008).

Estimated pressures from sample NL16-04 from the Cerro El Dátil locality indicate a possible average depth of emplacement of 8.31 km, considering 1 kbar = 2.7 km. This result is consistent with other calculated depths for Laramide granites in the state of Sonora. Zúñiga-Hernández (2010) reported emplacement depths of 7.05 km in the Rancho Las Cabecitas locality, in the central part of Sonora. Other studies in central Sonora show similar results (Barra *et al.*, 2005; Damon *et al.*, 1983b). While the granodiorite sample from the Cerro El Dátil locality and other Sonora state Laramide bodies shows similarities, it is important to consider that the calculated pressures may be affected by the alteration of the hornblende crystals. Therefore, this is a preliminary geothermobarometry study of the Caborca granitoids, and more systematic studies are required to properly understand the emplacement depths and temperatures for this magmatism.

$^{40}\text{Ar}/^{39}\text{Ar}$ geochronology results from the groundmasses of samples from the study area are consistent with the Sonora Laramide batholith emplacement timespan (Valencia-Moreno *et al.*, 2006; Ramos-Velázquez *et al.*, 2008). The age obtained from Cerro San Agustín (81.37 ± 0.81 Ma) shows very high MSWD values. The age difference between the two main localities could be explained as an older Laramide intrusion affecting the east part of the study area, although a partially open system is more likely to be the reason for this incorrect metamorphic age. Therefore, we suggest that the $^{40}\text{Ar}/^{39}\text{Ar}$ ages obtained from the metabasalts in the west part of the study area, should be considered as the closest approximation to the metamorphism age that affected the early Cambrian volcanism. The upper Cretaceous age obtained from the granodiorite at the Cerro El Dátil locality is consistent with the reported ages for Laramide intrusives in the region (Valencia-Moreno *et al.*, 2006, Paz-Moreno *et al.*, 2018). Although, due to the difference with the metamorphic ages obtained, younger intrusives may be buried closer to the Cambrian volcanism.

Figure 8 shows a cross section with the proposed interaction between the Neoproterozoic and Cambrian successions and the Laramide intrusive affecting them. Geologic and thermometric results suggest a very close influence of the Laramide intrusions, even though there are no visible granitic rock outcrops in the area. Combined results suggest that the geologic history of the Cerro Rajón Fm. volcanism started with a deposition followed by a subsidence event where the volcanic units were buried for approximately 8 km or more, a scenario consistent with platform deposits. Meanwhile, the volcanic unit were affected by an intrusive probably during the Paleocene. Finally, the extensional processes produced by the California peninsula separation (Martín-Barajas, 2000) exhumed the Neoproterozoic and Cambrian successions and the Laramide intrusive rocks. More studies are needed to properly understand the interaction between these rocks in the Caborca region.

Acknowledgements

Financial support for this project was generously provided by the University of Sonora PIFI (2015-2018). We thank Aimeé Orcí from ERNO-UNAM and Sheila Corral from UNISON for their work fabricating thin sections. We thank Ken Domanik for his support and guidance in the electron microprobe laboratory. We are thankful to the many local landowners who gave us permission to view outcrops on their property, especially R. Lizarraga and the Fresnillo mining company for assistance in Caborca. We thank Anthony Koppers from the OSU Argon Geochronology Laboratory and the

staff who helped in the samples processing. We would like to thank Alejandra Bocanegra-Castellanos and Concepción Arredondo-de La Rosa (CarMINLab) for their help with zircon mineral separation and SEM-CL characterization. In addition, we are very grateful to Carlos Ortega-Obregón (LEI) for his assistance calibrating LA-ICP-MS equipment and for supervising data reduction procedures for the U-Pb zircon geochronology. We are thankful with three anonymous reviewers which greatly contributed to improve the manuscript and with the revision from Pablo Paz Peñalba for the English grammar reviews.

References

- Arvizu, H., Iriondo, A., Izaguirre, A., Chávez-Cabello, G., Kamenov, G.D., Solís-Pichardo, G., Foster, D.A., and Lozano-Santa Cruz, R., 2009, Rocas graníticas pérmicas en la Sierra Pinta en el NW de Sonora, México: Magmatismo de subducción asociado al inicio del margen continental activo del SW de Norte América, *Revista Mexicana de Ciencias Geológicas*, v. 26(3), p. 709-728.
- Barra, F., Ruiz, J.; Valencia, V.A., Ochoa-Landin, L., Chesley, J.T., and Zurcher, L, 2005, Laramide porphyry Cu-Mo mineralization in northern Mexico: Age constraints from Re. Os Geochronology in molybdenite, *Economic Geology*, v. 100, p. 1605-1616.
- Barrón-Díaz, A.J., 2013, Caracterización petrogenética de las metabasitas anorogénicas del límite Cámbrico-Precámbrico, Municipio de Pitiquito, Sonora, México [M.S. thesis]: Universidad de Sonora, 95 p.
- Barrón-Díaz, A.J., Paz-Moreno, F.A., Lozano-Santa Cruz, R., Herrera-Urbina, S., Centeno-García, E. and López-Martinez, M., 2018, Early Cambrian alkaline volcanism on the southern margin of Laurentia: Evidence in the volcanoclastic units from the Puerto Blanco Formation in the Caborca Block, NW Mexico, *International Geology Review*. DOI: 10.1080/00206814.2018.1501619
- Barrón-Díaz, A.J., Paz-Moreno, F.A., and Hagadorn, J.W., 2019, The Cerro Cerro Rajón Formation—a new lithostratigraphic unit proposed for a Cambrian (Terreneuvian) volcano-sedimentary succession from the Caborca region, northwest Mexico, *Journal of South American Earth Science*, v. 89, p. 197-210.
- Coney, P.J., and Reynolds, S.J., 1977, Cordilleran Benioff zones, *Nature*, v. 270, p. 403–406.
- Coney, P.J., 1990, Terranes, tectonics and the Pacific rim, in Fouts, J., and Brennan, T., eds., *Proceedings, Pacific Rim Congress 90: Parkville, Victoria, Australian Institute of Mining and Metallurgy*, p. 19–30.
- Cooper, G.A., and Arellano A.R.V., 1952, Introduction and stratigraphy, in Cooper, G. A., Arellano, A. R. V., Johnson, J. H., Okulitch, V. J., Stoyanow, Alexander, and Lochman, Christina, eds., *Cambrian stratigraphy and paleontology near Caborca, northwestern Sonora, Mexico, Smithsonian Miscellaneous Collections*, v. 119, no. 1, p. 1-23.
- Damon, P.E., Shafiqullah, M., Roldán-Quintana, and J., Cochemé, J.J., 1983a, El batolito Laramide (90–40 Ma) de Sonora, *Pap. Memoir of the 15th National Convention of the AIMMGM, Guadalajara, Jalisco*, p. 63–95.
- Damon, P. E., Shafiqullah, and M., Clark, K. F., 1983, Geochronology of the porphyry copper deposits and related mineralization of Mexico: *Canadian Journal of Earth Sciences*, no. 20, p. 1052-1071.
- Dickinson, W.R., 2002, The Basin and Range Province as a Composite Extensional Domain, *International Geology Review*, v. 44, no. 1, p. 1-38.
- Eells, J.L., 1972, *Geology of the Sierra de La Berruga, north-western Sonora, Mexico* [M.S. thesis]: San Diego, California State University, 77 p.
- Eskola, P., 1920, The Mineral Facies of Rocks, *Norsk Geologisk Tidsskrift*, no. 6, p. 143-194.
- Eskola, P., 1939, Die metamorphen Gesteine, in T. F. W. Barth, C. W. Correns, and P. Eskola (eds.), *Die Entstehung der Gesteine*, Julius Springer, Berlin, p. 263–407.
- Fettes, D.J., Desmons, J., Árkai, P., and International Union of Geological Sciences, 2007, *Metamorphic rocks: A Classification and Glossary of Terms: recommendations of the International Union of Geological Sciences Subcommittee on the Systematics of Metamorphic Rocks*, Cambridge, Cambridge University Press.
- González-León, C.M., Solari, L., Valencia-Moreno, M., Rascón-Heimlel, M.A., Solé, J., González-Becuar, E., Lozano-Santacruz, R., and Pérez-Arvizu, O., 2016, Late Cretaceous to early Eocene magmatic evolution of the Laramide arc in the Nacozari quadrangle, northeastern Sonora, Mexico and its regional implications, *Ore Geology Reviews*.
- Holland, T., and Blundy, J., 1994, Non-ideal interactions in calcic amphiboles and their bearing on amphibole-plagioclase thermometry. *Contributions to Mineralogy and Petrology*, v. 116, p. 433-447.

- Iriondo, A., Premo, W.R., Martínez-Torres, L.M., Budahn, J.R., Atkinson Jr., W.W., Siems, D.F., and Guarás-González, B., 2004, Isotopic, geochemical, and temporal characterization of Proterozoic basement rocks in the Quitovac region, northwestern Sonora, Mexico: Implications for the reconstruction of the southwestern margin of Laurentia, *Geological Society of American Bulletin*, v. 116, no. 1. p. 154–170.
- Koppers, A.A.P., 2002, ArArCALC—Software for $^{40}\text{Ar}/^{39}\text{Ar}$ age calculations, *Comput. Geosci.*, v. 28, p. 605-619. [Available at <http://earthref.org/tools/ararcalc.htm>.]
- Koppers, A., Staudigel, H., Wijbrans, J.R., and Pringle, M., 2003, Short-lived and discontinuous intraplate volcanism in the South Pacific: Hot spots or extensional volcanism?, *Geochem. Geophys. Geosyst.*, v. 4, p. 1089. DOI:10.1029/2003GC000533.
- Kuiper, K.F., Deino, A., Hilgen, F.J., Krijgsman, W., Renne, P.R., and Wijbrans, J. R., 2008, Synchronizing rock clocks of Earth history, *Science*, v. 320, p. 500-504. DOI:10.1126/science.1154339.
- Leake, B.E., Woolley, A.R., Arps, C.E.S., Birch, W.D., Gilbert, M.C., Grice, J.D., Hawthorne, F.C., Kato, A., Kisch, H.J., Krivovichev, V.G., Linthout, K., Laird, J., Mandarin, J.A., Maresch, W.V., Nickel, E.H., Rock, N.M.S., Schumacher, J.C., Smith, D.C., Stephenson, N.C.N., Ungaretti, L., Whittaker, E.J.W., and Guo, Y., 1997, Nomenclature of amphiboles: Report of the subcommittee on amphiboles of the international mineralogical association, commission on new minerals and mineral names, *Canadian Mineralogist*, v. 35, p. 219–246.
- Leyva-Ruiz, N., Barrón-Díaz, A.J., Lozano-Santa Cruz, R., and Paz-Moreno, F.A., 2017, Petrografía y geoquímica de los intrusivos granitoides en el Cerro El Dátil, municipio de Pitiquito, Sonora, México, XXVII Congreso Nacional de Geoquímica, *Actas INAGEQ*, v. 23, p. 104.
- Longoria, J.F., González, M.A., Mendoza, J.J., and Pérez, V.A., 1978, Consideraciones estructurales en el Cuadrángulo Pitiquito-La Primavera, NW de Sonora [Structural considerations in the Pitiquito-La Primavera quadrangle, northwestern Sonora, Mexico]: *Universidad de Sonora, Departamento de Geología Boletín*, v. 1, p. 61-67.
- Longoria, J.F., 1981, Geologic features of northwest Sonora, in Longoria, Jose, ed., *Regional geology of northwest Sonora: Geological Society of America, Cordilleran Section Annual Meeting, Hermosillo, Sonora, Mexico, Proceedings*, p. 1-48.
- Loyd, S.J., Marengo, P.M., Hagadorn, J.W., Lyons, T.W., Kaufman, A.J., Sour-Tovar, F., and Corsetti, F.A., 2013, Local $\delta^{34}\text{S}$ variability in ~580 Ma carbonates of northwestern Mexico and the Neoproterozoic marine sulfate reservoir, *Precambrian Res.*, v. 224, p. 551–569.
- Ludwig, K.R., 2003. User's Manual for ISOPLOT 3.00: A geochronological toolkit for Microsoft Excel. Berkeley, Berkeley Geochronology Center, no. 4 (Special Publication), 74 p.
- Martín-Barajas, A., 2000, Volcanismo y extensión en la Provincia Extensional del Golfo de California, *Boletín de la Sociedad Geológica Mexicana*, v. 53, n. 1, p. 72-83.
- Min, K., Mundil, R., Renne, P. R., and Ludwig, K. R., 2000, A test for systematic errors in $^{40}\text{Ar}/^{39}\text{Ar}$ geochronology through comparison with U/Pb analysis of a 1.1-Ga rhyolite, *Geochim. Cosmochim. Acta*, v. 64, p. 73-98.
- Molina, F., Moreno, J.A., Castro, A., Rodríguez, C., and Fershtater, G.B., 2015, Calcic amphibole thermobarometry in metamorphic and igneous rocks: New calibrations based on plagioclase/amphibole Al-Si partitioning and amphibole/liquid Mg partitioning, *Lithos*, v. 232, p. 286-305.
- Paton, C., Woodhead, J.D., Hellstrom, J.C., Hergt, J.M., Greig, A., and Maas, R., 2010, Improved laser ablation U-Pb zircon geochronology through robust downhole fractionation correction. *Geochemistry, Geophysics, Geosystems*, 11, QOAA06. DOI: 10.1029/2009GC002618
- Paton, C., Hellstrom, J., Paul, B., Woodhead, J., and Hergt, J., 2011, Lolite: Freeware for the visualization and processing of mass spectrometric data. *Journal of Analytical Atomic Spectrometry*, v. 26, p. 2508–2518.
- Petrus, J.A., and Kamber, B.S., 2012, VizualAge: a novel approach to laser ablation ICP-MS U-Pb geochronology data reduction, *Geostand. Geoanal. Res.*, v. 36, p. 247–270.
- Paz-Moreno F.A., Izaguirre-Pompa A. and Iriondo A., 2018, Geoquímica y Geocronología del pórfido monzonítico Cretácico tardío del Cerro Gasolinera, norte de Caborca Sonora, México: una marca del magmatismo adakítico laramídico, XXVIII Congreso Nacional de Geoquímica, *Actas INAGEQ*, v. 24, no.1.
- Ramos Velázquez, E., Calmus, T., Valencia, V., Iriondo, A., and Bellon, H., 2008, U-Pb and $^{40}\text{Ar}/^{39}\text{Ar}$ geochronology of the coastal Sonora batholith: New insights on Laramide continental arc magmatism, *Revista Mexicana de Ciencias Geológicas*, v. 25, no. 2, p. 314-333.
- Radelli, L., Solis-Weiss, V., Dórame-Navarro, M., De la Cruz-Ortega, L. C., and Urrutia, J., 2008, Fossil content and structural relationships of the San Luis zone and Caborca zone of NW Sonora, Mexico. Suppression of the precambrian Z. of Caborca, *Boletín de Geología Universidad Industrial de Santander, Colombia*, v. 30, no. 2, p. 1-34.

- Raisz, E., 1964, Land forms of Mexico: Cambridge, MA, Office of Naval Research, Second Edition.
- Sláma, J., Košler, J., Condon, D.J., Crowley, J.L., Gerdes, A., Hanchar, J.M., Horstwood, M.S.A., Morris, G.A., Nasdala, L., Norberg, N., Schaltegger, U., Schoene, B., Tubrett, M.N., and Whitehouse, M.J., 2008, Plešovice zircon — A new natural reference material for U–Pb and Hf isotopic microanalysis: *Chemical Geology*, v. 249, p. 1–35.
- Solari, L.A., Gómez-Tuena, A., Bernal, J.P., Pérez-Arvizu, O., and Tanner, M., 2010, U-Pb zircon geochronology by an integrated LA-ICPMS microanalytical workstation: achievements in precision and accuracy: *Geostandards and Geoanalytical Research*, v. 34(1), p. 5–18.
- Sour-Tovar, F., Hagadorn, J.W., and Huitrón-Rubio, T., 2007, Ediacaran and Cambrian index fossils from Sonora, Mexico., *Paleontology*, v. 50, Part 1, p. 169-175.
- Steiger, R.H., and Jäger, E., 1977, Subcommittee of geochronology: convention on the use of decay constants in geo- and cosmochronology. *Earth and Planetary Science Letters*, v. 36, p. 59-362.
- Stewart, J.H., McMenamin, A.S., and Morales-Ramirez, J. M., 1984, Upper Proterozoic and Cambrian Rocks in the Caborca Region, Sonora, Mexico. *Physical Stratigraphy, Biostratigraphy, Paleocurrents Studies and Regional Relations.*, U. S. Geological Survey Professional Paper 1390.
- Stewart, J.H., Amaya-Martinez, R., and Palmer, A.R., 2002, Neoproterozoic and Cambrian strata of Sonora, Mexico: Rodinian supercontinent to Laurentian Cordilleran margin, *Geological Society of America, Special Paper 365*, p. 5-48.
- Taylor, J.R., 1997, *An Introduction to Error Analysis: The Study of Uncertainties in Physical Measurements*, Univ. Sci. Books, Mill Valley, Calif., 327 p.
- Urrutia-Bañuelos, J., Paz-Moreno F.A., Demant, A., and Meza-Figueroa, D.M., 2008, Estudio geoquímico del plutonismo laramídico del batolito San Hipólito, Sonora central, México, XVIII Congreso Nacional de Geoquímica, Actas INAGEQ, v. 18, no.1, p. 42-43.
- Valencia-Moreno, M., Ruiz, J., Barton, M.D., Patchett, P.J., Zurcher, L., Hodkinson, D.G., and Roldán-Quintana, J., 2001, A chemical and isotopic study of the Laramidic granitic belt of northwestern México: Identification of the southern edge of the North American Precambrian basement, *Geological Society of America Bulletin*, v. 113(11), p. 1409-1422.
- Valencia-Moreno, M., Iriondo, A., and González-León, C., 2006, Temporal constraints on the eastward migration of the Late Cretaceous-Early Tertiary magmatic arc of NW Mexico based on new ⁴⁰Ar/³⁹Ar hornblende geochronology of granitic rocks, *Journal of South American Earth Sciences*, v. 22(1-2), p. 22-38.
- York, D., 1969, Least squares fitting of a straight line with correlated errors, *Earth and Planetary Science Letters*, v. 5, p. 320-324.
- Wiedenbeck, M., Allé, P., Corfu, F., Griffin, W.L., Meier, M., Oberli, F., Von Quadt, A., Roddick, J.C., and Spiegel, W., 1995, Three natural zircon standards for U–Th–Pb, Lu–Hf, trace-element and REE analyses, *Geostandards Newsletter*, v. 19, p. 1–23.
- Zúñiga-Hernandez, L.G., 2010, Estudio geológico, geoquímico y metalogenético del cuadrángulo Huépac-Moctezuma, centro noreste de Sonora, México, [M.S. thesis]: Universidad de Sonora, 95 p.

Figure Captions

Fig. 1. Location map from the surrounding of the Rancho Bámori south from Caborca city. Studied localities where samples were taken are marked with a red star. Section A-B location (Fig. 8) is also marked. After Barrón-Díaz *et al.* (2018).

Fig. 2. Stratigraphic column of the type section of the Rajón Formation Fm. Metabasalts flows can be observed at the top of the succession in this locality. The position of the volcanic flows varies in the studied localities. For a detailed description of these variations see Fig. 8 in Barrón-Díaz *et al.*, 2019).

Fig. 3. A. Photograph from a metabasalt sample, Cerro Rajón locality. Porphyritic textures can be observed. Red arrow heads indicate green clinopyroxene pseudomorph (usually altered to actinolite and chlorite), white arrow heads indicate olivine pseudomorph and titanomagnetite. **B.** Metabasalt outcrop in the Cerro Rajón Type Section. Red dashed line separate the scoriaceous base from the rest of the volcanic flow. Hammer is 30cm long. **C.** Metabasalt flow in the Cerro Calaveras locality. A porphyritic texture can be observed. White arrowheads indicate holes probably produced by

crystal dissolution. Common desert weathering can be observed printing a glare in the surface of the rock. Knife is 7.6 cm long.

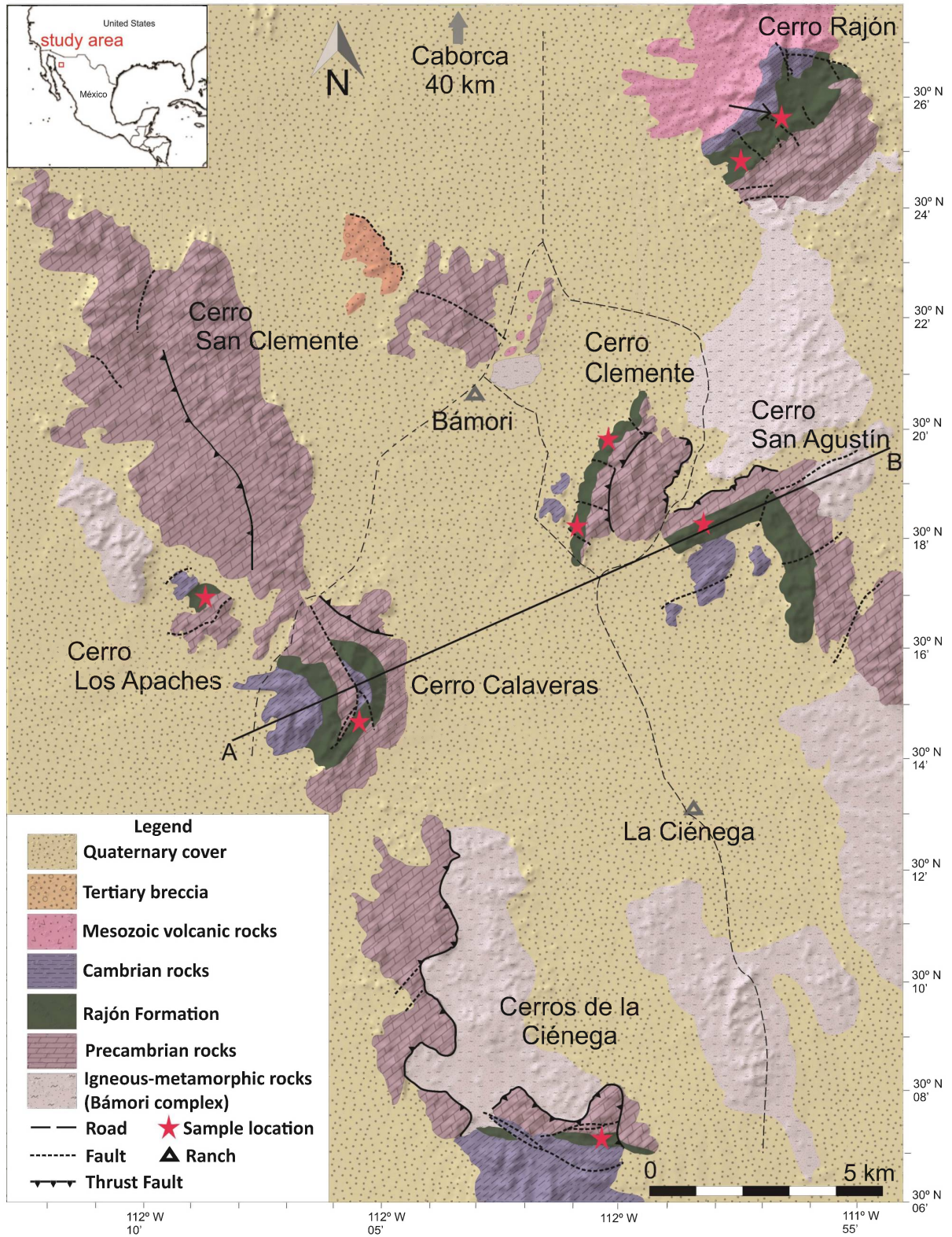
Fig. 4. **A.** Microphotograph of a metabasalt showing an actinolite-chlorite pseudomorph after clinopyroxene. Cerro Rajón. **B.** Actinolite-chlorite pseudomorph and epidote crystals from a metabasalt. Sample AB11-46 from Cerro Calaveras. **C.** Calcite and Ti-Fe pseudomorph after olivine. Sample AB15-20 from Cerro los Apaches. A calcite vein is cutting the porphyroblast. **D.** Picobasalt showing a diopside phenocryst in a diopside-sphene-titanomagnetite groundmass. Sample AB10-06B from Cerro San Agustín. **E.** Clinopyroxene crystal transformed to actinolite. Sphene and albite in the groundmass. **F.** Detailed of the groundmass in the metabasalts showing metamorphic minerals such as actinolite, chlorite, sphene and late stage crystallization albite. E and F are back-scattered electron images with the CAMECA SX100. Act=actinolite, chl=chlorite, ab=albite, ox=oxide, sph= sphene.

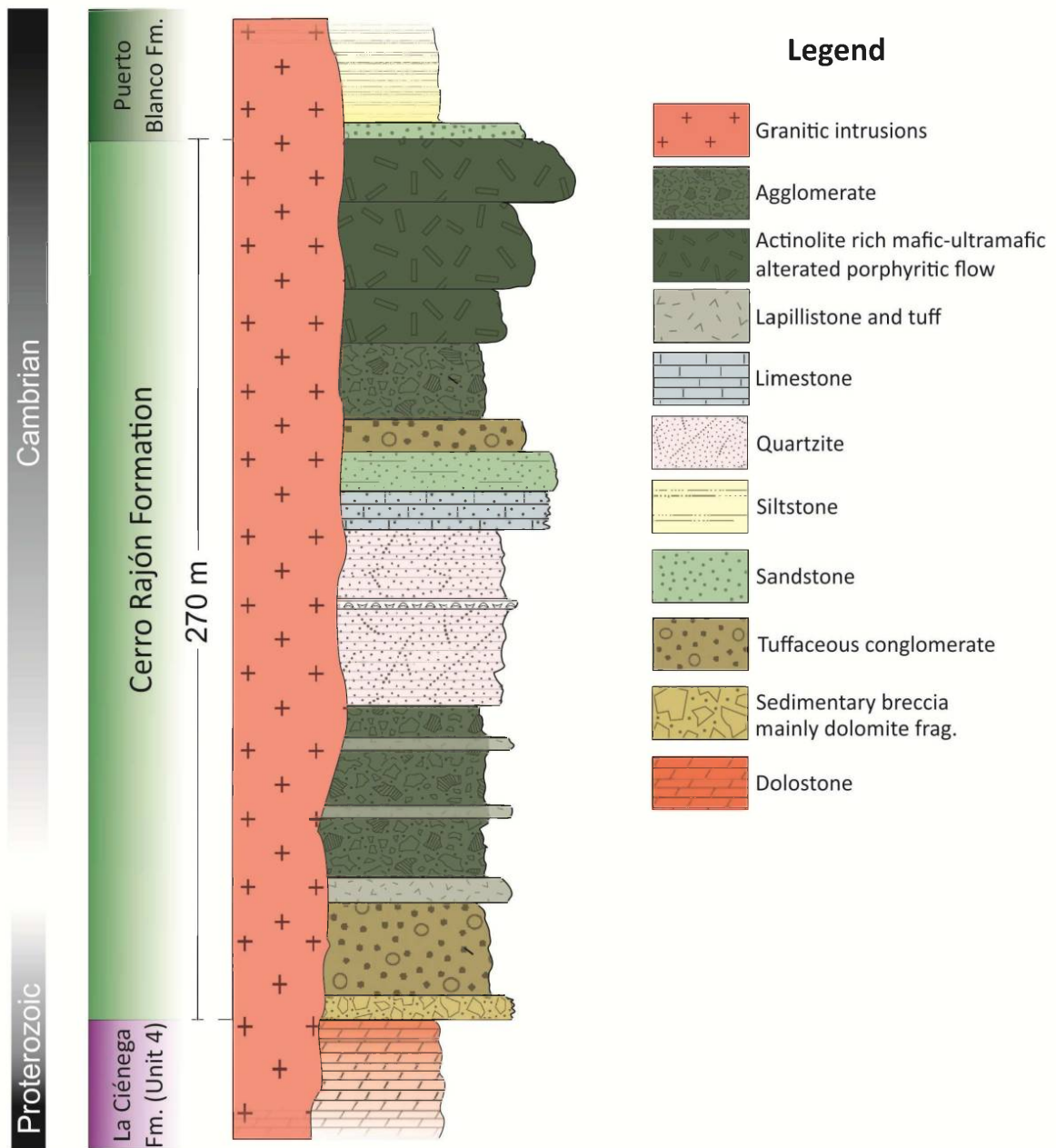
Fig. 5. **A.** Amphibole classification from Leake *et al.* (1997). Samples represent volcanic metabasalts from the Cerro Rajón Formation, except for sample NL16-04 which is a granodiorite from Cerro El Dátil locality. **B.** Ab-An-Or diagram for feldspars nomenclature. Albitization of plagioclase can be observed in the metabasalt lava flow samples.

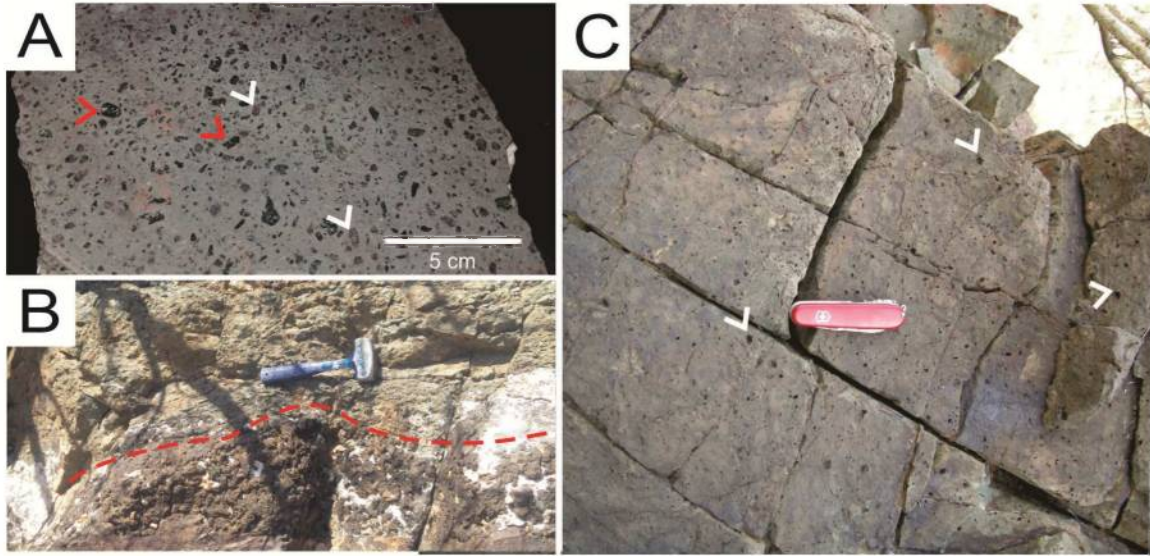
Fig. 6. $^{40}\text{Ar}/^{39}\text{Ar}$ plots for the metabasalt samples from the Rajón Formation. **A – B** metabasalt sample from Cerro Los Apaches. **C-D** metabasalt sample from Cerro Calaveras. Both samples are located west of the study area. **E** corresponds to the picobasalt sample in the east portion of the study area. The MSWD in this last sample is very high and therefore the age may be incorrect.

Fig. 7. **A.** Tera–Wasserburg concordia diagram and weighted mean age plot (**B.**) for granodiorite sample NL16-04. The most concordant U-Pb zircon analyses, used for the $^{206}\text{Pb}/^{238}\text{U}$ age calculation ($n = 19$), are shown as black-line error ellipses with black squares in the concordia diagram (**A.**) and as gray bars in weighted mean age plot (**B.**). **C.** SEM-Cathodoluminescence images of representative dated zircons from the granodiorite sample; yellow semicircles and the adjacent numbers represent the spot size ($\sim 23\mu\text{m}$) and the spot number, respectively. The $^{206}\text{Pb}/^{238}\text{U}$ ages are reported in Ma at the 2-sigma level of precision.

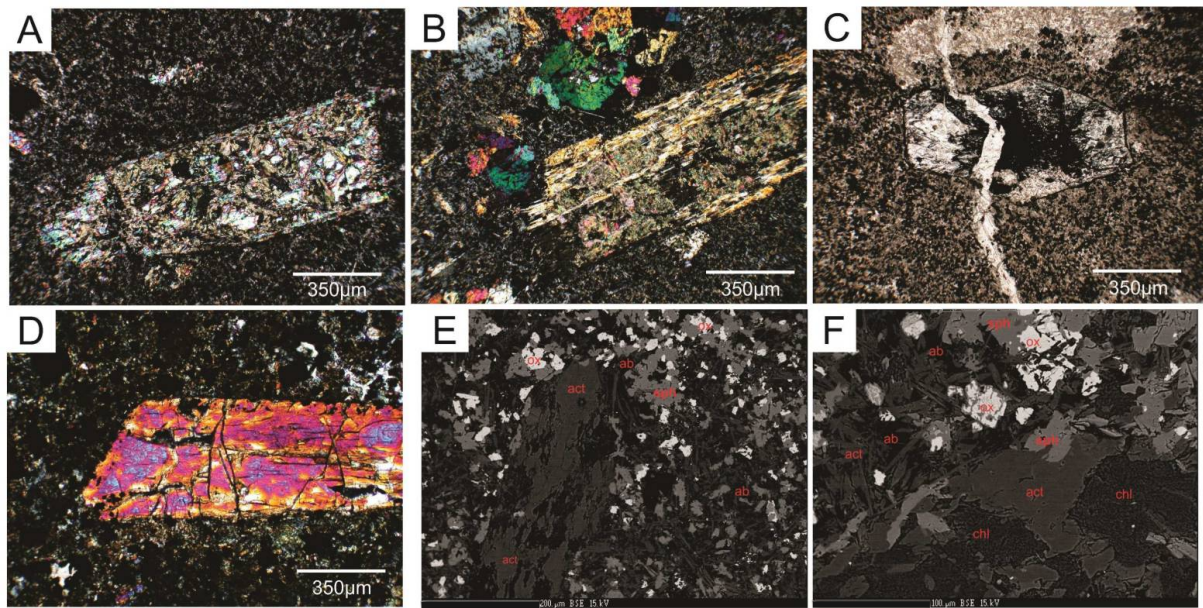
Fig. 8. Geologic cross section from southwest to northeast of the study area. Section A-B is marked in Fig. 1. Laramide intrusive position may not correspond to precise depths. Vertical scale is exaggerated x4 times to illustrate the pending roof position of the Neoproterozoic and Cambrian successions. Normal faulting in the Cerro Calaveras locality can be better observed in the geological map (Fig. 1), where a normal fault with a strike component is repeating a previously folded succession.



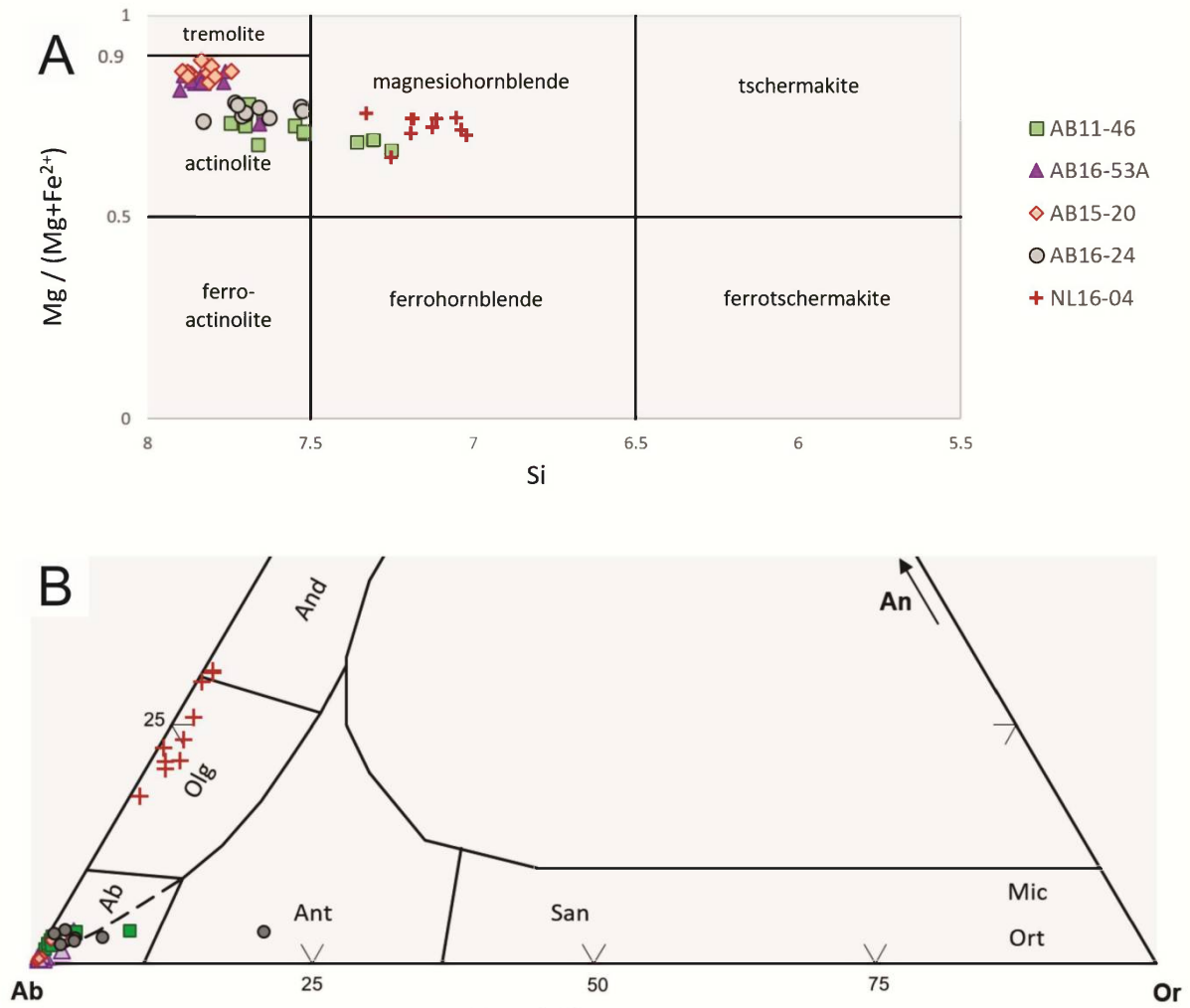


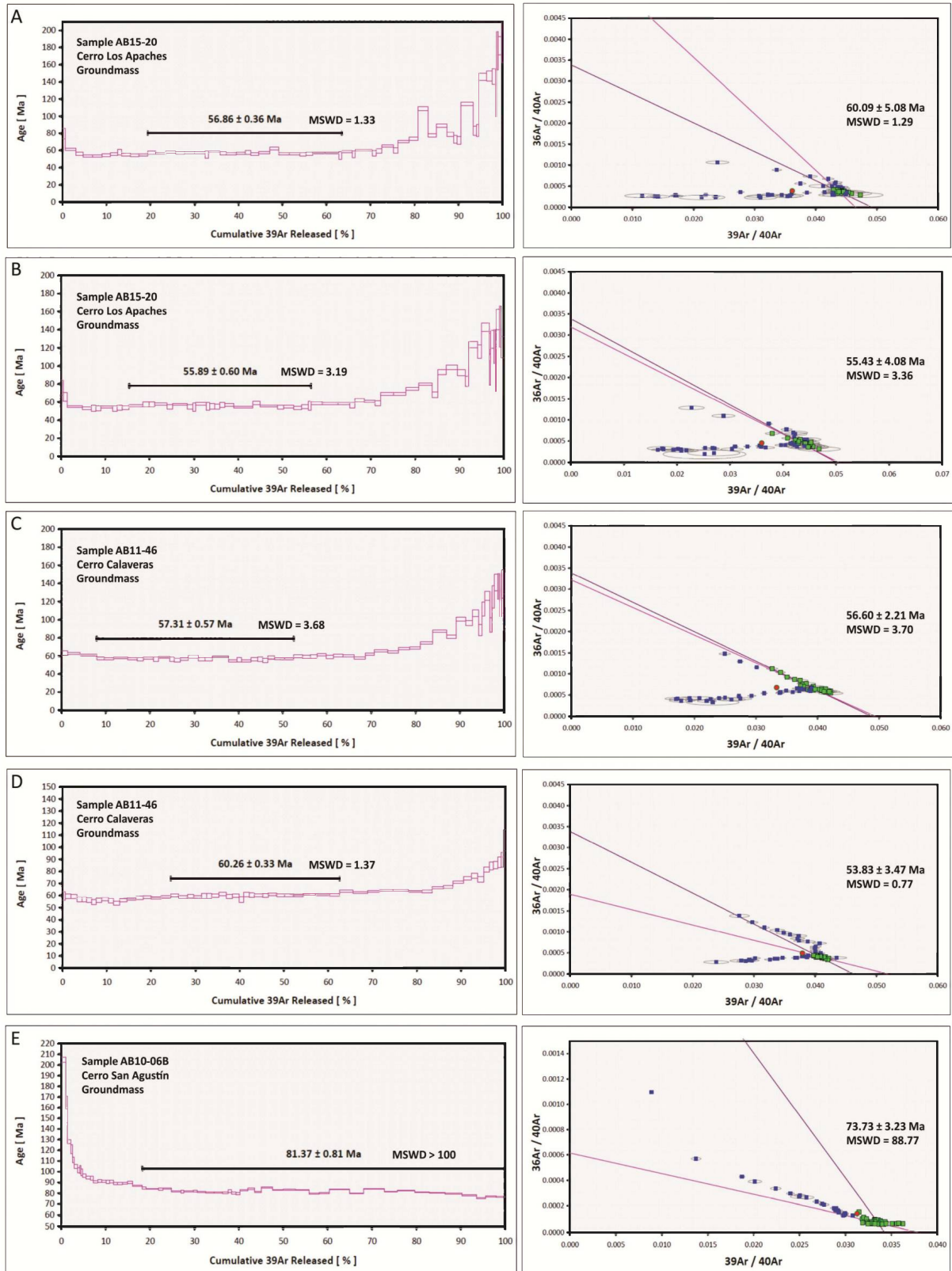


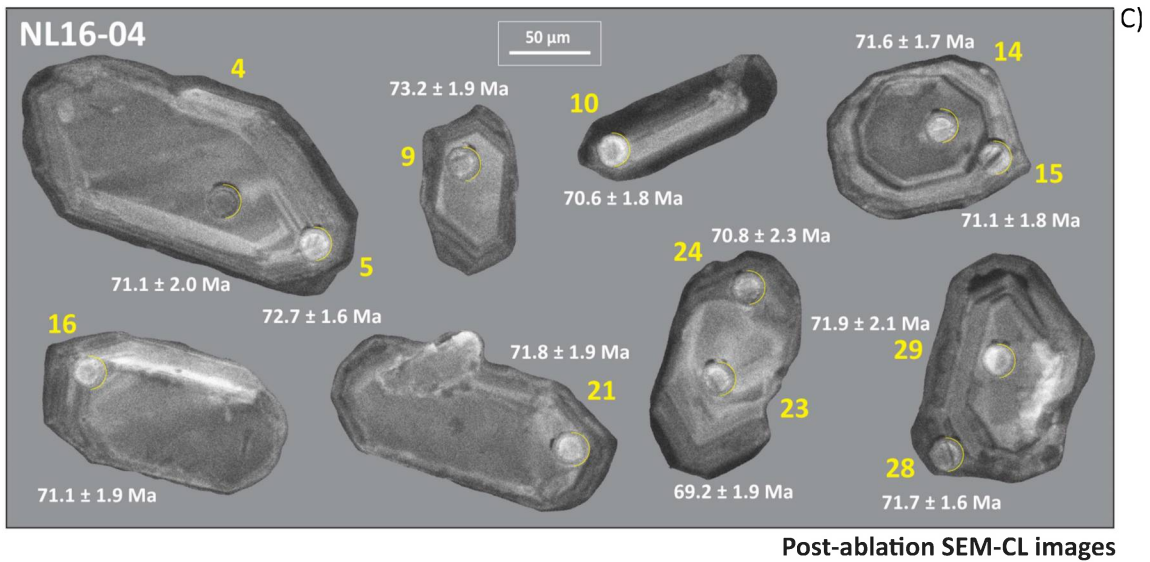
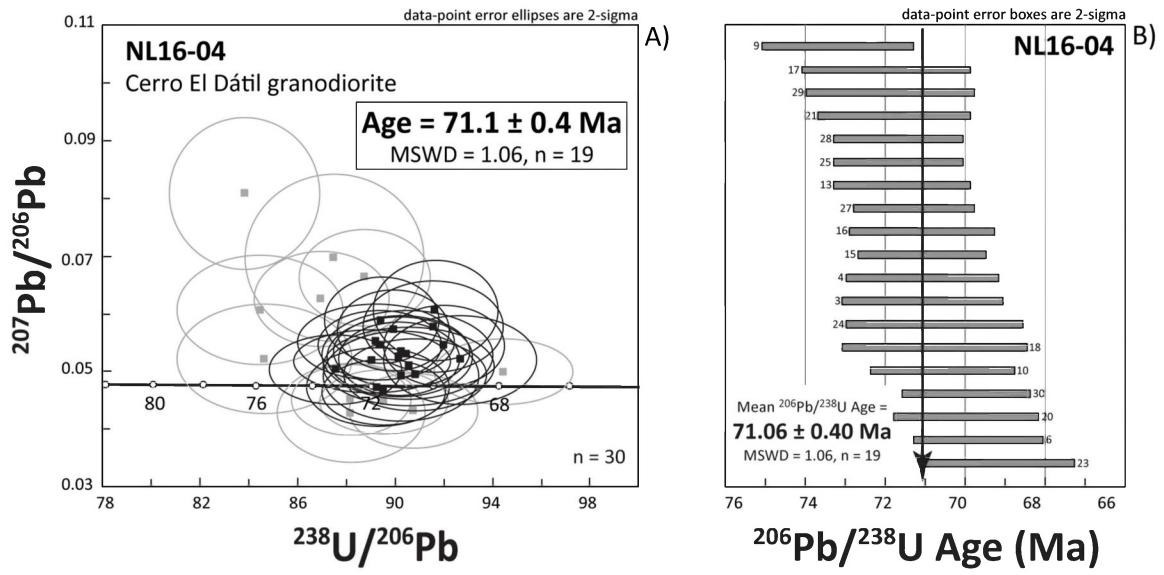
ACCEPTED MANUSCRIPT



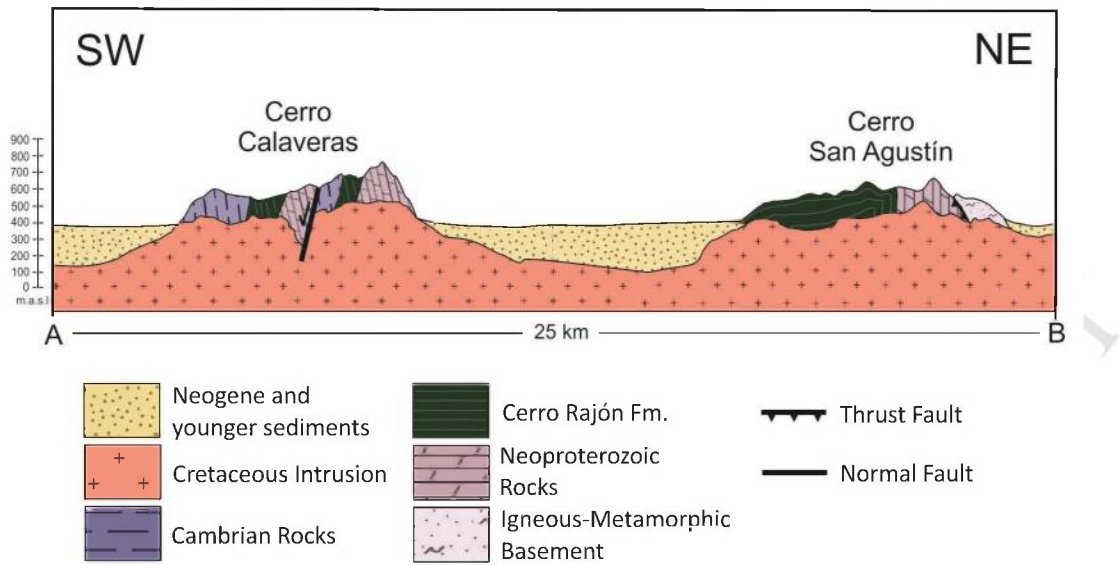
ACCEPTED MANUSCRIPT







ACCEPTED



ACCEPTED MANUSCRIPT

Highlights

1. Caborca Cambrian volcanism is affected by Laramide metamorphism
2. $^{40}\text{Ar}/^{39}\text{Ar}$ geochronology results show metamorphism ages of ~ 60 Ma
3. An U-Pb zircon age of 71.1 ± 0.4 Ma is reported for a nearby Laramide intrusive
4. Cambrian metabasalts show greenschist facies metamorphism ($T < 548$ °C)
5. Caborca block successions were rapidly exhumed by basin and range

5

CARACTERÍSTICAS PETROGENÉTICAS DEL MAGMATISMO MÁFICO- ULTRAMÁFICO DE LA FORMACIÓN CERRO RAJÓN

CARACTERÍSTICAS PETROGENÉTICAS DEL MAGMATISMO MÁFICO-ULTRAMÁFICO DE LA FORMACIÓN CERRO RAJÓN

5.1 Introducción

La Formación Cerro Rajón, definida por [Barrón-Díaz et al. \(2019a\)](#), contiene un volcanismo que ha sido caracterizado como productos máficos-ultramáficos derivados de un actividad estromboliana en un margen continental pasivo cercano a la línea de costa. Las características geoquímicas de este volcanismo fueron estudiadas por [Barrón-Díaz \(2013\)](#) y posteriormente por [Barrón-Díaz et al. \(2018\)](#) desde los clastos volcánicos contenidos en los conglomerados tufáceos de la Formación Cerro Rajón. Estos trabajos indican que el magmatismo es de naturaleza alcalino, producido por bajas tasas de fusión parcial.

En este trabajo se aborda un mayor número de estudios y una discusión más profunda que la expuesta en [Barrón-Díaz \(2013\)](#), incluyendo las unidades lávicas de la Formación Cerro Rajón y los sills ultramáficos contenidos en la Formación La Ciénega y FORMACIÓN El Arpa, los cuales no fueron contemplados en el trabajo de [Barrón-Díaz et al. \(2018\)](#). Esta discusión permitirá contextualizar geológicamente los eventos volcánicos ocurridos a inicios del Cámbrico en la región de Caborca, utilizando todos los elementos petrogenéticos que se han adquirido hasta la fecha. Para lo anterior, se presentan los resultados geoquímicos de estas unidades, los cuales contribuyen a las discusiones generales del presente estudio y complementan la petrogénesis descrita por [Barrón-Díaz et al. \(2018\)](#).

Antes de abordar esta descripción geoquímica, es importante mencionar que los productos magmáticos pueden diferenciarse en dos grupos según el enfoque de estudio desde el que se analicen. Desde su ocurrencia en el campo, las unidades pueden identificarse como productos volcánicos o unidades hipabisales (sills). De forma general los derrames presentan un mayor espesor (de 6 a 25 metros) que los sills (< 2 metros). Sin embargo, los derrames ubicados a la base de la columna estratigráfica del Cerro Los Apaches (ver Figura 8 en [Barrón-Díaz et al., 2019a](#)), son derrames excepcionales de 60 cm de espesor. Estas características dificultan la distinción entre algunos derrames y los sills cercanos al límite

de la Formación Cerro Rajón con la subyacente Formación La Ciénega del precámbrico. Los productos del magmatismo también pueden ser diferenciados desde sus características geoquímicas, en rocas máficas y ultramáficas. Esta discriminación también es sustentada por la mineralogía (abundancia Cpx>Ol y ausencia de Pl), en la cual la plagioclasa se manifiesta únicamente en los derrames más diferenciados. El derrame de picrobasaltos observado en la localidad del Cerro San Agustín, es un ejemplo de productos de poco espesor (6 m) con una mineralogía de Cpx > Ol y ausencia de plagioclasa. Mientras que los derrames del Cerro Calaveras y Cerro Rajón, son ejemplos donde los volúmenes son mayores y se manifiesta la plagioclasa en los términos más diferenciados.

5.2 Características geoquímicas y petrogenéticas del magmatismo.

Se seleccionaron y analizaron un total de 14 derrames y 5 sills. Estos últimos fueron obtenidos de las secuencias precámbricas Formación La Ciénega y uno de ellos de la Formación El Arpa. La geoquímica de los metabasaltos (incluye términos máficos y ultramáficos) y sills se caracteriza por tener valores bajos en SiO₂ (22.70% – 50.30%) y altos en TiO₂ (<6.49%). Los valores más bajos en SiO₂ se presentan en los sills, los cuales también presentan los menores espesores y una mayor lixiviación de los elementos mayores. El MgO en las rocas es generalmente alto (<14.55%), a diferencia de los clastos volcánicos, donde la alteración lixivió el Mg en muchas de las muestras (Barrón-Díaz *et al.*, 2018). Esta característica también permitió calcular el Mg#, el cual muestra un carácter primario del magmatismo (~70; [Tabla 1](#)). Las muestras presentan distintos grados de alteración según la historia geológica de cada localidad de estudio. Esta alteración también se correlaciona con el espesor del derrame o sill. Mientras que los derrames más potentes, como las muestras del Cerro Calaveras y Cerro Rajón suelen conservarse mejor, los sills y los derrames de la base del Cerro Los Apaches (ver Figura 8 en [Barrón-Díaz *et al.*, 2019a](#)) presentan los valores más altos de pérdida por ignición (LOI). Es importante mencionar que debido a estas características geoquímicas y petrográficas de los derrames y sills, estas rocas deben ser consideradas como metamórficas y por lo tanto se acuñe al prefijo meta.

El cálculo de la norma CIPW permite observar algunas características del magmatismo. Sin embargo, los criterios para la utilización de la norma CIPW solo se cumplen en algunas de las muestras que tienen los valores de LOI más bajos. En esta ocasión se presentan todos los resultados, ya que, a pesar de no cumplir con los requisitos, todas las muestras son consistentes. Solo una muestra (AB16-53) presenta cuarzo normativo. Esto se puede deber a que este derrame es del grupo que corona a la Formación Cerro Rajón, los cuales tienen ligeramente una mayor diferenciación, en este caso la muestra es una

Locality	C. de la Ciénega	Cerro Los Apaches				Cerro Calaveras				Cerro San Agustín		Cerro Clemente			Cerro Rajón				
MAYOR	AB16-24	AB11- 31	AB11- 30C	AB11- 23A	AB15-20	AB11- 50	AB11- 46	AB11- 48	AB11- 52	AB10- 06A	AB10- 06B	AB11-04	AB14-02	AB11-07	AB15- 06B	AB15- 02M	AB16-53	AB15- 12B	AB16- 59B
Formation	CR	CR	CR	LC	CR	CR	CR	CR	CR	CR	CR	LC	CR	LC	CR	CR	CR	LC	EA
SiO ₂	38.40	29.50	33.40	34.10	43.90	44.10	45.20	45.40	47.30	38.50	40.90	22.70	32.80	38.90	42.00	43.70	50.30	32.20	36.60
TiO ₂	5.96	4.30	2.36	6.05	4.90	4.35	4.55	4.75	4.24	6.35	6.49	4.04	4.99	4.86	4.97	5.60	3.23	4.48	2.99
Al ₂ O ₃	10.15	7.83	3.92	9.74	8.65	9.47	10.05	10.30	13.95	9.11	9.42	6.88	9.28	10.05	9.28	10.10	5.77	7.41	5.43
Fe ₂ O ₃	15.70	12.85	12.95	15.40	15.00	12.25	13.00	13.10	13.60	15.95	15.60	12.90	16.10	11.95	15.45	14.25	13.40	12.55	10.30
FeO		6.13	2.05	6.19		3.69	8.34	6.79	2.81	7.96	6.08	6.08		5.57					
MnO	0.36	0.34	0.26	0.11	0.11	0.23	0.19	0.18	0.18	0.15	0.20	0.23	0.15	0.14	0.13	0.19	0.15	0.15	0.12
MgO	9.04	11.70	10.30	9.17	7.77	9.09	10.05	9.85	5.42	7.92	8.86	14.55	12.65	7.25	7.92	9.13	7.98	13.45	11.85
CaO	10.20	12.75	15.15	8.38	9.63	10.50	10.35	10.00	4.40	12.20	12.90	13.95	10.35	12.90	8.81	8.79	10.80	9.89	11.55
Na ₂ O	0.75	0.02	0.04	0.03	3.74	2.95	1.58	1.68	4.40	1.04	1.23	0.01	0.21	0.24	2.79	2.35	1.90	0.02	0.01
K ₂ O	3.58	1.38	0.77	3.17	0.36	1.20	1.92	2.13	2.54	1.10	1.38	0.35	1.36	4.40	0.58	1.35	0.73	1.22	0.68
P ₂ O ₅	1.04	0.58	0.31	0.97	0.67	0.59	0.63	0.65	0.96	0.51	0.59	0.68	1.16	1.29	0.56	0.56	0.45	0.55	0.31
LOI	4.27	19.90	22.30	12.90	3.41	4.69	2.91	3.14	2.77	6.17	2.38	22.00	9.40	5.51	6.45	2.41	6.23	16.30	19.50
Total	99.75	101.34	102.00	100.15	98.31	99.64	100.65	101.43	99.98	99.20	100.00	98.60	98.68	97.90	99.04	98.63	101.20	98.38	99.53
NORM CIPW																			
Quartz	0.0	0.0	0.0	0.0	0.0	0.0	0.0	0.0	0.0	0.0	0.0	0.0	0.0	0.0	0.0	0.0	6.7	0.0	0.0
Plagioclase	14.7	19.9	10.3	18.6	33.7	24.4	24.2	25.4	44.1	17.9	17.1	21.8	23.2	13.8	38.1	34.7	22.6	20.5	16.3
Orthoclase	12.1	0.0	0.0	4.8	2.3	7.3	10.8	12.1	15.3	6.6	8.0	0.0	0.0	0.0	3.8	8.5	4.6	0.7	5.1
Nepheline	3.7	0.1	0.2	0.1	3.5	5.7	1.4	1.1	2.5	4.4	4.8	0.1	1.1	1.2	0.0	0.0	0.0	0.1	0.0
Leucite	8.2	7.4	4.5	12.2	0.0	0.0	0.0	0.0	0.0	0.0	0.0	0.0	7.2	21.1	0.0	0.0	0.0	6.4	0.0
Kalsilite	0.0	0.0	0.0	0.0	0.0	0.0	0.0	0.0	0.0	0.0	0.0	1.4	0.0	0.0	0.0	0.0	0.0	0.0	0.0
Diopside	26.1	1.8	42.5	16.3	33.0	32.9	25.7	24.7	4.0	33.8	35.5	0.0	20.7	29.5	26.0	23.0	39.9	28.7	43.2
Hypersthene	0.0	0.0	0.0	0.0	0.0	0.0	0.0	0.0	0.0	0.0	0.0	0.0	0.0	0.0	1.4	4.4	16.5	0.0	16.2
Olivine	18.2	41.9	24.5	29.5	13.7	17.4	25.2	23.7	21.3	20.5	18.1	51.5	30.9	16.5	16.5	14.6	0.0	29.3	9.2
Larnite	0.0	14.5	8.9	0.0	0.0	0.0	0.0	0.0	0.0	0.0	0.0	17.9	0.4	2.5	0.0	0.0	0.0	0.0	0.0
Ilmenite	12.1	9.5	5.6	12.5	10.0	8.5	8.2	8.7	8.2	12.1	12.0	9.4	10.8	9.6	10.4	11.2	6.6	10.5	7.2
Magnetite	2.4	3.3	2.7	3.5	2.3	2.4	3.1	2.9	2.5	3.6	3.2	3.5	2.7	2.7	2.5	2.2	2.1	2.3	1.9
Apatite	2.6	1.6	0.9	2.4	1.7	1.4	1.4	1.5	2.3	1.2	1.3	2.0	3.1	3.1	1.4	1.4	1.1	1.6	0.9
Mg#	57.53	58.34	68.17	65.17	54.93	63.58	64.51	63.88	48.39	53.87	57.19	72.62	58.79	64.90	54.67	60.12	58.35	71.60	73.02

Tabla 1. Concentración de elementos mayores de los derrames y filones (sills > diques) de la Formación Cerro Rajón, Formación La Ciénega y Formación El Arpa. CR: Formación Cerro Rajón, LC: Formación La Ciénega, EA: Formación El Arpa

andesita-basáltica. En los derrames y sills predomina una ligera subsaturación en sílice (Ne norm. < 5%), consistente con el carácter medianamente alcalino que mostraba el diagrama TAS. La presencia de Larnita normativa en algunas de las muestras se puede deber a la contaminación por Ca que aportó el hidrotermalismo.

El diagrama *Total Alcalis vs Silica* (TAS) de [Le Bas et al. \(1986\)](#), clasifica a la mayoría los metabasaltos como subalcalinos ([Fig. 1](#)). La discriminación de [Schwarzer & Rogers \(1974\)](#), les atribuye un carácter medianamente alcalino ([Fig. 1](#)). Sin embargo, este diagrama solo puede ser utilizado en rocas con bajos valores de LOI. Por lo anterior, las muestras que cumplen con estas características ([Tabla 1](#)), son el picrobasalto del Cerro San Agustín, los basaltos del Cerro Rajón y Cerro Calaveras, la andesita-basáltica del Cerro Rajón y la hawaita del Cerro Calaveras. Para poder obtener una mejor caracterización del magmatismo, se utilizó el diagrama Zr/Ti vs Nb/Y de [Pearce \(1982\)](#), el cual utiliza elementos fuertemente inmóviles. Este diagrama clasifica el magmatismo como basaltos alcalinos.

Las concentraciones de elementos traza ([Tabla 2](#)) confirman la hipótesis de que el metamorfismo, a pesar de haber afectado los elementos mayores, no provocó una movilización significativa de los elementos traza incompatibles. Los valores de Cr son ≥ 400 ppm para 14 de las 19 muestras, llegando hasta 1520 ppm. Y los valores de Ni son ≥ 219 ppm, llegando hasta 882 ppm. Estos valores evidencian el carácter primario del magmatismo. Las concentraciones de Ba llegan hasta 3270 ppm para una muestra

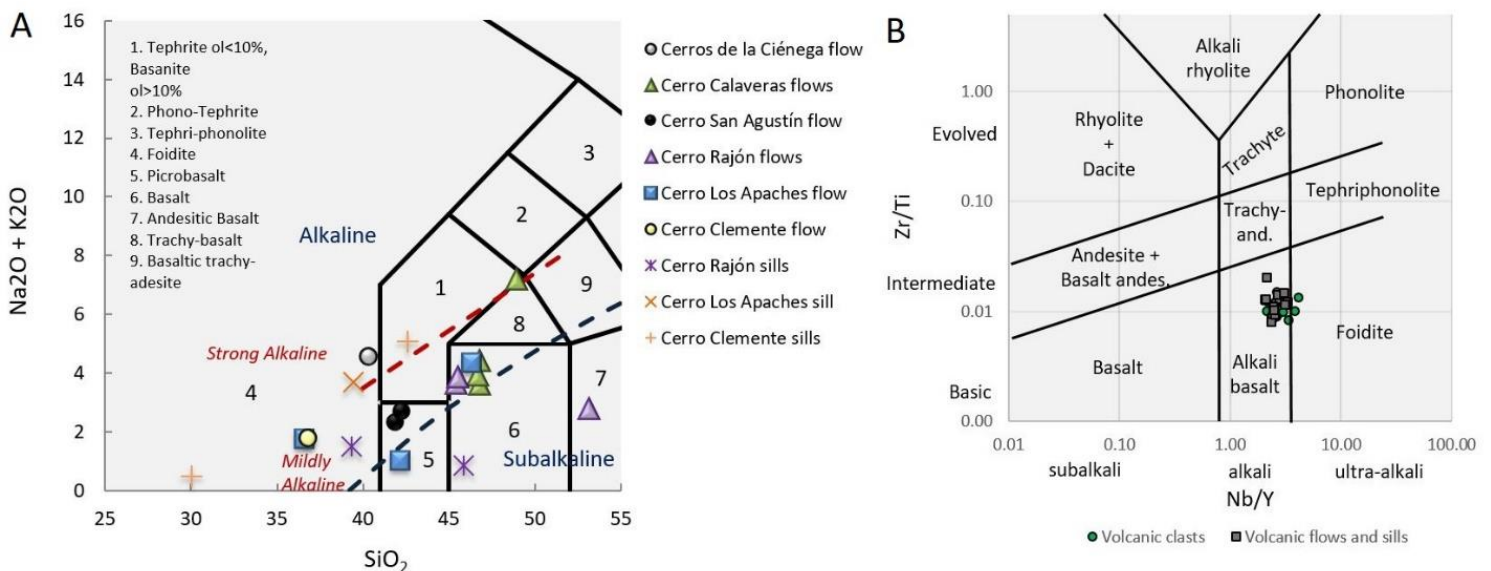


Figura 1. A. Diagrama de clasificación de rocas volcánicas Total Alcalis vs Silica de [Le Bas \(1986\)](#). Se graficaron las 19 muestras obtenidas de derrames y sills de las formaciones Cerro Rajón, La Ciénega y El Arpa. Sin embargo, solo algunas cumplen con los requisitos para utilizar este diagrama, el resto están representadas de forma comparativa. B. Diagrama de clasificación de rocas alteradas de [Pearce \(1982\)](#).

Locality	C. de la Ciénega	Cerro Los Apaches				Cerro Calaveras				Cerro San Agustín		Cerro Clemente			Cerro Rajón				
Formation	CR	CR	CR	LC	CR	CR	CR	CR	CR	CR	CR	LC	CR	LC	CR	CR	CR	LC	EA
SAMPLE	AB16-24	AB11-31	AB11-30C	AB11-23A	AB15-20	AB11-50	AB11-46	AB11-48	AB11-52	AB10-06A	AB10-06B	AB11-04	AB14-02	AB11-07	AB15-06B	AB15-02M	AB16-53	AB15-12B	AB16-59B
Ba	37	1715	262	47	851	249	727	554	756	1540	822	719	568	823	3270	61	585	683	161
Ce	55	136	98	52	174	143	105	113	115	172	122	123	132	202	105	106	111	75	107
Co	63	55	83	100	53	59	53	59	56	39	64	67	72	50	43	51	53	60	67
Cr	1320	310	980	1520	40	780	630	670	630	90	400	400	1360	390	<10	480	480	980	830
Cs	1	5	3	2	16	1	1	2	2	0	3	1	5	4	1	2	1	0	39
Cu	106	62	107	7	181	4	<5	98	96	46	240	316	91	181	170	8	113	8	164
Dy	4	8	6	3	9	7	7	7	7	10	8	8	6	8	8	6	7	4	6
Er	2	4	2	1	3	3	3	3	3	4	3	3	2	3	3	3	3	2	2
Eu	2	4	3	2	5	4	3	4	4	5	4	3	3	5	3	3	3	2	3
Ga	13	23	19	10	22	17	22	23	23	30	19	19	14	18	11	20	21	10	17
Gd	5	12	8	4	13	10	9	10	10	13	10	10	9	14	9	9	9	7	9
Hf	5	10	10	4	12	10	9	9	9	13	9	8	7	11	10	8	9	6	6
Ho	1	1	1	1	1	1	1	1	1	2	1	1	1	1	1	1	1	1	1
La	25	61	45	24	78	62	47	51	51	79	54	55	60	90	61	49	51	38	51
Lu	0	0	0	0	0	0	0	0	0	1	0	0	0	0	0	0	0	0	0
Mo	8	3	<2	2	<2	<1	<2	<2	2	2	2	2	<2	<1	<2	<1	<1	1	1
Nb	36	84	63	31	94	80	60	63	64	91	75	75	79	109	107	68	71	52	64
Nd	30	77	50	28	90	71	55	59	59	87	61	61	61	94	44	53	55	40	52
Ni	536	185	425	882	58	483	231	250	230	56	219	236	516	247	69	232	232	412	396
Pb	4	4	13	12	8	5	<5	6	6	5	5	9	9	<2	8	2	<2	4	2
Pr	7	17	12	7	22	17	13	14	14	21	15	15	16	24	12	13	14	10	13
Rb	22	53	52	30	109	7	16	62	52	20	38	24	19	36	44	20	26	8	64
Sm	6	16	10	6	17	14	12	12	12	18	12	12	11	18	10	11	11	8	11
Sn	1	3	2	1	4	3	3	3	3	4	3	3	2	3	3	2	3	2	3
Sr	57	561	243	150	249	281	433	534	543	352	754	647	342	716	575	194	444	365	128
Ta	2	6	5	2	7	5	4	4	4	6	5	5	5	7	5	4	4	3	4
Tb	1	2	1	1	2	1	1	1	1	2	1	1	1	2	1	1	1	1	1
Th	3	6	5	3	9	6	6	6	6	10	6	6	7	9	2	6	6	4	4
U	3	2	2	1	3	2	1	2	2	2	2	2	2	3	2	1	2	1	3
V	252	448	524	270	569	424	389	401	402	402	520	519	342	483	498	510	467	197	413
W	1	1	3	2	4	1	2	2	1	1	1	1	1	<1	1	1	<1	1	1
Y	16	35	24	13	34	28	29	31	31	43	31	32	24	34	35	28	29	17	25
Yb	1	3	1	1	2	2	2	2	2	3	2	2	2	2	2	2	2	1	2
Zn	134	141	299	144	186	98	139	149	147	165	186	177	734	130	131	119	137	83	112
Zr	178	400	365	144	471	407	338	357	363	521	338	316	299	484	428	308	347	222	252
ThTa	1.06	0.95	1.02	1.20	1.38	1.32	1.42	1.40	1.42	1.70	1.24	1.21	1.32	1.32	0.52	1.28	1.36	1.17	1.06

Tabla 2. Análisis de elementos traza en los derrames y filones (sills > diques) de la Formación Cerro Rajón, Formación La Ciénega y Formación El Arpa. CR: Formación Cerro Rajón, LC: Formación La Ciénega, EA: Formación El Arpa

de una peperita en el Cerro Rajón (AB15-06B), la cual esta mezclada con material detrítico.

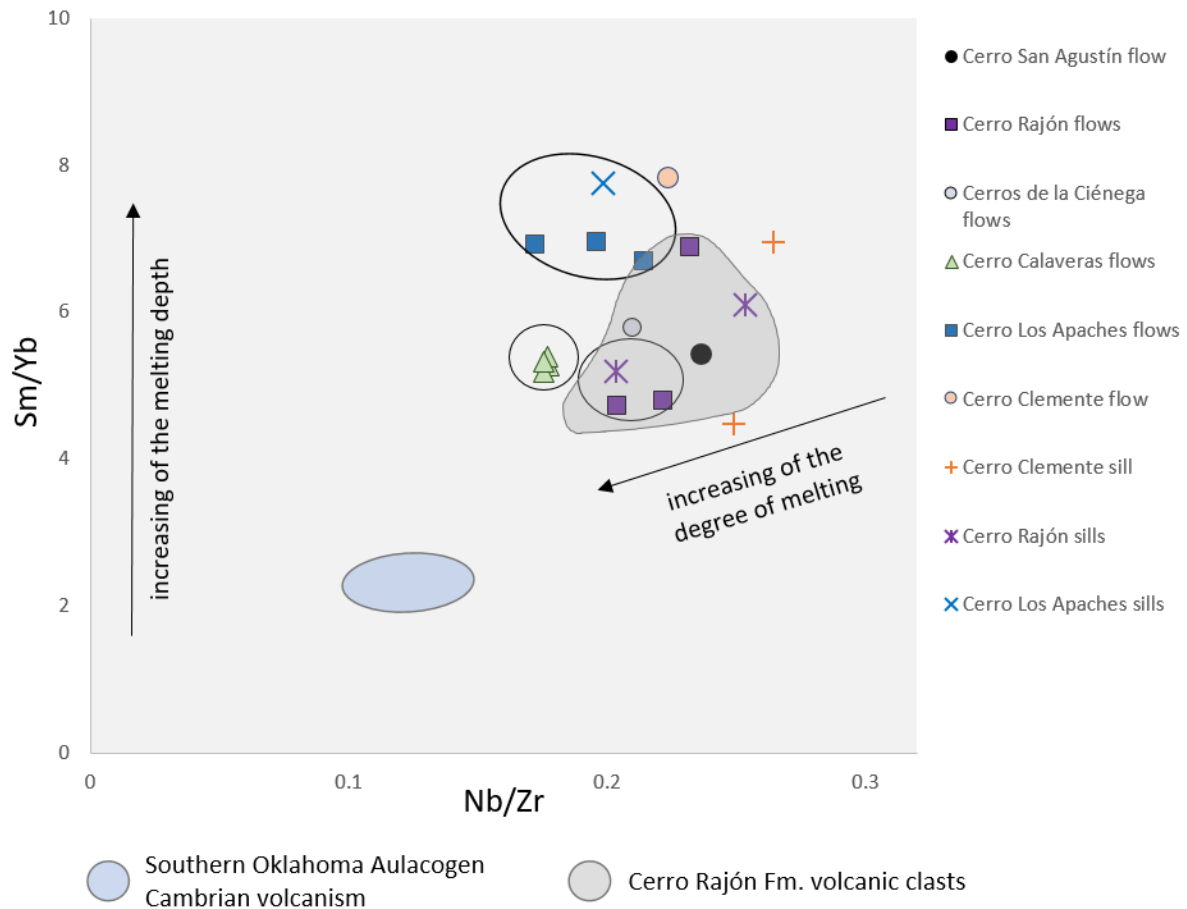


Figura 2. Diagrama Sm/Yb vs. Nb/Zr de He et al. (2010), de los derrames y sills de la Formación Cerro Rajón, Formación La Ciénega y Formación El Arpa. Los círculos indican una relación de la tasa de fusión y la profundidad en las muestras de las localidades del Cerro Los Apaches, Cerro Calaveras y Cerro Rajón.

Utilizando el diagrama de He et al. (2010), se puede observar que las muestras del Cerro Calaveras, Cerro Los Apaches y algunas del Cerro Rajón, se agrupan según su localidad (Fig. 2). Dentro de estos grupos, los sills presentan un ligero incremento en profundidad la fusión, lo cual es esperado. Las muestras de derrames y sills fueron evaluadas por métodos más precisos de estimación de las tasas de fusión parcial, pero debido a la alteración, no resultaron ser candidatos idóneos, por lo que se recurrió al diagrama cualitativo de He et al. (2010). A pesar de lo anterior, se puede apreciar como el magmatismo alcalino Cámbrico de la región de Caborca tiene tasas de fusión parcial menores a un volcanismo toleítico como el del aulacógeno del sur de Oklahoma.

El diagrama de tierras raras normalizado a los valores de la Condrita C1 (Sun y McDonough, 1989) muestra un paralelismo entre los espectros de los derrames y sills, los cuales siguen la trayectoria del

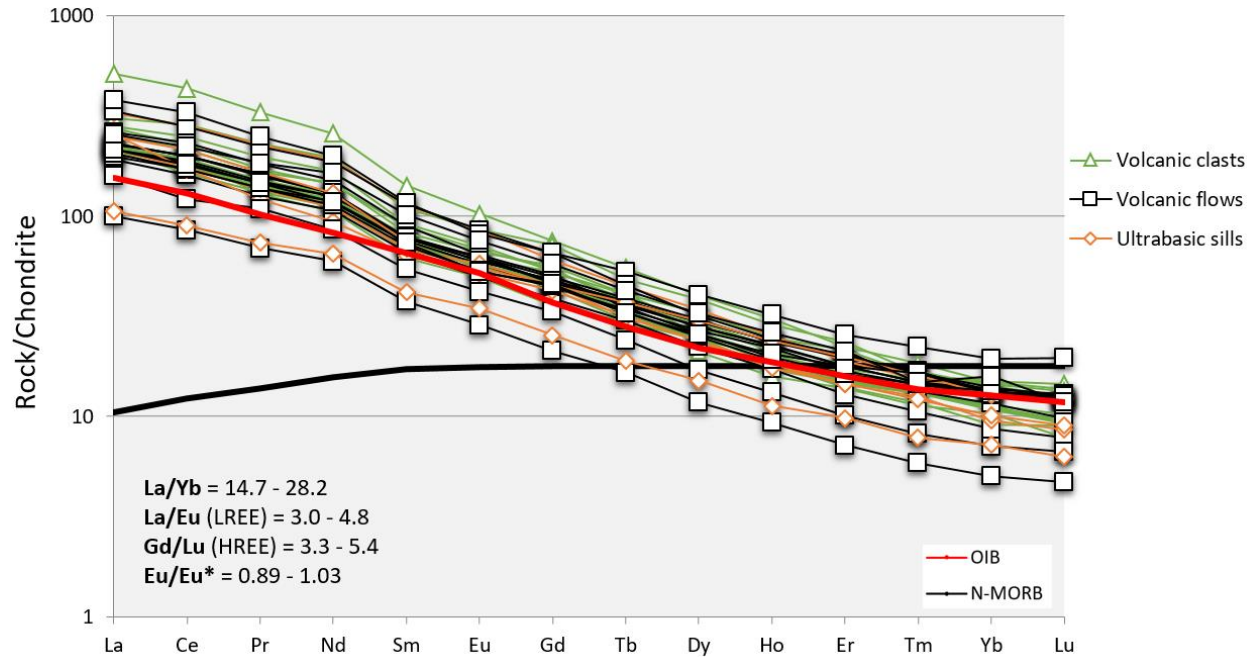


Figura 3. Diagrama de tierras raras normalizado a los valores de la Condrita C1 para los derrames y sills de la Formación Cerro Rajón, Formación La Ciénega y Formación El Arpa. Los espectros de clastos volcánicos (Barrón-Díaz *et al.*, 2018) son presentados como comparación. Los espectros OIB y N-MORB son obtenidos de Sun y McDonough (1989).

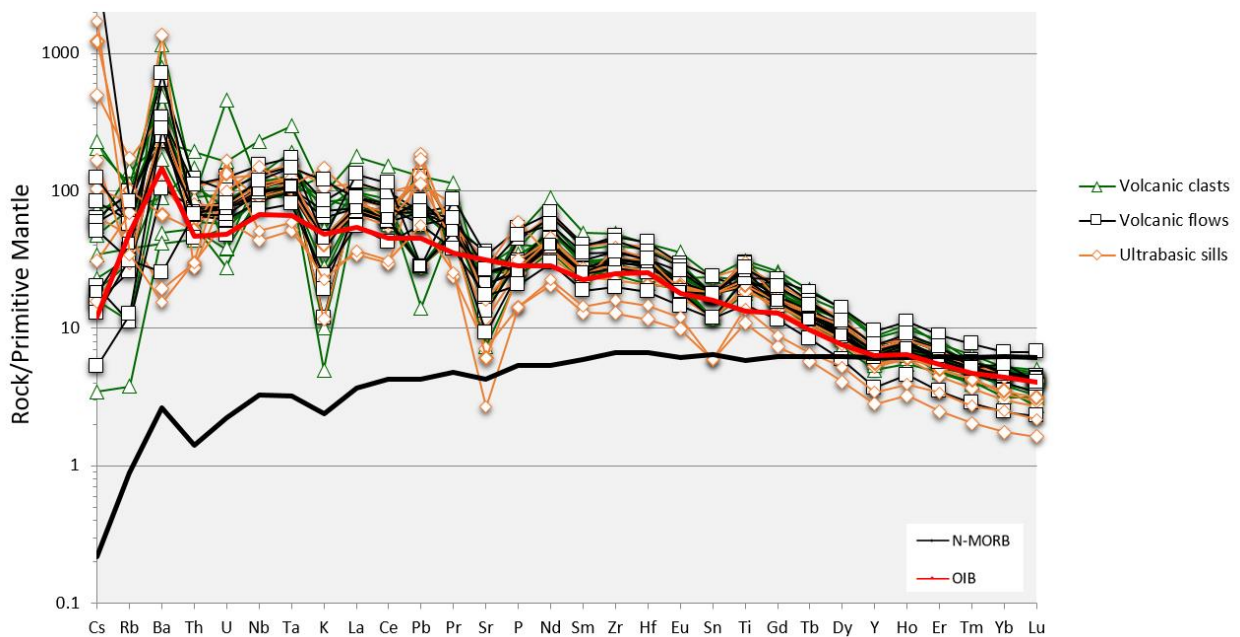


Figura 4. Diagrama de tipo *Spider* normalizado con manto primitivo para los derrames y sills de la Formación Cerro Rajón, Formación La Ciénega y Formación El Arpa. Los espectros de clastos volcánicos (Barrón-Díaz *et al.*, 2018) son presentados como comparación. Los espectros OIB y N-MORB son obtenidos de Sun y McDonough (1989).

espectro OIB. Las muestras describen patrones con un enriquecimiento en tierras raras ligeras y pendientes $La/Eu = 3.0 - 4.8$, el cual es más marcado en los derrames que en los sills, y un

empobrecimiento en tierras raras pesadas con pendientes $Gd/Lu = 3.3 - 5.4$ (Fig. 3). La anomalía en Eu está muy poco desarrollada y es ligeramente negativa ($Eu/Eu^* = 0.89 - 1.03$). Las concentraciones de LREE inician por encima de 100 ppm y en su mayoría se grafican por encima de la media de los valores OIB de la Condrita C1 de (Sun y McDonough, 1989). El diagrama multielemental normalizado con manto primitivo (Sun y McDonough, 1989) muestra un espectro en forma de joroba marcado por una anomalía positiva en Nb y Ta, siguiendo el espectro promedio OIB (Fig. 4). Se observa una fuerte dispersión en elementos trazas incompatibles, dentro de las cuales destaca una marcada anomalía positiva en Ba, probablemente por el efecto de la alteración en las muestras o asimilación de sedimentos, la cual también explica las anomalías positivas en Pb. El carácter especial de alto Ti se puede observar en la ligera anomalía positiva que presentan los espectros (Fig. 4). Se observa una fuerte anomalía negativa en Sr, probablemente provocada por una contaminación de sedimentos.

La preservación de los elementos traza inmóviles también permitió utilizar diagramas discriminación tectónica. El diagrama de Pearce (1983) es utilizado para distinguir los magmas que tienen

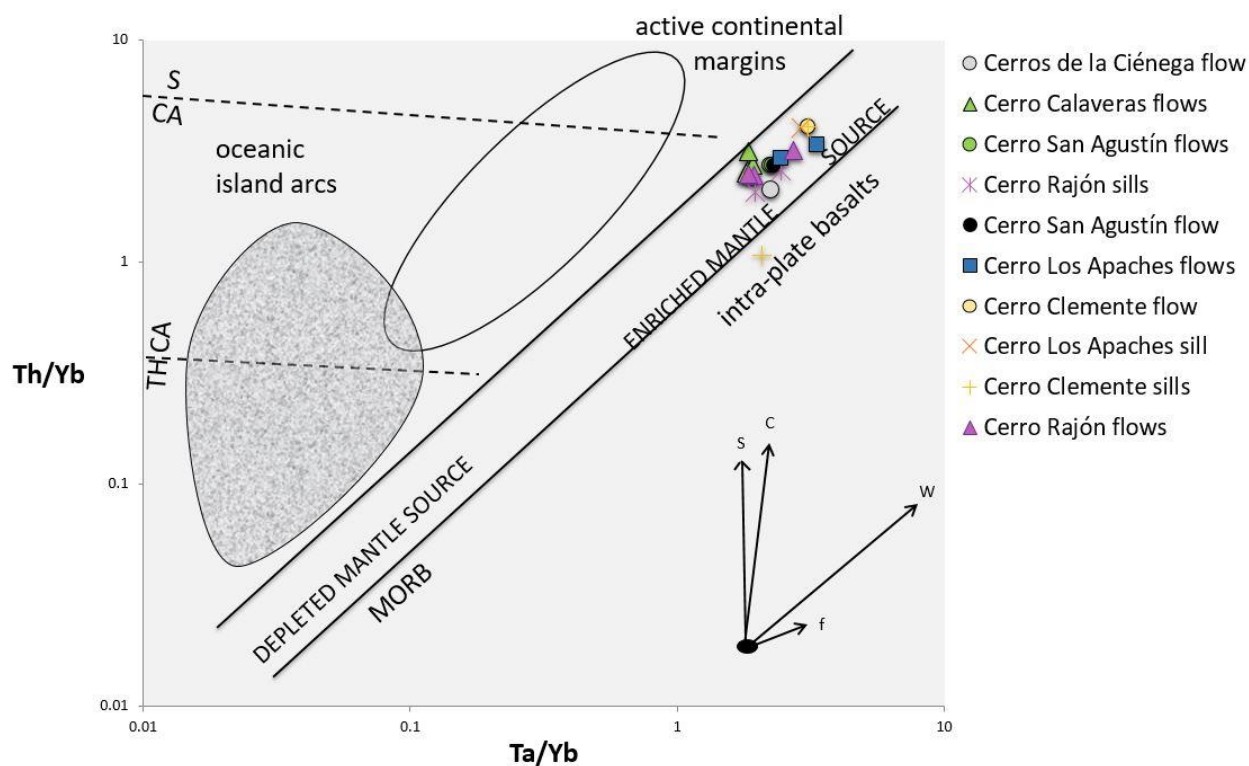


Figura 5. Diagrama de Pearce (1983) para distinguir entre fuentes del magmatismo. Utilizado para los derrames y sills de la Formación Cerro Rajón, Formación La Ciénega y Formación El Arpa. Los vectores muestran la influencia de componentes de subducción (S), enriquecimiento intraplaca (W), contaminación cortical (C) y cristalización fraccionada. Las líneas discontinuas indican los límites entre los dominios toleítico (TH), calco-alcalino (CA) y shoshonítico (S).

una fuente empobrecida de los que tienen una fuente enriquecida. En este caso las muestras entran casi en su totalidad en la zona de fuente enriquecida (Fig. 5). Este comportamiento es esperado debido a las características de un magmatismo con firmas tipo OIB. Nuevamente se observa como las muestras se agrupan según las localidades de estudio. El diagrama de discriminación de ambiente tectónico de Wood (1980) ubica a las muestras en el campo de basaltos alcalinos intraplaca (Fig. 6), con excepción de una sill de la localidad del Cerro Clemente el cual presenta una fuerte alteración la cual probablemente lo empobreció en Th. El ambiente tectónico es soportado también por el diagrama de Cabanis and Lecolle (1989), en el cual las muestras de los derrames y sills se ubican en el límite entre dominios alcalinos anorogénicos y dominios intra-continetales (Fig. 7). La incursión al dominio intra-continental, para este diagrama, se puede deber a la asimilación cortical.

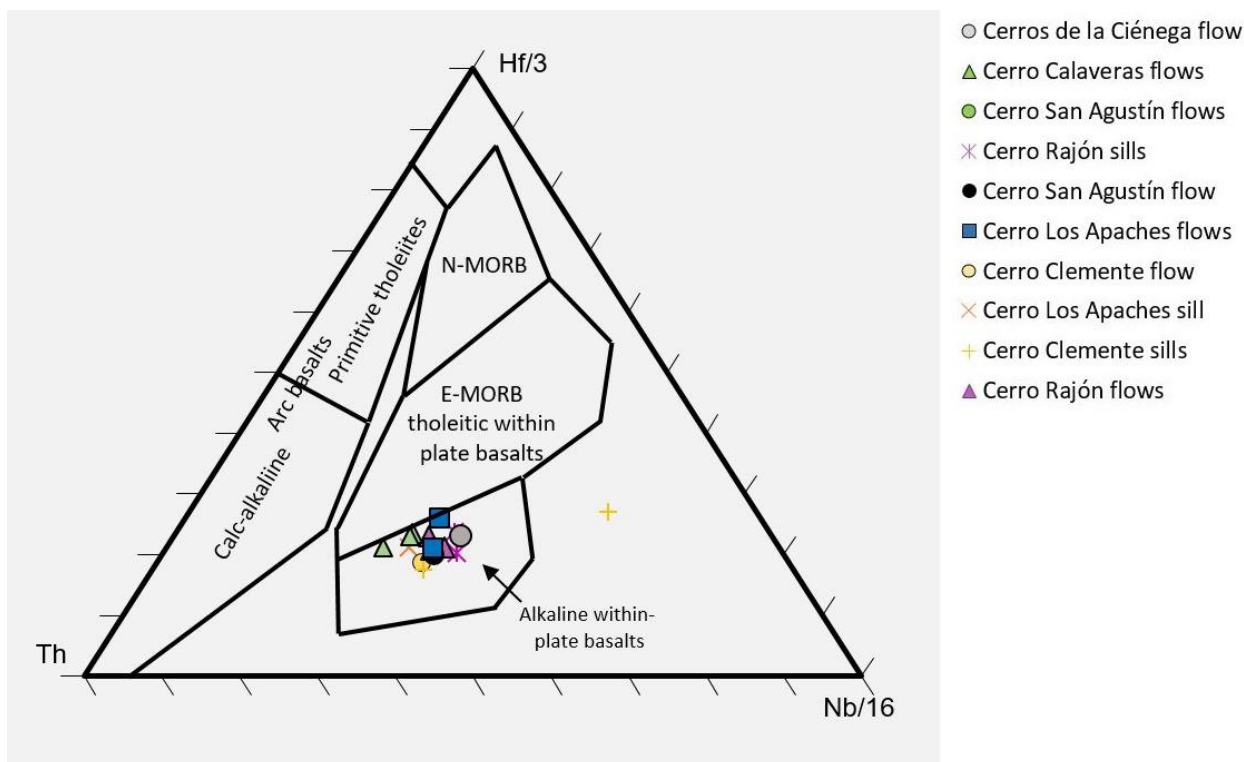


Figura 6. Diagrama de discriminación de ambiente tectónico de Wood (1980). Utilizado para los derrames y sills de la Formación Cerro Rajón, Formación La Ciénega y Formación El Arpa.

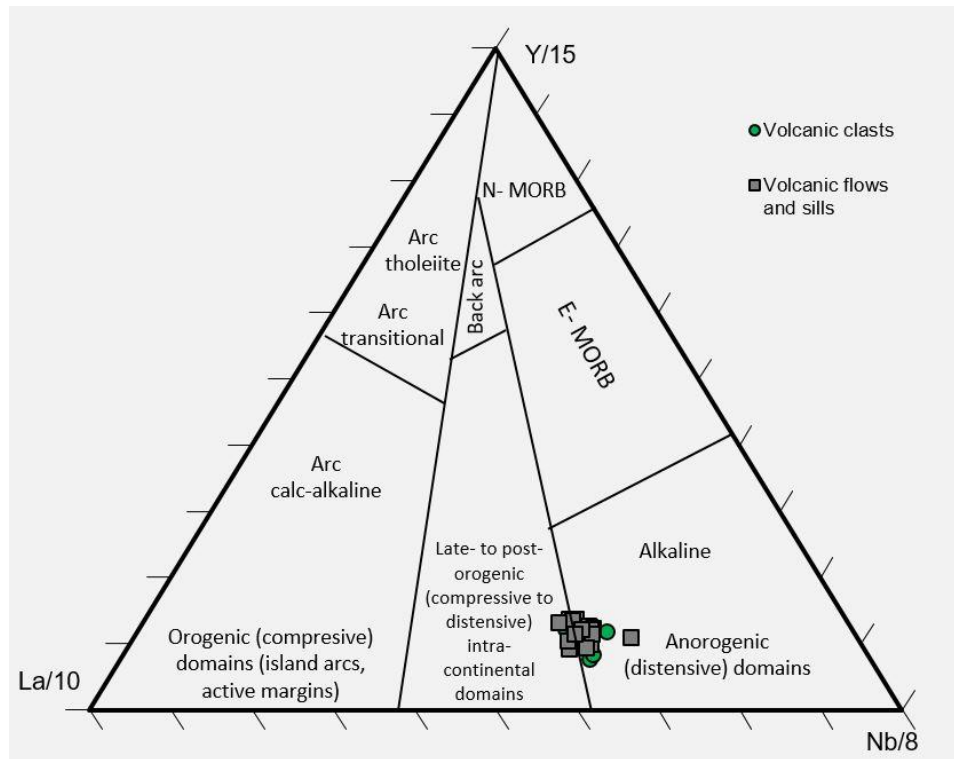


Figura 7. Diagrama de discriminación de ambiente tectónico de Cabanis and Lecolle (1989). Utilizado para los derrames y sills de la Formación Cerro Rajón, Formación La Ciénega y Formación El Arpa. También se presentan como comparación los clastos volcánicos de la Formación Cerro Rajón, tomados de Barrón-Díaz et al. (2018).

6

DISCUSIÓN Y CONCLUSIONES

DISCUSIÓN Y CONCLUSIONES

La base de la secuencia del Cámbrico en la región de Caborca, ha sido representada por la Fm. Puerto Blanco (Cooper y Arellano, 1952). Sin embargo, la presente investigación indica que su unidad basal (Unidad 1) difiere sustancialmente del resto de las unidades (Stewart *et al.* 1984; Barrón-Díaz *et al.*, 2019a). Este contraste se da principalmente por la presencia exclusiva de un volcanismo de características máfico-ultramáficas que puede ser observado en toda la unidad 1. Con base en lo anterior, la Unidad 1 de la Fm. Puerto Blanco ha sido redefinida y elevada a una formación litoestratigráfica formalmente definida con el nombre de Formación Cerro Rajón (Barrón-Díaz *et al.*, 2019a). Uno de las principales justificaciones para este cambio fue la importancia como indicador litológico y su exclusividad que representa el evento volcánico contenido en esta nueva formación. La Formación Cerro Rajón fue definida como una sucesión vulcano-sedimentaria de conglomerados tufáceos, metabasaltos, tobas máficas, lapillitas máficas, aglomerados máficos y cuarcita; con menor proporción de limolitas, calizas, dolomías y conglomerados.

El estudio del volcanismo de la Fm. Cerro Rajón indica que se trata de un evento que generó volúmenes bajos de material volcánico. Los principales elementos son rocas piroclásticas generadas por una intensa actividad estromboliana. El volcanismo puede haberse generado a través de pequeños edificios volcánicos, fisuras y conos de escoria (Fig. 8). Los aglomerados observados principalmente en las localidades de los Cerros de la Ciénega y el Cerro Rajón, están formados por una gran cantidad de bombas volcánicas y fragmentos de otras rocas piroclásticas. Lo anterior indica que posiblemente se formaron por la destrucción de los edificios volcánicos o en zonas muy cercanas a las fuentes de la actividad volcánica. Los conglomerados tufáceos también tienen una importante componente de material piroclástico. Estos se pudieron haber formado en zonas alejadas de las fuentes de la actividad volcánica, donde aún llegaba una importante cantidad de material piroclástico. O bien, se formaron por la erosión de derrames volcánicos y conos cineríticos. Los resultados geoquímicos indican que las tasas de fusión parcial del volcanismo en la Fm. Cerro Rajón son bajas (Fig. 2). Esto justifica los escasos derrames de metabasaltos que se encontraron, así como los espesores de entre 60 cm y 6m. Se propone que los afloramientos donde

estos espesores de metabasaltos llegan a tener hasta 25 metros, son producto de una acumulación de uno o varios eventos efusivos en paleocanales o bajos topográficos (Fig. 8). Los conductos alimentadores de este volcanismo no fueron observados, sin embargo, se encontraron al menos cinco sills con características ultramáficas intrusionando la Fm. La Ciénega y la Fm. El Arpa. Debido a sus características geoquímicas, estos cuerpos hipabisales son considerados como intrusiones con características primarias del magmatismo que estuvieron ligados a los conductos alimentadores del volcanismo en la Fm. Cerro Rajón. Se requiere un mayor estudio en estos sills para entender el metamorfismo y metasomatismo que los afecta, y la generación de minerales arcillosos que los conforman. La Figura 8 es un modelo de un posible escenario geológico en el cual se generó el volcanismo a inicios del Cámbrico del bloque Caborca.

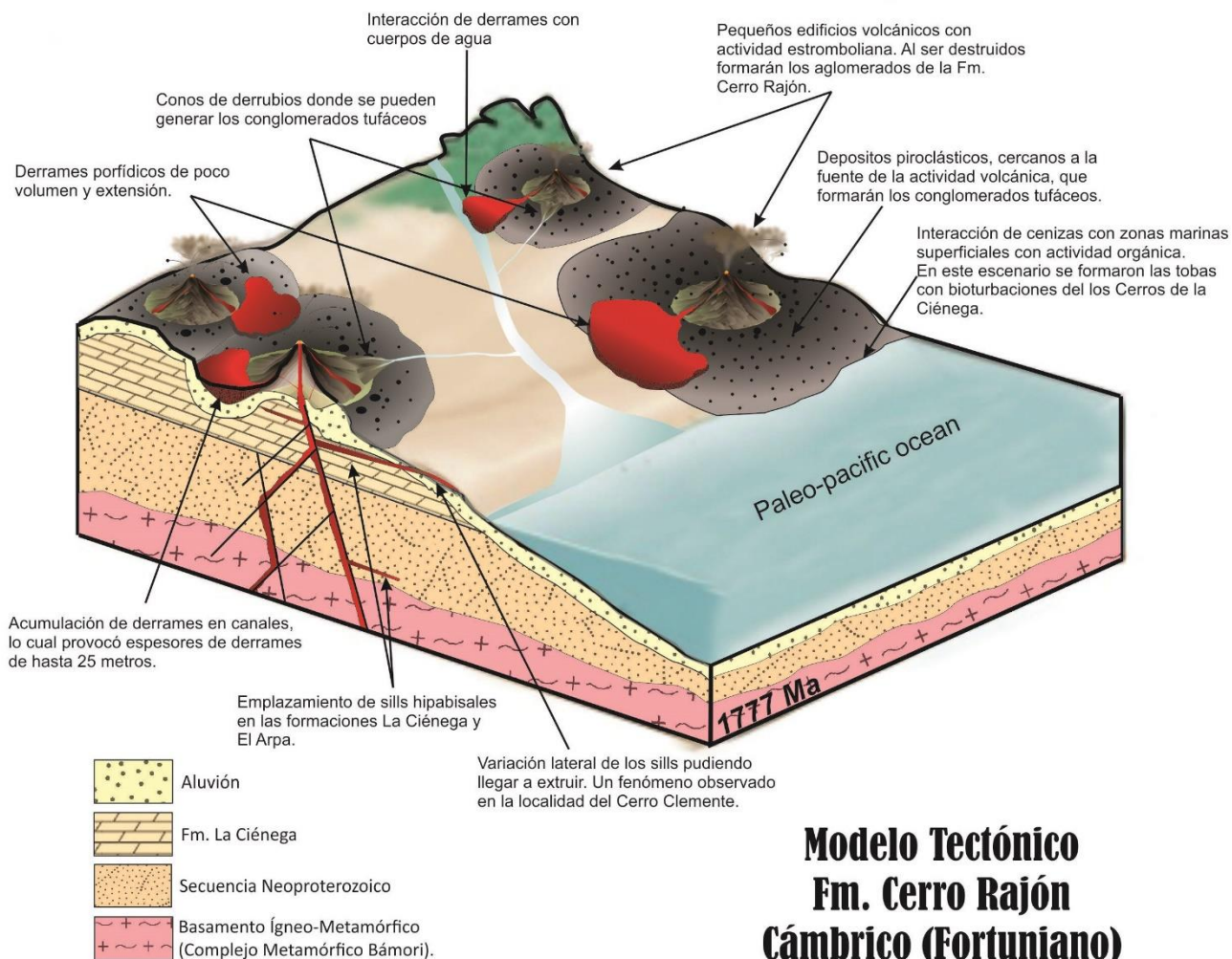


Figura 8. Modelo tectónico para el volcanismo de la Fm. Cerro Rajón ocurrido durante el Cámbrico (Fortuniano). Se presentan los principales escenarios geológicos en los que se desarrollaron las unidades de conglomerados tufáceos, tobas, lapillitas, aglomerados y derrames que caracterizan a la Fm. Cerro Rajón. Edad del basamento tomada de [Iriando \(2001\)](#).

Los resultados petrográficos de los derrames de metabasaltos y los clastos volcánicos contenidos en la Fm. Cerro Rajón, indican un volcanismo con diferentes grados de alteración. Los metabasaltos que presentan texturas porfidoblásticas con una alteración propilítica, tienen una paragénesis mineral metamórfica característica de un metamorfismo de bajo grado en facies de esquistos verdes. Sin embargo, en algunos derrames, la presencia de magnesio-hornblenda y abundante epidota, en conjunto con los resultados de geotermometría que muestran temperaturas mayores a 500 °C, indican que el metamorfismo podría estar alcanzando las facies de epidota-anfibolita. Todas las muestras presentan un hidrotermalismo, el cual está más acentuado en los clastos volcánicos. Estos presentan la mineralogía primaria casi en su totalidad remplazada por carbonatos. La petrografía también permitió distinguir el volcanismo en dos grupos según su diferenciación mineralógica. Un grupo de derrames tiene características ultramáficas, estos presenta una gran abundancia de cristales de clinopiroxeno y una ausencia de plagioclasas. El mejor ejemplo de este caso es el picrobasalto observado en la localidad del Cerro San Agustín (ver Fig. 4D en Barrón-Díaz *et al.*, 2019b). El segundo grupo de derrames presenta plagioclasas albitizadas en la matriz, estas características son más comunes en derrames de composición máfica. En ambos casos la matriz presenta una esfenitización, la cual podría derivar del titano lixiviado de los fenocristales de ilmenita. Con base en lo anterior, la petrografía clasifica a los derrames como granofels de actinolita-clorita-epidota y a los clastos volcánicos y sills como granofels de calcita. Los derrames que conservan la mineralogía primaria son clasificados petrográficamente como ankaramitas con una ligera alteración hidrotermal.

Los resultados geoquímicos del volcanismo de la Fm. Cerro Rajón, indican un magmatismo con características máficas-ultramáficas. Este magmatismo tiene bajas tasas de fusión relativas (Fig. 2) y produjo pequeños volúmenes de volcanismo. Los valores altos en TiO₂ son una importante característica de este volcanismo, los cuales no son producto de una alteración, ya que esa anomalía positiva se puede observar también en la química de los cristales de diopsida obtenidos de las muestras de un picrobasalto (Barrón-Díaz *et al.*, 2018). La reflexión en torno a los valores altos en Ti en este magmatismo, debe considerar que este evento tiene como fuente un manto Precámbrico, distinto al actual; además de que el Ti se acentúa por el carácter alcalino de las muestras, como se observa en la diferencia que este volcanismo presenta con las rocas toleíticas cámbricas del Aulacógeno del sur de Oklahoma (Brueseke *et al.*, 2016). No se observa una importante diferenciación en los productos volcánicos. Únicamente se distingue un ligero aumento en sílice entre los derrames de picrobasaltos y los metabasaltos y andesitas basálticas contenidos generalmente hacia la cima de la Fm. Cerro Rajón. Los sills contenidos en la Fm. La Ciénega y Fm. El Arpa, presentan una fuerte lixiviación en sílice. Sin embargo no es posible indicar, de

forma precisa, hasta donde esta lixiviación es producto de un efecto de metamorfismo y que tanto es una característica primaria de este magmatismo. La geoquímica de elementos mayores indica que se produjo un metasomatismo en un sistema parcialmente abierto. La variación de este intercambio químico varía según la localidad de estudio. Los álcalis son los óxidos principalmente afectados, así como el calcio que suele enriquecerse por el hidrotermalismo. La alteración está más acentuada en los clastos volcánicos de los conglomerados tufáceos, debido a la mayor susceptibilidad que presentan a eventos hidrotermales y circulaciones de fluidos. A pesar de la alteración observada en todas las muestras, la geoquímica de trazas indica que la mayoría de los derrames y sills conservan características primarias con valores elevados en Cr y Ni. Los diagramas multielementales y de tierras raras ayudan a confirmar algunas características del volcanismo, como los espectros del tipo OIB o el muy elevado enriquecimiento en LREE con grandes pendientes La/Lu, observable en magmas ultramáficos (Wilson, 1989). En conjunto, los resultados geoquímicos indican un volcanismo alcalino anorogénico del tipo OIB.

Los estudios de química mineral a través de microsonda electrónica, permitieron identificar la mineralogía de alteración y la mineralogía primaria en los metabasaltos. Esta última se reduce a fenocristales de ilmenita y cristales de diopsida parcialmente alterados a actinolita. Los resultados de geotermometría obtenidos con cristales de plagioclasas y hornblenda-actinolita, permitieron identificar un metamorfismo en facies de esquistos verdes. Sin embargo, las temperaturas llegaron a ser lo suficientemente altas para incursionar en un metamorfismo de grado medio, marcado por la facies de epidota-anfibolita. Este fenómeno se da en la región oeste del área de estudio, en la localidad del Cerro Calaveras, la cual pudo haber tenido una interacción más cercana con los cuerpos intrusivos de la región, explicando así el mayor grado de metamorfismo.

Uno de los principales objetivos de la presente investigación es el de obtener una edad de cristalización para el volcanismo contenido en la Fm. Cerro Rajón. Esta tarea resultó ser más complicada que lo que esperábamos en un inicio, sin embargo, se realizó un importante número de intentos a través de distintas técnicas radiométricas. Estos esfuerzos aún continúan y se espera poder obtener una edad radiométrica en un futuro cercano. A pesar de lo anterior, los estudios de estratigrafía, chemoestratigrafía y paleobiología en los que se colaboraron, permitieron acotar la edad de este volcanismo al Fortuniano (ver sección 3.3 en Barrón-Díaz *et al.*, 2019a). La geocronología $^{40}\text{Ar}/^{39}\text{Ar}$ permitió fechar con exactitud el evento metamórfico en los metabasaltos de la porción oeste del área de estudio. Mientras que los estudios de la porción este, resultaron con una mayor incertidumbre. Las edades obtenidas de las matrices volcánicas rondan alrededor de los 60 Ma. Estas edades son similares a las reportadas en los intrusivos

Laramídicos cercanos al área de estudio (Valencia-Moreno *et al.*, 2006; Ramos-Velázquez *et al.*, 2008; Paz-Moreno *et al.*, 2018). El intrusivo laramídico reportado más cercano a la Fm. Cerro Rajón, son los afloramientos de granodioritas en el Cerro El Dátil, del cual se obtuvo una edad de 71.1 ± 0.4 Ma. Esta edad es muy consistente con las reportadas en la región de estudio (ver discusiones en capítulo 4). Los resultados del cálculo de presión en la granodiorita del Cerro El Dátil indican valores cercanos 3 kbar, los cuales representan una profundidad de emplazamiento de ~ 8.31 km, consistente con el emplazamiento de intrusivos Laramídicos en el estado de Sonora (ver discusiones en Barrón-Díaz *et al.*, 2019b). Tomando en cuenta estos resultados, se considera que las secuencias del Neoproterozoico y Cámbrico de la región de Caborca tuvieron un importante enterramiento de al menos 8km, posteriormente sufrieron un metamorfismo provocado por un evento intrusivo de edad Laramídica y por último fueron exhumadas por los eventos de distensión en la región de Sonora. Esta reflexión se logra considerando el contexto tectónico regional, en el cual los batolitos laramídicos suelen presentarse como bloques que elevan las secuencias intrusionadas (ver Fig. 8 en Barrón-Díaz *et al.*, 2019b).

Los estudios de geoquímica de trazas inmóviles permitieron la utilización de diagramas de discriminación y ambiente tectónico para el magmatismo de la Fm. Cerro Rajón. Los resultados indican que el volcanismo está relacionado a un rift del tipo intraplaca continental (Barrón-Díaz *et al.*, 2018; ver también sección 5.2 en el capítulo 5). Sin embargo, los bajos volúmenes y el pobre fraccionamiento del volcanismo no coinciden con un evento ocurrido en la zona axial de un rift, más bien parece ser un evento relacionado a una zona distal del eje del rift o bien, el evento puede pertenecer a un rift abortado. Tomando en cuenta este escenario tectónico y la edad del evento volcánico, se propone que el volcanismo de la Fm. Cerro Rajón puede estar relacionado a los eventos ocurridos a finales del Neoproterozoico en el margen oeste de Laurentia, el cual estuvo activo de 780–570 Ma (Lund *et al.*, 2003). Esta correlación no se dio únicamente por la contemporaneidad de los eventos volcánicos, sino que también es importante destacar que la geoquímica de estas rocas es muy similar, especialmente las anomalías positivas en TiO_2 que comparte el volcanismo de la Fm. Cerro Rajón con el de margen occidental de Laurentia (Barrón-Díaz *et al.*, 2018). Las rocas volcánicas reportadas en el límite Cámbrico-Precámbrico por Kellogg (1963) y Stewart (1972) en Nevada, pudieran indicar el afloramiento más meridional, hasta la fecha, de este rift. De encontrarse relacionado, el volcanismo de la Fm. Cerro Rajón comprendería un evento en el extremo sur de este rift occidental de Laurentia, que se manifiesta en el bloque Caborca. Se requieren más estudios para correlacionar con las mismas técnicas analíticas el volcanismo de Caborca con el del oeste de Laurentia. En la presente investigación se consideraron también otras posibles correlaciones de este volcanismo (ver discusiones en Barrón-Díaz *et al.*, 2018 y Barrón-Díaz *et al.*, 2019a). Entre ellas destacan

el magmatismo que se encuentra en el Aulacógeno del Sur de Oklahoma (SOA), el cual se formó durante un proceso inicial de rift contemporáneo al magmatismo de Caborca (Thomas *et al.*, 2012). Sin embargo, la geoquímica indica que hay diferencias importantes entre estos eventos volcánicos, entre ellas se encuentra la gran diferencia en la tasa de fusión parcial y las concentraciones de TiO_2 (Barrón-Díaz *et al.*, 2018). Al término de la presente investigación, aún se tienen varias cuestiones por responder y trabajos pendientes, por lo que el estudio de este volcanismo y su relación con las secuencias en Norte América continuará siendo un tema de interés y una temática de investigación apasionante a profundizar.

7

REFERENCIAS

REFERENCIAS

**Se presentan únicamente las referencias mencionadas en los capítulos 1, 5 y 6. Las referencias de los capítulos 2, 3 y 4 se encuentran al final de dichas publicaciones.*

Barrón-Díaz, A.J., 2013, Caracterización petrogenética de las metabasitas anorogénicas del límite Cámbrico-Precámbrico, Municipio de Pitiquito, Sonora, México [M.S. thesis]: Universidad de Sonora, 95 p.

Barrón-Díaz, A.J., Paz-Moreno, F.A., Lozano-Santa Cruz, R., Herrera-Urbina, S., Centeno-García, E., & López-Martínez, M., 2018, Early Cambrian alkaline volcanism on the southern margin of Laurentia: evidence in the volcanoclastic units from the Puerto Blanco Formation in the Caborca block, NW Mexico, *International Geology Review*.

Barrón-Díaz, A.J., Paz-Moreno, F.A., & Hagadorn, J.W., 2019a, The Cerro Cerro Rajón Formation—a new lithostratigraphic unit proposed for a Cambrian (Terreneuvian) volcano-sedimentary succession from the Caborca region, northwest Mexico. *Journal of South American Earth Science*, v. 89, p. 197-210.

Barrón-Díaz, A.J., Paz-Moreno, F.A., Miggins, D.P., & Iriondo, A., 2019b, Geochronology and geothermometry of the Laramidic metamorphism in the Cambrian metabasalts from the Cerro Rajón Formation, Caborca region, northwest Mexico. *Journal of South American Earth Science*, In press.

Brueseke, M.E., Hobbs, J.M., Bulen, C.L., Mertzman, S.A., Puckett, R.E., Walker, J.D., & Feldman, J., 2016, Cambrian intermediate-mafic magmatism along the Laurentian margin: Evidence for flood basalt volcanism from well cuttings in the Southern Oklahoma Aulacogen (U.S.A.), *Lithos*, v. 260, p. 164–177.

Cabanis, B., & Lecolle, M., 1989, Le diagramme La/10 - Y/15 - Nb/8; un outil pour la discrimination des series volcaniques et la mise en evidence de processus de melange et/ou de contamination crustale, *C. R. Acad. Sci. Ser. II*, v. 309, p. 2023 - 2090.

- González-León, C.M., & Jacques-Ayala, C., 1988, Estratigrafía de las rocas Cretácico en el área de Cerro de Oro, Sonora central, Universidad de Sonora, Departamento de Geología Boletín, v. 5, p. 1-23.
- Centeno-García, E., Maytorena, F., Calmus, T., Solis-Pichardo, G. & Lozano-Santa Cruz, R., 2002, Proterozoic OIB magmatism in the Caborca terrane, northwestern Mexico, in Denver Annual Meeting, Colorado Convention Center: C205, Session No. 245.
- Cooper, G.A. & Arellano A.R.V., 1952, Introduction and stratigraphy, in Cooper, G. A., Arellano, A. R. V., Johnson, J. H., Okulitch, V. J., Stoyanow, Alexander, & Lochman, Christina, eds., Cambrian stratigraphy and paleontology near Caborca, northwestern Sonora, Mexico: Smithsonian Miscellaneous Collections, v. 119, no. 1, p. 1-23.
- He, Q., Xiao, L., Balta, B., Gao, R., & Chen, J., 2010, Variety and complexity of the Late–Permian Emeishan basalts: Reappraisal of plume–lithosphere interaction processes, *Lithos* 119, p. 91–107.
- Iriondo, A., 2001. Proterozoic basements and their Laramide juxtaposition in NW Sonora, Mexico: Tectonic constraints on the SW margin of Laurentia. [Ph.D. thesis]: University of Colorado, 222 p.
- North American Commission on Stratigraphic Nomenclature, 2005, North American Stratigraphic Code; AAPG Bulletin, v. 89, no. 11, p. 1547-1591.
- Kellogg, H.E., 1963, Paleozoic Stratigraphy of the Southern Egan Range, Nevada. GSA Bulletin, vol. 74, p. 685–708.
- Le Bas, M.J., Le Maitre, R.W., Streckeisen, A., & Zanettin, B., 1986, A chemical classification of volcanic rocks based on the total alkali–silica diagram, *Journal of Petrology*, Oxford, v.27, p.745–750.
- Lund, K., Aleinikoff, J., Evans, K. & Fanning, C., 2003, SHRIMP U-Pb geochronology of Neoproterozoic Windermere Supergroup, central Idaho: Implications for rifting of western Laurentia and synchronicity of Sturtian glacial deposits: *Bulletin of the Geological Society of America*, v. 115, no. 3, p. 349-372.
- Longoria, J. F., Gonzalez, M. A., Mendoza, J. J., & Perez, V.A., 1978, Consideraciones estructurales en el Cuadrangulo Pitiquito-La Primavera, NW de Sonora [Structural considerations in the Pitiquito-La Primavera quadrangle, northwestern Sonora, Mexico], Universidad de Sonora, Departamento de Geología Boletín, v. 1, p. 61-67.

- Paz-Moreno F. A., Izaguirre-Pompa A., & Iriondo A., 2018, Geoquímica y Geocronología del pórfido monzonítico Cretácico tardío del Cerro Gasolinera, norte de Caborca Sonora, México: una marca del magmatismo adakítico laramídico. XXVIII Congreso Nacional de Geoquímica, Actas INAGEQ, v. 24, no.1.
- Pearce, J.A., 1982, Trace elements characteristics of lavas from destructive plate boundaries, In: Thorpe, R. S., *Andesites*, Wiley & Sons, p. 525-548.
- Pearce, J.A., 1983, Role of the Subcontinental Lithosphere in Magma Genesis at Continental Margins In: C. J. Hawkesworth & M. J. Norry, Eds., *Continental Basalts and Mantle Xenoliths*, Shiva Publishing, Cheshire, p. 230-249.
- Ramos-Velázquez E., Calmus, T., Valencia, V., Iriondo, A., Valencia-Moreno, M., & Bellon, H., 2008, U-Pb and $^{40}\text{Ar}/^{39}\text{Ar}$ geochronology of the coastal Sonora batholith: New insights on Laramide continental arc magmatism, *Revista Mexicana de Ciencias Geológicas*, v. 25, no. 2, p. 314 - 333.
- Stewart, J.H., 1972. Initial deposits of the Cordilleran geosyncline: evidence of a late Precambrian (850 m.y.) continental separation. *Geological Society of America Bulletin*, vol. 83, p. 1345–1360.
- Stewart, J.H., 1982, Regional relations of Proterozoic Z and Lower Cambrian rocks in the western United States and northern Mexico, in Cooper, J. D., Troxel, B. W., and Wright, L. A., eds., *Geology of selected areas in the San Bernardino Mountains, western Mojave Desert, and southern Great Basin, California: Geological Society of America, Cordilleran Section Annual Meeting, Anaheim, California., 1982, Guidebook and Volume*, p. 171-186.
- Stewart, J.H., McMenamin, A.S., & Morales-Ramirez, J. M., 1984, Upper Proterozoic and Cambrian Rocks in the Caborca Region, Sonora, Mexico. *Physical Stratigraphy, Biostratigraphy, Paleocurrents Studies and Regional Relations.*, U. S. Geological Survey Professional Paper 1390.
- Stewart, J.H., Amaya-Martinez, R., & Palmer, A.R., 2002, Neoproterozoic and Cambrian Strata of Sonora, Mexico: Rodinian Supercontinent to Laurentian Cordilleran Margin, *Geológicas Society of América*, p. 5–48 Special Paper 365.
- Sun, S.S., & McDonough, W.F., 1989, Chemical and Isotopic Systematics of Oceanic Basalts: Implications for Mantle Composition and Processes, In: Saunders, A.D. and Norry, M.J., Eds., *Magmatism in the Ocean Basins*, v. 42, Geological Society, Special Publications, London, p. 313-345.

- Schwarzer, R.R., & Rogers J.J.W., 1974, A worldwide comparison of alkali olivine basalts and their differentiation trends, *Earth Planet. Sci., Lett.*, 23, p. 286–296.
- Thomas, W.A., Tucker, R.D., Astini, R.A., & Denison, R.E., 2012, Ages of pre-rift basement and synrift rocks along the conjugate rift and transform margins of the Argentine Precordillera and Laurentia, *Geosphere* 8, p. 1–18.
- Valencia-Moreno, M., Iriondo, A., & González-León, C., 2006, Temporal constraints on the eastward migration of the Late Cretaceous–early Tertiary magmatic arc of NW Mexico based on new $^{40}\text{Ar}/^{39}\text{Ar}$ hornblende geochronology of granitic rocks, *Journal of South American Earth Science* 22, p. 22-38.
- Wilson, M., 1989, *Igneous petrogénesis*, London, Unwin Hyman.
- Wood, D.A., 1980, The Application of a Th-Hf-Ta Diagram to Problems of Tectonomagmatic Classification and to Establishing the Nature of Crustal Contamination of Basaltic Lavas of the British Tertiary Volcanic Province. *Earth and Planetary Science Letters*, 50, p. 11-30.

8



ANEXOS

ANEXOS

Supplementary files de la publicación: *“Early Cambrian alkaline volcanism on the southern margin of Laurentia: evidence in the volcanoclastic units from the Puerto Blanco Formation in the Caborca block, NW Mexico”*pag. 88-103

Supplementary files de la publicación: *“Geochronology and geothermometry of the Laramidic metamorphism in the Cambrian metabasalts from the Cerro Rajón Formation, Caborca region, northwest Mexico.”* pag. 104-128

Supplementary file 1. Petrography descriptions

Description of the petrographic thin sections for the volcanic clast samples from the tuffaceous conglomerates and the agglomerate bombs.
Sample AB10-06B a microbasalt flow partially fresh is also included.

Sample Id	Locality	Rock type	Rock name	Preserved volcanic mineralogy	Secondary Mineralogy	Pseudomorph crystals	Texture	Alteration	Observations
AB15-05A	Cerro Rajón	volcanic clast from tuffaceous conglomerate	albite-sphene-actinolite granofel	Fe-Ti oxides	ab>sf>act>ox>chl>ep	Cpx	porphyritic	propylitic	Cpx pseudomorph crystals replaced with actinolite and in minor proportions chlorite. Groundmass with abundant albite crystals and actinolite microcrystals, also abundant sphene in a dusty or cloudy habit.
AB15-05B	Cerro Rajón	volcanic clast from tuffaceous conglomerate	sphene-titanomagnetite-actinolite granofel	-	sf>ox>act>cal>chl>qz>ep	Cpx	porphyritic	propylitic	Altered mafic flow with pseudomorph crystals up to 6mm large. They are replaced by actinolite. Groundmass with abundant sphene and cpx microcrystals. No albite observed. Calcite filling amygdule.
AB15-08A	Cerro Rajón	volcanic clast from tuffaceous conglomerate	actinolite-sphene-calcite granofel	-	act>sf>cal>chl>ox>ep>qz	Cpx>Ol	porphyritic, amygdaloid	propylitic	Porphyritic rock rich in pseudomorphs and filled amygdule. Calcite is mainly replacing the pseudomorph crystals. Actinolite is replacing the original cpx crystals. Groundmass with abundant actinolite in decussate fabric and sphene in dusty habit. Calcite filling cavities. This samples is probably a fragment from the base of a flow.
AB15-08B	Cerro Rajón	volcanic clast from tuffaceous conglomerate	actinolite-sphene granofel	-	act>sf>ox>cal>ep	Cpx>Ol	porphyritic	propylitic	Abundant pseudomorph replaced with actinolite and titanomagnetite. Groundmass with abundant dusty sphene, oxides and albite in minor proportions.
AB16-49B	Cerro Rajón	volcanic bomb from agglomerate	albite-sphene granofel	-	ab>sf>ox>qz>act>chl>cal>ser>hem	-	aphanitic	silicification	Silicified clast with quartz and calcite veins. The veins have little amounts of hematite and sericite. Groundmass with abundant albite and actinolite in a decussate texture.

AB16-49D	Cerro Rajón	volcanic bomb from agglomerate	quartz-sphene granofel	Fe-Ti oxides	qz>sf>chl>hem	Cpx=Ol	aphanitic	silicification	The thin section show only one pseudomorph from cpx, now replaced with oxides. There is a intense silicification affecting all the samples. Quartz is filling amygdule. The groundmass has abundant sphene crystals. A partial crystal orientation has been developed.
AB11-40C	Cerro Calaveras	volcanic clast from tuffaceous conglomerate	calcite granofel	-	cal>hem and ox>> ab and qz	Cpx>Ol	porphyritic	carbonatization	Strong carbonatization replacing almost entirely the original mineralogy. Calcite veins and patches. Most pseudomorph crystals are replaced by hematite and Fe-Ti oxides.
AB11-39	Cerro Calaveras	volcanic clast from tuffaceous conglomerate	meta-peperite	-	ox>sf>>cal>ser>chl>qz	Frag. Rx	peperitic	propylitic	An orientated texture and rounded small grain from sedimentary origin, can be observed. Original rock texture was erased but it might have been pyroclastic. Groundmass with abundant sphene, and Fe-Ti oxides.
AB16-02C	Cerro Calaveras	volcanic clast from tuffaceous conglomerate	albite-sphene-actinolite granofel	Fe-Ti oxides	ab>sf>act>cal>chl>ep	Cpx>Ol	porphyritic	propylitic	Actinolite and chlorite replacing pseudomorphs crystals up to 3mm long. Groundmass is made of acicular actinolite microcrystals in a decussate texture. Albite and sphene are also present in the groundmass. Calcite is present in veins with up to 250 microns wide.
AB16-02A	Cerro Calaveras	volcanic clast from tuffaceous conglomerate	albite-sphene-actinolite granofel	Fe-Ti oxides	ab>sf>act>chl>cal>ep	Cpx>Ol	porphyritic	propylitic	Primary mineralogy shapes are recognized as cpx and olivine crystals, now replaced with actinolite and chlorite. Groundmass with abundant albite in a late stage of crystalization. Abundant sphene in the groundmass and ocationally calcite veins.
AB11-47C	Cerro Calaveras	volcanic clast from tuffaceous conglomerate	calcite-chlorite granofel	Fe-Ti oxides	cal>chl>act>sf>ep>ox> qz	Cpx>>Ol	porphyritic	propylitic	Pseudomorph crystals altered to chlorite, actinolite and calcite. Epidote is also growing in the large crystals. Groundmass formed of actinolite, sphene and less abundant Fe-Ti oxides. Calcite amygdules. Calcite veins.

AB14-05A	Cerro San Agustín	volcanic clast from tuffaceous conglomerate	calcite granofel	Fe-Ti oxides	cal>hem>sf>ox>ab	Cpx>Ol>Amig.	porphyritic	carbonatization	Strong carbonatization present in the groundmass and pseudomorph crystals. It is possible to observe cpx shapes now altered. Groundmass with abundant sphene.
AB14-05B	Cerro San Agustín	volcanic clast from tuffaceous conglomerate	calcite granofel	Fe-Ti oxides	cal>sf>ab?	Ol y Amig.	porphyritic	carbonatization	Calcite abundant in the groundmass and replacing the original mineralogy. Groundmass with abundant sphene, Fe-Ti oxides and plagioclase?
AB10-06B	Cerro San Agustín	volcanic flow	ankaramite	Cpx, Fe-Ti oxides, pl	sf, ab	Ol	porphyritic	minor alteration	Picrobasalt flow with fresh diopside euhedral to subhedral phenocrysts. Olivine shapes, now recrystallized, can be observed. The groundmass is mainly formed by a second generation of diopside microcrystals, titanomagnetite and sphene in a cloudy habit and include both andesine and albite in a late stage of crystallization.
AB11-20C	Cerros de la Ciénega	volcanic clast from tuffaceous conglomerate	calcite granofel	-	cal>ox>ab>sf	Ol>Cpx	porphyritic	carbonatization	Carbonate veins and an original mineralogy entirely replaced with carbonates. Fe-Ti oxides are abundant in the groundmass and less abundant albite. Calcite in patches.
AB11-20F	Cerros de la Ciénega	volcanic clast from tuffaceous conglomerate	albite-calcite granofel	-	ab>cal>ox	Ol	micro-porphyritic	carbonatization	Presents large calcite patches up to 0.5 mm, calcite veins and albite on the groundmass. pseudomorph crystals are replaced with oxides and calcite.
AB11-200	Cerros de la Ciénega	volcanic clast from tuffaceous conglomerate	calcite-albite granofel	-	cal>ab>ox>ser	Cpx>Ol	porphyritic	carbonatization	Groundmass with abundant albite, calcite in patches. The primary mineralogy is completely replaced with carbonates, oxides and sericite.

AB11-20D	Cerros de la Ciénega	volcanic clast from tuffaceous conglomerate	quartz granofel	-	qz>ox>ab?	NA	aphanitic	silicification	Oxides are observed as microcryst in the matrix. It has abundant quartz veins. The smaller microcrystals may be albite.
AB11-20L	Cerros de la Ciénega	volcanic clast from tuffaceous conglomerate	albite-sphene granofel	-	alb>sf>ox>cal	NA	aphanitic	carbonatization	Melanocratic sample with aphanitic texture with abundant albite, sphene and oxides. Thin calcite veins can be observed.

act = actinolite, ab = albite, cal = calcite, chl = chlorite, hem = hematite, ox = Fe-Ti oxides (mainly titanomagnetite), qz = quartz, ser = sericite, sf = sphene, cpx = clinopyroxene.

Supplementary file 2. Thermometric data

Calculations after Blundy, J. D. & Holland, T. J. B. 1990.

Hbl-Plag thermometry calibration reaction edenite + 4 quartz = tremolite + albite

		1		
	Sample	Temperature °C	Temp. Average	Temp. Std. Deviation
Alkaline Metabasalt Cerro Rajon locality	AB15-05A	446	455	21
		450		
		429		
		487		
		435		
		451		
		463		
		429		
		473		
		485		
Alkaline Metabasalt Cerro Calaveras locality	AB16-02C	507	493	20
		518		
		500		
		492		
		509		
		481		
		451		
		508		
		492		
		472		

Supplementary file 3. Mayor elements and Norm CIPW

Mayor earth elements results obtained by ICP-MS and XRF. Most of the rock samples includes significant amounts of loss of ignition due to the alteration. Norm CIPW and the Mgv are included at the bottom. nm = no measured. Volcanic clasts from Cerro San Agustín show Na₂O values below the detection limit (0.03). IGLa-1 standard from Lozano and Bernal (2005). Sample AB10-06 is a microbasalt flow, it represents the lava flows which the volcanoclastic units were generated from.

Locality	Cerros de la Ciénega					Cerro Calaveras					Cerro San Agustín			Cerro Rajón					Standard	
MAYOR	AB11-20C	AB11-20F	AB11-20O	AB11-20D	AB11-20L	AB11-40C	AB16-02C	AB11-39	AB11-47C	AB16-02A	AB14-05A	AB14-05B	AB10-06B	AB15-08A	AB15-05B	AB15-08B	AB15-05A	AB16-49B	AB16-49D	IGLa-1
SiO ₂	38.27	38.70	44.52	44.82	45.38	29.60	46.78	38.50	43.57	43.95	28.31	29.27	40.90	40.02	41.51	42.64	45.84	42.75	47.52	60.52
TiO ₂	5.20	5.10	4.93	4.69	6.56	5.12	5.03	6.75	3.39	4.87	4.94	3.86	6.49	3.38	3.69	4.08	4.05	6.28	5.25	1.08
Al ₂ O ₃	10.23	9.77	12.11	10.34	12.19	8.17	10.76	10.80	7.49	9.75	7.86	8.79	9.42	9.06	9.37	10.09	11.25	11.43	11.94	17.39
Fe ₂ O ₃	15.11	16.48	11.19	20.17	19.01	8.76	12.87	11.33	9.23	11.79	14.75	13.94	8.85	10.03	12.31	9.10	10.73	14.35	15.80	1.96
FeO	0.30	0.38	0.45	0.70	0.40	2.51	nm	4.61	1.25	nm	nm	nm	6.08	4.10	2.95	4.50	3.50	nm	nm	3.74
MnO	0.15	0.09	0.09	0.09	0.05	0.28	0.15	0.16	0.16	0.16	0.26	0.25	0.20	0.23	0.22	0.23	0.15	0.21	0.14	0.102
MgO	1.66	0.17	0.40	1.85	0.70	1.81	6.84	4.97	5.55	7.69	9.51	12.35	8.86	11.89	10.15	12.15	7.30	8.37	5.12	1.97
CaO	13.77	14.05	10.63	6.86	5.58	20.96	8.80	8.45	14.89	11.68	14.64	13.54	12.90	9.57	9.76	7.22	6.47	7.33	5.24	5.18
Na ₂ O	5.32	5.85	7.16	5.39	6.85	3.63	3.15	0.33	3.18	2.53	<DL	<DL	1.23	1.04	1.64	1.62	2.59	3.21	5.40	4.80
K ₂ O	0.27	0.15	0.23	0.31	0.30	0.85	2.58	2.84	1.19	2.49	1.59	0.72	1.38	3.15	2.71	2.60	3.84	2.18	1.22	2.14
P ₂ O ₅	0.58	0.52	0.76	0.54	0.74	0.55	0.67	1.07	0.48	0.62	0.59	0.64	0.59	0.70	0.82	0.75	0.88	0.84	0.78	0.43
LOI	9.11	8.72	7.45	4.16	2.16	17.49	2.37	9.19	9.35	4.44	16.56	15.93	2.38	6.12	4.47	4.40	2.81	3.00	1.58	0.06
Total	99.96	99.98	99.92	99.92	99.92	99.72	100.00	99.00	99.73	99.97	99.01	99.29	99.28	99.29	99.59	99.38	99.40	99.96	99.99	99.37
Fe ₂ O ₃ /FeO	50.36	43.36	24.86	28.81	47.51	3.49	nm	2.46	7.38	nm	nm	nm	1.46	2.45	4.17	2.02	3.06	nm	nm	0.52
Mg#	20.18	2.31	7.45	17.24	7.84	26.94	55.57	41.54	55.17	60.55	60.27	67.58	67.58	65.73	60.50	66.96	54.02	57.85	43.26	

Supplementary file . Classification results from MagClAMSys

Results from the online program for altered igneous rock classification MagClAMSys from Verma et al. (2017)

CO	S	C	T	M	SiO	TiO	LO	F _T	O	MO	MGO	CO	O	O	PO	M	MAGMA_DISC_M (MagClAMSys_ilr)
1				AB11-20C	38.27	5.20	10.23	15.11	0.15	1.66	13.77	5.32	0.27	0.58		ULTRABASIC	
2				AB11-20F	38.70	5.10	9.77	16.48	0.09	0.17	14.05	5.85	0.15	0.52		ULTRABASIC	
3				AB11-20O	44.52	4.93	12.11	11.19	0.09	0.40	10.63	7.16	0.23	0.76		ULTRABASIC	
4				AB11-20D	44.82	4.69	10.34	20.17	0.09	1.85	6.86	5.39	0.31	0.54		BASIC	
5				AB11-20L	45.38	6.56	12.19	19.01	0.05	0.70	5.58	6.85	0.30	0.74		BASIC	
6				AB11-40C	29.60	5.12	8.17	8.76	0.28	1.81	20.96	3.63	0.85	0.55		ULTRABASIC	
7				AB16-02C	46.78	5.03	10.76	12.87	0.15	6.84	8.80	3.15	2.58	0.67		ULTRABASIC	
8				AB11-39	38.50	6.75	10.80	11.33	0.16	4.97	8.45	0.33	2.84	1.07		BASIC	
9				AB11-47C	43.57	3.39	7.49	9.23	0.16	5.55	14.89	3.18	1.19	0.48		ULTRABASIC	
10				AB16-02A	43.95	4.87	9.75	11.79	0.16	7.69	11.68	2.53	2.49	0.62		ULTRABASIC	
11				AB14-05A	28.31	4.94	7.86	14.75	0.26	9.51	14.64	0.01	1.59	0.59		BASIC	
12				AB14-05B	29.27	3.86	8.79	13.94	0.25	12.35	13.54	0.01	0.72	0.64		BASIC	
13				AB10-06B	40.90	6.49	9.42	8.85	0.20	8.86	12.90	1.23	1.38	0.59		ULTRABASIC	
14				AB15-08A	40.02	3.38	9.06	10.03	0.23	11.89	9.57	1.04	3.15	0.70		ULTRABASIC	
15				AB15-05B	41.51	3.69	9.37	12.31	0.22	10.15	9.76	1.64	2.71	0.82		ULTRABASIC	
16				AB15-08B	42.64	4.08	10.09	9.10	0.23	12.15	7.22	1.62	2.60	0.75		ULTRABASIC	
17				AB15-05A	45.843	4.051	11.254	10.725	0.146	7.296	6.467	2.591	3.838	0.881		ULTRABASIC	
18				AB16-49B	42.75	6.28	11.43	14.35	0.214	8.37	7.33	3.213	2.18	0.839		ULTRABASIC	
19				AB16-49D	47.52	5.25	11.94	15.8	0.143	5.12	5.24	5.4	1.22	0.781		ULTRABASIC	
SIO2adj1	TIO2adj1	AL2O3	FE2O3	MNOad	MGOad	CAOadj	NA2Oa	KK2Oa	PP2O5		ilrTIO2	ilrAL2	ilrFE2O3T	ilrMNOm1	ilrMGOm1		
42.26	5.74	11.30	16.68	0.17	1.83	15.21	5.88	0.30	0.64		1.41	0.26	-0.15	3.99	1.08		
42.58	5.61	10.75	18.13	0.10	0.19	15.46	6.44	0.17	0.57		1.43	0.30	-0.24	4.47	3.07		
48.38	5.35	13.16	12.16	0.10	0.43	11.55	7.78	0.25	0.83		1.56	0.16	0.19	4.48	2.27		
47.15	4.93	10.88	21.21	0.09	1.95	7.22	5.67	0.32	0.56		1.60	0.28	-0.38	4.58	0.94		
46.61	6.74	12.52	19.52	0.05	0.72	5.73	7.04	0.31	0.76		1.37	0.28	-0.18	5.15	1.81		
37.13	6.43	10.24	10.99	0.35	2.27	26.29	4.55	1.06	0.69		1.24	0.34	0.18	3.21	0.92		
47.92	5.15	11.02	13.18	0.15	7.01	9.01	3.23	2.64	0.69		1.58	0.29	0.05	4.05	-0.21		
45.19	7.92	12.68	13.30	0.19	5.83	9.92	0.39	3.33	1.26		1.23	0.33	0.19	3.96	0.09		
48.89	3.80	8.40	10.36	0.18	6.23	16.70	3.57	1.34	0.53		1.81	0.40	0.10	3.68	-0.21		
46.01	5.10	10.21	12.34	0.16	8.05	12.23	2.65	2.61	0.65		1.56	0.33	0.07	3.92	-0.35		
34.33	5.99	9.53	17.89	0.32	11.53	17.75	0.01	1.93	0.72		1.23	0.33	-0.31	3.37	-0.53		
35.11	4.63	10.54	16.72	0.30	14.81	16.24	0.01	0.86	0.77		1.43	0.16	-0.29	3.37	-0.81		
45.03	7.15	10.37	9.75	0.22	9.76	14.20	1.35	1.52	0.65		1.30	0.45	0.37	3.68	-0.46		
44.93	3.79	10.17	11.26	0.26	13.35	10.74	1.17	3.54	0.78		1.75	0.20	0.06	3.42	-0.81		
45.03	4.00	10.16	13.36	0.24	11.01	10.58	1.78	2.94	0.89		1.71	0.23	-0.08	3.54	-0.61		
47.12	4.51	11.15	10.06	0.26	13.42	7.98	1.79	2.87	0.83		1.66	0.22	0.24	3.46	-0.78		
49.24	4.35	12.09	11.52	0.16	7.84	6.95	2.78	4.12	0.95		1.72	0.16	0.15	3.96	-0.34		
44.09	6.48	11.79	14.80	0.22	8.63	7.56	3.31	2.25	0.87		1.36	0.29	0.01	3.77	-0.27		
48.29	5.33	12.13	16.05	0.15	5.20	5.32	5.49	1.24	0.79		1.56	0.23	-0.08	4.15	0.12		

Supplementary File 5. ra e elements

Trace elements results obtained by ICP-MS and XRF. The strongly immobile elements were used for tectonic setting calculation. In some samples, the hydrothermal alteration provoked a lixiviation of important trace elements. nm = no measured. DL = Detection Limits (inferior). IGLa-1 standard and DL from Lozano and Bernal (2005). ICP-MS DL from ALS CHEMEX laboratories. Sample AB10-06 is a microbasalt flow, it represents the lava flows which the volcanoclastic units were generated from.

Lo allity	Cerros de la Ci ne a					Cerro Cala eras				Cerro San A ust n			Cerro Ra n					DL		Standard
Met od	XRF	ICP-MS	XRF	XRF	ICP-MS	ICP-MS	ICP-MS	XRF	ICP-MS	ICP-MS	ICP-MS	ICP-MS	XRF	XRF	ICP-MS	ICP-MS	ICP-MS	ICP-MS	XRF	XRF
SAMPL	AB11-20C	AB11-20F	AB11-20O	AB11-20D	AB11-20L	AB11-40C	AB11-39	AB11-47C	AB16-O2A	AB14-05A	AB14-05B	AB10-06B	AB15-08A	AB15-05B	AB15-08B	AB15-05A	AB16-49B	-	-	IGLa-1
Ba	215	119	464	199	411	100	545	1148	2760	215	297	719	1926	803	1175	1895	796	0.5	11	930
Co	22	4	14	24	8	32	70	43	38	63	65	67	50	46	46	31	56	1	3	10
Cr	919	990	355	792	230	870	220	645	300	640	660	400	549	345	250	10	90	10	2	27
Cs	nm	0	nm	nm	1	1	2	nm	1	2	1	0	nm	nm	7	6	2	0.01	nm	nm
Cu	58	26	72	37	17	81	11	5	36	25	256	316	3624	15	29	70	5	1	0.7	17
Ga	nm	21	nm	nm	14	11	28	nm	19	18	18	19	nm	nm	20	16	22	0.1	nm	nm
f	nm	8	nm	nm	9	8	13	nm	10	8	7	8	nm	nm	7	8	12	0.2	nm	nm
Li	nm	nm	nm	nm	10	10	nm	nm	10	30	50	nm	nm	nm	40	20	20	10	nm	nm
Nb	75	63	113	64	82	63	164	42	70	92	65	75	62	60	79	61	97	0.2	0.7	20
Ni	99	40	51	165	61	178	173	178	167	301	341	236	292	132	134	19	213	1	0.5	7
Pb	6	5	5	5	2	10	9	3	2	5	2	9	3	4	<2	<2	4	2	4	11
Rb	5	2	2	6	7	24	89	7	19	47	21	24	71	54	64	71	57	0.2	2	32
Sc	nm	nm	nm	nm	28	29	nm	nm	27	25	28	nm	nm	nm	24	11	28	1	nm	nm
Sn	nm	3	nm	nm	3	2	4	nm	4	3	2	3	nm	nm	2	2	3	1	nm	nm
Sr	252	155	226	167	270	541	345	294	733	529	547	647	219	326	306	590	266	0.1	1	592
Ta	nm	5	nm	nm	5	4	12	nm	5	8	4	5	nm	nm	5	4	6	0.1	nm	nm
Th	3	4	12	2	5	4	16	2	9	12	5	6	3	3	8	5	8	0.05	2	<2
	nm	1	nm	nm	2	1	3	nm	2	1	1	2	nm	nm	10	1	2	0.05	nm	nm
V	500	487	317	454	475	319	448	228	400	463	439	519	344	358	445	325	513	5	5	97
	29	27	43	28	31	23	40	20	33	24	26	32	19	20	30	29	39	0.5	0.5	22
n	52	126	12	32	26	140	188	74	63	253	168	177	135	105	131	93	120	2	1.5	74
r	281	290	450	254	363	319	548	205	366	303	272	316	171	222	313	313	450	2	0.5	224
Th/Ta	nm	1.0	nm	nm	1.0	0.9	1.4	nm	2.0	1.6	1.3	1.2	nm	nm	1.5	1.2	1.3	-	-	-
R	AB11-20C	AB11-20F	AB11-20O	AB11-20D	AB11-20L	AB11-40C	AB11-39	AB11-47C	AB16-O2A	AB14-05A	AB14-05B	AB10-06B	AB15-08A	AB15-05B	AB15-08B	AB15-05A	AB16-49B	-	-	-
La	nm	52.8	nm	nm	65.5	52.0	122.0	nm	60.5	66.9	52.3	54.5	nm	nm	51.7	50.3	73.2	0.5	-	-
Ce	nm	118.0	nm	nm	139.0	113.5	266.0	nm	132.0	153.0	109.0	123.0	nm	nm	119.0	101.0	176.0	0.5	-	-
Pr	nm	12.2	nm	nm	16.5	13.8	31.3	nm	15.8	18.9	13.2	15.4	nm	nm	14.5	12.5	21.8	0.03	-	-
Nd	nm	49.2	nm	nm	67.3	56.8	121.0	nm	68.1	78.1	56.0	60.8	nm	nm	60.2	52.2	91.3	0.1	-	-
Sm	nm	9.5	nm	nm	13.6	10.6	21.8	nm	12.7	14.1	11.6	12.0	nm	nm	12.3	10.4	16.7	0.03	-	-
u	nm	2.9	nm	nm	3.9	3.4	6.0	nm	3.9	4.1	3.3	3.5	nm	nm	3.6	3.3	5.0	0.03	-	-
Gd	nm	7.4	nm	nm	11.2	8.8	15.5	nm	11.6	10.9	9.8	9.8	nm	nm	10.8	9.7	14.8	0.05	-	-
Tb	nm	1.1	nm	nm	1.4	1.1	2.1	nm	1.5	1.4	1.3	1.4	nm	nm	1.5	1.2	1.8	0.01	-	-
Dy	nm	6.2	nm	nm	7.5	5.4	10.2	nm	8.4	6.6	6.1	7.6	nm	nm	7.1	6.6	9.7	0.05	-	-
o	nm	1.2	nm	nm	1.3	0.9	1.8	nm	1.4	1.0	1.0	1.4	nm	nm	1.2	1.2	1.6	0.01	-	-
r	nm	2.7	nm	nm	3.0	2.3	3.7	nm	3.6	2.3	2.5	3.3	nm	nm	2.9	2.8	3.9	0.03	-	-
Tm	nm	0.4	nm	nm	0.4	0.3	0.5	nm	0.4	0.3	0.3	0.4	nm	nm	0.4	0.4	0.4	0.01	-	-
b	nm	1.9	nm	nm	2.4	1.8	2.5	nm	2.6	1.6	1.9	2.2	nm	nm	2.3	2.2	2.5	0.03	-	-
Lu	nm	0.3	nm	nm	0.3	0.2	0.4	nm	0.4	0.2	0.2	0.3	nm	nm	0.3	0.3	0.3	0.01	-	-

Supplementary file . Electron microprobe analysis

Cpx PhC = Clinopyroxene phenocryst

Cpx McC = Clinopyroxene microcrystals

Sample	AB15-05A	AB15-05A	AB15-05A	AB15-05A	AB15-05A	AB15-05A	AB15-05A	AB15-05A	AB15-05A	AB15-05A	AB15-05A
Mineral	Chlorite	Chlorite	Chlorite	Chlorite	Chlorite	Chlorite	Chlorite	Chlorite	Chlorite	Chlorite	Actinolite
SiO	29.70	29.54	29.69	29.83	30.38	29.91	29.52	29.28	30.58	29.98	56.12
l O	18.87	18.73	18.81	18.72	18.46	18.75	17.83	19.28	18.31	18.54	0.80
FeO	12.83	13.24	13.48	12.74	12.77	13.02	12.78	13.28	12.75	13.15	6.80
MnO	0.45	0.55	0.54	0.47	0.54	0.49	0.53	0.55	0.46	0.50	0.38
MgO	25.02	24.68	24.98	24.56	24.58	25.01	24.22	24.63	24.43	24.79	19.63
CaO	0.11	0.11	0.13	0.25	0.14	0.11	0.04	0.01	0.20	0.16	13.00
a O	0.01	0.02	0.00	0.05	0.02	0.01	0.02	0.00	0.02	0.01	0.21
O	0.10	0.31	0.02	0.08	0.02	0.06	0.00	0.01	0.19	0.03	0.03
TiO	0.02	0.02	0.05	0.12	0.00	0.01	0.02	0.07	0.02	0.03	0.00
Total	87.12	87.30	87.71	86.84	86.92	87.39	84.98	87.12	86.98	87.18	96.98

Sample	AB15-05A	AB15-05A	AB15-05A	AB15-05A	AB15-05A	AB15-05A	AB15-05A	AB15-05A	AB15-05A	AB15-05A	AB15-05A
Mineral	Actinolite	Actinolite	Actinolite	Actinolite	Actinolite	Actinolite	Actinolite	Actinolite	Actinolite	Actinolite	Actinolite
SiO	56.17	55.60	55.85	55.18	56.10	55.81	56.44	56.52	55.80	54.83	55.97
l O	0.83	1.06	0.92	1.17	0.75	1.11	0.62	0.74	1.02	1.51	1.68
FeO	6.78	6.83	6.75	7.36	6.72	7.63	7.19	7.06	7.47	8.53	8.42
MnO	0.38	0.41	0.38	0.42	0.38	0.43	0.46	0.36	0.43	0.40	0.36
MgO	19.98	19.58	19.84	19.47	19.77	18.99	19.51	19.60	19.32	18.41	18.66
CaO	13.01	12.91	13.05	12.87	13.01	12.89	12.95	12.97	13.03	12.93	12.82
a O	0.23	0.20	0.23	0.29	0.24	0.30	0.23	0.17	0.26	0.33	0.35
O	0.03	0.05	0.04	0.06	0.03	0.05	0.04	0.04	0.06	0.07	0.05
TiO	0.00	0.00	0.01	0.05	0.03	0.06	0.00	0.01	0.00	0.01	0.03
Total	97.41	96.69	97.07	96.88	97.03	97.26	97.46	97.49	97.41	97.09	98.38

Sample	AB15-05A	AB15-05A	AB15-05A	AB15-05A	AB15-05A	AB15-05A	AB15-05A	AB15-05A	AB15-05A	AB15-05A	AB15-05A
Mineral	Actinolite	Actinolite	Actinolite	Actinolite	Actinolite	Titano magnetite	Titano magnetite	Titano magnetite	Titano magnetite	Titano magnetite	Titano magnetite
SiO	56.34	57.04	56.71	55.02	56.44	0.86	0.40	1.12	0.09	1.87	0.26
I O	0.66	1.68	1.26	1.66	0.67	0.05	0.13	0.29	0.05	0.56	0.08
FeO	7.07	7.26	7.57	8.06	6.59	70.10	89.14	89.47	72.94	83.58	79.18
MnO	0.41	0.45	0.46	0.47	0.48	0.08	0.03	0.07	0.06	0.07	0.11
MgO	19.86	18.51	19.05	18.52	19.87	0.00	0.11	0.03	0.01	0.92	0.10
CaO	13.04	12.04	12.46	12.28	12.62	1.38	0.25	0.29	0.02	0.16	0.06
a O	0.19	0.66	0.44	0.54	0.31	0.00	0.25	0.06	0.00	0.06	0.05
O	0.03	0.12	0.07	0.17	0.08	0.01	0.04	0.03	0.01	0.44	0.02
TiO	0.01	0.04	0.11	0.06	0.10	18.69	0.34	0.15	7.70	0.08	7.46
Total	97.61	97.80	98.12	96.79	97.14	91.21	90.73	92.01	81.39	87.74	87.56

Sample	AB15-05A	AB15-05A	AB15-05A	AB15-05A	AB15-05A	AB15-05A	AB15-05A	AB15-05A	AB15-05A	AB15-05A	AB15-05A
Mineral	Titano magnetite	Titano magnetite	Albite	Albite	Albite	Albite	Albite	Albite	Albite	Albite	Albite
SiO	0.69	0.05	67.51	68.06	67.28	67.95	66.55	67.99	67.88	67.63	67.80
I O	0.21	0.01	19.79	20.29	20.16	20.05	19.96	19.95	20.03	20.08	20.49
FeO	71.87	65.17	0.42	0.25	0.37	0.25	1.96	0.28	0.44	0.61	0.28
MnO	0.06	0.04	0.00	0.03	0.00	0.01	0.00	0.02	0.00	0.04	0.00
MgO	0.17	0.01	0.34	0.01	0.01	0.01	0.00	0.01	0.01	0.86	0.00
CaO	0.35	0.08	0.42	0.28	0.23	0.22	0.23	0.20	0.19	0.12	0.28
a O	0.01	0.00	11.01	11.89	11.35	12.04	11.70	11.78	11.98	11.92	11.81
O	0.03	0.00	0.76	0.12	0.11	0.15	0.31	0.16	0.11	0.29	0.10
TiO	18.11	30.06	0.03	0.01	0.02	0.04	0.18	0.04	0.12	0.03	0.02
Total	91.52	95.43	100.28	100.94	99.53	100.71	100.91	100.43	100.77	101.61	100.79

Sample	AB15-05A	AB15-05A	AB15-05A	AB15-05A
Mineral	Albite	Albite	Sphene	Epidote
SiO	67.99	68.06	30.20	37.12
I O	20.13	20.35	1.19	22.32
FeO	0.11	0.09	1.04	13.53
MnO	0.05	0.02	0.02	0.18
MgO	0.01	0.02	0.00	0.00
CaO	0.20	0.21	28.29	22.91
a O	11.52	11.88	0.00	0.01
O	1.11	0.11	0.01	0.00
TiO	0.02	0.03	37.39	0.10
Total	101.16	100.75	98.16	96.18

Sample	AB16-02C	AB16-02C	AB16-02C	AB16-02C	AB16-02C	AB16-02C	AB16-02C	AB16-02C	AB16-02C	AB16-02C	AB16-02C	AB16-02C
Mineral	Actinolite	Actinolite	Actinolite	Actinolite	Actinolite	Actinolite	Actinolite	Actinolite	Actinolite	Actinolite	Actinolite	Actinolite
SiO	55.74	47.29	56.43	55.75	54.48	52.61	55.40	55.77	55.72	56.08	57.01	
I O	1.64	2.24	1.36	2.05	2.79	2.98	2.52	1.84	2.26	1.55	1.05	
FeO	6.31	6.39	6.35	7.38	7.68	7.62	7.34	7.05	7.07	6.60	6.27	
MnO	0.33	0.32	0.56	0.37	0.40	0.41	0.39	0.47	0.44	0.50	0.56	
MgO	19.76	18.30	19.96	19.45	18.99	18.22	19.36	19.32	19.30	19.70	20.33	
CaO	12.83	12.25	12.53	12.83	12.74	13.88	12.58	12.58	12.65	12.79	12.52	
a O	0.34	0.39	0.40	0.31	0.42	0.42	0.42	0.42	0.37	0.31	0.35	
O	0.04	0.06	0.10	0.09	0.15	0.16	0.17	0.10	0.10	0.10	0.10	
TiO	0.03	0.03	0.12	0.11	0.16	0.38	0.12	0.09	0.18	0.07	0.08	
Total	97.14	87.59	97.82	98.36	97.82	96.70	98.29	97.66	98.09	97.71	98.28	

Sample	AB16-02C	AB16-02C	AB16-02C	AB16-02C	AB16-02C	AB16-02C	AB16-02C	AB16-02C	AB16-02C	AB16-02C	AB16-02C
Mineral	Actinolite	Albite	Albite	Albite	Albite	Albite	Albite	Albite	Albite	Albite	Albite
SiO	56.43	67.94	67.71	69.13	66.33	67.79	65.58	65.40	66.23	65.51	65.80
I O	1.70	20.30	19.83	19.15	21.13	20.31	20.88	18.41	18.65	18.14	19.57
FeO	7.16	0.23	0.51	0.44	0.22	0.44	0.89	1.04	0.86	0.71	0.70
MnO	0.51	0.00	0.01	0.01	0.00	0.00	0.05	0.04	0.06	0.04	0.02
MgO	19.46	0.02	0.43	0.42	0.01	0.19	0.66	2.29	1.57	0.87	0.75
CaO	12.74	0.29	0.79	0.46	0.97	0.33	1.25	1.96	1.86	2.52	1.81
a O	0.36	11.22	11.55	11.30	11.15	11.63	10.68	9.57	11.22	11.06	10.88
O	0.07	0.92	0.28	0.70	0.08	0.08	0.48	0.39	0.10	0.09	0.43
TiO	0.36	0.05	0.12	0.04	0.18	0.20	0.19	0.10	0.14	2.45	0.08
Total	98.80	101.05	101.25	101.65	100.09	100.97	100.73	99.25	100.72	101.40	100.09

Sample	AB16-02C	AB16-02C	AB16-02C	AB16-02C	AB16-02C	AB16-02C	AB16-02C	AB16-02C	AB16-02C
Mineral	Albite	Epidote	Epidote	Sphene	Sphene	Sphene	Sphene	Quartz	Orthoclase
SiO	65.36	37.28	36.89	30.51	30.67	29.98	29.54	95.86	63.76
I O	19.81	22.33	22.10	1.59	2.50	1.09	1.19	0.18	18.65
FeO	0.67	13.20	13.55	2.04	1.98	2.76	1.39	0.31	0.72
MnO	0.03	0.20	0.17	0.02	0.03	0.04	0.01	0.00	0.06
MgO	0.65	0.00	0.01	0.44	0.05	0.08	0.00	0.65	0.37
CaO	2.00	22.72	22.17	26.99	27.44	27.25	27.20	0.03	0.29
a O	11.42	0.00	0.01	0.06	0.05	0.03	0.07	0.00	0.24
O	0.19	0.00	0.00	0.06	0.07	0.09	0.03	0.17	14.19
TiO	0.36	0.20	0.07	35.66	34.21	36.70	38.73	0.03	0.35
Total	100.52	95.95	94.97	97.37	96.99	98.03	98.15	97.25	101.03

Sample	AB10-06B	AB10-06B	AB10-06B	AB10-06B	AB10-06B	AB10-06B	AB10-06B	AB10-06B	AB10-06B	AB10-06B	AB10-06B
Mineral	Cpx PhC	Cpx PhC	Cpx PhC	Cpx PhC	Cpx PhC	Cpx PhC	Cpx PhC	Cpx PhC	Cpx PhC	Cpx PhC	Cpx PhC
SiO	48.43	48.27	50.08	47.96	45.19	47.58	48.14	49.20	47.87	49.26	47.41
I O	3.97	4.32	2.90	4.28	6.69	4.44	4.58	3.41	4.52	3.26	4.97
FeO	5.75	5.77	6.04	6.26	7.36	6.26	6.49	5.68	6.59	5.62	6.51
MnO	0.08	0.07	0.09	0.10	0.10	0.10	0.07	0.07	0.13	0.11	0.10
MgO	14.27	14.49	15.01	13.97	12.29	14.18	14.03	14.88	13.96	14.95	13.83
CaO	22.92	23.16	22.77	22.87	22.71	23.02	23.17	23.15	22.89	23.28	23.10
a O	0.35	0.38	0.36	0.45	0.52	0.37	0.45	0.40	0.45	0.30	0.41
O	0.00	0.00	-0.01	0.00	0.00	-0.01	0.00	0.00	0.00	0.00	0.00
TiO	2.16	2.31	1.90	2.38	4.09	2.60	2.57	1.80	2.50	1.76	2.79
Total	98.39	99.28	99.44	98.57	98.98	98.88	99.70	99.10	99.02	99.04	99.25

Sample	AB10-06B	AB10-06B	AB10-06B	AB10-06B	AB10-06B	AB10-06B	AB10-06B	AB10-06B	AB10-06B	AB10-06B
Mineral	Cpx McC	Cpx McC	Cpx McC	Cpx McC	Cpx McC	Cpx McC	Cpx McC	Cpx McC	Cpx McC	Cpx McC
SiO	45.11	48.33	44.50	44.80	46.45	46.80	47.26	45.19	47.08	0.16
I O	6.13	3.70	7.06	6.57	5.35	5.59	4.24	6.50	4.16	0.10
FeO	7.37	7.14	7.61	7.47	8.76	7.37	7.51	7.36	7.76	66.49
MnO	0.10	0.12	0.09	0.10	0.15	0.10	0.11	0.12	0.15	0.14
MgO	12.71	14.15	12.52	12.57	12.91	13.14	13.83	12.52	13.87	0.06
CaO	22.91	22.53	22.57	23.03	22.10	22.86	22.76	22.91	22.56	0.19
a O	0.41	0.29	0.46	0.39	0.34	0.46	0.32	0.51	0.28	-0.02
O	0.01	0.00	0.00	0.01	0.00	0.00	0.00	0.02	0.00	0.01
TiO	3.84	2.75	4.25	3.86	3.95	3.11	2.99	4.16	3.18	23.86
Total	98.71	99.19	99.56	99.13	100.12	99.74	99.13	99.31	99.15	93.52

Sample	AB10-06B	AB10-06B	AB10-06B	AB10-06B
Mineral	Titano magnetite	Titano magnetite	Titano magnetite	Titano magnetite
SiO	0.26	0.14	1.00	55.81
l O	3.44	1.61	0.85	27.88
FeO	61.42	60.93	63.93	0.38
MnO	0.38	0.47	0.09	0.01
MgO	0.06	0.04	0.86	0.03
CaO	0.09	0.16	0.30	8.84
a O	-0.09	-0.02	0.01	6.11
O	0.00	0.00	0.03	0.72
TiO	23.47	24.80	25.13	0.19
Total	92.69	93.01	92.40	99.99

Sample	AB10-06B	AB10-06B	AB10-06B	AB10-06B	AB10-06B	AB10-06B	AB10-06B	AB10-06B	AB10-06B	AB10-06B	AB10-06B
Mineral	Plagioclase	Plagioclase	Plagioclase	Plagioclase	Plagioclase	Plagioclase	Plagioclase	Plagioclase	Plagioclase	Plagioclase	Plagioclase
SiO	58.57	54.90	55.39	54.48	55.07	64.02	55.05	59.70	62.69	55.59	55.41
l O	25.58	28.69	28.22	28.37	28.17	22.00	28.39	23.91	19.37	27.69	28.35
FeO	0.38	0.50	0.40	0.48	0.92	0.44	0.48	1.04	0.72	0.51	0.49
MnO	0.00	0.00	0.00	-0.01	0.02	0.01	0.00	0.00	0.01	0.00	0.00
MgO	0.03	0.05	0.05	0.03	0.15	0.28	0.03	0.12	0.24	0.06	0.03
CaO	6.32	10.03	9.53	9.59	7.53	1.50	9.60	4.29	0.06	8.98	9.63
a O	7.07	5.56	5.70	5.78	5.12	8.61	5.95	7.05	0.25	6.13	5.72
O	1.19	0.49	0.62	0.47	2.77	2.52	0.57	2.44	17.29	0.55	0.59
TiO	0.18	0.18	0.19	0.21	0.20	0.05	0.21	0.15	0.01	0.19	0.21
Total	99.32	100.39	100.10	99.41	99.96	99.45	100.29	98.70	100.63	99.71	100.44

Supplementary file 7. $^{40}\text{Ar}/^{39}\text{Ar}$ Geochronology data

Sample AB 10 06 Picrobasalt

Laser step-heating experiments on groundmass concentrate

Pwr	$^{39}\text{Ar} \times 10^{-6}$	F ^{39}Ar	$^{40}\text{Ar}^*/^{39}\text{Ar}_K$	1σ	Age in Ma	1σ				% $^{40}\text{Ar}^*$	$^{40}\text{Ar}/^{36}\text{Ar}$	$^{37}\text{Ar}_{Ca}/^{39}\text{Ar}_K$	
0.40	2.529	0.0095	16.77	3.48	99.24	20.02	a	†	‡	§	24.94	393.71	2.99
1.00	12.065	0.0450	16.10	0.69	95.42	4.01	b	†	‡	§	61.39	765.26	19.85
1.60	16.447	0.0613	16.17	0.61	95.83	3.49	c	†	‡	§	78.10	1349.39	18.93
2.20	28.114	0.1060	16.33	0.22	96.73	1.26	d	†	‡		91.59	3514.60	1.24
3.00	37.318	0.1408	18.02	0.16	106.47	0.93	e	†	‡		96.29	7966.98	0.76
4.00	40.470	0.1526	18.95	0.16	111.77	0.91	f	†	‡		98.41	18545.60	0.86
4.60	26.556	0.1002	17.95	0.23	106.04	1.34	g	†	‡		98.92	27258.69	0.91
5.40	18.173	0.0685	15.38	0.27	91.26	1.58	h			§	99.10	32748.60	2.08
6.50	33.853	0.1272	14.86	0.21	88.21	1.23	i			§	97.81	13488.50	6.12
8.00	50.447	0.1889	17.46	0.18	103.24	1.04	j	†	‡		95.09	6015.09	12.02
0.30	5.046	0.0067	15.20	2.06	90.20	11.94	k		‡	§	19.63	367.67	2.657
0.90	26.592	0.0351	14.44	0.31	85.81	1.82	l		‡	§	56.04	672.20	2.105
1.50	53.741	0.0710	13.50	0.20	80.32	1.14	m				78.50	1374.26	1.921
2.00	78.473	0.1037	14.72	0.15	87.44	0.84	n				88.03	2468.67	1.260
2.50	63.945	0.0845	17.82	0.14	105.28	0.82	o		‡		95.22	6177.01	0.569
3.50	115.493	0.1526	18.39	0.08	108.55	0.46	p		‡		97.04	9991.25	0.560
4.50	86.878	0.1148	19.34	0.11	114.00	0.62	q				97.93	14293.83	1.084
6.00	147.126	0.1938	15.53	0.07	92.10	0.40	r			§	96.97	9748.19	5.505
9.00	180.879	0.2379	15.41	0.07	91.43	0.39	s			§	94.12	5024.53	7.925

Integrated results

$^{39}\text{Ar} \times 10^{-6}$	$^{40}\text{Ar}^*/^{39}\text{Ar}_K$	1σ	Age in Ma	1σ	% $^{40}\text{Ar}^*$	$^{40}\text{Ar}/^{36}\text{Ar}$	$^{37}\text{Ar}_{Ca}/^{39}\text{Ar}_K$
265.0	17.08	0.09	101.03	0.63	90.66	3163.30	5.73
756.4	16.30	0.05	96.56	0.42	89.99	2951.81	3.57

$$J = 0.003373 \pm 0.000012$$

$$\dagger \quad t_c = 105.80 \pm 2.24 \text{ Ma}, (^{40}\text{Ar}/^{36}\text{Ar})_i = 282 \pm 65, \text{MSWD} = 20 \text{ for } n = 8$$

$$\ddagger \quad t_c = 108.57 \pm 1.50 \text{ Ma}, (^{40}\text{Ar}/^{36}\text{Ar})_i = 251 \pm 30, \text{MSWD} = 32 \text{ for } n = 13$$

$$\S \quad t_c = 91.67 \pm 0.55 \text{ Ma}, (^{40}\text{Ar}/^{36}\text{Ar})_i = 287 \pm 10, \text{MSWD} = 3 \text{ for } n = 9$$

Sample AB 11 46

Porphyritic metabasalt

Laser step-heating experiments on groundmass concentrate

Pwr	$^{39}\text{Ar} \times 10^{-6}$	F ^{39}Ar	$^{40}\text{Ar}^*/^{39}\text{Ar}_K$	1 σ	Age in Ma	1 σ		% $^{40}\text{Ar}^*$	$^{40}\text{Ar}/^{36}\text{Ar}$	$^{37}\text{Ar}_{Ca}/^{39}\text{Ar}_K$
0.40	13.923	0.0108	5.37	0.59	32.38	3.54	a ‡	21.19	374.98	0.457
0.80	37.337	0.0290	6.25	0.18	37.65	1.09	b ‡	66.35	878.08	0.700
1.20	68.032	0.0528	8.68	0.10	52.06	0.61	c ‡	89.37	2780.33	0.716
1.60	63.931	0.0496	9.32	0.09	55.84	0.51	d	92.77	4086.50	0.942
2.00	59.698	0.0464	9.43	0.10	56.47	0.61	e	94.91	5803.53	0.289
2.44	99.028	0.0769	9.22	0.08	55.27	0.48	f	93.98	4907.14	0.303
3.00	138.189	0.1073	9.28	0.06	55.62	0.33	g	96.51	8477.86	0.792
3.60	187.610	0.1456	9.33	0.05	55.92	0.28	h	96.33	8057.18	1.803
4.50	224.491	0.1742	9.66	0.03	57.85	0.20	i	94.61	5486.10	2.234
6.00	245.700	0.1907	9.64	0.05	57.69	0.27	j	93.48	4532.80	1.209
8.00	49.418	0.0382	12.71	0.15	75.74	0.90	k ‡	95.78	6998.43	5.795
10.00	101.385	0.0784	12.94	0.09	77.06	0.52	l ‡	91.48	3467.47	6.657

Integrated results

$^{39}\text{Ar} \times 10^{-6}$	$^{40}\text{Ar}^*/^{39}\text{Ar}_K$	1 σ	Age in Ma	1 σ	% $^{40}\text{Ar}^*$	$^{40}\text{Ar}/^{36}\text{Ar}$	$^{37}\text{Ar}_{Ca}/^{39}\text{Ar}_K$
1287	9.68	0.02	57.98	0.25	91.54	3492.65	1.857

$$J = 0.003373 \pm 0.000012$$

the plateau age was calculated with the weighted mean of fractions d to h

$$t_p = 55.78 \pm 0.15 \text{ Ma}, \text{ 42.58\% of } ^{39}\text{Ar} \text{ released in 5 consecutive fractions, MSWD} = 0.7$$

$$t_c = \mathbf{52.58 \pm 2.00 \text{ Ma}}, (^{40}\text{Ar}/^{36}\text{Ar})_i = 717 \pm 189, \text{ MSWD} = 3.2 \text{ for } n = 7$$

‡ fraction ignored in the isochron given in the figure

Supplementary file 1. Electron microprobe analysis

Spreadsheet from La Ford Anderson (anderson@usc.edu).

Sample	AB16-53A	AB16-53A	AB16-53A	AB16-53A	AB16-53A	AB16-53A	AB16-53A	AB16-53A	AB16-53A	AB16-53A	AB16-53A
Mineral	Alite	Alite	Alite	Alite	Alite	Alite	Alite	Alite	Alite	Alite	Actinolite
SiO	65.93	68.05	65.52	68.19	67.00	67.98	67.37	68.16	67.49	67.07	56.27
TiO	0.04	0.03	0.02	0.04	0.04	0.01	0.04	0.00	0.11	0.02	0.08
IO	19.66	20.15	19.45	19.91	20.40	20.10	19.94	19.96	20.14	20.06	0.61
FeO	1.02	0.28	0.96	0.22	0.37	0.36	0.64	0.25	0.28	0.54	7.35
MgO	1.46	0.02	1.85	0.12	0.36	0.01	0.34	0.03	0.01	0.64	19.42
MnO	0.03	0.02	0.02	0.01	0.00	0.01	0.04	0.00	0.00	0.00	0.64
CaO	0.29	0.15	0.10	0.10	0.74	0.15	0.16	0.11	0.20	0.11	12.85
aO	10.73	11.96	11.22	11.72	11.33	11.89	11.83	12.15	11.63	11.88	0.24
O	0.34	0.06	0.15	0.11	0.38	0.16	0.11	0.08	0.09	0.08	0.03
Total	99.51	100.75	99.28	100.42	100.67	100.70	100.49	100.76	99.96	100.40	97.50

Sample	AB16-53A	AB16-53A	AB16-53A	AB16-53A	AB16-53A	AB16-53A	AB16-53A	AB16-53A	AB16-53A	AB16-53A	AB16-53A
Mineral	Actinolite	Actinolite	Actinolite	Actinolite	Actinolite	Actinolite	Actinolite	Actinolite	Actinolite	Actinolite	Chlorite
SiO	55.02	55.53	55.35	55.96	56.00	54.85	55.58	55.27	55.29	52.98	29.43
TiO	0.03	0.04	0.04	0.05	0.15	0.02	0.09	0.11	0.09	0.08	0.04
IO	1.31	1.16	0.86	0.74	1.04	1.67	0.76	0.98	1.25	2.57	18.45
FeO	7.59	7.43	7.94	7.13	7.94	8.07	7.65	7.61	8.42	11.66	13.57
MgO	18.74	18.92	18.76	19.20	18.44	18.51	18.87	18.72	18.75	15.91	23.93
MnO	0.55	0.54	0.65	0.65	0.64	0.51	0.57	0.61	0.53	0.23	0.67
CaO	12.86	12.92	12.43	12.75	12.49	12.75	12.73	12.71	12.44	12.67	0.08
aO	0.33	0.29	0.43	0.24	0.47	0.36	0.30	0.36	0.33	0.37	0.00
O	0.04	0.06	0.05	0.03	0.10	0.08	0.03	0.05	0.07	0.11	0.05
Total	96.73	97.08	96.50	96.76	97.28	96.85	96.58	96.44	97.17	96.57	86.87

Sample	AB16-53A	AB16-53A	AB16-53A	AB16-53A	AB16-53A
Mineral	Chlorite	Chlorite	Chlorite	Chlorite	Chlorite
SiO	30.37	29.15	29.41	29.58	30.69
TiO	0.01	0.03	0.04	0.01	0.04
I O	17.84	19.04	17.85	18.21	17.39
FeO	13.86	13.70	13.58	13.79	13.83
MgO	23.80	23.97	24.10	23.94	23.87
MnO	0.68	0.77	0.70	0.67	0.66
CaO	0.18	0.07	0.11	0.11	0.20
a O	0.00	0.00	0.01	0.02	0.03
O	0.03	0.05	0.03	0.01	0.05
Total	86.96	86.79	85.89	86.62	86.76

Sample	AB11-46	AB11-46	AB11-46	AB11-46	AB11-46	AB11-46	AB11-46	AB11-46	AB11-46	AB11-46	AB11-46
Mineral	Al ite	Al ite	Al ite	Al ite	Al ite	Al ite	Al ite	Al ite	Al ite	Actinolite	Actinolite
SiO	66.72	61.75	67.73	67.61	67.46	67.23	67.49	67.82	67.63	52.98	52.23
TiO	0.06	0.14	0.02	0.02	0.01	0.05	0.05	0.04	0.07	0.08	0.08
I O	20.03	20.20	20.31	20.29	20.36	20.45	20.39	20.18	20.20	2.57	2.63
FeO	0.58	3.11	0.23	0.19	0.26	0.37	0.25	0.25	0.22	11.66	11.21
MgO	0.26	3.01	0.03	0.06	0.00	0.09	0.02	0.00	0.01	15.91	15.89
MnO	0.00	0.05	0.01	0.00	0.02	0.00	0.00	0.03	0.01	0.23	0.15
CaO	0.71	0.70	0.33	0.44	0.53	0.63	0.44	0.49	0.40	12.67	12.41
a O	11.23	10.04	11.70	11.76	11.69	11.76	11.58	11.72	11.73	0.37	0.39
O	0.43	1.21	0.09	0.10	0.11	0.10	0.21	0.20	0.17	0.11	0.08
Total	100.04	100.23	100.46	100.48	100.44	100.68	100.44	100.75	100.46	96.57	95.39

Sample	AB11-46	AB11-46	AB11-46	AB11-46	AB11-46	AB11-46	AB11-46	AB11-46	AB11-46	AB11-46	AB11-46
Mineral	Actinolite	Actinolite	Actinolite	Actinolite	Actinolite	Actinolite	Actinolite	Horn lende	Horn lende	Horn lende	Epidote
SiO	51.11	52.12	53.28	51.57	51.21	53.22	52.81	49.93	49.51	48.92	36.88
TiO	0.09	0.35	0.04	0.02	0.05	0.31	0.03	0.05	0.10	0.11	0.07
l O	3.60	2.58	1.95	3.46	3.39	2.00	2.29	4.66	4.94	5.58	22.45
FeO	12.61	12.92	11.38	12.13	12.69	10.28	11.54	13.96	14.05	14.46	12.91
MgO	14.81	14.70	16.01	15.29	14.90	16.78	15.77	13.98	13.85	13.22	0.00
MnO	0.15	0.25	0.20	0.14	0.16	0.16	0.16	0.22	0.15	0.13	0.15
CaO	12.43	12.43	12.56	12.45	12.45	12.02	12.52	12.35	12.20	12.12	22.52
a O	0.49	0.47	0.29	0.49	0.45	0.39	0.38	0.66	0.72	0.79	0.02
O	0.12	0.11	0.06	0.10	0.11	0.57	0.08	0.22	0.20	0.27	0.00
Total	95.67	96.05	96.09	95.79	95.79	96.24	96.01	96.11	95.87	95.86	95.09

Sample	AB11-46	AB11-46	AB11-46	AB11-46	AB11-46	AB11-46	AB11-46	AB11-46	AB11-46	AB11-46
Mineral	Epidote	Epidote	Epidote	Epidote	Epidote	Epidote	Epidote	Epidote	Epidote	uart
SiO	36.59	36.69	36.85	36.89	36.94	37.01	36.81	36.61	36.79	98.71
TiO	0.13	0.04	0.10	0.07	0.12	0.03	0.07	0.22	0.06	0.08
l O	22.46	22.77	23.43	22.22	22.85	22.54	22.43	21.70	22.70	0.05
FeO	12.67	12.53	11.85	13.18	12.75	13.01	13.11	13.45	12.44	0.21
MgO	0.00	0.01	0.02	0.00	0.00	0.00	0.00	0.00	0.00	0.00
MnO	0.08	0.15	0.08	0.14	0.23	0.13	0.12	0.10	0.13	0.00
CaO	22.89	22.47	22.87	22.51	22.45	22.75	22.47	22.47	22.77	0.05
a O	0.01	0.05	0.03	0.01	0.02	0.01	0.07	0.02	0.01	0.01
O	0.01	0.00	0.01	0.00	0.00	0.00	0.01	0.00	0.00	0.00
Total	94.99	94.88	95.31	95.09	95.41	95.55	95.16	94.92	94.97	99.13

Sample	AB15-20	AB15-20	AB15-20	AB15-20	AB15-20	AB15-20	AB15-20	AB15-20	AB15-20	AB15-20	AB15-20
Mineral	Al ite	Al ite	Al ite	Al ite	Al ite	Al ite	Al ite	Al ite	Al ite	Al ite	Actinolite
SiO	68.25	67.63	69.04	67.67	67.22	67.83	68.14	67.75	67.79	68.19	54.91
TiO	0.05	0.05	0.03	0.05	0.07	0.03	0.05	0.00	0.03	0.01	0.02
I O	20.13	19.68	19.94	19.82	19.88	19.73	19.93	20.10	20.02	20.06	1.39
FeO	0.27	0.38	0.17	0.66	0.75	0.18	0.21	0.10	0.20	0.31	6.85
MgO	0.01	0.50	0.02	0.11	0.25	0.01	0.02	0.01	0.00	0.02	19.31
MnO	0.02	0.04	0.01	0.01	0.00	0.00	0.00	0.00	0.00	0.00	0.28
CaO	0.09	0.66	0.06	0.13	0.16	0.54	0.12	0.07	0.14	0.12	12.82
a O	11.67	11.39	12.11	11.72	11.76	12.06	11.70	11.72	11.55	11.67	0.30
O	0.07	0.35	0.06	0.08	0.11	0.10	0.07	0.07	0.05	0.08	0.04
Total	100.56	100.71	101.45	100.26	100.21	100.49	100.28	99.83	99.79	100.47	96.25

Sample	AB15-20	AB15-20	AB15-20	AB15-20	AB15-20	AB15-20	AB15-20	AB15-20	AB15-20	AB15-20
Mineral	Actinolite	Actinolite	Actinolite	Actinolite	Actinolite	Actinolite	Actinolite	Actinolite	Actinolite	uart
SiO	55.57	55.91	56.11	56.15	55.87	54.45	55.48	55.21	54.94	97.63
TiO	0.04	0.01	0.03	0.11	0.04	0.03	0.07	0.04	0.01	0.09
I O	1.09	0.94	1.14	0.90	1.10	1.59	1.10	1.58	1.40	1.04
FeO	6.47	6.12	6.51	5.97	6.69	7.19	6.61	7.26	7.46	0.29
MgO	19.58	19.91	19.94	20.05	19.43	19.13	19.74	18.85	18.97	0.02
MnO	0.29	0.24	0.28	0.22	0.31	0.28	0.29	0.33	0.31	0.00
CaO	12.89	13.05	12.67	13.03	12.86	12.82	12.85	12.84	12.75	0.09
a O	0.30	0.25	0.24	0.24	0.29	0.31	0.28	0.35	0.31	0.03
O	0.03	0.03	0.04	0.03	0.05	0.04	0.04	0.04	0.06	0.00
Total	96.62	96.84	97.01	97.05	97.05	96.14	96.66	96.68	96.55	99.21

Sample	AB16-24	AB16-24	AB16-24	AB16-24	AB16-24	AB16-24	AB16-24	AB16-24	AB16-24	AB16-24	AB16-24
Mineral	Al ite	Al ite	Al ite	Al ite	Al ite	Al ite	Al ite	Actinolite	Actinolite	Actinolite	Actinolite
SiO	67.24	67.18	65.39	66.01	67.15	67.49	67.49	54.95	53.66	54.00	52.48
TiO	0.11	0.12	0.11	0.20	0.07	0.06	0.07	0.05	0.04	0.02	0.04
I O	20.34	20.32	20.29	20.08	20.38	20.51	20.34	1.40	2.20	2.07	3.55
FeO	0.32	0.65	1.10	0.51	0.30	0.23	0.30	10.99	10.70	10.20	11.30
MgO	0.15	0.40	1.07	0.16	0.03	0.03	0.11	16.46	16.50	16.91	16.07
MnO	0.00	0.01	0.00	0.01	0.00	0.00	0.00	0.52	0.50	0.49	0.51
CaO	0.56	0.42	0.58	0.73	0.74	0.65	0.51	12.74	12.73	12.64	12.46
a O	11.21	11.54	10.80	9.40	11.33	11.14	11.06	0.23	0.29	0.28	0.43
O	0.47	0.31	0.89	3.50	0.24	0.09	0.48	0.06	0.09	0.07	0.10
Total	100.43	100.95	100.35	101.02	100.24	100.22	100.44	97.47	96.76	96.75	96.96

Sample	AB16-24	AB16-24	AB16-24	AB16-24	AB16-24	AB16-24	AB16-24	AB16-24	AB16-24	AB16-24	AB16-24
Mineral	Actinolite	Actinolite	Actinolite	Actinolite	Actinolite	Actinolite	Titanomag.	Ilmenite	Sphene	Sphene	Epidote
SiO	53.23	52.47	52.29	53.71	54.22	53.73	0.40	0.03	30.21	28.38	36.53
TiO	0.07	0.02	0.04	0.03	0.04	0.04	37.76	48.79	36.07	40.00	0.08
I O	2.60	3.21	2.88	2.21	1.92	2.18	0.20	0.00	1.91	1.63	21.94
FeO	10.28	11.90	10.81	11.42	10.07	10.71	49.16	39.15	1.64	1.80	13.15
MgO	16.73	15.96	15.92	16.25	17.19	16.50	0.27	0.16	0.90	0.49	0.01
MnO	0.41	0.46	0.51	0.49	0.47	0.47	7.82	10.23	0.05	0.06	0.29
CaO	12.70	12.52	12.61	12.53	12.73	12.79	0.31	0.01	26.58	26.13	21.50
a O	0.35	0.45	0.38	0.36	0.29	0.33	0.03	0.01	0.01	0.01	0.01
O	0.08	0.16	0.10	0.06	0.05	0.09	0.05	0.00	0.12	0.01	0.00
Total	96.50	97.19	95.59	97.09	97.12	96.87	96.18	98.42	97.54	98.56	93.55

Sample	AB16-24	AB16-24	AB16-24	AB16-34
Mineral	Epidote	uart	uart	uart
SiO	36.90	99.21	99.21	98.77
TiO	0.20	0.00	0.02	0.03
l O	21.13	0.05	0.27	0.23
FeO	14.26	0.11	0.09	0.25
MgO	0.00	0.04	0.00	0.04
MnO	0.21	0.00	0.00	0.00
CaO	22.31	0.00	0.01	0.04
a O	0.03	0.00	0.03	0.00
O	0.02	0.00	0.00	0.01
Total	95.08	99.44	99.63	99.36

Sample	NL16-04	NL16-04	NL16-04	NL16-04	NL16-04	NL16-04	NL16-04	NL16-04	NL16-04	NL16-04
Mineral	Oligoclase	Oligoclase	Oligoclase	Oligoclase	Oligoclase	Oligoclase	Oligoclase	Andesine	Oligoclase	Oligoclase
SiO	62.09	62.38	62.52	61.58	61.24	60.15	63.70	59.90	62.74	59.99
TiO	0.00	0.00	0.01	0.01	0.00	0.00	0.02	0.01	0.00	0.01
l O	24.02	23.66	23.74	24.40	23.95	25.48	23.04	25.42	23.14	25.41
FeO	0.12	0.15	0.15	0.23	0.17	0.18	0.16	0.22	0.18	0.13
MgO	0.00	0.00	0.00	0.00	0.01	0.00	0.01	0.00	0.01	0.00
MnO	0.00	0.00	0.03	0.00	0.00	0.00	0.06	0.00	0.01	0.00
CaO	4.80	4.53	4.55	5.42	4.92	6.42	3.73	6.44	4.32	6.28
a O	9.04	8.98	9.20	8.47	8.68	7.94	9.58	8.03	9.10	8.27
O	0.09	0.47	0.25	0.28	0.32	0.15	0.16	0.18	0.31	0.08
Total	100.18	100.16	100.45	100.40	99.29	100.30	100.45	100.20	99.81	100.17

Sample	NL16-04	NL16-04	NL16-04	NL16-04	NL16-04	NL16-04	NL16-04	NL16-04	NL16-04	NL16-04
Mineral	Amphi ole	Amphi ole	Amphi ole	Amphi ole	Amphi ole	Amphi ole	Amphi ole	Amphi ole	Amphi ole	Amphi ole
SiO	51.22	51.00	51.68	53.71	51.31	49.83	49.56	50.49	51.00	51.49
TiO	0.34	0.24	0.24	0.13	0.31	0.74	0.90	0.42	0.24	0.23
l O	3.84	3.67	3.37	2.36	3.77	4.99	5.55	4.29	3.67	3.24
Cr O	0.00	0.00	0.00	0.00	0.01	0.00	0.01	0.01	0.00	0.00
FeO	12.66	12.50	12.38	11.84	12.41	13.17	14.06	12.74	12.50	12.11
MgO	15.23	15.42	15.58	16.14	15.44	14.22	13.08	15.05	15.42	15.67
CaO	12.12	12.08	12.16	12.34	12.10	11.89	11.74	12.06	12.08	12.31
MnO	0.57	0.60	0.54	0.60	0.52	0.59	0.63	0.57	0.60	0.58
a O	0.67	0.56	0.63	0.37	0.69	1.02	1.20	0.67	0.56	0.51
O	0.27	0.23	0.20	0.13	0.26	0.43	0.54	0.32	0.23	0.21
Total	96.93	96.31	96.78	97.62	96.81	96.88	97.24	96.63	96.31	96.35

Supplementary file . Thermometric data

Calculations after Holland & Blundy estimated error is ± 1 C
 Ideal Plagioclase thermometry calibration reaction edenite + quartz = tremolite + albite

	Sample	Temperature C	Temp. range	Std. Deviation
I aline Meta asalt Cerro Ra on locality	1	1	1	
		1		
		1		
I aline Meta asalt Cerro Cala eras locality	11	1		
		1		
		1		

	Sample	Temperature C	Temp. range	Std. Deviation
I aline Meta asalt Cerro Los paches locality	1			
			1	
			1	
I aline Meta asalt Cerros de la Ci nega locality	1			
			11	

Holland and Blundy (1993) thermometry calibration reaction edenite + albite = richterite + anorthite
 recommended by Anderson (1981) for aplitic rocks

Sample	Temperature (C)	Temp. range	Std. Deviation
Granodiorite Cerro Divil locality	1		1
	1		
	1		

Supplementary file . Geo aromether calculations

Calculations after Molina *et al.* 2015

Used for the granodiorite from Cerro El Dátil locality

Calcic amphibole thermobarometry in metamorphic and igneous rocks

New calibrations based on plagioclase/amphibole Al-Si partitioning and amphibole/li uid Mg partitioning

Amphibole

Sample	Author	SiO2	TiO2	Al2O3	Cr2O3	NiO	FeO	MnO	MgO	CaO	Na2O	K2O
NL16-04 anf1	Barrón-Díaz et al.	51.22	0.34	3.84	0.00	0.00	12.66	0.57	15.23	12.12	0.67	0.27
NL16-04 anf2	Barrón-Díaz et al.	51.00	0.24	3.67	0.00	0.00	12.50	0.60	15.42	12.08	0.56	0.23
NL16-04 anf3	Barrón-Díaz et al.	51.68	0.24	3.37	0.00	0.00	12.38	0.54	15.58	12.16	0.63	0.20
NL16-04 anf4	Barrón-Díaz et al.	53.71	0.13	2.36	0.00	0.00	11.84	0.60	16.14	12.34	0.37	0.13
NL16-04 anf5	Barrón-Díaz et al.	51.31	0.31	3.77	0.01	0.00	12.41	0.52	15.44	12.10	0.69	0.26
NL16-04 anf6	Barrón-Díaz et al.	49.83	0.74	4.99	0.00	0.00	13.17	0.59	14.22	11.89	1.02	0.43
NL16-04 anf7	Barrón-Díaz et al.	49.56	0.90	5.55	0.01	0.00	14.06	0.63	13.08	11.74	1.20	0.54
NL16-04 anf8	Barrón-Díaz et al.	50.49	0.42	4.29	0.01	0.00	12.74	0.57	15.05	12.06	0.67	0.32
NL16-04 anf9	Barrón-Díaz et al.	51.00	0.24	3.67	0.00	0.00	12.50	0.60	15.42	12.08	0.56	0.23
NL16-04 anf10	Barrón-Díaz et al.	51.49	0.23	3.24	0.00	0.00	12.11	0.58	15.67	12.31	0.51	0.21

F	Cl	Total	Si	Ti	Al	Cr	Ni	Fet	Mn	Mg	Ca	Na	K	F
0.00	0.00	96.93	0.85	0.00	0.08	0.00	0.00	0.18	0.01	0.38	0.22	0.02	0.01	0.00
0.00	0.00	96.31	0.85	0.00	0.07	0.00	0.00	0.17	0.01	0.38	0.22	0.02	0.00	0.00
0.00	0.00	96.78	0.86	0.00	0.07	0.00	0.00	0.17	0.01	0.39	0.22	0.02	0.00	0.00
0.00	0.00	97.62	0.89	0.00	0.05	0.00	0.00	0.16	0.01	0.40	0.22	0.01	0.00	0.00
0.00	0.00	96.82	0.85	0.00	0.07	0.00	0.00	0.17	0.01	0.38	0.22	0.02	0.01	0.00
0.00	0.00	96.88	0.83	0.01	0.10	0.00	0.00	0.18	0.01	0.35	0.21	0.03	0.01	0.00
0.00	0.00	97.25	0.82	0.01	0.11	0.00	0.00	0.20	0.01	0.32	0.21	0.04	0.01	0.00
0.00	0.00	96.64	0.84	0.01	0.08	0.00	0.00	0.18	0.01	0.37	0.22	0.02	0.01	0.00
0.00	0.00	96.31	0.85	0.00	0.07	0.00	0.00	0.17	0.01	0.38	0.22	0.02	0.00	0.00
0.00	0.00	96.35	0.86	0.00	0.06	0.00	0.00	0.17	0.01	0.39	0.22	0.02	0.00	0.00

Cl	13CNK	Si_23O	Ti_23O	Al_23O	Cr_23O	Ni_23O	FeT_23O	Mn_23O	Mg_23O	Ca_23O	Na_23O	K_23O	F_23O	Cl_23O
0.00	8.70	7.42	0.04	0.66	0.00	0.00	1.53	0.07	3.29	1.88	0.19	0.05	0.00	0.00
0.00	8.73	7.41	0.03	0.63	0.00	0.00	1.52	0.07	3.34	1.88	0.16	0.04	0.00	0.00
0.00	8.69	7.48	0.03	0.57	0.00	0.00	1.50	0.07	3.36	1.89	0.18	0.04	0.00	0.00
0.00	8.58	7.67	0.01	0.40	0.00	0.00	1.41	0.07	3.44	1.89	0.10	0.02	0.00	0.00
0.00	8.69	7.42	0.03	0.64	0.00	0.00	1.50	0.06	3.33	1.88	0.19	0.05	0.00	0.00
0.00	8.78	7.28	0.08	0.86	0.00	0.00	1.61	0.07	3.10	1.86	0.29	0.08	0.00	0.00
0.00	8.82	7.27	0.10	0.96	0.00	0.00	1.73	0.08	2.86	1.85	0.34	0.10	0.00	0.00
0.00	8.73	7.34	0.05	0.73	0.00	0.00	1.55	0.07	3.26	1.88	0.19	0.06	0.00	0.00
0.00	8.73	7.41	0.03	0.63	0.00	0.00	1.52	0.07	3.34	1.88	0.16	0.04	0.00	0.00
0.00	8.73	7.48	0.03	0.56	0.00	0.00	1.47	0.07	3.39	1.92	0.14	0.04	0.00	0.00

Fe3	Fe2	AlIV_23O	AlVI_23O	CaM4_23O	NaA_23O	A_23O	x1v_si_a	x1v_ti_a	x1v_al_a	x1v_cr_a	x1v_ni_a	x1v_fet_a	x1v_mn_a	x1v_mg_a
0.44	1.10	0.58	0.07	0.12	0.07	0.12	0.46	0.00	0.04	0.00	0.00	0.10	0.00	0.21
0.53	0.99	0.59	0.04	0.12	0.04	0.08	0.46	0.00	0.04	0.00	0.00	0.09	0.00	0.21
0.44	1.06	0.52	0.05	0.11	0.06	0.10	0.47	0.00	0.04	0.00	0.00	0.09	0.00	0.21
0.34	1.07	0.33	0.06	0.11	-0.01	0.01	0.48	0.00	0.02	0.00	0.00	0.09	0.00	0.21
0.45	1.06	0.58	0.07	0.12	0.07	0.12	0.46	0.00	0.04	0.00	0.00	0.09	0.00	0.21
0.32	1.28	0.72	0.14	0.14	0.15	0.23	0.46	0.01	0.05	0.00	0.00	0.10	0.00	0.19
0.16	1.57	0.73	0.23	0.15	0.19	0.29	0.45	0.01	0.06	0.00	0.00	0.11	0.00	0.18
0.49	1.06	0.66	0.07	0.12	0.07	0.13	0.46	0.00	0.05	0.00	0.00	0.10	0.00	0.20
0.53	0.99	0.59	0.04	0.12	0.04	0.08	0.46	0.00	0.04	0.00	0.00	0.09	0.00	0.21
0.41	1.06	0.52	0.04	0.08	0.06	0.10	0.47	0.00	0.03	0.00	0.00	0.09	0.00	0.21

x1v_ca_a	x1v_na_a	x1v_k_a	x1v_fe3	x1v_fe2	x1v_aliv	x1v_alvi	x1v_nam	x1v_naa	tk1	tk2	lnDAISi	RTlnDAISi_	RTlnDAISi_	XAIT1
0.12	0.01	0.00	0.03	0.07	0.04	0.00	0.01	0.00	273.15	273.15	1.99	4525.50	4525.50	0.15
0.12	0.01	0.00	0.03	0.06	0.04	0.00	0.01	0.00	273.15	273.15	2.07	4690.15	4690.15	0.15
0.12	0.01	0.00	0.03	0.07	0.03	0.00	0.01	0.00	273.15	273.15	1.50	3399.63	3399.63	0.13
0.12	0.01	0.00	0.02	0.07	0.02	0.00	0.01	0.00	273.15	273.15	1.85	4200.33	4200.33	0.08
0.12	0.01	0.00	0.03	0.07	0.04	0.00	0.01	0.00	273.15	273.15	1.60	3639.87	3639.87	0.14
0.12	0.02	0.01	0.02	0.08	0.04	0.01	0.01	0.01	273.15	273.15	1.11	2519.23	2519.23	0.18
0.12	0.02	0.01	0.01	0.10	0.05	0.01	0.01	0.01	273.15	273.15	2.00	4538.90	4538.90	0.18
0.12	0.01	0.00	0.03	0.07	0.04	0.00	0.01	0.00	273.15	273.15	#iDIV/0!	#iDIV/0!	#iDIV/0!	0.17
0.12	0.01	0.00	0.03	0.06	0.04	0.00	0.01	0.00	273.15	273.15	#iDIV/0!	#iDIV/0!	#iDIV/0!	0.15
0.12	0.01	0.00	0.03	0.07	0.03	0.00	0.01	0.00	273.15	273.15	#iDIV/0!	#iDIV/0!	#iDIV/0!	0.13

Plagioclase

Sample	SiO2	Al2O3	FeO	MnO	MgO	CaO	Na2O	K2O	Total	Si	Al	Fet
NL16-04 pl1	62.09	24.02	0.12	0.00	0.00	4.80	9.04	0.09	100.17	1.03	0.47	0.00
NL16-04 pl2	62.38	23.66	0.15	0.00	0.00	4.53	8.98	0.47	100.16	1.04	0.46	0.00
NL16-04 pl3	62.52	23.74	0.15	0.03	0.00	4.55	9.20	0.25	100.44	1.04	0.47	0.00
NL16-04 pl4	61.58	24.40	0.23	0.00	0.00	5.42	8.47	0.28	100.39	1.03	0.48	0.00
NL16-04 pl5	61.24	23.95	0.17	0.00	0.01	4.92	8.68	0.32	99.28	1.02	0.47	0.00
NL16-04 pl6	60.15	25.48	0.18	0.00	0.00	6.42	7.94	0.15	100.30	1.00	0.50	0.00
NL16-04 pl7	63.70	23.04	0.16	0.06	0.01	3.73	9.58	0.16	100.43	1.06	0.45	0.00
NL16-04 pl8	59.90	25.42	0.22	0.00	0.00	6.44	8.03	0.18	100.19	1.00	0.50	0.00
NL16-04 pl9	62.74	23.14	0.18	0.01	0.01	4.32	9.10	0.31	99.81	1.04	0.45	0.00
NL16-04 pl10	59.99	25.41	0.13	0.00	0.00	6.28	8.27	0.08	100.16	1.00	0.50	0.00

Mn	Mg	Ca	Na	K	factor_80	Si_80	Al_80	FeT_80	Mn_80	Mg_80	Ca_80	Na_80	K_80	Ab
0.00	0.00	0.09	0.29	0.00	2.28	2.36	1.07	0.00	0.00	0.00	0.20	0.67	0.00	0.77
0.00	0.00	0.08	0.29	0.01	2.28	2.37	1.06	0.00	0.00	0.00	0.18	0.66	0.02	0.76
0.00	0.00	0.08	0.30	0.01	2.27	2.37	1.06	0.00	0.00	0.00	0.18	0.68	0.01	0.77
0.00	0.00	0.10	0.27	0.01	2.28	2.34	1.09	0.01	0.00	0.00	0.22	0.62	0.01	0.73
0.00	0.00	0.09	0.28	0.01	2.30	2.34	1.08	0.01	0.00	0.00	0.20	0.64	0.02	0.75
0.00	0.00	0.11	0.26	0.00	2.29	2.29	1.14	0.01	0.00	0.00	0.26	0.59	0.01	0.69
0.00	0.00	0.07	0.31	0.00	2.27	2.41	1.03	0.00	0.00	0.00	0.15	0.70	0.01	0.82
0.00	0.00	0.11	0.26	0.00	2.29	2.28	1.14	0.01	0.00	0.00	0.26	0.59	0.01	0.69
0.00	0.00	0.08	0.29	0.01	2.28	2.38	1.04	0.01	0.00	0.00	0.18	0.67	0.02	0.78
0.00	0.00	0.11	0.27	0.00	2.29	2.29	1.14	0.00	0.00	0.00	0.26	0.61	0.00	0.70

RESULTS

Sample	P(kbar) Plg-amp- bar (at TC=1)	P(kbar) Plg-amp- bar (at TC=2)	Si 230	Ti 230	Al 230	Cr 230	Ni 230	FeT 230	Mn 230	Mg 230	Ca 230	Na 230
NL16-04 anf1	2.61	2.61	7.42	0.04	0.66	0.00	0.00	1.53	0.07	3.29	1.88	0.19
NL16-04 anf2	2.53	2.53	7.41	0.03	0.63	0.00	0.00	1.52	0.07	3.34	1.88	0.16
NL16-04 anf3	2.71	2.71	7.48	0.03	0.57	0.00	0.00	1.50	0.07	3.36	1.89	0.18
NL16-04 anf4	4.49	4.49	7.67	0.01	0.40	0.00	0.00	1.41	0.07	3.44	1.89	0.10
NL16-04 anf5	3.13	3.13	7.42	0.03	0.64	0.00	0.00	1.50	0.06	3.33	1.88	0.19
NL16-04 anf6	3.67	3.67	7.28	0.08	0.86	0.00	0.00	1.61	0.07	3.10	1.86	0.29
NL16-04 anf7	2.16	2.16	7.27	0.10	0.96	0.00	0.00	1.73	0.08	2.86	1.85	0.34
NL16-04 anf8	3.48	3.48	7.34	0.05	0.73	0.00	0.00	1.55	0.07	3.26	1.88	0.19
NL16-04 anf9	2.29	2.29	7.41	0.03	0.63	0.00	0.00	1.52	0.07	3.34	1.88	0.16
NL16-04 anf10	3.69	3.69	7.48	0.03	0.56	0.00	0.00	1.47	0.07	3.39	1.92	0.14

K 230	F 230	Cl 230	Fe3 230	Fe2 230	AlIV 230	AlVI 230	CaM4 230	NaA 230	A 230
0.05	0.00	0.00	0.44	1.10	0.58	0.07	0.12	0.07	0.12
0.04	0.00	0.00	0.53	0.99	0.59	0.04	0.12	0.04	0.08
0.04	0.00	0.00	0.44	1.06	0.52	0.05	0.11	0.06	0.10
0.02	0.00	0.00	0.34	1.07	0.33	0.06	0.11	-0.01	0.01
0.05	0.00	0.00	0.45	1.06	0.58	0.07	0.12	0.07	0.12
0.08	0.00	0.00	0.32	1.28	0.72	0.14	0.14	0.15	0.23
0.10	0.00	0.00	0.16	1.57	0.73	0.23	0.15	0.19	0.29
0.06	0.00	0.00	0.49	1.06	0.66	0.07	0.12	0.07	0.13
0.04	0.00	0.00	0.53	0.99	0.59	0.04	0.12	0.04	0.08
0.04	0.00	0.00	0.41	1.06	0.52	0.04	0.08	0.06	0.10

Pressure range	3.08	3.08
Std. Deviation	0.75	0.75

Supplementary file . Mineral Structural Formulae Amphibole

Sample L1 from Cerro ID til

Oxygens in mineral formula basis

23

Oxide Formula weights (g mol)

SiO ₂	TiO ₂	Al ₂ O ₃	Cr ₂ O ₃	FeO	MgO	CaO	MnO	Na ₂ O	K ₂ O	F	Cl	Fe ₂ O ₃	H ₂ O
60.08	79.87	101.96		71.84	40.30	56.08	70.94	61.98	94.20	19.00	35.45	159.7	18.02

Oxide t

Sample Analysis	Sample Name	SiO ₂	TiO ₂	Al ₂ O ₃	Cr ₂ O ₃	FeO	MgO	CaO	MnO	Na ₂ O	K ₂ O	F	Cl	Total
1	NL16-04	51.22	0.34	3.84	0.00	12.66	15.23	12.12	0.57	0.67	0.27	0.00	0.00	96.93
2	NL16-04	51.00	0.24	3.67	0.00	12.50	15.42	12.08	0.60	0.56	0.23	0.00	0.00	96.31
3	NL16-04	51.68	0.24	3.37	0.00	12.38	15.58	12.16	0.54	0.63	0.20	0.00	0.00	96.78
4	NL16-04	53.71	0.13	2.36	0.00	11.84	16.14	12.34	0.60	0.37	0.13	0.00	0.00	97.62
5	NL16-04	51.31	0.31	3.77	0.01	12.41	15.44	12.10	0.52	0.69	0.26	0.00	0.00	96.82
6	NL16-04	49.83	0.74	4.99	0.00	13.17	14.22	11.89	0.59	1.02	0.43	0.00	0.00	96.88
7	NL16-04	49.56	0.90	5.55	0.01	14.06	13.08	11.74	0.63	1.20	0.54	0.00	0.00	97.25
8	NL16-04	50.49	0.42	4.29	0.01	12.74	15.05	12.06	0.57	0.67	0.32	0.00	0.00	96.64
9	NL16-04	51.00	0.24	3.67	0.00	12.50	15.42	12.08	0.60	0.56	0.23	0.00	0.00	96.31
10	NL16-04	51.49	0.23	3.24	0.00	12.11	15.67	12.31	0.58	0.51	0.21	0.00	0.00	96.35

Amphibole Formula

Tetrahedral site				M1 M2 M3 sites							M4 site			A site				
Si	Al(IV)	Ti(IV)	Total	Al(VI)	Ti	Cr	Fe3	Mg	Fe2	Mn	Total	Fe2	Ca	Na	Total	Na	K	Total
7.417	0.583	0.000	8.000	0.072	0.037	0.000	0.437	3.288	1.096	0.070	5.000	0.000	1.881	0.119	2.000	0.070	0.050	0.120
7.411	0.589	0.000	8.000	0.040	0.027	0.000	0.532	3.341	0.986	0.074	5.000	0.000	1.881	0.119	2.000	0.040	0.042	0.082
7.476	0.524	0.000	8.000	0.050	0.026	0.000	0.439	3.361	1.059	0.066	5.000	0.000	1.885	0.115	2.000	0.061	0.038	0.099
7.667	0.333	0.000	8.000	0.064	0.014	0.001	0.339	3.435	1.074	0.073	5.000	0.000	1.888	0.102	1.990	0.000	0.024	0.024
7.425	0.575	0.000	8.000	0.069	0.034	0.001	0.445	3.331	1.056	0.064	5.000	0.000	1.876	0.124	2.000	0.069	0.048	0.116
7.280	0.720	0.000	8.000	0.140	0.081	0.000	0.325	3.097	1.284	0.073	5.000	0.000	1.862	0.138	2.000	0.150	0.080	0.230
7.274	0.726	0.000	8.000	0.234	0.099	0.001	0.159	2.862	1.567	0.078	5.000	0.000	1.846	0.154	2.000	0.187	0.101	0.288
7.338	0.662	0.000	8.000	0.072	0.046	0.001	0.489	3.261	1.059	0.071	5.000	0.000	1.878	0.122	2.000	0.068	0.060	0.128
7.411	0.589	0.000	8.000	0.040	0.027	0.000	0.532	3.341	0.986	0.074	5.000	0.000	1.881	0.119	2.000	0.040	0.042	0.082
7.482	0.518	0.000	8.000	0.037	0.025	0.000	0.414	3.394	1.057	0.072	5.000	0.000	1.916	0.084	2.000	0.060	0.039	0.099

Sample 1 from Cerro Ra n

Oxide t

Sample Analysis	Sample Name	SiO2	TiO2	Al2O3	Cr2O3	FeO	MgO	CaO	MnO	Na2O	K2O	F	Cl	Total
1	AB16-53A	55.02	0.03	1.31	0.00	7.59	18.74	12.86	0.55	0.33	0.04	0.00	0.00	96.45
2	AB16-53A	55.53	0.04	1.16	0.00	7.43	18.92	12.92	0.54	0.29	0.06	0.00	0.00	96.87
3	AB16-53A	55.35	0.04	0.86	0.00	7.94	18.76	12.43	0.65	0.43	0.05	0.00	0.00	96.50
4	AB16-53A	55.96	0.05	0.74	0.00	7.13	19.20	12.75	0.65	0.24	0.03	0.00	0.00	96.75
5	AB16-53A	56.00	0.15	1.04	0.00	7.94	18.44	12.49	0.64	0.47	0.10	0.00	0.00	97.28
6	AB16-53A	54.85	0.02	1.67	0.00	8.07	18.51	12.75	0.51	0.36	0.08	0.00	0.00	96.82
7	AB16-53A	55.58	0.09	0.76	0.00	7.65	18.87	12.73	0.57	0.30	0.03	0.00	0.00	96.57
8	AB16-53A	55.27	0.11	0.98	0.00	7.61	18.72	12.71	0.61	0.36	0.05	0.00	0.00	96.43
9	AB16-53A	55.29	0.09	1.25	0.00	8.42	18.75	12.44	0.53	0.33	0.07	0.00	0.00	97.17
10	AB16-53A	52.98	0.08	2.57	0.00	11.66	15.91	12.67	0.23	0.37	0.11	0.00	0.00	96.56

Amphibole Formula

Tetrahedral site				M1 M2 M3 sites							M4 site				A site			
Si	Al(IV)	Ti(IV)	Total	Al(VI)	Ti	Cr	Fe3	Mg	Fe2	Mn	Total	Fe2	Ca	Na	Total	Na	K	Total
7.832	0.168	0.000	8.000	0.051	0.003	0.000	0.089	3.976	0.814	0.066	5.000	0.000	1.962	0.038	2.000	0.052	0.007	0.059
7.864	0.136	0.000	8.000	0.057	0.004	0.000	0.061	3.995	0.819	0.065	5.000	0.000	1.960	0.040	2.000	0.040	0.010	0.050
7.860	0.140	0.000	8.000	0.004	0.004	0.000	0.216	3.971	0.726	0.078	5.000	0.000	1.892	0.108	2.000	0.010	0.010	0.020
7.907	0.093	0.000	8.000	0.030	0.005	0.000	0.118	4.045	0.724	0.078	5.000	0.000	1.931	0.067	1.997	0.000	0.006	0.006
7.912	0.088	0.000	8.000	0.085	0.016	0.000	0.044	3.883	0.895	0.077	5.000	0.000	1.891	0.109	2.000	0.019	0.017	0.037
7.783	0.217	0.000	8.000	0.062	0.002	0.000	0.160	3.915	0.798	0.062	5.000	0.000	1.938	0.062	2.000	0.037	0.014	0.052
7.892	0.108	0.000	8.000	0.020	0.009	0.000	0.109	3.994	0.799	0.069	5.000	0.000	1.937	0.063	2.000	0.019	0.005	0.024
7.870	0.130	0.000	8.000	0.034	0.012	0.000	0.085	3.974	0.821	0.073	5.000	0.000	1.939	0.061	2.000	0.039	0.009	0.048
7.790	0.207	0.003	8.000	0.000	0.007	0.000	0.334	3.938	0.658	0.064	5.000	0.000	1.878	0.090	1.969	0.000	0.012	0.012
7.676	0.324	0.000	8.000	0.115	0.009	0.000	0.133	3.436	1.279	0.028	5.000	0.000	1.967	0.033	2.000	0.070	0.020	0.090

Sample 11 from Cerro Calaveras

Oxide t

Sample Analysis	Sample Name	SiO2	TiO2	Al2O3	Cr2O3	FeO	MgO	CaO	MnO	Na2O	K2O	F	Cl	Total
1	AB11-46	51.11	0.09	3.60		12.61	14.81	12.43	0.15	0.49	0.12	0.00	0.00	95.42
2	AB11-46	52.12	0.35	2.58		12.92	14.70	12.43	0.25	0.47	0.11	0.00	0.00	95.92
3	AB11-46	53.28	0.04	1.95		11.38	16.01	12.56	0.20	0.29	0.06	0.00	0.00	95.77
4	AB11-46	51.57	0.02	3.46		12.13	15.29	12.45	0.14	0.49	0.10	0.00	0.00	95.64
5	AB11-46	51.21	0.05	3.39		12.69	14.90	12.45	0.16	0.45	0.11	0.00	0.00	95.40
6	AB11-46	53.22	0.31	2.00		10.28	16.78	12.02	0.16	0.39	0.57	0.00	0.00	95.73
7	AB11-46	52.81	0.03	2.29		11.54	15.77	12.52	0.16	0.38	0.08	0.00	0.00	95.59
8	AB11-46	52.98	0.08	2.57		11.66	15.91	12.67	0.23	0.37	0.11	0.00	0.00	96.56
9	AB11-46	52.23	0.08	2.63		11.21	15.89	12.41	0.15	0.39	0.08	0.00	0.00	95.08

Amphibole Formula

Tetrahedral site				M1 M2 M3 sites							M4 site			A site				
Si	Al(IV)	Ti(IV)	Total	Al(VI)	Ti	Cr	Fe3	Mg	Fe2	Mn	Total	Fe2	Ca	Na	Total	Na	K	Total
7.534998	0.465002	0	8	0.161	0.01	0	0.194	3.255	1.361	0.019	5	0	1.964	0.036	2	0.105	0.022	0.127
7.669	0.331	0.000	8.000	0.117	0.038	0.000	0.063	3.224	1.527	0.031	5.000	0.000	1.960	0.040	2.000	0.095	0.020	0.115
7.768	0.232	0.000	8.000	0.103	0.004	0.000	0.105	3.480	1.283	0.024	5.000	0.000	1.962	0.038	2.000	0.043	0.011	0.054
7.557	0.443	0.000	8.000	0.155	0.002	0.000	0.219	3.339	1.267	0.017	5.000	0.000	1.954	0.046	2.000	0.093	0.018	0.111
7.549	0.451	0.000	8.000	0.137	0.005	0.000	0.222	3.274	1.342	0.019	5.000	0.000	1.966	0.034	2.000	0.094	0.021	0.115
7.724	0.276	0.000	8.000	0.066	0.034	0.000	0.191	3.632	1.057	0.019	5.000	0.000	1.869	0.109	1.977	0.000	0.105	0.105
7.729	0.271	0.000	8.000	0.123	0.004	0.000	0.091	3.441	1.321	0.020	5.000	0.000	1.964	0.036	2.000	0.070	0.015	0.086
7.676	0.324	0.000	8.000	0.115	0.009	0.000	0.133	3.436	1.279	0.028	5.000	0.000	1.967	0.033	2.000	0.070	0.020	0.090
7.666	0.334	0.000	8.000	0.121	0.008	0.000	0.166	3.476	1.210	0.019	5.000	0.000	1.951	0.049	2.000	0.063	0.016	0.079

Sample 1 from Cerro Los paches

Oxide t

Analysis	Sample Name	SiO2	TiO2	Al2O3	Cr2O3	FeO	MgO	CaO	MnO	Na2O	K2O	F	Cl	Total
1	AB15-20	55.57	0.04	1.09	0.00	6.47	19.58	12.89	0.29	0.30	0.03	0.00	0.00	96.26
2	AB15-20	55.91	0.01	0.94	0.00	6.12	19.91	13.05	0.24	0.25	0.03	0.00	0.00	96.47
3	AB15-20	56.11	0.03	1.14	0.00	6.51	19.94	12.67	0.28	0.24	0.04	0.00	0.00	96.98
4	AB15-20	56.15	0.11	0.90	0.00	5.97	20.05	13.03	0.22	0.24	0.03	0.00	0.00	96.71
5	AB15-20	55.87	0.04	1.10	0.00	6.69	19.43	12.86	0.31	0.29	0.05	0.00	0.00	96.66
6	AB15-20	54.45	0.03	1.59	0.00	7.19	19.13	12.82	0.28	0.31	0.04	0.00	0.00	95.83
7	AB15-20	55.48	0.07	1.10	0.00	6.61	19.74	12.85	0.29	0.28	0.04	0.00	0.00	96.46
8	AB15-20	55.21	0.04	1.58	0.00	7.26	18.85	12.84	0.33	0.35	0.04	0.00	0.00	96.50
9	AB15-20	54.94	0.01	1.40	0.00	7.46	18.97	12.75	0.31	0.31	0.06	0.00	0.00	96.22
10	AB15-20	54.91	0.02	1.39	0.00	6.85	19.31	12.82	0.28	0.30	0.04	0.00	0.00	95.90

Amphibole Formula

Tetrahedral site				M1 M2 M3 sites							M4 site				A site			
Si	Al(IV)	Ti(IV)	Total	Al(VI)	Ti	Cr	Fe3	Mg	Fe2	Mn	Total	Fe2	Ca	Na	Total	Na	K	Total
7.876	0.124	0.000	8.000	0.057	0.004	0.000	0.054	4.136	0.714	0.035	5.000	0.000	1.958	0.042	2.000	0.041	0.006	0.047
7.898	0.102	0.000	8.000	0.054	0.001	0.000	0.020	4.193	0.703	0.029	5.000	0.000	1.975	0.025	2.000	0.044	0.006	0.050
7.853	0.147	0.000	8.000	0.041	0.003	0.000	0.225	4.160	0.537	0.033	5.000	0.000	1.901	0.065	1.966	0.000	0.008	0.008
7.903	0.097	0.000	8.000	0.052	0.011	0.000	0.018	4.207	0.685	0.027	5.000	0.000	1.966	0.034	2.000	0.032	0.006	0.038
7.893	0.107	0.000	8.000	0.076	0.004	0.000	0.039	4.092	0.751	0.038	5.000	0.000	1.947	0.053	2.000	0.028	0.009	0.037
7.768	0.232	0.000	8.000	0.036	0.003	0.000	0.178	4.068	0.680	0.034	5.000	0.000	1.959	0.041	2.000	0.046	0.006	0.052
7.837	0.163	0.000	8.000	0.021	0.007	0.000	0.154	4.157	0.627	0.035	5.000	0.000	1.945	0.055	2.000	0.022	0.007	0.030
7.840	0.160	0.000	8.000	0.104	0.004	0.000	0.038	3.990	0.824	0.040	5.000	0.000	1.953	0.047	2.000	0.049	0.008	0.057
7.816	0.184	0.000	8.000	0.050	0.001	0.000	0.148	4.022	0.739	0.038	5.000	0.000	1.943	0.057	2.000	0.029	0.010	0.039
7.818	0.182	0.000	8.000	0.050	0.002	0.000	0.127	4.099	0.688	0.033	5.000	0.000	1.955	0.045	2.000	0.038	0.007	0.044

Sample 1 from Cerros de la Ci nega

Oxide

Sample Analysis	Sample Name	SiO2	TiO2	Al2O3	Cr2O3	FeO	MgO	CaO	MnO	Na2O	K2O	F	Cl	Total
1	AB16-24	53.23	0.07	2.60	0.00	10.28	16.73	12.70	0.41	0.35	0.08	0.00	0.00	96.45
2	AB16-24	52.47	0.02	3.21	0.00	11.90	15.96	12.52	0.46	0.45	0.16	0.00	0.00	97.16
3	AB16-24	52.29	0.04	2.88	0.00	10.81	15.92	12.61	0.51	0.38	0.10	0.00	0.00	95.54
4	AB16-24	53.71	0.03	2.21	0.00	11.42	16.25	12.53	0.49	0.36	0.06	0.00	0.00	97.07
5	AB16-24	54.22	0.04	1.92	0.00	10.07	17.19	12.73	0.47	0.29	0.05	0.00	0.00	96.99
6	AB16-24	53.73	0.04	2.18	0.00	10.71	16.50	12.79	0.47	0.33	0.09	0.00	0.00	96.84
7	AB16-24	54.95	0.05	1.40	0.00	10.99	16.46	12.74	0.52	0.23	0.06	0.00	0.00	97.41
8	AB16-24	53.66	0.04	2.20	0.00	10.70	16.50	12.73	0.50	0.29	0.09	0.00	0.00	96.71
9	AB16-24	54.00	0.02	2.07	0.00	10.20	16.91	12.64	0.49	0.28	0.07	0.00	0.00	96.67
10	AB16-24	52.48	0.04	3.55	0.00	11.30	16.07	12.46	0.51	0.43	0.10	0.00	0.00	96.95

Amphibole Formula

Tetrahedral site				M1 M2 M3 sites							M4 site			A site				
Si	Al(IV)	Ti(IV)	Total	Al(VI)	Ti	Cr	Fe3	Mg	Fe2	Mn	Total	Fe2	Ca	Na	Total	Na	K	Total
7.669	0.331	0.000	8.000	0.110	0.007	0.000	0.172	3.594	1.066	0.051	5.000	0.000	1.961	0.039	2.000	0.059	0.015	0.074
7.545	0.455	0.000	8.000	0.089	0.002	0.000	0.347	3.421	1.084	0.056	5.000	0.000	1.929	0.071	2.000	0.055	0.029	0.084
7.645	0.355	0.000	8.000	0.140	0.004	0.000	0.128	3.470	1.194	0.063	5.000	0.000	1.976	0.024	2.000	0.085	0.018	0.103
7.712	0.288	0.000	8.000	0.086	0.003	0.000	0.228	3.479	1.144	0.060	5.000	0.000	1.928	0.072	2.000	0.029	0.010	0.039
7.749	0.251	0.000	8.000	0.072	0.005	0.000	0.181	3.663	1.022	0.057	5.000	0.000	1.950	0.050	2.000	0.029	0.010	0.038
7.737	0.263	0.000	8.000	0.107	0.004	0.000	0.093	3.542	1.197	0.057	5.000	0.000	1.973	0.027	2.000	0.066	0.016	0.082
7.865	0.135	0.000	8.000	0.101	0.006	0.000	0.040	3.513	1.277	0.064	5.000	0.000	1.955	0.045	2.000	0.017	0.010	0.028
7.729	0.271	0.000	8.000	0.103	0.004	0.000	0.133	3.543	1.156	0.061	5.000	0.000	1.965	0.035	2.000	0.046	0.016	0.063
7.747	0.253	0.000	8.000	0.097	0.003	0.000	0.176	3.617	1.048	0.059	5.000	0.000	1.943	0.057	2.000	0.019	0.013	0.032
7.535	0.465	0.000	8.000	0.136	0.005	0.000	0.347	3.441	1.009	0.062	5.000	0.000	1.917	0.083	2.000	0.038	0.018	0.056

Supplementary file . Mineral Structural Formulae Plagioclase

Sample L1 from Cerro ID til

O ygens in mineral formula asis

8

	1	2	3	4	5	6	7	8	9	10
SiO2	62.09076	62.525	61.584	61.237	60.149	63.695	59.898	62.735	59.986	
Al2O3	24.0244	23.74	24.402	23.948	25.476	23.037	25.423	23.142	25.413	
FeOt	0.119441	0.15	0.15	0.23	0.17	0.18	0.16	0.22	0.18	0.13
MnO	0.000013	0.00	0.03	0.00	0.00	0.00	0.06	0.00	0.01	0.00
MgO	0.000017	0.00	0.00	0.00	0.01	0.00	0.01	0.00	0.01	0.00
CaO	4.804574	4.53	4.55	5.42	4.92	6.42	3.73	6.44	4.32	6.28
Na2O	9.043498	8.98	9.20	8.47	8.68	7.94	9.58	8.03	9.10	8.27
K2O	0.089554	0.47	0.25	0.28	0.32	0.15	0.16	0.18	0.31	0.08
TiO2	0.002779	0.00	0.01	0.01	0.00	0.00	0.02	0.01	0.00	0.01
Total	100.175	100.16	100.45	100.40	99.29	100.30	100.45	100.20	99.81	100.17

Si	2.748512	2.76	2.76	2.73	2.74	2.67	2.80	2.67	2.79	2.67
Al	1.253256	1.2352	1.2357	1.273	1.2623	1.3333	1.1951	1.3335	1.2108	1.3324
Fet	0.004422	0.0055	0.0056	0.0086	0.0065	0.0065	0.0058	0.0081	0.0065	0.0047
Mn	4.87E-07	5E-07	0.001	5E-07	5E-07	5E-07	0.0023	5E-07	0.0002	5E-07
Mg	0	0.00	0.00	0.00	0.00	1E-06	0.0008	1E-06	0.0005	0.0001
Ca	0	0.22	0.22	0.26	0.24	0.3053	0.1758	0.307	0.2056	0.2994
Na	1	0.77	0.79	0.73	0.75	0.6834	0.8177	0.6933	0.7837	0.7134
K	0	0.03	0.01	0.02	0.02	0.0084	0.009	0.0101	0.0177	0.0046
Ti	0	0.00	0.00	0.00	0.00	6E-07	0.0007	0.0005	6E-07	0.0004
Total	5	5.02	5.02	5.01	5.02	5.0081	5.0111	5.0184	5.0101	5.0237

An	23	21.23	21.16	25.72	23.41	30.621	17.538	30.384	20.415	29.431
A	77	76.14	77.45	72.69	74.76	68.539	81.569	68.62	77.825	70.115
Or	1	2.63	1.39	1.59	1.83	0.8396	0.8928	0.9954	1.7603	0.4541

	For diagram									
	11.79183	13.24	11.97	14.45	13.53	16.15	9.66	16.19	11.97	15.17
Y	19.55606	18.39	18.32	22.27	20.27	26.52	15.19	26.31	17.68	25.49

Sample 1 from Cerro Ra n

	1	2	3	4	5	6	7	8	9	10
SiO2	65.92683	.	65.518	68.193	67.001	67.978	67.374	68.156	67.486	67.075
Al2O3	19.66294	20.154	19.447	19.906	20.398	20.099	19.944	19.963	20.14	20.061
FeOt	1.019169	0.28	0.96	0.22	0.37	0.36	0.64	0.25	0.28	0.54
MnO	0.027419	0.02	0.02	0.01	0.00	0.01	0.04	0.00	0.00	0.00
MgO	1.463781	0.02	1.85	0.12	0.36	0.01	0.34	0.03	0.01	0.64
CaO	0.285072	0.15	0.10	0.10	0.74	0.15	0.16	0.11	0.20	0.11
Na2O	10.73414	11.96	11.22	11.72	11.33	11.89	11.83	12.15	11.63	11.88
K2O	0.344376	0.06	0.15	0.11	0.38	0.16	0.11	0.08	0.09	0.08
TiO2	0.037779	0.03	0.02	0.04	0.04	0.01	0.04	0.00	0.11	0.02
Total	99.50151	100.73	99.28	100.42	100.62	100.68	100.48	100.74	99.95	100.40

Si	2.919424	2.96	2.91	2.97	2.93	2.96	2.95	2.97	2.96	2.94
Al	1.026124	1.0334	1.018	1.0225	1.0509	1.0319	1.0283	1.024	1.0402	1.035
Fet	0.037743	0.0102	0.0358	0.0079	0.0136	0.0132	0.0234	0.0092	0.0104	0.0196
Mn	0.001028	0.0009	0.0007	0.0005	5E-07	0.0003	0.0014	5E-07	5E-07	5E-05
Mg	0	0.00	0.12	0.01	0.02	0.0007	0.0223	0.0018	0.0004	0.0419
Ca	0	0.01	0.00	0.00	0.03	0.0071	0.0073	0.005	0.0095	0.0053
Na	1	1.01	0.97	0.99	0.96	1.0046	1.0036	1.0255	0.988	1.0083
K	0	0.00	0.01	0.01	0.02	0.0091	0.006	0.0043	0.0052	0.0043
Ti	0	0.00	0.00	0.00	0.00	0.0002	0.0015	0.0001	0.0036	0.0005
Total	5	5.03	5.07	5.01	5.03	5.029	5.0415	5.0363	5.0151	5.0517

An	1	0.71	0.47	0.45	3.43	0.6985	0.7204	0.4834	0.946	0.523
A	97	98.99	98.67	98.94	94.50	98.405	98.69	99.103	98.536	99.053
Or	2	0.30	0.86	0.61	2.07	0.8961	0.5895	0.4134	0.5185	0.424

	For diagram									
	2.746287	0.66	1.10	0.83	3.78	1.25	0.95	0.66	0.99	0.69
Y	1.227033	0.61	0.41	0.39	2.97	0.60	0.62	0.42	0.82	0.45

Sample 11 from Cerro Caleras

	1	2	3	4	5	6	7	8	9	10
SiO2	66.72423	1.	67.728	67.611	67.46	67.228	67.489	67.823	67.633	67.075
Al2O3	20.03059	20.2	20.312	20.29	20.365	20.449	20.387	20.179	20.205	20.061
FeOt	0.578308	3.11	0.23	0.19	0.26	0.37	0.25	0.25	0.22	0.54
MnO	0.000013	0.05	0.01	0.00	0.02	0.00	0.00	0.03	0.01	0.00
MgO	0.264263	3.01	0.03	0.06	0.00	0.09	0.02	0.00	0.01	0.64
CaO	0.712439	0.70	0.33	0.44	0.53	0.63	0.44	0.49	0.40	0.11
Na2O	11.2309	10.04	11.70	11.76	11.69	11.76	11.58	11.72	11.73	11.88
K2O	0.428794	1.21	0.09	0.10	0.11	0.10	0.21	0.20	0.17	0.08
TiO2	0.059252	0.14	0.02	0.02	0.01	0.05	0.05	0.04	0.07	0.02
Total	100.0288	100.22	100.46	100.47	100.43	100.67	100.44	100.73	100.44	100.40

Si	2.937006	2.78	2.95	2.95	2.95	2.93	2.95	2.95	2.95	2.94
Al	1.039038	1.071	1.0442	1.0436	1.0484	1.052	1.0493	1.036	1.0398	1.035
Fet	0.021288	0.1171	0.0085	0.0068	0.0094	0.0136	0.009	0.0091	0.0079	0.0196
Mn	4.85E-07	0.0021	0.0004	5E-07	0.0007	0.0001	0.0002	0.0009	0.0004	5E-05
Mg	0	0.20	0.00	0.00	0.00	0.0056	0.0015	1E-06	0.0003	0.0419
Ca	0	0.03	0.02	0.02	0.02	0.0294	0.0208	0.0229	0.0187	0.0053
Na	1	0.88	0.99	1.00	0.99	0.9954	0.9807	0.9903	0.9936	1.0083
K	0	0.07	0.01	0.01	0.01	0.0054	0.0117	0.011	0.0094	0.0043
Ti	0	0.00	0.00	0.00	0.00	0.0016	0.0016	0.0014	0.0022	0.0005
Total	5	5.15	5.02	5.03	5.03	5.0379	5.0224	5.0265	5.0258	5.0517

An	3	3.44	1.53	2.03	2.42	2.8548	2.0525	2.2395	1.832	0.523
A	94	89.46	97.95	97.43	96.98	96.624	96.794	96.685	97.248	99.053
Or	2	7.09	0.51	0.53	0.60	0.5208	1.1534	1.0755	0.92	0.424

	For diagram									
	4.022609	8.82	1.28	1.55	1.81	1.95	2.18	2.20	1.84	0.69
Y	2.863479	2.98	1.33	1.76	2.09	2.47	1.78	1.94	1.59	0.45

Sample 1 from Cerro Los paches

	1	2	3	4	5	6	7	8	9	10
SiO2	68.25069	.	69.042	67.672	67.22	67.827	68.142	67.753	67.793	68.189
Al2O3	20.13326	19.678	19.937	19.821	19.878	19.733	19.931	20.105	20.024	20.06
FeOt	0.26995	0.38	0.17	0.66	0.75	0.18	0.21	0.10	0.20	0.31
MnO	0.020816	0.04	0.01	0.01	0.00	0.00	0.00	0.00	0.00	0.00
MgO	0.008921	0.50	0.02	0.11	0.25	0.01	0.02	0.01	0.00	0.02
CaO	0.092093	0.66	0.06	0.13	0.16	0.54	0.12	0.07	0.14	0.12
Na2O	11.66871	11.39	12.11	11.72	11.76	12.06	11.70	11.72	11.55	11.67
K2O	0.065043	0.35	0.06	0.08	0.11	0.10	0.07	0.07	0.05	0.08
TiO2	0.046241	0.05	0.03	0.05	0.07	0.03	0.05	0.00	0.03	0.01
Total	100.5557	100.68	101.44	100.25	100.21	100.49	100.26	99.83	99.79	100.47

Si	2.969529	2.95	2.98	2.96	2.95	2.96	2.97	2.97	2.97	2.97
Al	1.032312	1.0127	1.0138	1.0226	1.0278	1.0161	1.0249	1.0379	1.034	1.0298
Fet	0.009822	0.0138	0.0061	0.0242	0.0277	0.0066	0.0077	0.0037	0.0075	0.0113
Mn	0.000767	0.0014	0.0002	0.0005	5E-07	5E-07	5E-07	5E-07	5E-07	5E-07
Mg	0	0.03	0.00	0.01	0.02	0.0008	0.0014	0.0004	1E-06	0.0014
Ca	0	0.03	0.00	0.01	0.01	0.0253	0.0058	0.0033	0.0067	0.0058
Na	1	0.96	1.01	0.99	1.00	1.0217	0.9901	0.9953	0.9809	0.9856
K	0	0.02	0.00	0.00	0.01	0.0057	0.0038	0.004	0.0031	0.0047
Ti	0	0.00	0.00	0.00	0.00	0.0011	0.0018	6E-07	0.0009	0.0003
Total	5	5.03	5.02	5.02	5.04	5.041	5.0092	5.0127	5.0035	5.0094

An	0	3.05	0.29	0.61	0.76	2.406	0.5842	0.3338	0.6728	0.5793
A	99	95.02	99.38	98.94	98.65	97.05	99.036	99.269	99.017	98.952
Or	0	1.92	0.33	0.45	0.59	0.5436	0.3793	0.3972	0.31	0.4684

	For diagram									
	0.580142	3.45	0.48	0.76	0.97	1.75	0.67	0.56	0.65	0.76
Y	0.374687	2.64	0.25	0.53	0.65	2.08	0.51	0.29	0.58	0.50

Sample 1 from Cerros de la Ci nega

	1	2	3	4	5	6	7
SiO2	67.23629	.1	65.39	66.011	67.145	67.487	67.489
Al2O3	20.33766	20.316	20.289	20.079	20.383	20.51	20.337
FeOt	0.321405	0.65	1.10	0.51	0.30	0.23	0.30
MnO	0.000013	0.01	0.00	0.01	0.00	0.00	0.00
MgO	0.148911	0.40	1.07	0.16	0.03	0.03	0.11
CaO	0.560249	0.42	0.58	0.73	0.74	0.65	0.51
Na2O	11.21377	11.54	10.80	9.40	11.33	11.14	11.06
K2O	0.470953	0.31	0.89	3.50	0.24	0.09	0.48
TiO2	0.108388	0.12	0.11	0.20	0.07	0.06	0.07
Total	100.3976	100.95	100.24	100.60	100.23	100.21	100.35

Si	2.941721	2.93	2.89	2.92	2.94	2.95	2.95
Al	1.048613	1.0441	1.0568	1.0481	1.0521	1.0559	1.0477
Fet	0.01176	0.0238	0.0407	0.0189	0.0108	0.0086	0.0108
Mn	4.82E-07	0.0002	0.0002	0.0004	5E-07	5E-07	5E-07
Mg	0	0.03	0.07	0.01	0.00	0.002	0.0072
Ca	0	0.02	0.03	0.03	0.03	0.0305	0.0237
Na	1	0.98	0.93	0.81	0.96	0.9437	0.9373
K	0	0.02	0.05	0.20	0.01	0.0052	0.0268
Ti	0	0.00	0.00	0.01	0.00	0.002	0.0023
Total	5	5.04	5.07	5.05	5.02	4.9961	5.0059

An	3	1.92	2.75	3.34	3.45	3.1138	2.3955
A	95	96.35	92.24	77.63	95.22	96.359	94.887
Or	3	1.73	5.02	19.03	1.34	0.5269	2.7177

	For diagram						
	3.926643	2.69	6.39	20.70	3.06	2.08	3.92
Y	2.265773	1.66	2.38	2.89	2.99	2.70	2.07

Table 1. U-Th analytical data for MS spot analyses on zircon grains for granodiorite sample from ID til, northwestern Sonora, Mexico.

Sample	Zircon U ^{ppm}	Th ^{ppm}	Th/U	CORRECTED ISOTOPIC RATIOS								Rho	CORRECTED AGES (Ma)				Best Age (Ma) ± 2s
				²⁰⁷ Pb/ ²⁰⁶ Pb	err %	²⁰⁷ Pb/ ²³⁵ U	err %	²⁰⁶ Pb/ ²³⁸ U	err %	²⁰⁸ Pb/ ²³² Th	err %		²⁰⁶ Pb/ ²³⁸ U ± 2s	²⁰⁷ Pb/ ²³⁵ U ± 2s	²⁰⁷ Pb/ ²⁰⁶ Pb ± 2s	²⁰⁸ Pb/ ²³² Th ± 2s	
Sample NL16-04(e)	Granodiorite (erro 1D til, northwestern Sonora, Mexico) Mount -11 (November 01)																
16-0 e-19	6	0	0.0	0.0000	10.0	0.0	0.0	0.010	0.000	0.1	0.6	6.1	1.1	6.6	1.0	1.0	6.1
16-0 e-23	1	1	0.0	0.0160	1.0	0.0	0.1	0.010	0.000	1.1	0.0	6.1	1.1	6.1	1.0	0.0	69.2 ± 1.9
16-0 e-6			0.0	0.000	11.0	0.0	0.160	0.010	0.000	1.1	0.0	6.1	1.6	6.1	0.0	0.0	69.7 ± 1.6
16-0 e-20		0	0.0	0.000	11.6	0.0	0.00	0.010	0.6	0.0	1.1	0.0	1.1	0.0	0.0	0.0	70.0 ± 1.8
16-0 e-30		16	0.0	0.061	0.11	0.0	0.110	0.010	1.1	0.0	1.1	0.1	0.0	1.6	1.1	10.0	70.0 ± 1.6
16-0 e-10		0	0.66	0.000	11.0	0.0	0.00	0.01101	0.6	0.0	6.1	0.6	1.1	0.0	1.0	0.0	70.6 ± 1.8
16-0 e-22		1	0.1	0.000	1.1	0.06	0.1	0.0110	0.000	1.1	0.1	0.6	1.1	6.1	-160	0.0	0.6
16-0 e-18	1	1	0.6	0.060	1.1	0.0	0.060	0.0110	0.000	1.1	0.0	1.6	1.1	6.1	0.6	0.0	70.8 ± 2.2
16-0 e-24	01	1	0.0	0.000	11.0	0.0	0.60	0.0110	0.000	1.0	0.0	0.0	0.0	0.0	0.60	0.0	70.8 ± 2.3
16-0 e-3			0.0	0.000	10.0	0.0	0.0	0.0110	0.000	6.1	0.0	1.1	1.6	0.0	0.60	0.0	71.1 ± 1.6
16-0 e-4		6	0.0	0.060	1.6	0.0	0.10	0.0110	0.000	6.1	0.1	1.1	0.0	0.0	110	0.0	71.1 ± 2.0
16-0 e-15		6	0.0	0.060	0.0	0.0	1.0	0.0110	0.000	0.1	0.0	1.1	1.1	0.0	10	00	71.1 ± 1.8
16-0 e-16		0	1.1	0.61	0.0	0.0	0.0	0.0110	0.000	1.1	0.0	1.1	1.1	0.0	10	0.0	71.1 ± 1.9
16-0 e-27		1	0.6	0.000	10.1	0.0	0.0	0.0111	0.1	0.0	1.6	1.1	1.1	0.1	0.0	10	71.3 ± 1.5
16-0 e-13	1	1	0.0	0.060	10.0	0.0	1.0	0.0111	0.000	61	1.1	0.0	1.6	1.1	6.0	0.0	71.6 ± 1.7
16-0 e-14	16	1	1.01	0.000	10.0	0.06	0.0	0.0111	0.000	0.1	0.0	1.6	1.1	6.1	6.0	-0.10	1.6
16-0 e-25		1	0.0	0.000	11.1	0.0	0.0	0.0111	0.1	0.0	1.0	0.0	1.1	1.6	0.0	0.0	71.7 ± 1.6
16-0 e-28	1		0.6	0.000	0.0	0.0	0.0	0.0111	0.000	1.1	0.0	1.1	1.6	0.0	0.0	00	71.7 ± 1.6
16-0 e-21		1	0.0	0.060	1.0	0.0	0.00	0.0110	0.000	0.1	0.0	1.1	1.1	1.1	0.0	0.0	71.8 ± 1.9
16-0 e-29	1	1	1.0	0.060	10.6	0.0	0.0	0.0111	0.000	1.1	0.0	1.1	0.1	0.0	0.0	10	71.9 ± 2.1
16-0 e-17		1	0.6	0.000	0.0	0.0	0.0	0.011	0.000	1.1	0.0	0.0	0.1	0.0	6.0	0.10	72.0 ± 2.1
16-0 e-26			0.1	0.06600	10.6	0.10	0.00	0.011	0.000	1.1	0.0	0.0	1.1	0.1	10.0	0.0	0.0
16-0 e-5	0	1	0.6	0.000	11.6	0.0	0.0	0.011	0.000	6.1	0.0	0.0	1.6	6.1	0.0	0.0	0.0
16-0 e-11	1	11	0.0	0.010	1.1	0.06	0.00	0.011	0.000	1.0	0.1	0.0	0.1	6.0	11.0	0.0	0.0
16-0 e-9	6		0.0	0.000	10.0	0.0	0.0	0.011	0.000	6.1	0.0	0.0	1.1	0.6	0.0	0.0	73.2 ± 1.9
16-0 e-2	1	1	0.0	0.100	1.1	0.11000	1.1	0.011	0.000	1.1	1.6	0.1	0.0	10.0	1.0	60	0.0
16-0 e-7		1	0.6	0.060	11.0	0.0	0.0	0.0110	0.6	0.0	1.1	0.0	1.1	0.0	660	0.0	0.0
16-0 e-8	1	6	0.6	0.061	0.1	0.0	0.0	0.011	0.000	1.6	0.1	0.0	0.0	6.0	1.0	0.0	00
16-0 e-1	1	1	0.6	0.010	1.1	0.0	0.0	0.011	0.000	11	1.6	0.0	0.0	0.0	1.0	0.0	6.0
16-0 e-12	1	10	0.0	0.010	1.1	0.1	0.00	0.011	0.000	1.1	1.0	0.0	0.0	1.6	1.0	60	6.0

n = 0

Mean ²⁰⁶Pb/²³⁸U Age = 71.1 ± 0.4

(sigma, MS D = 1.06 n = 1)

and Th concentrations (ppm) are calculated relative to analyses of trace-element glass standard ST 610.

isotopic ratios are corrected relative to 1.00 standard zircon for mass bias and down-hole fractionation (1.00 with an age 106 Ma Jochen *et al.*, 1998). isotopic ²⁰⁶Pb/²³⁸U ratios, ages and errors are calculated following *aton et al.* All errors in isotopic ratios are in percentage whereas ages are reported in absolute and given at the 1-sigma level. The weighted mean ²⁰⁶Pb/²³⁸U age is also reported in absolute values at the 1-sigma level. The uncertainties have been propagated following the methodology discussed by *aton et al.* (2010).

rho is the error correlation value for the isotopic ratios ²⁰⁶Pb/²³⁸U and ²⁰⁷Pb/²³⁵U calculated by dividing these two percentage errors. The rho value is required for plotting concordia diagrams.

percentage discordance values are obtained using the following equation (100 * ((edad ²⁰⁶Pb/²³⁸U) - (edad ²⁰⁷Pb/²³⁵U)) / edad ²⁰⁶Pb/²³⁸U). positive and negative values indicate normal and inverse discordance, respectively.

individual zircon ages in bold were used to calculate the weighted mean ²⁰⁶Pb/²³⁸U age and MS D (Mean Square of Weighted Deviates) using the computational program *soplot* (udwig, 2003).